To the Graduate Council:

I am submitting herewith a dissertation written by Shima Najem Clarke entitled "Analysis of Fatigue Prone Details on a Continuous Steel Girder Bridge." I have examined the final copy of this dissertation for form and content and recommend that it be accepted in partial fulfillment of the requirements for the degree of Doctor of Philosophy, with a major in Civil Engineering.

David W. Goodpasture, Major Professor

We have read this dissertation
and recommend its acceptance:

Harold Deatherage

John D. Lemcles

Richard M. Bennett

Accepted for the Council:

Associate Vice Chancellor
and Dean of The Graduate School

ANALYSIS OF FATIGUE PRONE DETAILS ON A CONTINUOUS STEEL GIRDER BRIDGE

A Dissertation

Presented for the

Doctor of Philosophy

Degree

The University of Tennessee, Knoxville

Shima Najem Clarke

May 1997

Copyright 1997 by Shima Najem Clarke

All rights reserved

DEDICATION

This dissertation is dedicated to my father, Dr. G. Reza Najem.

Thank you, Father, for being the best parent and mentor a girl could have.

Thanks also for encouraging me to believe that nothing is impossible,

it may be difficult but not impossible.

My dearest Father, you will always be my inspiration.

ACKNOWLEDGMENTS

I am eternally indebted to many individuals who made the accomplishment of this degree possible. I would like to thank Dr. David W. Goodpasture, my Committee Chair, for his guidance and insight throughout the course of this research. I would also like to thank the other committee members, Dr. Richard M. Bennett, Dr. J. Harold Deatherage, and Dr. John D. Landes, for their time, willingness to serve, comments, and the benefit of their individual expertise. Additionally, I would like to thank Dr. Edwin G. Burdette for the vote of confidence in my pursuit of this degree and for his time spent on this project.

Thanks are extended to the Tennessee Department of Transportation for their assistance and financial support of this research: Messrs. Larry Hinds, Ed Wasserman, Mitch Hiles, Jack Lowe, Bud Turbyville, Joe Varnell, and Larry Bayless. A special note of appreciation to Bud Turbyville for his cooperation and assistance. Thanks are also extended to others helping with instrumentation, drawings, computer programming, bridge engineering practices, and gathering and reducing data: Mike Sanders, Jim Barham, Joele Fowler, Mark Mayhew, Joe Swann, Chris Schmidt, Ali Jawad Najem, David Clarke, Ali Jahed Najem, Marc Matulich, Joe Giordano, and Sam Teague.

On a personal note, I would like to thank God for giving me a second chance. I would like to thank my father, Dr. G. Reza Najem, for his guidance, encouragement, and words of wisdom. I thank my brothers, Jawad, Jahed, and Ali Najem, and my sister, Nazifa Given, for their continuous encouragement and confidence in me. I thank my mother, Hafiza Hassan, for her prayers. I thank my in-laws, Drs. Ellen and James Clarke, not only for their encouragement but also for the many times that they kept my children so that I could get some uninterrupted work done on this research. I thank my children, Robert, Christopher, and Kathleen for allowing me to be just a little bit selfish in wanting to pursue this degree. Finally, I would like to express my thanks to my husband, Dr. David Clarke, for his understanding, patience, and encouragement during this effort. Without his support, this accomplishment would have not been possible.

ABSTRACT

The most important parameters in fatigue life evaluation of existing steel highway bridges are the detail type, the truck traffic volume, the number of stress cycles per truck, and the effective stress range. The uncertainties in predicting remaining fatigue life can be attributed to any one of these parameters. Field testing of a six lane long span continuous highway girder bridge under normal traffic was conducted to determine the number of stress cycles per truck passage for various fatigue stress category details in both main and secondary members; to evaluate the effect of cycle counting methods, stress-range frequency of occurrence histogram construction, and field test duration on the effective stress range and the number of cycles per truck; and based on field observations, develop a formula for the present truck volume. Analysis of field test results revealed that the provisions of the AASHTO Guide specifications with respect to these parameters do not reflect actual conditions on a bridge.

A refined remaining fatigue life estimation procedure, based on the widely accepted method of comparing the number of cycles to date with the number of cycles to failure, was developed. A comparison of remaining fatigue life estimates based on the AASHTO Guide procedure and on the refined procedure showed that the refined procedure gave a more accurate estimate of the actual remaining fatigue life than the AASHTO Guide procedure.

As part of this research an impact study was conducted. Crawl and full speed test data were analyzed to examine the influence of bridge approach, surface condition, and truck velocity on impact factors for fatigue prone details in both main and secondary bridge members. The measured impact factors for fatigue stress categories A, B, E, and E' details were compared to values obtained using the AASHTO Standard specification formula. For fatigue prone details, the test results showed that surface roughness, truck velocity, and bridge approach affect the impact factor. Measured impact factors varied with the location of the detail. Also, the study showed that the AASHTO design impact factors were unconservative for details located in the approach (end) span.

TABLE OF CONTENTS

CHAPTER 1. INTRODUCTION 1

1.1 Problem 1

1.2 Review of AASHTO Standard Specification 2
AASHTO Standard Design Equations 8
AASHTO Standard Design Number of Cycles 8

1.3 Review of AASHTO Guide Specification 9
Stress Range 11
Remaining Life 13

1.4 Assessment of the AASHTO Specifications 14

1.5 Research Objective and Scope 16

1.6 Organization of the Dissertation 17

CHAPTER 2. BACKGROUND AND GAGE LOCATION 18

2.1 Description of the Structure 18

2.2 History of the Bridge and the Crack 22

2.3 History of the Repairs and Retrofit 24

2.4 Instrumentation 28
Strain Gages 28
Data Acquisition System 30

2.5 Description of Gage Location 30

CHAPTER 3. IMPACT STUDY 32

3.1 Introduction 32

3.2 Literature Review 33

3.3 Description of Impact Test 34
Instrumentation 34
Test Procedure 40

3.4 Test Results and discussion 45

3.5 Conclusions 55

CHAPTER 4. SENSITIVITY ANALYSIS 57

4.1 Literature Review 57
Cycle Counting Methods 57

Histogram Construction 64
Test Duration 65

4.2 Cycle Counting Methods 65
Evaluation Procedure 66
Evaluation Results and Discussion 69

4.3 Histogram Construction 79
Evaluation Procedure 79
Evaluation Results and Discussion 82

4.4 Test Duration 95
Evaluation Procedure 96
Evaluation Results and Discussion 100

4.5 Conclusions 141

CHAPTER 5. REMAINING FATIGUE LIFE ESTIMATION 147

5.1 Literature Review 147
Stress Cycles per truck 147
Remaining Life 148

5.2 Fatigue Testing Procedure 153

5.3 Present Truck Volume 154

5.4 Stress Cycles per Truck 158

5.5 Remaining Fatigue Life Procedure 161
Refined Procedure 161
Comparison of Remaining Life Calculation Results 164

5.6 Conclusions 171

CHAPTER 6. CONCLUSIONS AND RECOMMENDATIONS 174

6.1 Summary of Research Findings 174

6.2 Recommendations for Further Research 178

REFERENCES 180

APPENDIX 185

VITA 215

LIST OF TABLES

Table 1-1. Parameters of SN-Curve Regression Line for Redundant Members 5

Table 1-2. AASHTO Allowable Fatigue Stress Range 6

Table 1-3. AASHTO Stress Cycles 6

Table 3-1. Summary of Holston River Bridge Impact Test Details 39

Table 3-2. Impact Factors for Main Longitudinal Steel Bridge Members 51

Table 3-3. Impact Factors for Secondary Steel Bridge Members 52

Table 3-4. Measured Impact Factor Mean and Standard Deviation Values 54

Table 3-5. Measured Impact Factors for AASHTO Fatigue Stress Categories 54

Table 4-1. Summary of Cycle Counting Methods Fatigue Prone Details 67

Table 4-2. Cycle Counting Sensitivity Results for Fatigue Prone Details in Bridge Main Members 70

Table 4-3. Cycle Counting Sensitivity Results for Fatigue Prone Details in Bridge Secondary Members 71

Table 4-4. Summary of Cycle Counting Sensitivity Analysis 75

Table 4-5. Cycle Counting Regression Analysis 77

Table 4-6. Summary of Histogram Construction Details 80

Table 4-7. Percent Difference Results for Histograms of Gages G52 and G318 84

Table 4-8. Histogram Construction Results for Bridge Main Member Details 86

Table 4-9. Histogram Construction Results for Bridge Secondary Member Details. 87

Table 4-10. Histogram Construction Fatigue Damage Results 88

Table 4-11. Percent Difference Between Histograms for Bridge Main Member Details 89

Table 4-12. Percent Difference Between Histograms for Secondary Member Details 91

Table 4-13. Percent Difference Between Histograms for Fatigue Damage of Bridge Main Member Details 92

Table 4-14. Percent Difference Between Histograms for Fatigue Damage of Bridge Secondary Member Details 94

Table 4-15. Summary of Test Duration Details 97

Table 4-16. Test Duration Example Calculation for Gage 58D 98

Table 4-17. Summary of Test Duration Results 121
Table 4-18. Field Test Duration for AASHTO Fatigue Stress Categories 141
Table 5-1. AASHTO Guide's Number of Stress Cycles per Truck Passage 147
Table 5-2. Detail Constant, K, and Limiting Stress Range, S_{FL}, Values 150
Table 5-3. Percentage of Trucks Producing a Measurable Strain Range Reading... 155
Table 5-4. Holston River Bridge Truck Traffic Characteristics 157
Table 5-5. Present Truck Volume Based on Equations (5.5) and (5.9) 157
Table 5-6. Measured Stress Cycles per Truck Values 160
Table 5-7. Measured *CPT* Values for AASHTO Fatigue Stress Categories 161
Table 5-8. AASHTO Guide's Remaining Fatigue Life Estimates, Equation (5.4).. 165
Table 5-9. Estimations of the ADTT and the T Parameters 166
Table 5-10. Refined Procedure's Remaining Fatigue Life Estimates 167
Table A-1. Strain Gage Information 186

LIST OF FIGURES

Figure 1-1. AASHTO *Standard* Design Curves for Redundant Members 7

Figure 1-2. AASHTO *Standard* Fatigue Specification for Redundant Members 7

Figure 1-3. Illustration of the Mathematical Equivalence Between AASHTO Design and Actual Design Values for Category E Detail 10

Figure 1-4. AASHTO *Guide*'s Fatigue Truck 12

Figure 2-1. Holston River Bridge Elevation 19

Figure 2-2. Holston River Bridge Partial Plan View 20

Figure 2-3. Holston River Bridge Cross-Sections 21

Figure 2-4. Fracture of Girder Number 4 23

Figure 2-5. Holston River Bridge Girder Number 4 Cracked Section 25

Figure 2-6. Holston River Bridge Repair Process 26

Figure 2-7. Holston River Bridge Repairs at Failure Section 27

Figure 2-8. The Retrofit 29

Figure 3-1. Partial Plan of the Holston River Bridge: Impact Test Location 35

Figure 3-2. Gage Locations for Test Locations 1A, 1C, and 1D 36

Figure 3-3. Gage Locations for Test Locations 2 and 7 37

Figure 3-4. Gage Locations for Test Locations 1C, 1D, 2, and 7 38

Figure 3-5. Impact Study Test Truck 41

Figure 3-6. West Knoxville Weigh Station Truck Weight Histogram Summary 42

Figure 3-7. Strain Trace for Gage 135 with the Truck in the Middle Lane 44

Figure 3-8. Rough and Smooth Surface Condition Measured Impact Factors for Main and Secondary Steel Bridge Members (These are the Results of One Test) 46

Figure 3-9. Truck Velocity vs Measured Impact Factor for Main and Secondary Steel Bridge Members 47

Figure 3-10. Measured Impact Factors for Main and Secondary Steel Bridge Member Gages Located in the Approach (End) Span and in the Third Span 49

Figure 4-1. Level-Crossing Counting (Bannantine et al., 1990) 58

Figure 4-2. Simple-Range Counting (Bannantine et al., 1990) 59

Figure 4-3. Peak Counting (Bannantine et al., 1990) 61

Figure 4-4. Mean-Crossing-Peak Counting 62

Figure 4-5. Rainflow Counting (Bannantine et al., 1990) 63

Figure 4-6. Main Bridge Member Rainflow and Mean-Crossing-Peak Average Values for Stress-Range Frequency-of-Occurrence Histogram Starting at 1000 psi 73

Figure 4-7. Secondary Bridge Member Rainflow and Mean-Crossing-Peak Average Values for Stress-Range Frequency-of-Occurrence Histogram Starting at 1000 psi 74

Figure 4-8. Plot Showing the Degree of Correlation Between Rainflow and Mean-Crossing-Peak Counting Methods for all Fatigue Prone Details with Stress-Range Frequency-of-Occurrence Histogram Starting at 1000 psi 78

Figure 4-9. G105: Stress-Range Frequency-of-Occurrence Histograms, Interval Widths (From Top to Bottom) of 250, 350, 500, 600, & 1000 psi. Histograms (from Top to Bottom) Start at (A) 250, 350, 500, 600, & 1000 psi and (B) 500 psi 81

Figure 4-10. Category E' Detail Frequency-of-Occurrence Stress-Range Histogram for Histogram Interval Widths (from Top to Bottom) of 250 psi, 350 psi, 600 psi, and 1000 psi 83

Figure 4-11. The Effect of Field Test Duration on the Effective Stress Range (RMC), the Number of Cycles Per Truck (CPT), and the Total Fatigue Life for Category A Main Bridge Member Detail, Gage G58D 101

Figure 4-12. The Effect of Field Test Duration on the Effective Stress Range (RMC), the Number of Cycles Per Truck (CPT), and the Total Fatigue Life for Category B Main Bridge Member Detail, Gage G5 102

Figure 4-13. The Effect of Field Test Duration on the Effective Stress Range (RMC), the Number of Cycles Per Truck (CPT), and the Total Fatigue Life for Category B Main Bridge Member Detail, Gage G58 103

Figure 4-14. The Effect of Field Test Duration on the Effective Stress Range (RMC), the Number of Cycles Per Truck (CPT), and the Total Fatigue Life for Category B Main Bridge Member Detail, Gage G58 (Without Outlier Data Point) 104

Figure 4-15. The Effect of Field Test Duration on the Effective Stress Range (RMC), the Number of Cycles Per Truck (CPT), and the Total Fatigue Life for Category C Main Bridge Member Detail, G58B 105

Figure 4-16. The Effect of Field Test Duration on the Effective Stress Range (RMC), the Number of Cycles Per Truck (CPT), and the Total Fatigue Life for Category E Main Bridge Member Detail, Gage G47 106

Figure 4-17. The Effect of Field Test Duration on the Effective Stress Range (RMC), the Number of Cycles Per Truck (CPT), and the Total Fatigue Life for Category E' Main Bridge Member Detail, Gage G51 107

Figure 4-18. The Effect of Field Test Duration on the Effective Stress Range (RMC), the Number of Cycles Per Truck (CPT), and the Total Fatigue Life for Category E' Main Bridge Member Detail, Gage G73 108

Figure 4-19. The Effect of Field Test Duration on the Effective Stress Range (RMC), the Number of Cycles Per Truck (CPT), and the Total Fatigue Life for Category E' Main Bridge Member Detail, Gage G110 109

Figure 4-20. The Effect of Field Test Duration on the Effective Stress Range (RMC), the Number of Cycles Per Truck (CPT), and the Total Fatigue Life for Category E' Main Bridge Member Detail, Gage G116 110

Figure 4-21. The Effect of Field Test Duration on the Effective Stress Range (RMC), the Number of Cycles Per Truck (CPT), and the Total Fatigue Life for Category A Secondary Bridge Member Detail, Gage G35 113

Figure 4-22. The Effect of Field Test Duration on the Effective Stress Range (RMC), the Number of Cycles Per Truck (CPT), and the Total Fatigue Life for Category B Secondary Bridge Member Detail, Gage G2 114

Figure 4-23. The Effect of Field Test Duration on the Effective Stress Range (RMC), the Number of Cycles Per Truck (CPT), and the Total Fatigue Life for Category C Secondary Bridge Member Detail, Gage G32 115

Figure 4-24. The Effect of Field Test Duration on the Effective Stress Range (RMC), the Number of Cycles Per Truck (CPT), and the Total Fatigue Life for Category E Secondary Bridge Member Detail, Gage G34 116

Figure 4-25. The Effect of Field Test Duration on the Effective Stress Range (RMC), the Number of Cycles Per Truck (CPT), and the Total Fatigue Life for Category E Secondary Bridge Member Detail, Gage G105 117

Figure 4-26. The Effect of Field Test Duration on the Effective Stress Range (RMC), the Number of Cycles Per Truck (CPT), and the Total Fatigue Life for Category E Secondary Bridge Member Detail, Gage G305 118

Figure 4-27. The Effect of Field Test Duration on the Effective Stress Range (RMC), the Number of Cycles Per Truck (CPT), and the Total Fatigue Life for Category E' Secondary Bridge Member Detail, Gage G117 119

Figure 4-28. The Effect of Field Test Duration on the Effective Stress Range (RMC), the Number of Cycles Per Truck (CPT), and the Total Fatigue Life for Category E' Secondary Bridge Member Detail, Gage G317 120

Figure 4-29. Top Plot Showing the Relationship Between RMC and Truck Count and Bottom Plot Showing the Relationship Between CPT and Truck Count for Category A Main Bridge Member Detail, G58D 122

Figure 4-30. Top Plot Showing the Relationship Between RMC and Truck Count and Bottom Plot Showing the Relationship Between CPT and Truck Count for Category B Main Bridge Member Detail, G5 123

Figure 4-31. Top Plot Showing the Relationship Between RMC and Truck Count and Bottom Plot Showing the Relationship Between CPT and Truck Count for Category B Main Bridge Member Detail, G58 124

Figure 4-32. Top Plot Showing the Relationship Between RMC and Truck Count and Bottom Plot Showing the Relationship Between CPT and Truck Count for Category C Main Bridge Member Detail, G58B 125

Figure 4-33. Top Plot Showing the Relationship Between RMC and Truck Count and Bottom Plot Showing the Relationship Between CPT and Truck Count for Category E Main Bridge Member Detail, G47 126

Figure 4-34. Top Plot Showing the Relationship Between RMC and Truck Count and Bottom Plot Showing the Relationship Between CPT and Truck Count for Category E' Main Bridge Member Detail, G51 127

Figure 4-35. Top Plot Showing the Relationship Between RMC and Truck Count and Bottom Plot Showing the Relationship Between CPT and Truck Count for Category E' Main Bridge Member Detail, G73 128

Figure 4-36. Top Plot Showing the Relationship Between RMC and Truck Count and Bottom Plot Showing the Relationship Between CPT and Truck Count for Category E' Main Bridge Member Detail, G110 129

Figure 4-37. Top Plot Showing the Relationship Between RMC and Truck Count and Bottom Plot Showing the Relationship Between CPT and Truck Count for Category E' Main Bridge Member Detail, G116 130

Figure 4-38. Top Plot Showing the Relationship Between RMC and Truck Count and Bottom Plot Showing the Relationship Between CPT and Truck Count for Category A Secondary Bridge Member Detail, G35 132

Figure 4-39. Top Plot Showing the Relationship Between RMC and Truck Count and Bottom Plot Showing the Relationship Between CPT and Truck Count for Category B Secondary Bridge Member Detail, G2 133

Figure 4-40. Top Plot Showing the Relationship Between RMC and Truck Count and Bottom Plot Showing the Relationship Between CPT and Truck Count for Category C Secondary Bridge Member Detail, G32 134

Figure 4-41. Top Plot Showing the Relationship Between RMC and Truck Count and Bottom Plot Showing the Relationship Between CPT and Truck Count for Category E Secondary Bridge Member Detail, G34 135

Figure 4-42. Top Plot Showing the Relationship Between RMC and Truck Count and Bottom Plot Showing the Relationship Between CPT and Truck Count for Category E Secondary Bridge Member Detail, G105 136

Figure 4-43. Top Plot Showing the Relationship Between RMC and Truck Count and Bottom Plot Showing the Relationship Between CPT and Truck Count for Category E Secondary Bridge Member Detail, G305 137

Figure 4-44. Top Plot Showing the Relationship Between RMC and Truck Count and Bottom Plot Showing the Relationship Between CPT and Truck Count for Category E' Secondary Bridge Member Detail, G117 138

Figure 4-45. Top Plot Showing the Relationship Between RMC and Truck Count and Bottom Plot Showing the Relationship Between CPT and Truck Count for Category E' Secondary Bridge Member Detail, G317 139

Figure 5-1. Estimation of Remaining Fatigue Life 152

Figure 5-2. Average Daily Truck Traffic Volume (*ADTT*) Variation with Time 152

Figure 5-3. Typical Gage Locations Throughout the First Three Spans 155

Figure 5-4. The Yearly ADT for the Holston River Bridge 166

CHAPTER 1

INTRODUCTION

1.1 Problem

Because of the high cost of replacing, strengthening, or repairing bridges, the remaining service life of existing bridges has become an important issue to highway engineers. Steel is a common type of highway bridge material in this country. The steel in bridges is subjected to repeated loading over time, potentially leading to fatigue cracks which may grow with time and thus shorten the life of the bridge. Eighty to ninety percent of the failures in steel structures are related to fatigue and fracture (ASCE Committee, 1982). At present, approximately 50 percent of all highway steel bridges in the United States are over 30 years old, with many of them at or over their design life of 50 years (Zhao et al., 1994).

The remaining service life of a highway steel bridge is dependent on the fatigue and fracture resistance of its components, that is, its members and connection details. Currently, the highway engineer in this country is bound by the fatigue provisions of two specifications for design and evaluation of steel bridges. These specifications are the American Association of State Highway and Transportation Officials (AASHTO) *Standard Specification for Highway Bridges* (1992) and the AASHTO *Guide Specifications for Fatigue Evaluation of Existing Steel Bridges* (1990). The remaining fatigue life evaluation procedures of the *Guide* evolved from the fatigue design provisions of the *Standard* specification. Since the decision to initiate bridge rehabilitation projects are based on the results of the fatigue-life calculations performed in accordance with the

AASHTO specifications, it is imperative that these specifications accurately reflect actual bridge conditions. The problem is that the current fatigue life estimation procedures of the AASHTO specifications may not accurately reflect actual conditions in steel bridges. A review and an assessment of the current AASHTO *Standard* and *Guide* fatigue specification are presented.

1.2 Review of AASHTO Standard Specification

The present fatigue design requirements in the AASHTO *Standard Specification* were developed from the results of several National Cooperative Highway Research Program (NCHRP) projects investigating the fatigue strength of welded bridge details. The outcome of these projects were reported in NCHRP reports 102, 147, 188, 206, 227, 267, and 286. Of these reports, NCHRP Reports 102 and 147 contributed the most to the current fatigue design requirements. In NCHRP Report 102 (Fisher et al., 1970), 374 10-ft long beams were tested under a two-point constant amplitude stress range varying from 12 to 36 ksi. Of the total, 204 were fabricated with cover plates, 84 were fabricated with flange splices, and 86 were plain rolled beams and girders. In NCHRP Report 147 (Fisher et al., 1974), 157 10-ft to 20-ft long steel beams were tested under two-point constant amplitude cyclic loading. Of the total, 29 were plain rolled steel beams, 47 beams and 22 girders were fabricated with transverse stiffeners on one side, and 59 beams were fabricated with flange attachments. Three types of steel were used for both studies: A36, A441, and A514. The regression analysis model used to relate the number of cycles to failure (N) to the stress range (S_r) at the crack initiation point was

$$\log N = \log A - B \log S_r$$
$$or \qquad (1.1)$$
$$N = AS_r^{-B}$$

The coefficients A and B were obtained through a least-square fit. These studies concluded that the stress range was the only significant factor for designing a given detail against fatigue. Each type of detail in these studies was then classified into stress categories A through E. Category A represented details with the highest fatigue strength while Category E represented details with the lowest fatigue strength. Category A fatigue cracks initiated at surface defects. Category B fatigue cracks initiated at an internal discontinuity in the weld metal and propagated into both web and flange plates until failure occurred. Category C marked the transition between the initial defect and the geometrical stress concentration influencing the fatigue strength. Crack growth initiated at the transverse weld toe termination and propagated into the web plate. Category D was the transition zone between the high and low fatigue strength details. Category E fatigue cracks initiated at the longitudinal weld toe termination and propagated into the web and flange plate. For each stress category, an allowable fatigue stress range (F_{sr}), based on a 95 percent confidence limit for 95 percent survival, was recommended for N equal to 100,000 cycles, 500,000 cycles, 2,000,000 cycles, and over 2,000,000 cycles. Subsequent to these two reports, four other NCHRP projects were conducted on fatigue strength of welded bridge details. In NCHRP report 206 (Fisher et al., 1979), full-size coverplated A36 and A588 rolled beams were tested under constant amplitude stress range varying from 4 to 8 ksi. The results contributed to a new stress category, Category E'. In NCHRP report 227 (Fisher et al., 1980), 18 full-size A36 rolled beams with web and flange lateral

attachment plates were tested under constant amplitude stress range varying from 6 to 15 ksi. Detail types tested were: web gusset plates, flange gusset plates, web attachments with either fillet or groove welds, web attachments inserted through the web plate, and flange plates. The fatigue strength of these details were defined either as category E or E' depending on the plate thickness of the attachments. NCHRP reports 188 (Schilling et al., 1978) and 267 (Fisher et al., 1983) dealt with fatigue behavior of welded details subjected to variable amplitude loading. Two important conclusions were drawn from these two reports. First, both Miner's cumulative damage rule and the root-mean-square (RMS) stress range method can be used to relate random variable stress cycles to constant cycle data. That is, for equal number of cycles, the effective constant amplitude stress range will cause the same fatigue damage as the sequence of variable amplitude stress range it replaces. The effective stress range was defined by

$$S_{re} = \left[\sum \alpha_i S_{ri}^{B}\right]^{1/B} \tag{1.2}$$

in which S_{ri} is the midwidth of the *ith* interval in a frequency-of-occurrence histogram defining the variable amplitude spectrum and α_i is the fraction of stress range within that interval. B is the slope of the constant amplitude SN curve for Miner's Rule. And, the value of B is 2.0 for the RMS stress range method. Miner's rule is described by the following equation (Bannantine et al., 1990):

$$\sum D_i = \sum \frac{n_i}{N_i} \geq 1 \tag{1.3}$$

in which D_i is the damage fraction and is defined as the fraction of life used at stress range level S_{ri}, n_i is the number of cycles at stress range level S_{ri}, and N_i is the number of

cycles to failure under constant amplitude stress range S_{ri}. The second conclusion was that if one stress cycle exceeded the constant amplitude fatigue limit than all stress cycles contributed to the fatigue damage. The regression coefficients, A and B, and the stress range standard deviation, σ, for the six Categories A through E' are summarized in Table 1-1 (Albrecht, 1983).

NCHRP Report 286 (Keating et al., 1986) examined the adequacy of the AASHTO fatigue resistance curves by comparing them to the results of other fatigue studies conducted in this country and other countries. This review resulted in normalizing the AASHTO fatigue curves to a constant slope of -3.0. Also, a new fatigue curve, Category B', was added to better estimate the fatigue strength of partial penetration longitudinal groove welds and longitudinal welds with backing bars. Tables 1-2 and 1-3 list the present AASHTO allowable fatigue stress range for each stress category and the stress cycles, respectively. Figures 1-1 and 1-2 shows the AASHTO design curves and specification for redundant members. Figure 1-1 shows the current set of AASHTO

Table 1-1. Parameters of SN-Curve Regression Line for Redundant Members

Category	Type of Detail Tested	Number of Data Points	Regression Coefficients		σ	F_{sr} (ksi) for Over 2,000,000 Cycles
			A	B		
A	Rolled Beam	28	11.121	3.178	0.221	24
B	Welded Beam	55	10.87	3.372	0.147	16
C	Stiffener	135	10.085	3.097	0.158	12
	2-inch Attachments	14	10.038	3.25	0.063	10
D	4-inch Attachments	44	9.603	3.071	0.108	7
E	Coverplate End	193	9.292	3.095	0.101	5
E'	Coverplate End, t > 0.8"	18	9.166	3.2	0.194	2.6

Note: F_{sr} = Allowable fatigue stress range

Table 1-2. AASHTO Allowable Fatigue Stress Range

	Redundant Load Path Structures				Nonredundant Load Path Structures			
	Allowable Range of Stress, F_{sr} (ksi)				Allowable Range of Stress, F_{sr} (ksi)			
Category	For 100,000 Cycles	For 500,000 Cycles	For 2,000,000 Cycles	For over 2,000,000 Cycles	For 100,000 Cycles	For 500,000 Cycles	For 2,000,000 Cycles	For over 2,000,000 Cycles
A	63	37	24	24	50	29	24	24
B	49	29	18	16	39	23	16	16
B'	39	23	14.5	12	31	18	11	11
C	35.5	21	13	10	28	16	10	9
D	28	16	10	7	22	13	8	5
E	22	13	8	4.5	17	10	6	2.3
E'	16	9.2	5.8	2.6	12	7	4	1.3
F	15	12	9	8	12	9	7	6

Source: AASHTO Standard Specification (1992)

Table 1-3. AASHTO Stress Cycles

			Main (Longitudinal) Load Carrying Members		Transverse Members and Details Subjected to Wheel Loads
Type of Road	Case	One Way ADTT	Truck Loading	Lane Loading	Truck Loading
Freeways, Expressways, Major Highways, and Streets	I	2,500 or more	2,000,000 and over	500,000	over 2,000,000
Freeways, Expressways, Major Highways, and Streets	II	less than 2,500	500,000	100,000	2,000,000
Other Highways and Streets	III	-	100,000	100,000	500,000

Source: AASHTO Standard Specification (1992)

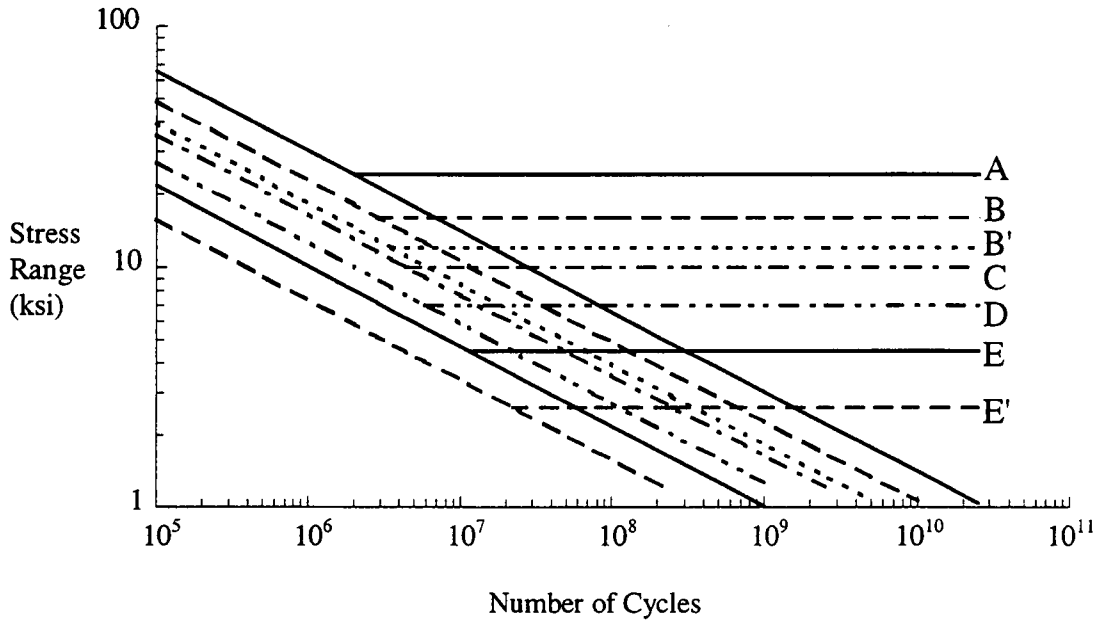


Figure 1-1. AASHTO *Standard* Design Curves for Redundant Members

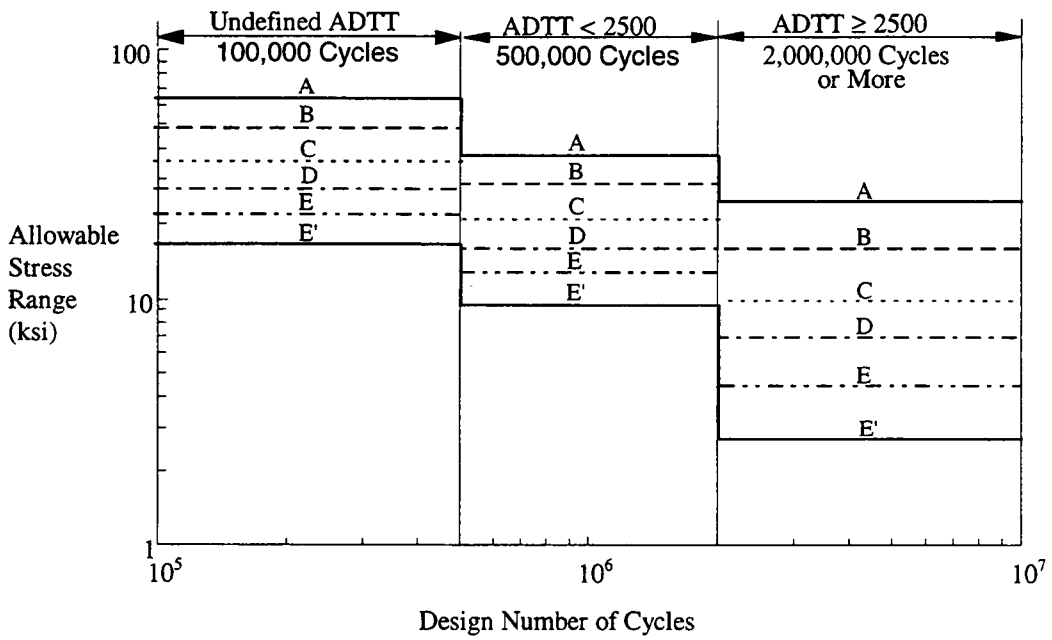


Figure 1-2. AASHTO *Standard* Fatigue Specification for Redundant Members

fatigue design curves. These lines are drawn two-standard deviations to the left and parallel to the mean curves. Therefore, the probability that the test results for a given detail fall below this design line is 2.5 percent. Figure 1-2 is an illustration of Tables 1-2 and 1-3.

AASHTO *Standard* Design Equations

The AASHTO requirement for bridges designed for two or more traffic lanes is

$$f_{sr} = \frac{M_r(1+I)}{S_x}\frac{S}{7} \le F_{sr} \quad \{F_{sr} \text{ for } 2\times10^6 \text{ cycles} - \text{Case I} \tag{1.4}$$

and for one traffic lane,

$$f_{sr} = \frac{M_r(1+I)}{S_x}\frac{S}{5.5} \le F_{sr} \quad \begin{cases} F_{sr} \text{ for over } 2\times10^6 \text{ cycles} - \text{Case I} \\ F_{sr} \text{ for } 5\times10^5 \text{ cycles} - \text{Case II} \\ F_{sr} \text{ for } 1\times10^5 \text{ cycles} - \text{Case III} \end{cases} \tag{1.5}$$

in which M_r is the moment range caused by wheel loads of a HS20 truck, I is the impact factor, S is the average stringer spacing, $S/5.5$ and $S/7$ are the lateral distribution factors, S_x is the section modulus, and F_{sr} is the allowable fatigue stress range.

AASHTO *Standard* Design Number of Cycles

During the 1940's AASHTO adopted the American Welding Society (AWS) bridge specifications for welded structures (Fisher, 1977). These provisions were based on small plate specimen test data, and 2,000,000 cycles was generally assumed to be the run-out or infinite life condition. Albrecht (1983) showed that AASHTO's choice of 2,000,000 cycles of allowable design stress range, F_{sr}, is mathematically equivalent to the

design life number of cycles of an equivalent constant amplitude stress range, f_{re}. For a longitudinal member, f_{re} is related to F_{sr} by

$$f_{re} = 0.705\phi\, F_{sr} \tag{1.6}$$

and for a transverse member

$$f_{re} = 0.705\phi\, F_{sr}\left(\frac{F_{sr}\ for 2\times10^{6}\ cycles}{F_{sr}\ for over 2\times10^{6}\ cycles}\right) \tag{1.7}$$

in which ϕ is the ratio of measured-to-computed stress range for the design load. The value of ϕ for all stress categories is 0.5. Figure 1-3 illustrates equation (1.6) for a Category E detail with ADTT = 2500 and a design life of 50 years.

1.3 Review of AASHTO Guide Specification

From the mid-seventies to the mid-eighties, many investigators attempted to improve on the AASHTO fatigue specifications. Their main concerns were that:

- The fatigue provisions were based on approximations of actual conditions in steel bridges.
- These provisions combined an artificially high stress range with an artificially low number of stress cycles to produce a reasonable design.
- These provisions were intended for design applications and not intended for rating or assessing the remaining fatigue life of existing steel bridges.
- These provisions did not provide consistent levels of reliability for different cases.

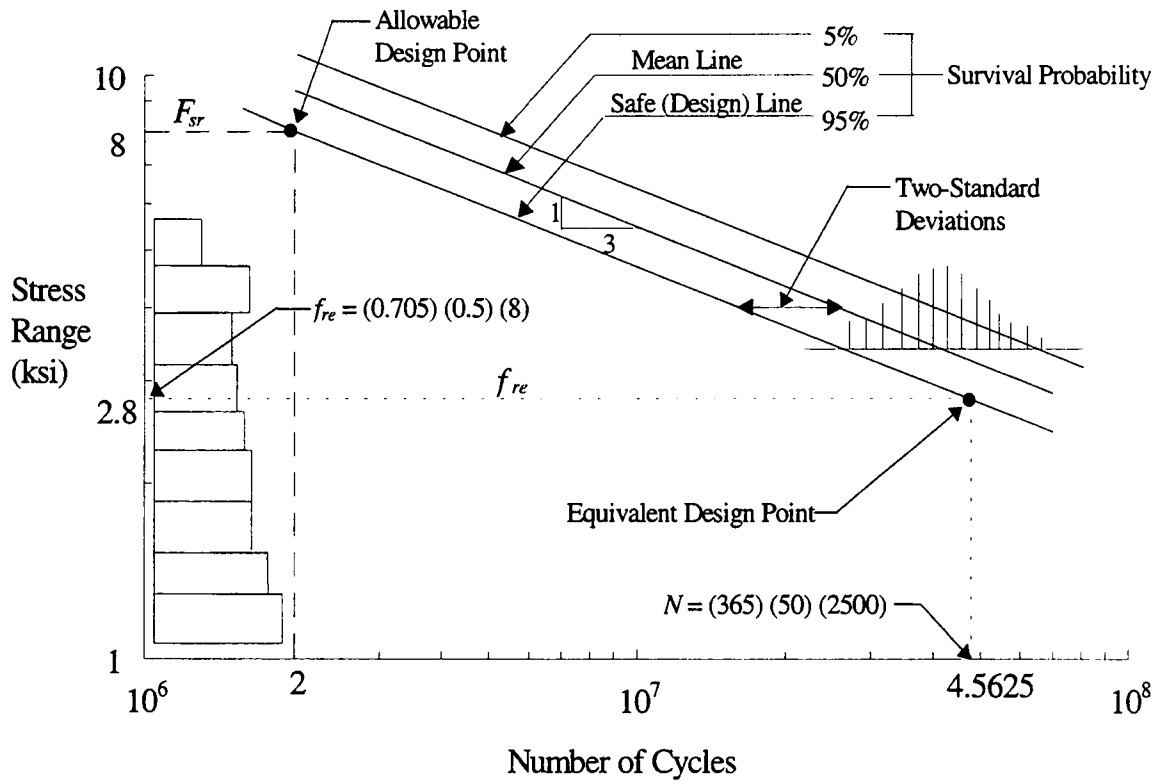


Figure 1-3. Illustration of the Mathematical Equivalence Between AASHTO Design and Actual Design Values for Category E Detail

In an attempt to address these concerns, AASHTO published the *Guide* specification. The *Guide*, based on methodology developed in NCHRP Report 299 (Moses et al., 1987), presents evaluation procedures that better reflect the actual fatigue conditions in steel bridges when compared to AASHTO *Standard s*pecification procedures. Sections 2 and 3 of the *Guide* outline an evaluation procedure for calculating the stress range and for estimating the remaining fatigue life, respectively.

Stress Range

The *Guide* provides two options for obtaining the stress range. One option is to calculate the stress range by

$$S_r = \frac{M_r(1+I)}{S_x} DF \tag{1.8}$$

in which M_r is the moment range, I is the impact factor, S_x is the section modulus, and DF is the lateral load distribution factor. The moment range for a given bridge detail is calculated by passage of a fatigue truck across the bridge. For longitudinal members, the fatigue truck is placed at different positions that would cause the algebraic maximum and minimum moments; the algebraic difference between the two is the moment range. For transverse members, the moment range equals the moment at the detail when the fatigue truck is at the center of the traffic lane that results in the highest moment. Figure 1-4 illustrates the fatigue truck. The *Guide* gives four alternatives for adjusting the fatigue truck's gross weight when site specific data on truck weights or classification are known. The evaluation procedure uses an impact factor of 10 percent for smooth road surfaces and a factor ranging from 10 to 30 percent for rough surfaces. The section modulus is

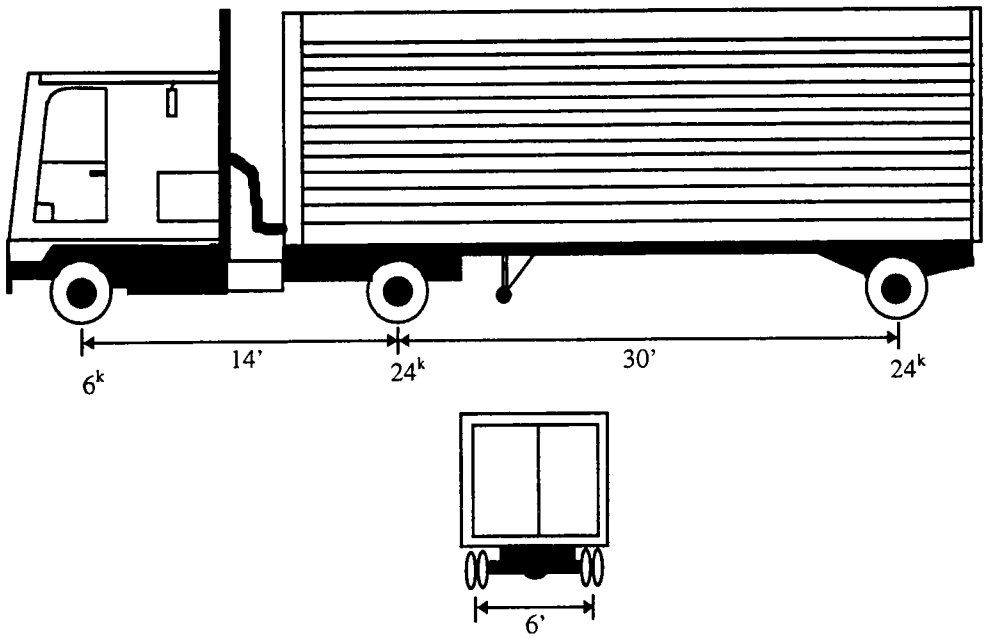


Figure 1-4. AASHTO *Guide*'s Fatigue Truck

calculated by dividing the moment of inertia of the bending member by the distance from the neutral axis to expected crack initiation location of the detail under consideration. The lateral distribution factors used in this evaluation procedure are given in the *S/D* format, where *S* is the girder spacing in feet and *D* is equal to 17, 19, 20, 22, 23 for spans in feet of 30 or less, 40, 60, 90, and 120 or more, respectively. The *S/D* factors are based on the full truck moment rather than 1/2 of the truck moment as in the present AASHTO factors. As an alternative, the stress range may be determined from stress range histograms obtained from field measurements on the bridge under normal traffic. Equation (1.2) with *B* equal to 3.0 is used to calculate the effective stress range.

Remaining Life

Section 3 of the *Guide* outlines a procedure for calculating the remaining fatigue life of an existing steel bridge. The remaining fatigue life for an estimated lifetime average daily truck volume is calculated by

$$Y_f = \left(\frac{f K \times 10^6}{T_a C (R_s S_r)^3} \right) - a \tag{1.9}$$

in which Y_f is the remaining fatigue life in years, K is the detail constant, T_a is the estimated average daily truck volume (ADTT) in the outer lane, C is the number of stress cycles per truck passage, S_r is the stress range in ksi, R_s is the reliability factor, a is the present age of the bridge in years, and f is 1.0 for calculating safe life and 2.0 for calculating mean life.

This evaluation procedure is applicable to uncracked and unrepaired members subjected to primary stresses that are normally calculated in design. The *Guide's* remaining mean life is the best possible estimate of the actual life; there is a 50 percent probability that the actual remaining life will exceed the remaining mean life. The *Guide's* remaining safe life provides a much higher degree of safety; the probability that the actual remaining life will exceed the remaining safe life is 97.7 percent. The detail constant K is calculated by

$$K = \frac{A}{365 \times 10^6} \tag{1.10}$$

where A is obtained from equation (1.1) for N equal to 2,000,000 cycles and S_r equal to the allowable stress range values of Table 1-1. For longitudinal members with spans greater than 40-ft and for transverse members with girder spacing greater than 20-ft, C is

taken as 1.0. As an alternative, the number of stress cycles per passage of the fatigue truck across a given span can be calculated by

$$N_e = 1 + \sum \left(\frac{S_{ri}}{S_{rp}} \right)^3 \tag{1.11}$$

in which N_e is the equivalent number of primary cycles for a complex cycle, S_{ri} is the stress range for a higher order cycle, and S_{rp} is the stress range for the primary cycle. In this approach, the complex cycle is decomposed into a primary cycle and one or more higher order (secondary, tertiary, etc.) cycles. Fatigue damage is proportional to the stress range, S_r, cubed. Thus, each higher order cycle does $(S_{ri}/S_{rp})^3$ times as much damage as the primary cycle. The *Guide* allows the shape of the complex cycle to either be calculated for a given span by using an influence line or obtained from a field measured stress-time plot of a typical truck passage. The lifetime ADTT in the outer lane is estimated from the present ADTT in the outer lane, T, the present age of the bridge, a, and the annual growth rate, g. The present ADTT, T, is calculated by

$$T = (ADT) F_T F_L \tag{1.12}$$

in which ADT is the present average daily traffic volume (both directions) on the bridge, F_T is the fraction of trucks (excluding panel, pickup, and 2-axle/4-wheel trucks) in the traffic, and F_L is the fraction of trucks in the outer lane.

1.4 Assessment of the AASHTO Specifications

The current AASHTO *Standard* and *Guide* fatigue specifications were presented to illustrate the deficiencies in their fatigue life estimation procedures in reflecting actual conditions in steel bridges. The AASHTO *Standard* SN curves, which are based on 30

year old laboratory investigations conducted at constant stress range, can at best be considered an approximation of actual conditions in steel bridges. There are no provisions in the *Standard* fatigue design procedures for calculating remaining fatigue life. The detail type, the truck traffic volume, the number of stress cycles per truck, and the stress range are the most important parameters in fatigue life evaluation of steel bridges, as shown in equation (1.9). The uncertainties in predicting life can be attributed to any one of these parameters. Therefore, the provisions of the *Guide* with respect to these parameters should reflect actual conditions on a bridge as much as possible. In regards to truck traffic volume, the *Guide*'s requirement of estimating T_a for the outer lane may be unconservative for bridges with 4 or more traffic lanes. Also, assigning fixed values for F_T may be unconservative. In regards to cycles per truck, the *Guide*'s provisions are based on analytical results. Field measurement data are needed to validate the analytical results. In regards to calculated stress range, the impact factor of equation (1.8) is solely a function of surface roughness and the value of 10 percent for this parameter was based on the results of only two field measurement studies. Clearly, more field data is required in this area. In regards to field measured stress range, the *Guide* provides no provisions for cycle counting methods, stress-range frequency-of-occurrence histogram construction, and test duration. All could have a significant affect on the effective stress range.

1.5 Research Objectives and Scope

The objectives of this research were to:

1. Conduct an impact study to (a) examine the influence of bridge approach, truck velocity and surface condition on impact factors for fatigue prone details in both main and secondary members, and (b) to determine impact factors for various fatigue stress category details.
2. Conduct fatigue testing under normal traffic (a) to determine the number of stress cycles per truck for various fatigue stress category details in both main and secondary members, (b) to evaluate the effect of cycle counting methods, stress-range frequency-of-occurrence histogram construction, and field testing duration on the effective stress range and the number of cycles per truck, and (c) based on field observations, develop a formula for T (present truck volume) that more accurately reflects actual bridge conditions than equation (1.12).
3. Develop a more refined procedure than equation (1.9) for calculating the remaining fatigue life and compare the results with that of equation (1.9).
4. Based on the results of the first four objectives, make recommendations on how to improve the *Guide*'s remaining fatigue life evaluation procedure if necessary.

The scope of this study is limited to fatigue prone details on long span continuous steel girder bridges. The focus of this research is experimental; the test bridge is the Holston River Bridge on I-40, located in east Knox county, Tennessee.

1.6 Organization of the Dissertation

The remainder of this dissertation is divided into five chapters. Chapter 2 provides a structural description of the Holston River Bridge, a history of the bridge, and a description of instrumentation and strain gage locations. Chapter 3 discusses the impact study; included in this chapter are test description, procedure, results, and conclusions. A sensitivity analysis addressing the effect of cycle counting methods, stress-range frequency-of-occurrence histogram construction, and test duration on the effective stress range and the number of cycles per truck is conducted in Chapter 4. In Chapter 5, a more refined remaining fatigue life calculation procedure than AASHTO *Guide*'s procedure is presented. The number of cycles per truck for various stress category details and a formula for the present truck volume are also developed in this chapter. Chapter 6 summarizes the research findings and provides suggestions for improving the AASHTO *Guide*'s remaining life evaluation procedure. Included in each chapter is a literature review pertaining to the chapter's subject matter.

CHAPTER 2

BACKGROUND AND GAGE LOCATION

This chapter presents a structural description of the Holston River Bridge, a brief history of the bridge, a history of the bridge cracking and repairs, a description of the instrumentation, and a description of gage locations.

2.1 Description of the Structure

The Holston River Bridge on I-40 is located in east Knox county, Tennessee. The eight-span structure consists of four continuous longitudinal girders at 26 ft spacing. The spans are 100 ft, 3 at 135 ft, 145 ft, 165 ft, 240 ft, and 135 ft, as shown in Figure 2-1. The continuous girders are haunched over two of the seven reinforced concrete two-post piers and are supported on rockers at the reinforced concrete abutments. The bridge's lateral bracing system is shown in Figure 2-2.

The bridge's 7.5 inch reinforced concrete deck, which is composite in positive moment regions, is supported by the four continuous longitudinal girders, cantilever (outrigger) brackets, and by six continuous longitudinal stringers. The stringers are supported either by transverse cross-frames or by transverse floorbeams. The transverse members are connected to the four main girders as shown in Figure 2-3. The structural steel is A36 except for some girder flange steel which is A588, and all bolts are A325 high strength bolts. There are approximately 500 occurrences of Category E details and 150 occurrences of Category E' details throughout the bridge.

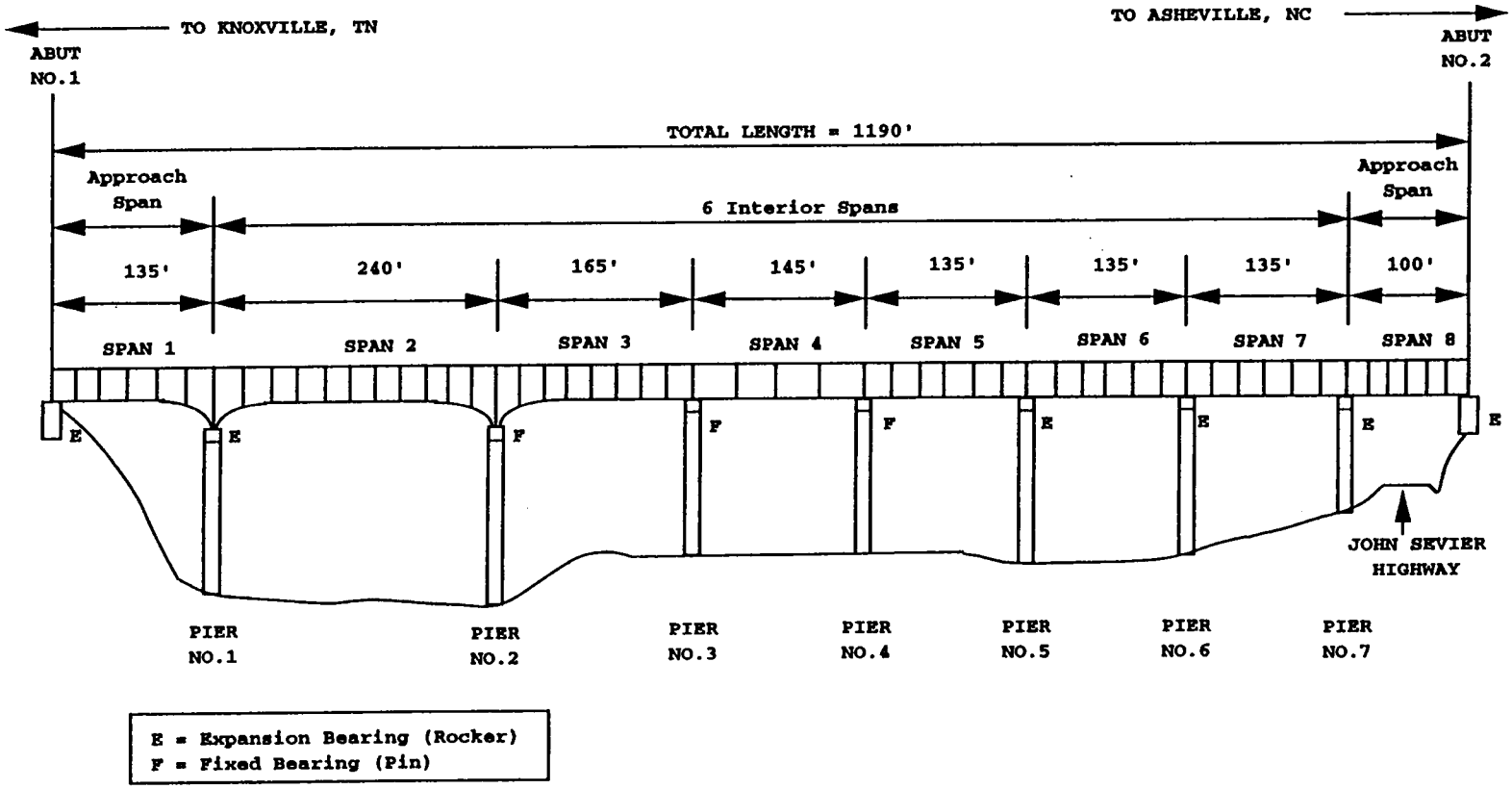


Figure 2-1. Holston River Bridge Elevation

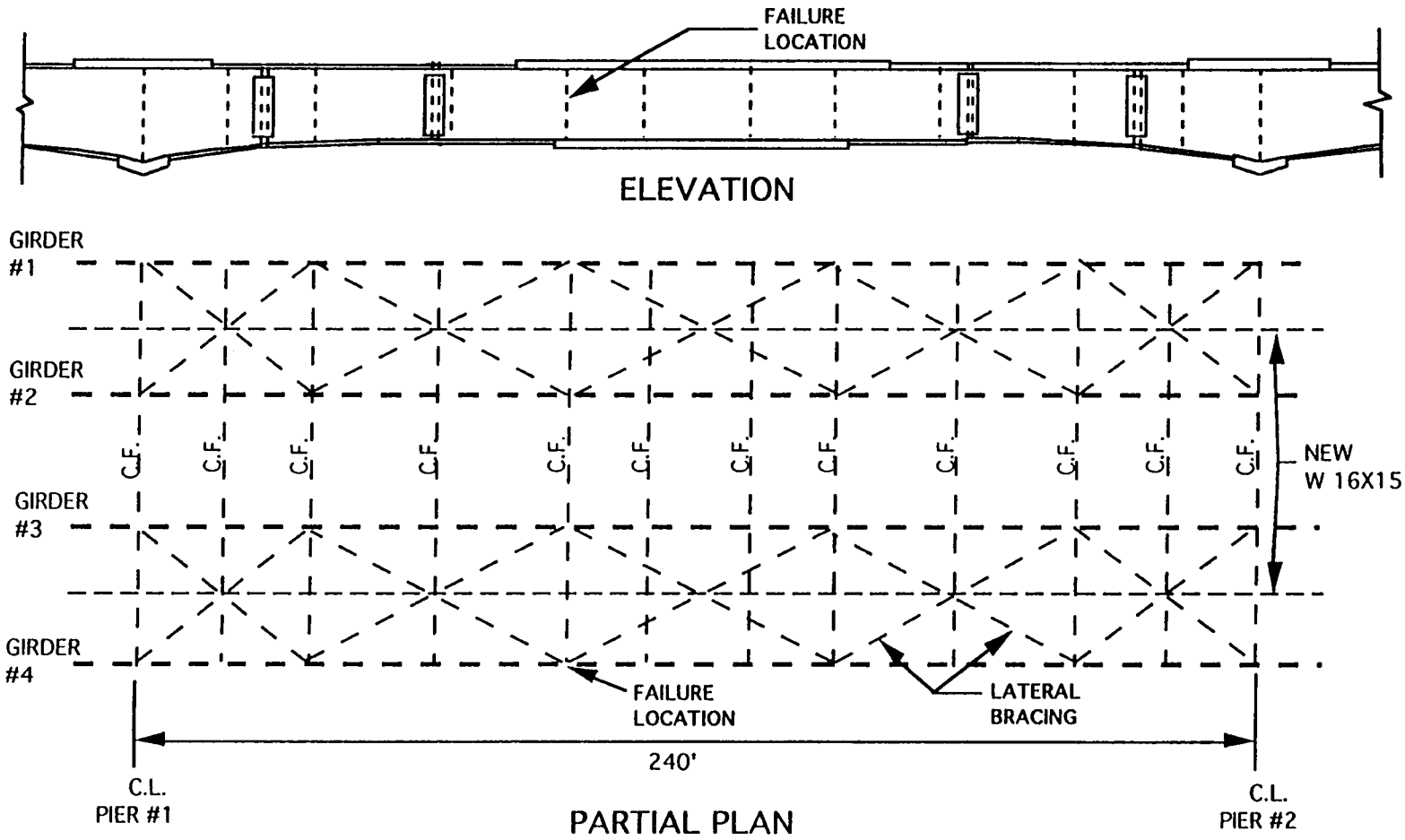


Figure 2-2. Holston River Bridge Partial Plan View

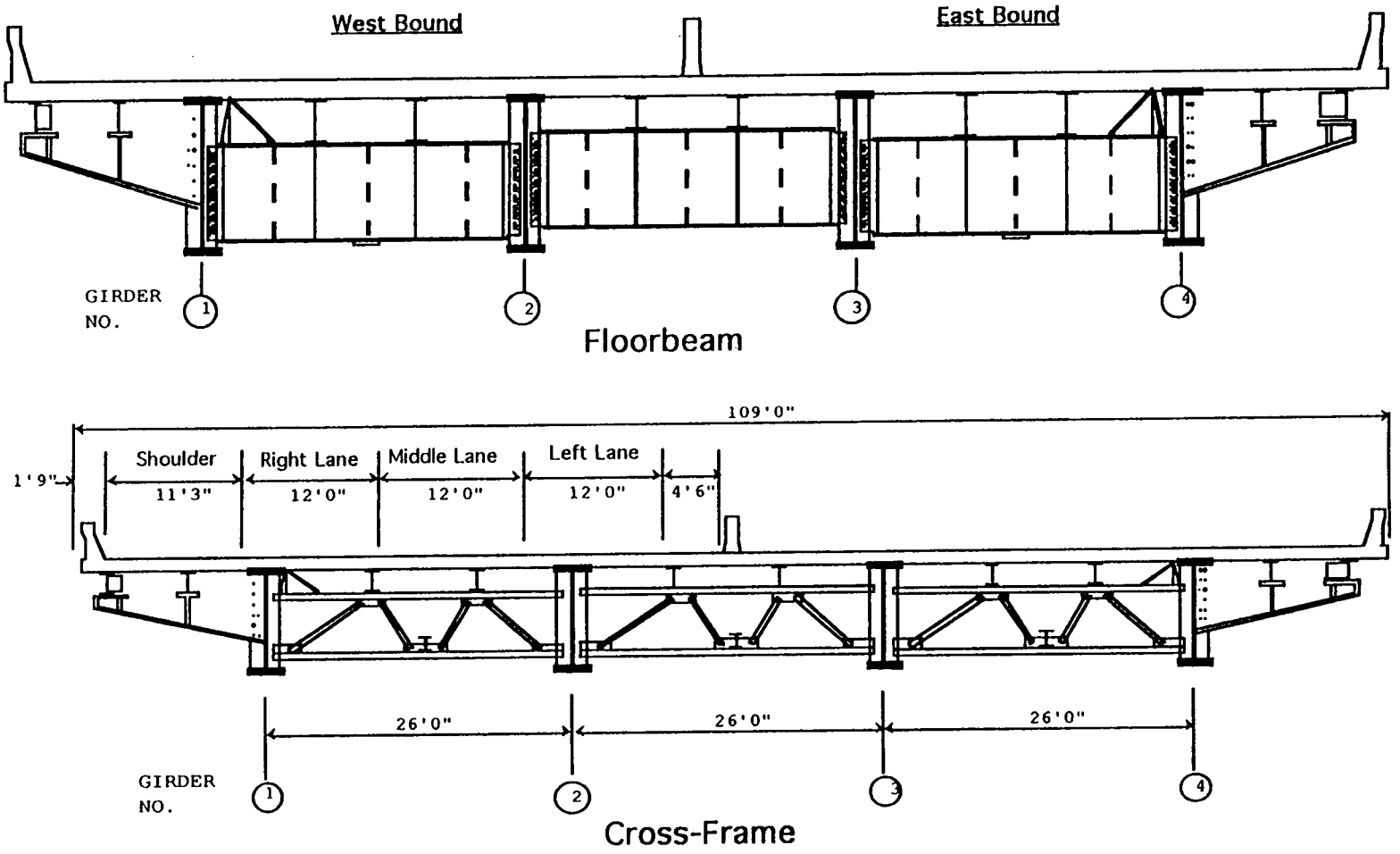
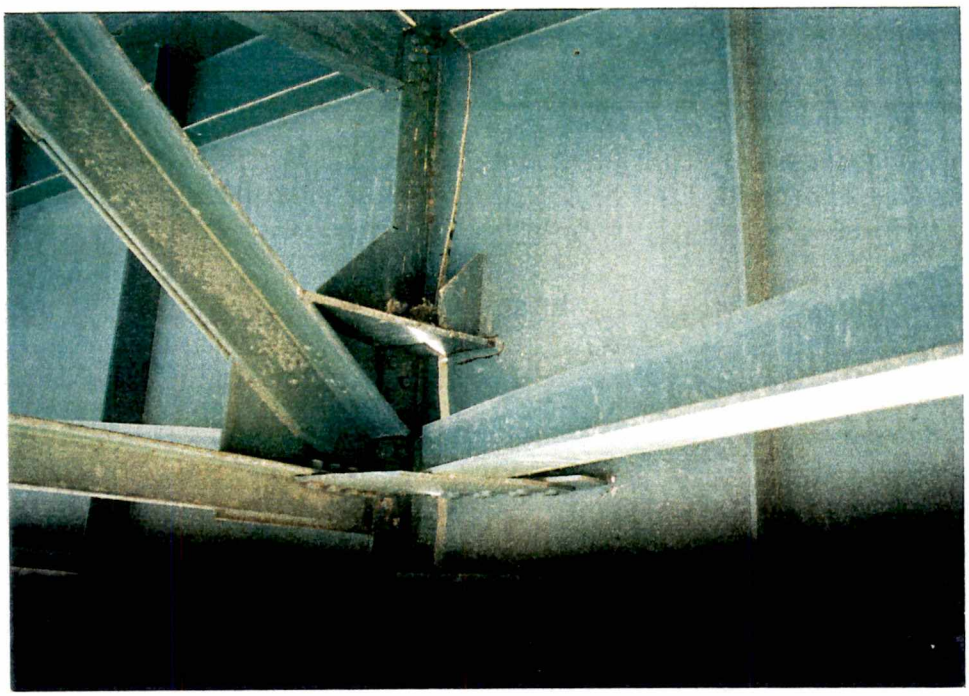


Figure 2-3. Holston River Bridge Cross-Sections

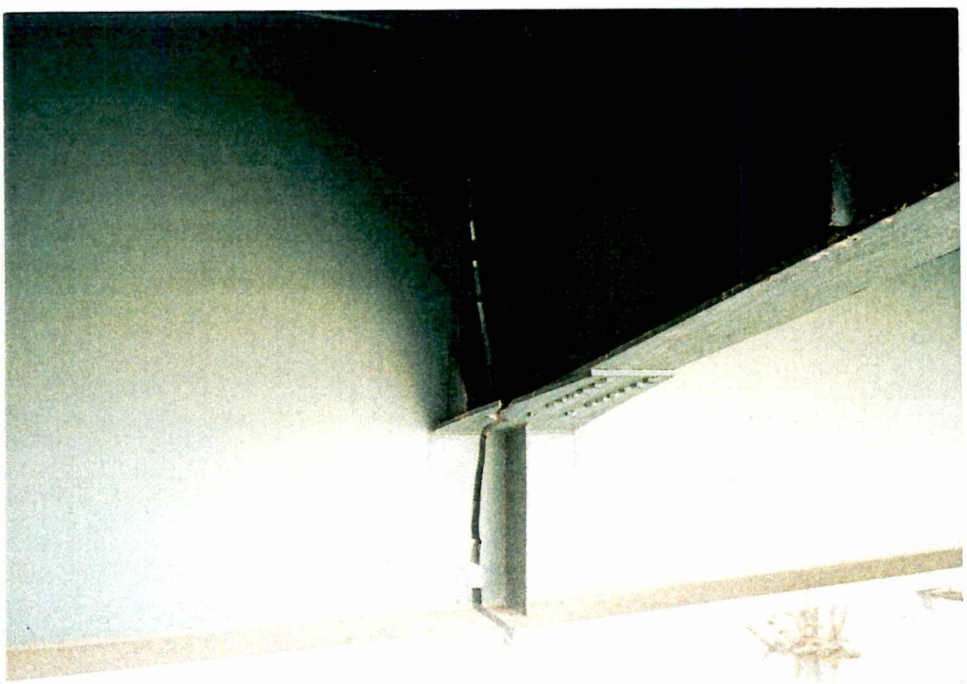
2.2 History of the Bridge and the Crack

The Holston River Bridge was originally designed as a four lane structure when construction began in 1970. In 1972 the bridge was redesigned to carry six lanes of traffic. The revised design called for cantilever (outrigger) brackets to widen the bridge from four lanes to six lanes, with the cantilever brackets supporting part of the right lane and shoulder in each direction of traffic. The bridge was designed for HS20 loading. Since its opening to traffic in 1974, the bridge has undergone several routine maintenance repairs and one collision repair for damage at the east end over the John Sevier Highway.

On January 22, 1992, a crack that had completely penetrated the bottom flange and nearly the full height of the web of the east bound fascia girder was discovered. The cracked section was located at the fourth cross-frame from pier number 1 in the second span. Figure 2-4 contains photographs of the crack at the time of the discovery. As illustrated in the photographs, the crack had also penetrated the gusset plate for the cross-frame and for the cantilever. The crack not only separated the fascia girder flange to form a wide gap, approximately 1.5 to 2 inches wide, but the flange sections were also displaced laterally in different directions. This horizontal offset was measured to be approximately 3/8 inch. It was also noted that 2 to 3 inches of the fascia girder's cracked web surface at the lateral bracing gusset plate attachment was rusted while the remaining portion of the cracked web surface had no rust. Other surface cracks were discovered at the outside edge of the attachment of the lateral bracing gusset plate on both sides of the cracked section. There was also a 6 inch long tear in the fascia girder



INSIDE VIEW



OUTSIDE VIEW

Figure 2-4. Fracture of Girder Number 4

web about 15 inches from the cracked section. Figure 2-5 illustrates the cracked section. An inspection of the bridge also revealed a cracked cross-frame gusset plate, several bent cross-frame gusset plates, and loose bolts at the fracture location. Bent cross-frame gusset plates and loose bolts were also discovered at adjacent transverse cross-frames. A profile of the top of the east bound parapet indicated that the bridge had sagged approximately 4.5 inches at the fracture location.

2.3 History of the Repairs and Retrofit

Immediately after the discovery of the fracture, the east bound outside traffic lane was closed, and actions were taken to repair the damaged bridge. The repair work began on January 24, 1992. Hydraulic jacks, hanger rods, and high strength rods were used to close the gap as much as possible, as shown in Figure 2-6. The gap was then repaired by welding, and splice plates were added to further strengthen the repair. Plates were bolted to both sides of the bottom flange and to both sides of the girder web, as shown in Figure 2-7. A profile of the top of the east bound parapet after the repairs showed that the bridge still had a sag of approximately 3.8 inches at the fracture location. This method of repairs reduced the fractured girder deflection by about half an inch.

A retrofit of the cantilever bracket to fascia girder flange connection was used to eliminate the situation that was believed to be responsible for the fracture in the girder. The crack was believed to have been initiated by out-of-plane forces exerted on the girder web at the bottom of the cantilever to girder connection. The intent of the

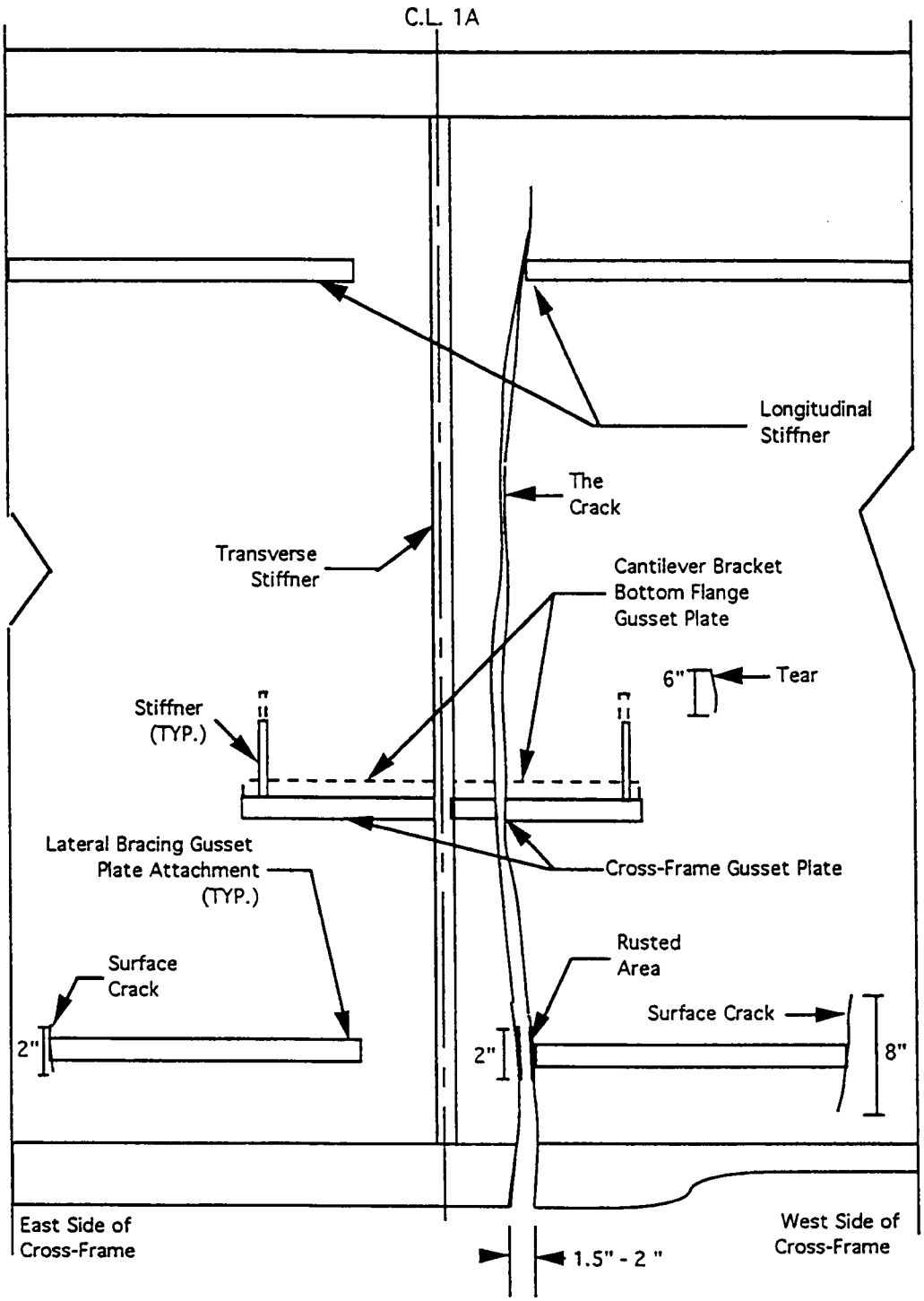
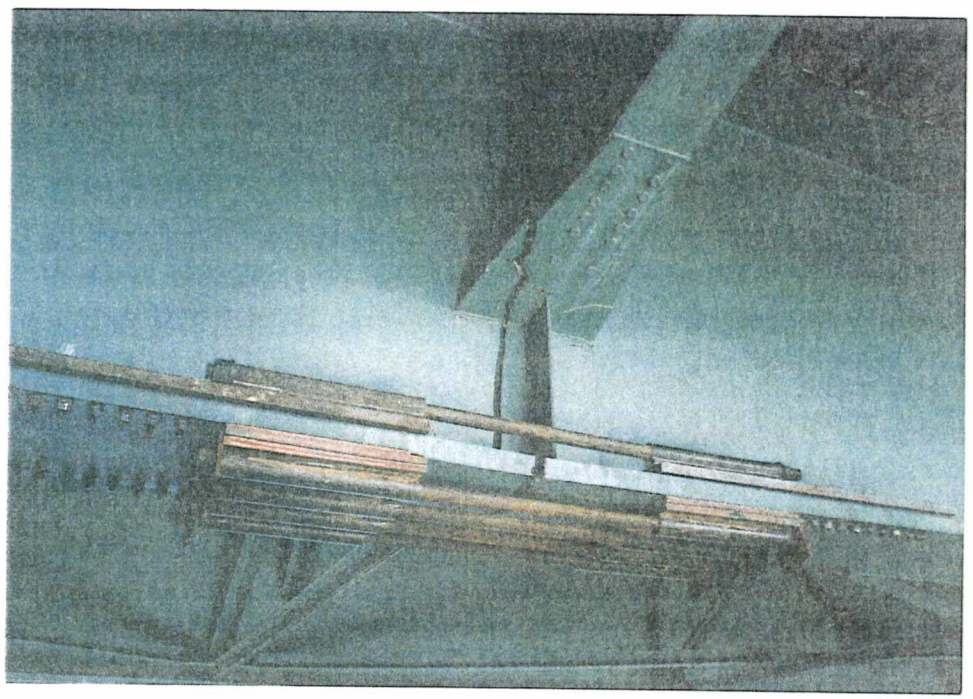


Figure 2-5. Holston River Bridge Girder Number 4 Cracked Section



FOUR BEAMS WITH HANGER RODS



HIGH STRENGTH RODS

Figure 2-6. Holston River Bridge Repair Process

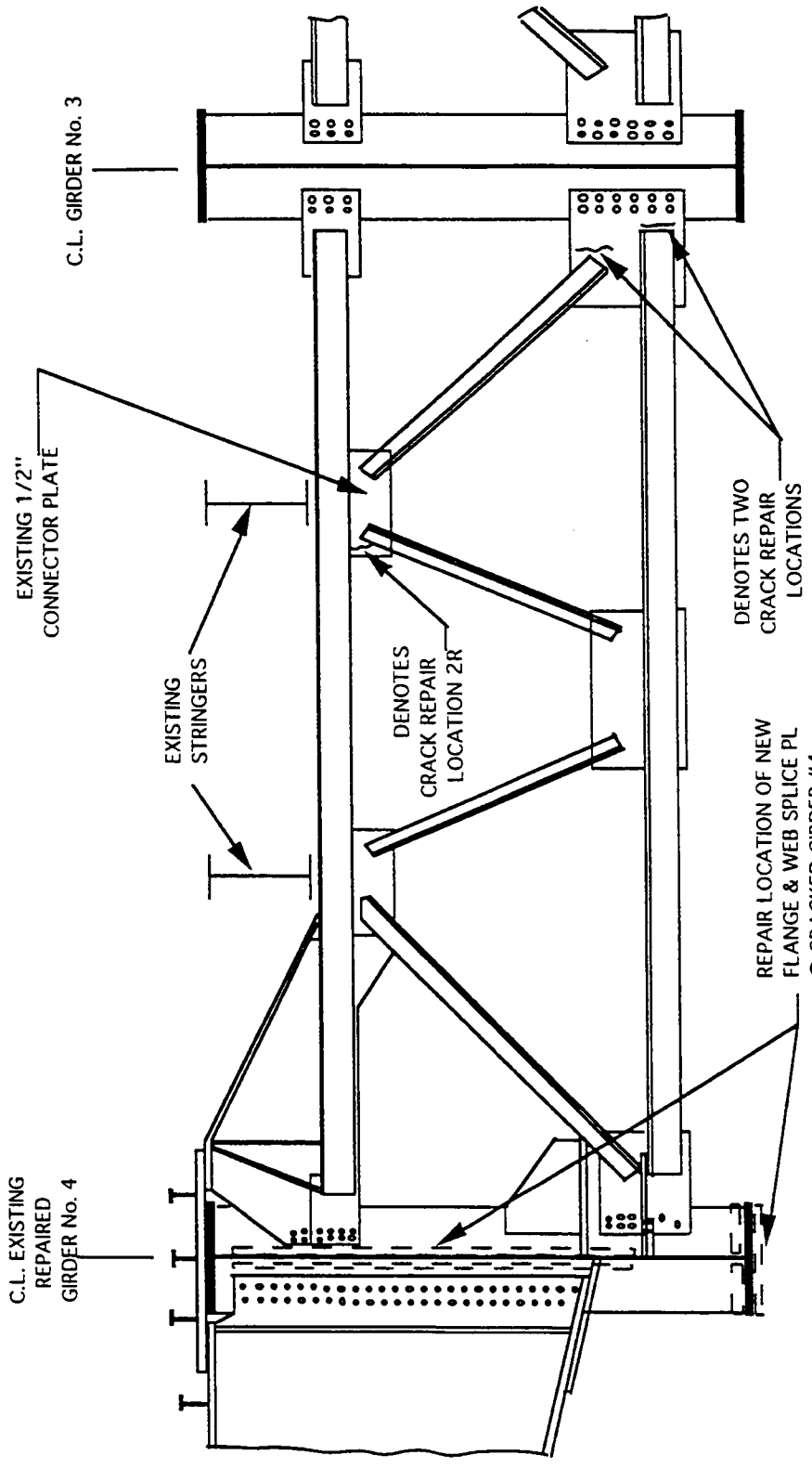


Figure 2-7. Holston River Bridge Repairs at Failure Section

corrective measure was to assure that any forces from the cantilever would now be transferred directly into the cross-frame, thereby greatly reducing the out-of-plane web distortion. This retrofit was added to every cantilever bracket opposite a cross-frame on both the east and west bound sides. Figure 2-8 illustrates the retrofit.

After the repair of the fractured fascia girder was complete, additional repairs and retrofitting of the bridge began. These included drilling holes at the ends of the fascia girder web cracks on either side of the lateral bracing gusset plate attachment, replacing cross-frame cracked gusset plates, and welding the lateral bracing members to their gusset plates in areas where the bolts were loosened by the fracture.

2.4 Instrumentation

The following is a discussion of the instrumentation and data acquisition system used on this research project.

Strain Gages

Electrical resistance foil strain gages were used to measure static and dynamic strain during testing. The strain gages were Micro-Measurements types CEA-06-250UW-350, CEA-06-125UW-350, and CEA-06-250UR-350 having a resistance of 350 ohms and a gage factor of 2.1. Gage lengths were either 1/4-inch or 1/8-inch. The 1/8-inch gages were used in the web gaps and the 1/4-inch gages were used in all other locations. The strain gages were installed according to manufacturer's instructions after the steel surface was stripped clean of paint and mill scale. With exception of the rosette strain gages, all strain gages measured longitudinal strains. The rosette strain gages measured longitudinal strains, transverse strains, and strains at 45 degrees.

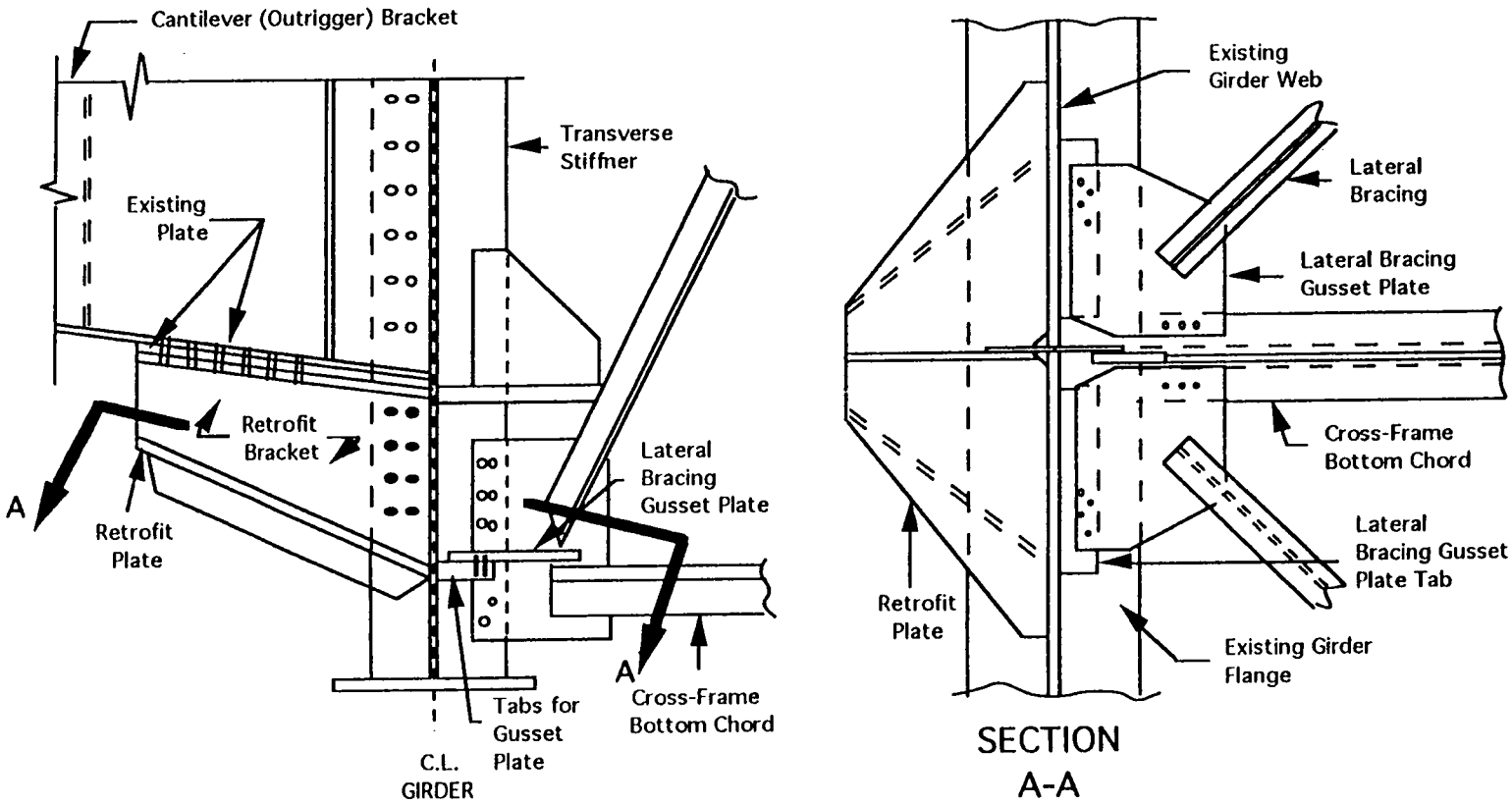


Figure 2-8. The Retrofit

Data Acquisition System

The Optim MEGADAC 5017A series data acquisition system was used to capture dynamic analog data from the strain gages in real time. The MEGADAC converts the analog data into digital data and sends it to a host personal computer (PC) for storage. Optim's Test Control Software (TCS) management package was used to interface between the MEGADAC and the PC. The MEGADAC has a 32 channel capacity. Each channel of strain gage sensor data represented the output of a Wheatstone bridge circuit with one active arm. The sampling rate was 50 scans per second.

2.5 Description of Gage Locations

The strain gage locations were determined on the basis of the following evaluations. The bridge plans were reviewed to identify fatigue prone details and their locations. A literature review was conducted to see if other similar type bridges with some of the same fatigue prone details experienced any fatigue cracking. An analytical evaluation of the bridge was performed to identify areas of high stress that would be susceptible to fatigue damage. The selected locations were then inspected and the gage locations were selected. Additional gage locations were selected for more information to permit an evaluation of strain distribution in the bridge. These gages would provide information pertaining to lateral distribution of loads, dynamic impact, stress distribution along the depth of the main longitudinal girders, out-of-plane distortions, and member forces.

The gage locations were all within the first three spans of the bridge, as shown in the Appendix. In span one, the approach (end) span, transverse floorbeams span between the main longitudinal girders. The fatigue prone details of this span are fairly typical of all

other spans of the bridge, excluding span two. Span one was chosen as the location for study of these typical details due to the ease of access. In span two, the location of the main girder fatigue failure, transverse cross-frames instead of floorbeams span between the main girders. Four separate locations within this span were identified as areas of high stress and were extensively instrumented. Span three was instrumented to compare the effects of the bridge approach on similar fatigue prone details. Table A-1 summarizes the gage locations shown in the Appendix. This table lists the gage number, the gage sample location, the applicable AASHTO fatigue stress category, and the gage detail description. There were a total of 164 strain gages monitored at various times during the research project.

CHAPTER 3

IMPACT STUDY

3.1 Introduction

This chapter describes an impact study on the Holston River Bridge. The bridge was initially instrumented in 1993 and then reinstrumented in 1995 for the Tennessee Department of Transportation to estimate the remaining life of the bridge, to determine the effectiveness of recent bridge repairs and retrofits, and to identify potential future fatigue problems. As part of this research two impact studies were conducted. The first study was conducted in 1993 to determine a dynamic impact factor for a few locations on the bridge. This study (Deatherage et al., 1995) concluded that the impact factors obtained using the AASHTO *Standard*'s (1992) formula were unconservative when compared to measured impact factors.

The AASHTO *Standard* specification requires that highway live loads be increased to allow for dynamic, vibratory and impact effects. The amount of impact allowance or increment is expressed as a fraction of the live load stress and is determined by the empirical formula

$$I = \frac{50}{L+125} \leq 30\% \tag{3.1}$$

in which I is the impact fraction or load amplification factor and L is the bridge span length in feet. This formula is strictly a function of length; it does not consider other parameters that may affect impact in highway bridges. The AASHTO *Guide* (1990) requires that the gross weight of the fatigue truck be increased by 10% to account for

impact on smooth road surfaces. For poor joint or pavement roughness, the *Guide* requires that the gross weight of the fatigue truck be increased above 10% but not above 30%. The *Guide*'s impact allowance is solely a function of surface roughness. While there has been a considerable amount of research on factors affecting impact for nonfatigue design, there has been little research on impact factors for fatigue design of steel highway bridges. This lack of research in conjunction with the results of the 1993 impact study was the motivation for the second impact study. This study examines the influence of bridge approach, surface condition, and truck velocity on impact factors for fatigue prone details in both main and secondary steel bridge members. The AASHTO *Standard* classifies common steel bridge structural details into fatigue stress categories A through E'. This study also determines impact factors for various fatigue stress category details and compares the results to AASHTO values.

3.2 Literature Review

Since the 1950s, extensive experimental and analytical studies have been conducted to examine factors affecting impact in highway bridges. Analytical findings of Peterson and Kostem (1973) showed that the dynamic load factor is a function of vehicle speed and that the dynamic response of the beams tends to oscillate about the static response. They noted that exterior beams have a higher dynamic load factor than interior beams and that beams that are not directly under the load tend to have a higher amplification of moment than those beams directly under the load. Ghosn et al. (1986) found that the observed impact value is less than AASHTO *Standard*'s specified value and is a function of surface roughness rather than length. In NCHRP Report 301 (Moses

et al., 1987), it was determined that the main parameters affecting impact are the bridge approach and grade, bumps and other pavement roughness. Biggs (1964) and Nowak et al. (1991) found that the major factors influencing dynamic load are the road roughness, bridge dynamics (frequency of vibrations) and vehicle dynamics (suspension system). Schilling (1982) concluded that while the AASHTO formula is based only on span length, the impact factors given by this formula are representative of actual bridge loadings and, therefore, appropriate for fatigue design. Nowak and Nassif (1995) recommend an impact factor (1+*I*) of 1.30 in lieu of the AASHTO *Standard*'s formula for design and analysis of steel highway bridges. Yang et al. (1995) concluded that impact factors can far exceed the limit of 0.30 set by the AASHTO *Standard* specification. The Ontario Code (1983) sets a limit of 0.40 for impact factors. The American Railway Engineering Association (AREA) Code (1990) has no set limit for impact factors.

3.3 Description of Impact Tests

Instrumentation

The bridge was instrumented with strain gages as shown in Figures 3-1, 3-2, 3-3 and 3-4. The fatigue prone details illustrated in these figures are typical throughout the bridge. The test locations shown in Figure 3-1 were identified as areas of high stress and thus susceptible to fatigue damage. Table 3-1 provides a summary of the various bridge details that were instrumented. This table lists the gage number, the applicable AASHTO fatigue stress category, and the description of the detail.

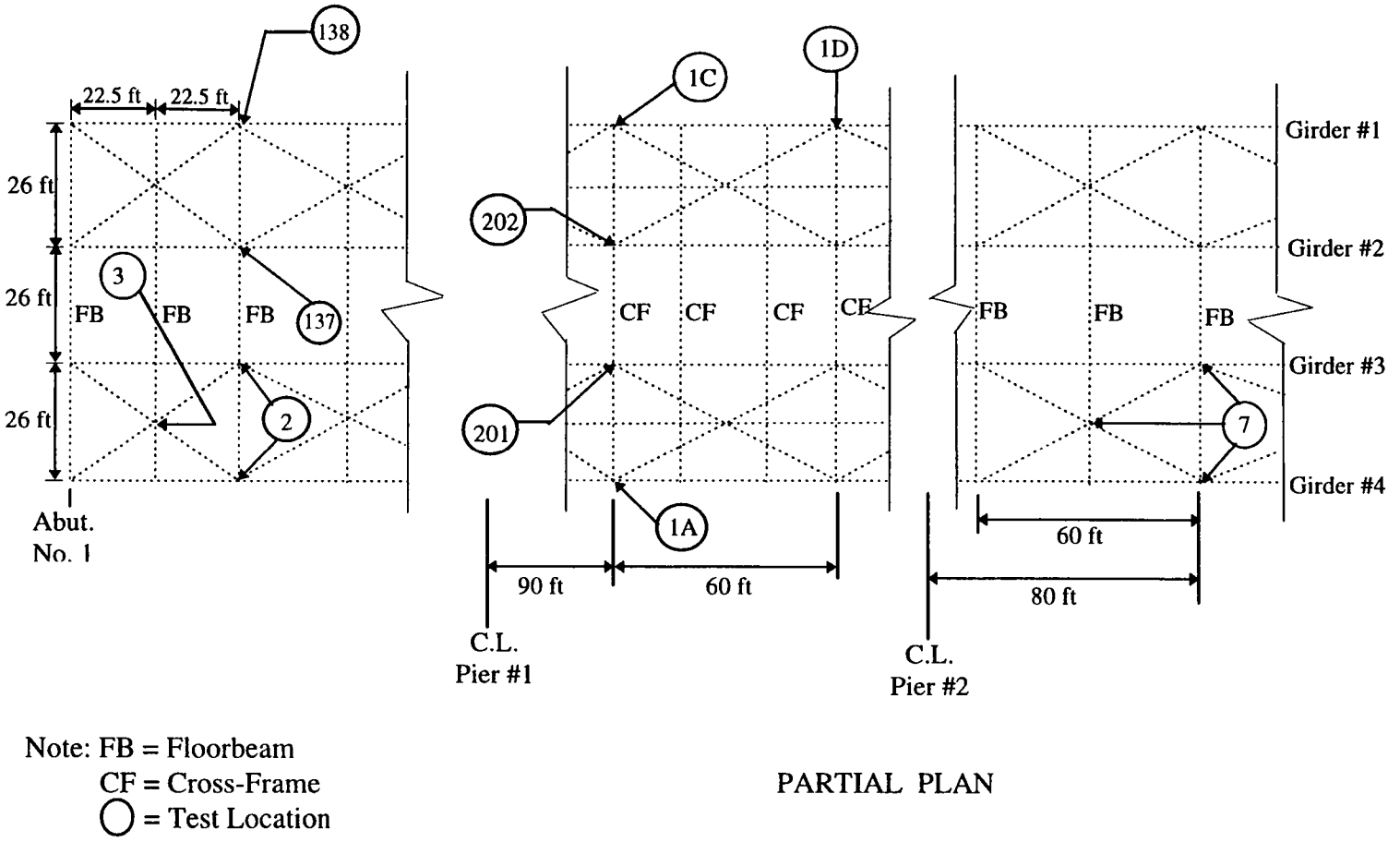


Figure 3-1. Partial Plan of the Holston River Bridge: Impact Test Location

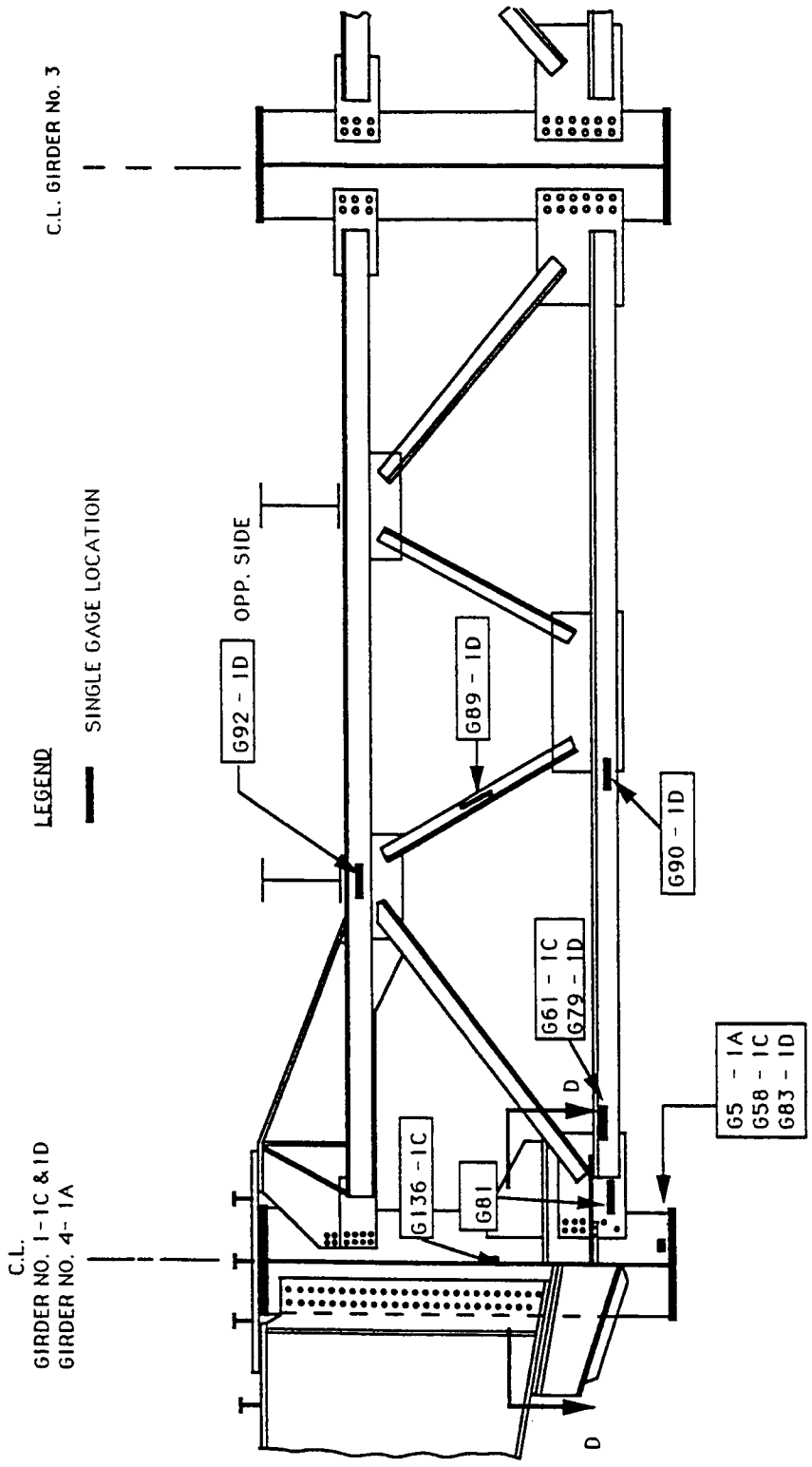


Figure 3-2. Gage Locations for Test Locations 1A, 1C, and 1D

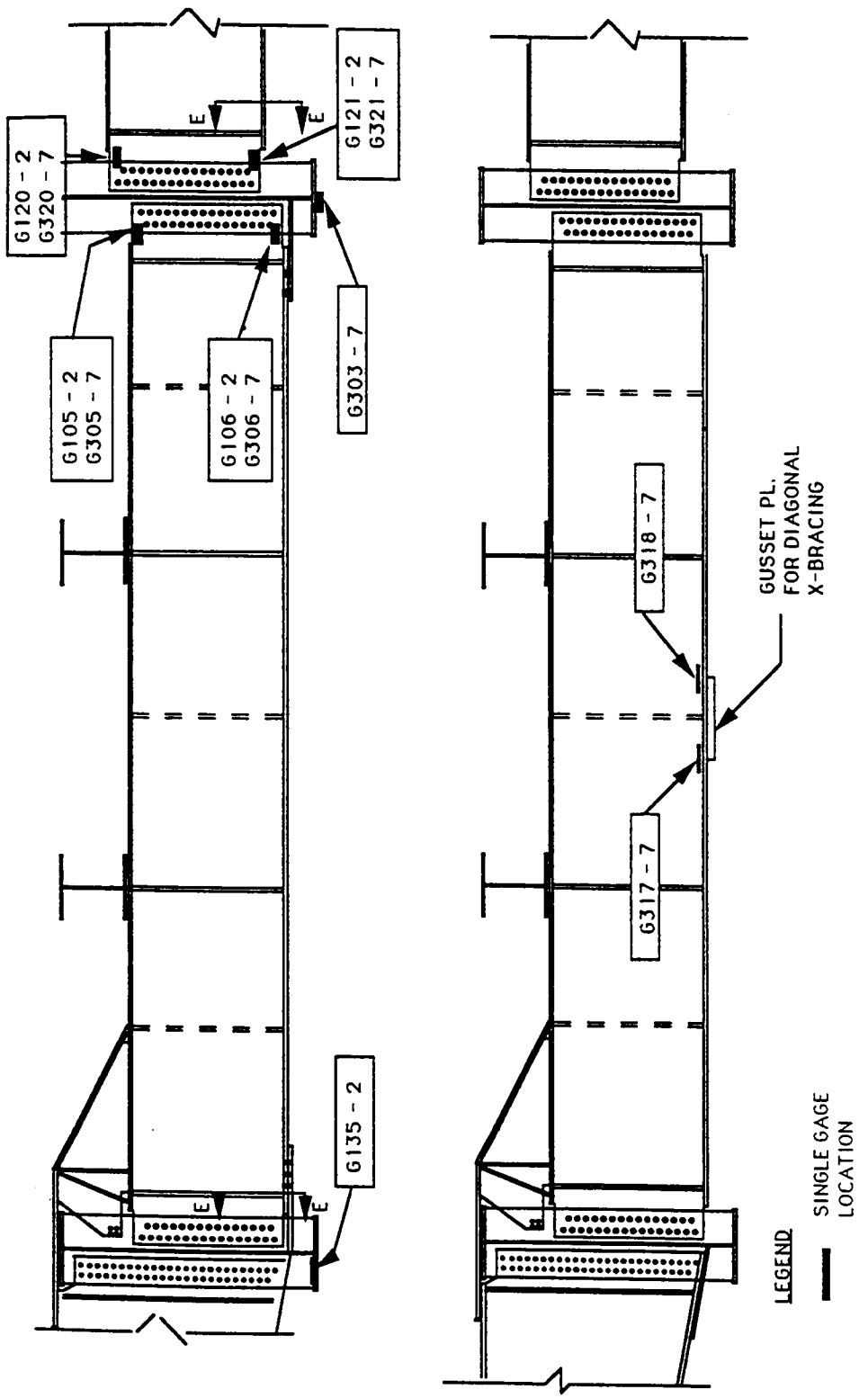


Figure 3-3. Gage Locations for Test Locations 2 and 7

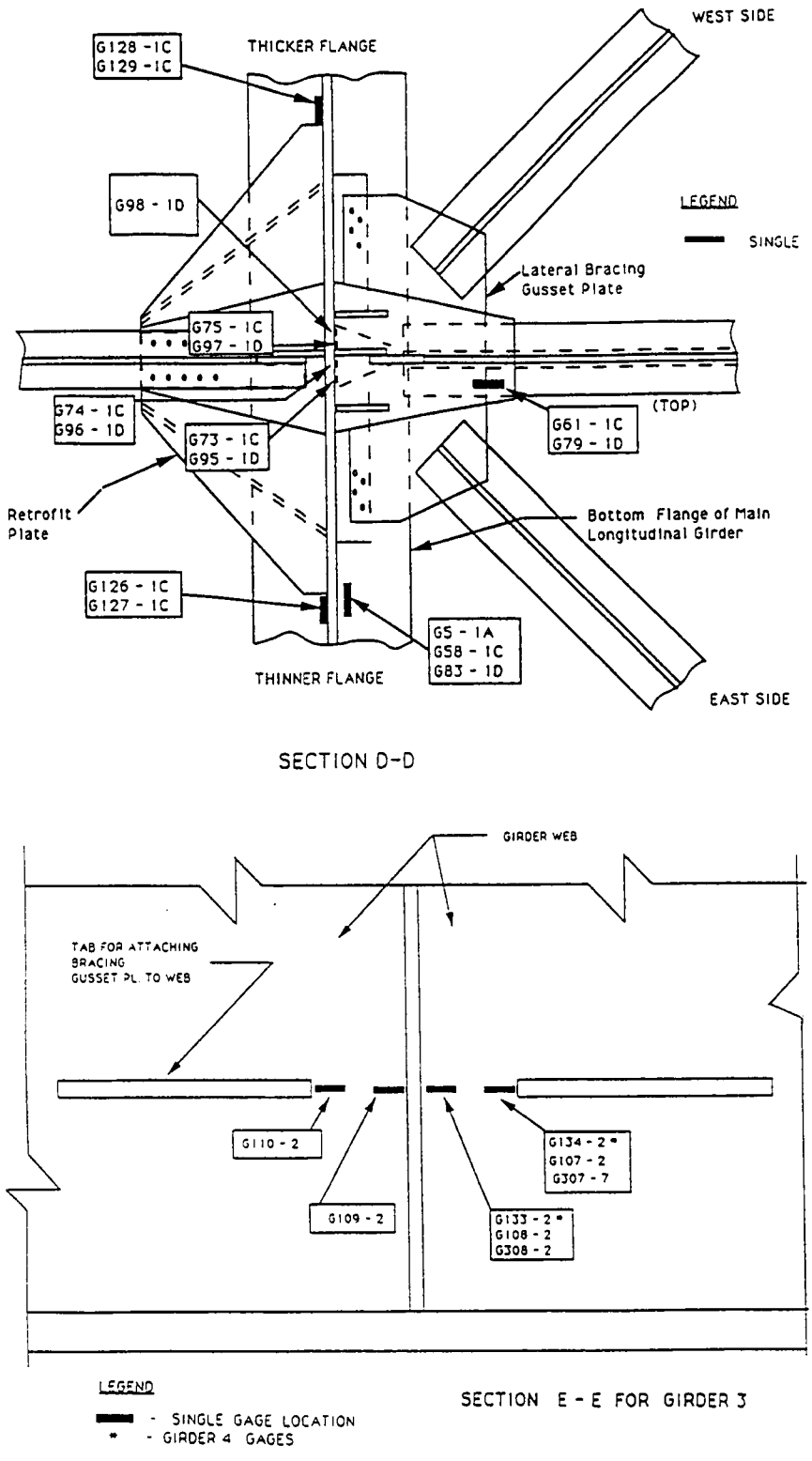


Figure 3-4. Gage Locations for Test Locations 1C, 1D, 2, and 7

Table 3-1. Summary of Holston River Bridge Impact Test Details

Gage Number	Gage Location	Fatigue Category	Detail Description
135,137,138	Span 1	B	Top of the bottom flange of main longitudinal
5,58,83,201,202	Span 2	B	girders (MLG) near the web-to-flange weld
303	Span 3	A	Bottom of the bottom flange of MLG
136	Span 2	A	Web of MLG
126,127,128,129	Span 2	E	End of longitudinal welded retrofit plate to MLG web
73-75, 95-98	Span 2	E'	Gages are attached to the MLG web in the
107-110,	Span 1	E'	horizontal gap between the transverse stiffener weld
133,134	Span 1	E'	and the longitudinal welds attaching the lateral
307,308	Span 3	E'	bracing connection plate to the girder web
61,79,90	Span 2	E	Cross-frame bottom chord at end of longitudinal welded gusset plate
81	Span 2	B	Cross-frame bottom chord bolted connection
89	Span 2	A	Cross-frame diagonal
92	Span 2	B	Cross-frame top chord near a longitudinal weld
105,106,120,121	Span 1	E	Floorbeam web at top and bottom flange termination
305,306,320,321	Span 3	E	weld
317,318	Sapn 3	E'	Floorbeam top of bottom flange at end of welded gusset plate

Test Procedure

The first impact study was carried out between 2 AM and 5 AM on August 5, 1993. During all test runs no other traffic was allowed on the bridge, and a member of the research team was in the test truck to ensure the driver was in the proper lane and traveling at the proper speed with the truck positioned in the center of each lane. The test truck was a tandem axle dump truck with weights and measurements as shown in Figure 3-5. A survey of truck weights in actual traffic was taken at a weigh station in west Knoxville, as shown in Figure 3-6. The west Knoxville weigh station is the closest weigh station to the bridge. Over 40% of the trucks surveyed weighed between 70 to 80 kips, with an effective gross weight of 67 kips. Approximately 60% of the 5-axle semitrailers (3S2) weighed between 70 to 80 kips, with an effective gross weight of 69 kips. It is these 3S2s that do most of the fatigue damage to bridges (Moses et al., 1987). The effective gross weight, W, is defined as

$$W = \left(\sum f_i W_i^3\right)^{1/3} \tag{3.2}$$

in which f_i is the fraction of gross weights within interval i and W_i is the midwidth of interval i (Moses et al., 1987). The total test truck weight (76.8 kips, 79.2 kips) was slightly heavier than a HS20-44 AASHTO design truck (72 kips). An effort was made to use the heaviest possible truck in order to obtain maximum strain gage response. The bridge's blacktop was removed due to scheduled maintenance. Thus, the exposed reinforced concrete surface had grooves and bumps that made it rough. The removal of the asphalt caused a vertical offset of about 2 inches between the bridge approach (end) span and the roadway at the expansion joint.

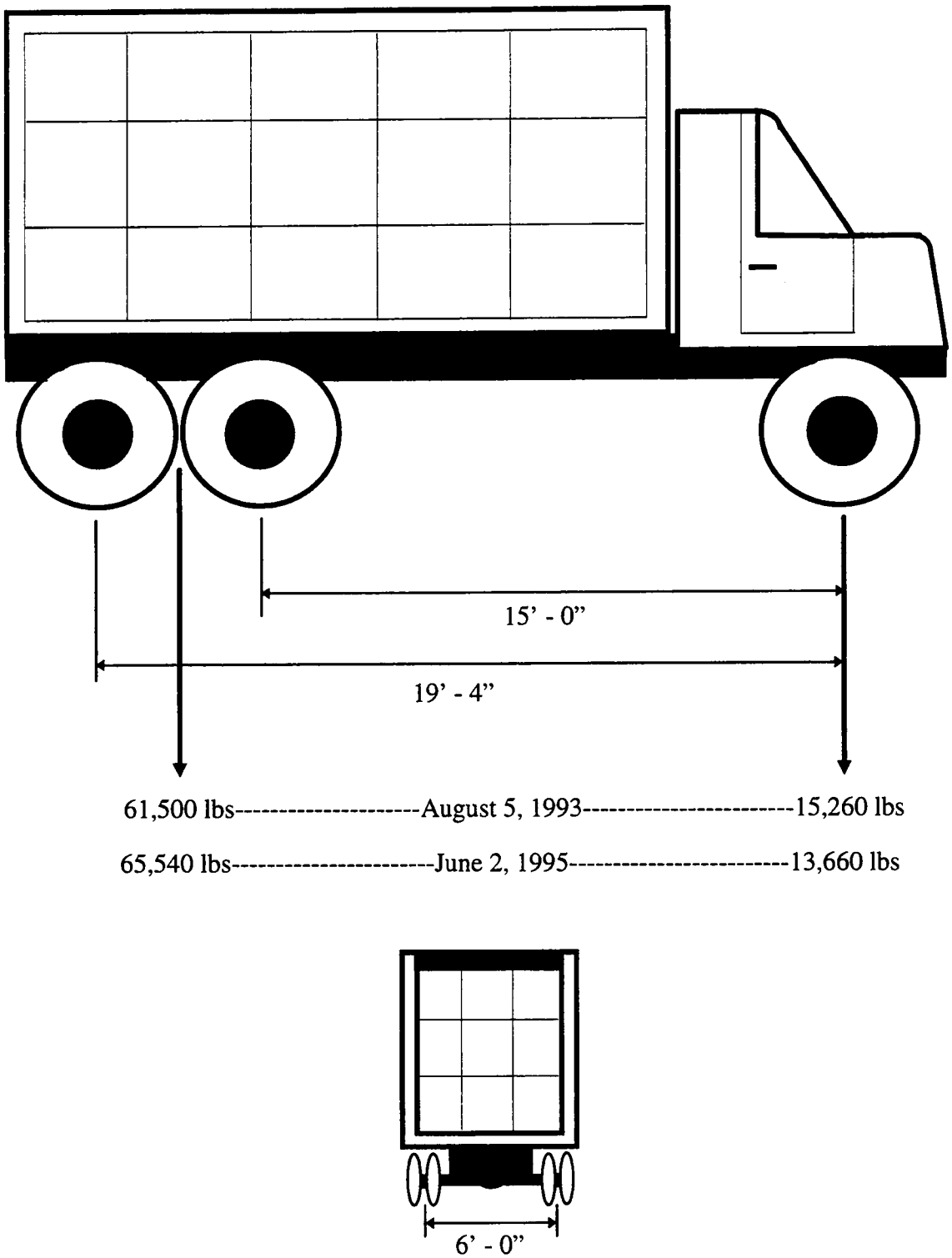
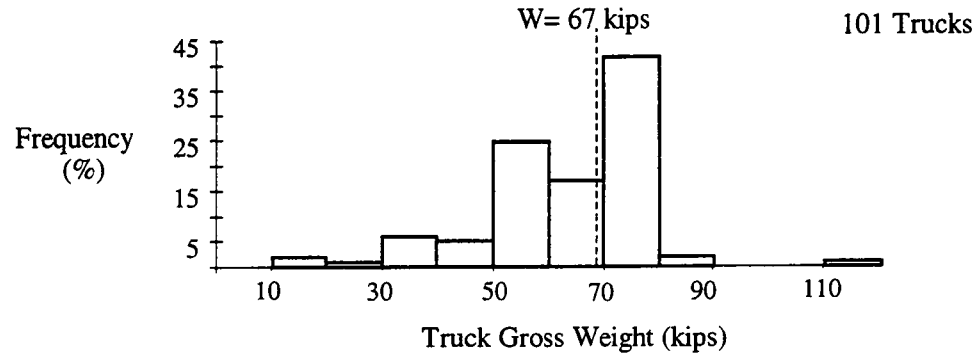
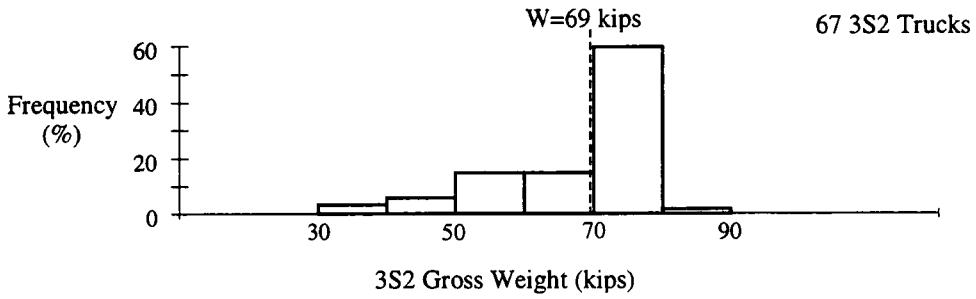


Figure 3-5. Impact Study Test Truck





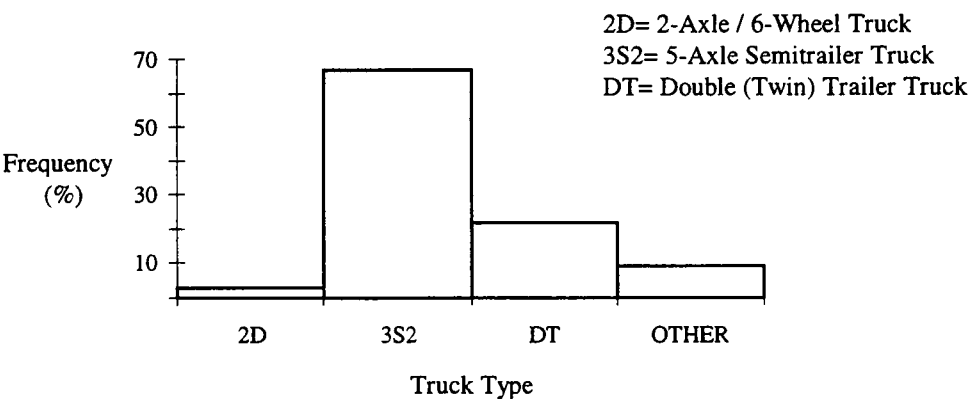
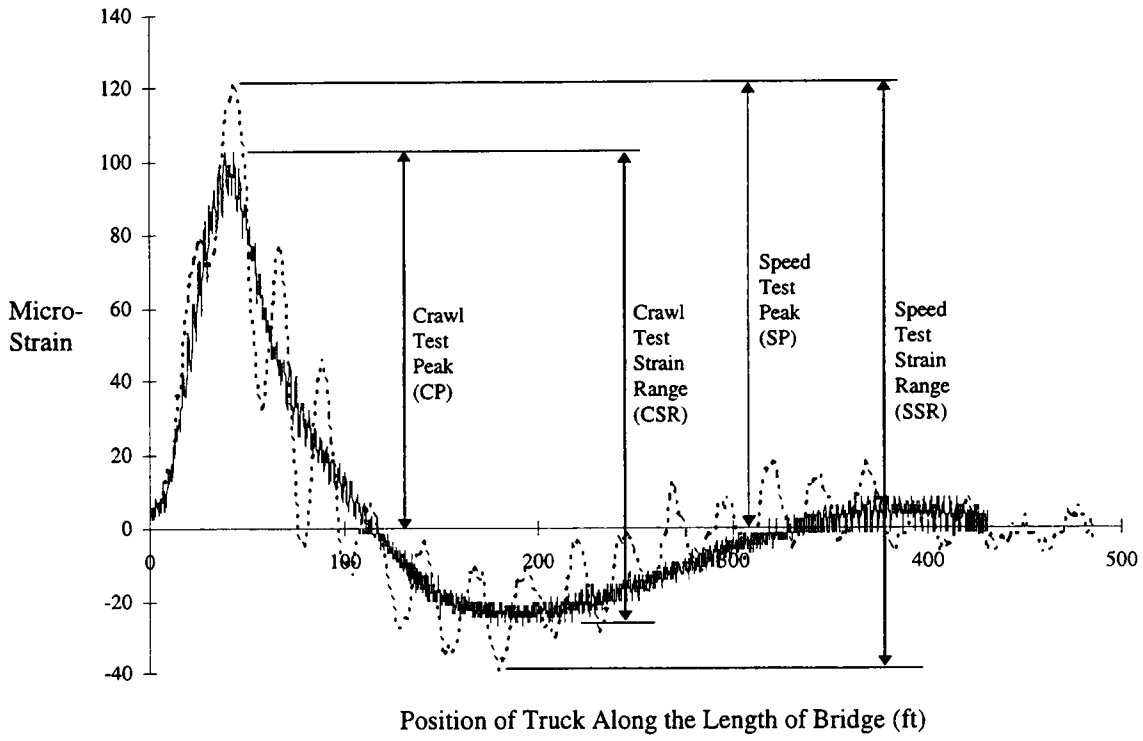


Figure 3-6. West Knoxville Weigh Station Truck Weight Histogram Summary

The 1993 impact test consisted of a crawl and a dynamic test (Moses et al., 1974; Schilling, 1982). The crawl speed tests were conducted to determine the structure's response to a static load. A constant speed of 5 mph was maintained throughout the test. Data were taken for when the test truck was in each of the six traffic lanes. The dynamic tests were conducted to determine the structure's response to a moving load. Data for the three eastbound and the three westbound traffic lanes were taken at speeds of 50 mph and 60 mph, respectively.

The second impact study was carried out between 1 AM and 4 AM on June 2, 1995. The test setup and procedure were identical to the first impact test with a few exceptions. The bridge surface condition was smooth. The test truck was slightly heavier, as shown in Figure 3-5. Dynamic test data for the three eastbound lanes were taken at speeds of 30 mph and 50 mph to determine the effect of velocity on impact factor. The bridge's third span was instrumented to determine the effect of bridge approach on impact factor.

An impact factor for each test run was calculated by taking the maximum stress obtained from the speed test, 50 mph, and dividing it by the maximum stress obtained from the crawl test, 5 mph. Stress-Range impact factors were calculated in the same manner except maximum stress ranges were compared. Figure 3-7 illustrates the measured impact factor for gage 135 with the control load truck in the middle line. It should be noted that the inherent noise in the data acquisition system and the outside noise interferences due to the nature of this type of test masks the strain gage readings for stress ranges below 1000 psi (35 $\mu\varepsilon$). Therefore, test runs which produced stress ranges



Note:
Impact Factor = SP / CP
Stress Range Impact Factor = SSR / CSR

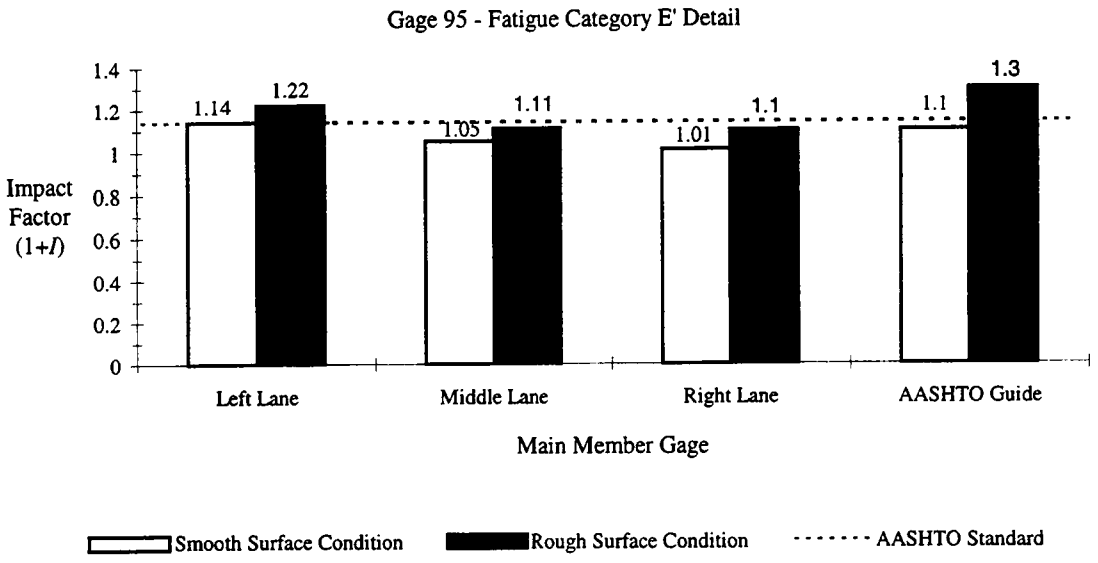
Figure 3-7. Strain Trace for Gage 135 with the Truck in the Middle Lane

below 1000 psi were not included in the impact factor calculations. The AASHTO *Standard* impact factors for main longitudinal girders were calculated using the bridge span length in feet for *L*. The secondary transverse bridge members are load carrying members; thus, the AASHTO *Standard* impact factors were calculated using the span length of the member center-to-center of supports.

3.4 Test Results and Discussion

The influence of surface condition was examined using the results of the 1993 and the 1995 impact studies. The surface condition of the 1993 test was rough while the surface of the 1995 test was smooth. The test results indicate that the impact factor for a rough surface condition is higher than that for a smooth surface condition. Plots of test results for gages 95 and 106, as shown in Figure 3-8, illustrate the influence of surface condition on the impact factor. Gage 95 is a fatigue category E' main longitudinal girder web gap gage while gage 106 is a fatigue category E secondary member flange termination gage. For all three traffic lanes, gage 95's impact factor for rough surface is an average of 7% greater than that for smooth surface. Gage 106's rough surface impact factor is an average of 10% greater than that for smooth surface.

Three speed tests were conducted to determine the effects of truck velocity on the impact factor for fatigue prone details. Test results show that the impact factor increases with increased truck velocity. The influence of velocity on the impact factor is more apparent in the first span than in the third span due to the influence of the expansion joint. Increase in truck velocity has essentially the same influence on the impact factor for both main and secondary bridge members. These results are illustrated in Figure 3-9. Gages



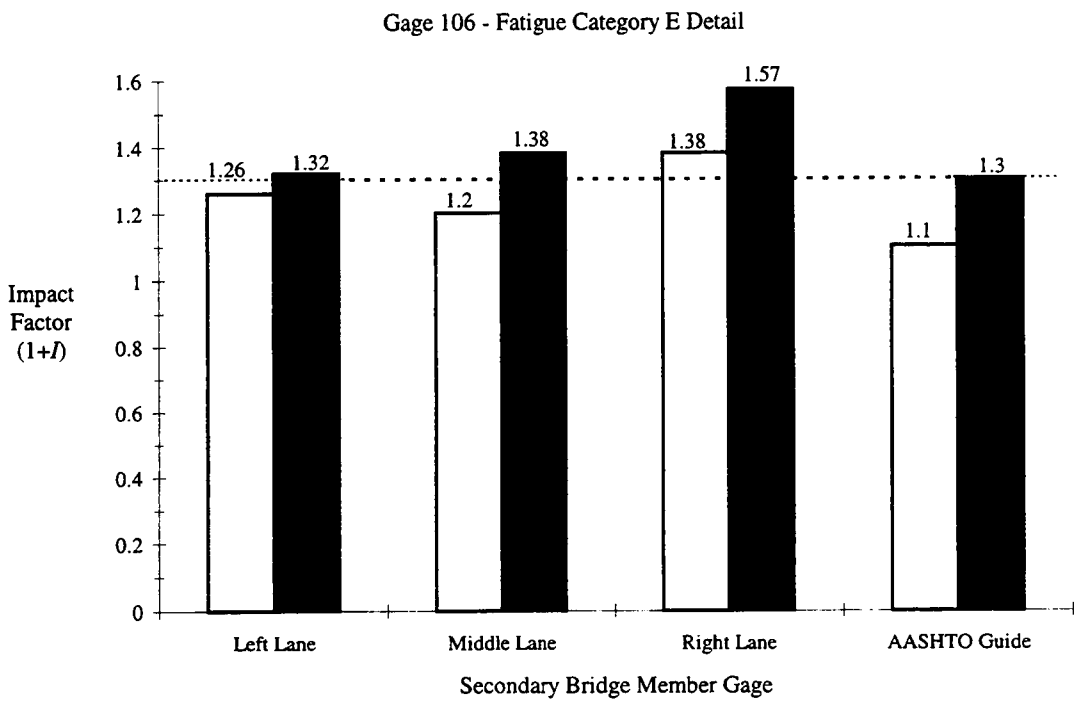


Figure 3-8. Rough and Smooth Surface Condition Measured Impact Factors for Main and Secondary Steel Bridge Members (These are the Results of One Test)

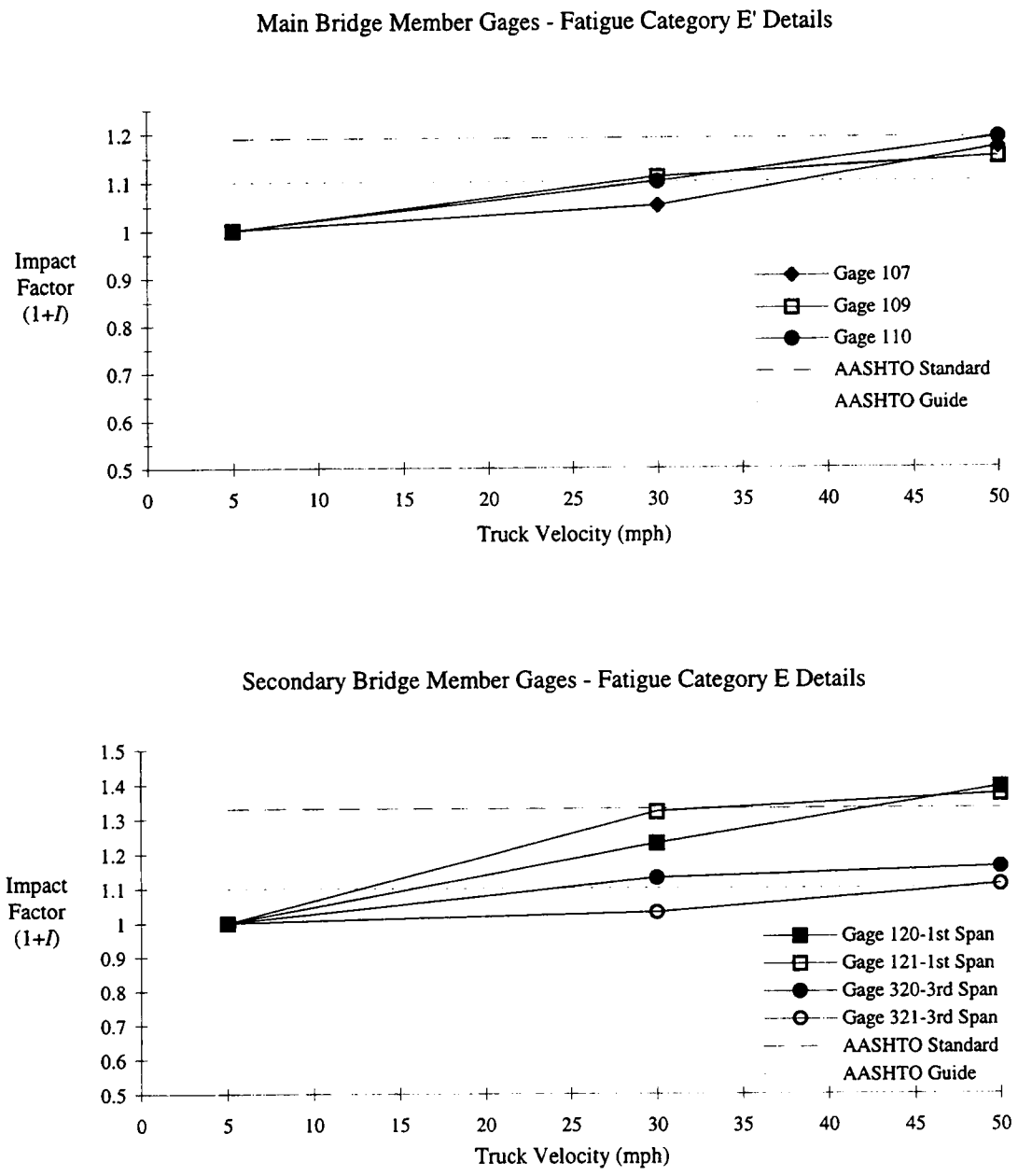


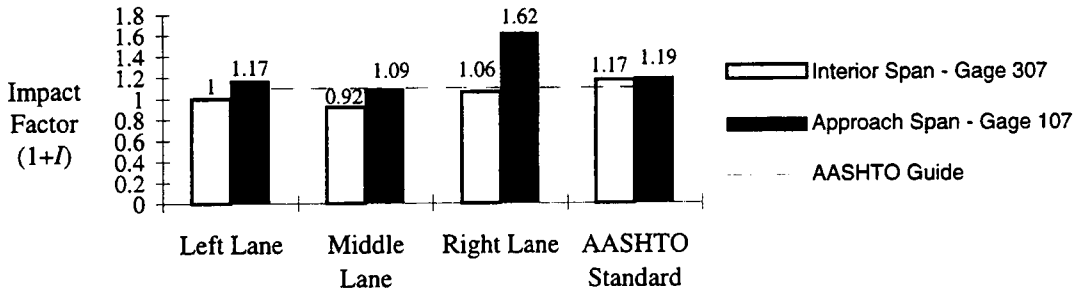
Figure 3-9. Truck Velocity vs Measured Impact Factor for Main and Secondary Steel Bridge Members

107, 109, and 110 are fatigue category E' main longitudinal girder web gap gages. Gages 120, 121, 320, and 321 are fatigue category E secondary member flange termination gages. Test results for gages 110 and 120 show a linear relationship between truck velocity and impact factor. Gage 110's measured impact factor exceeds AASHTO *Standard*'s impact factor for a truck velocity of 50 mph. The measured impact factor for gages 109, 110, 120, 121, and 320 exceeds the AASHTO *Guide*'s impact factor for truck velocity greater than 30 mph.

The effect of bridge approach, which for this bridge is only the expansion joints, on impact factors was investigated by testing strain gages in the same location for both the first and third spans of the bridge. Test results show that the bridge approach increases impact factors for fatigue prone details, as illustrated in Figure 3-10. Gages 107 and 307 are fatigue category E' main longitudinal girder web gap gages. Gages 106 and 306 are fatigue category E secondary member flange termination gages. The impact factor for bridge main member gages in the approach span is an average of 29% greater than its counterpart in the third span. For secondary bridge member gages, there is an average of 18% increase in impact factor. This increase in impact factor is attributed to the effect of the expansion joint. The percent increase in impact factor for the approach (end) span over the third span was determined by calculating the percent increase in impact factor for each lane of traffic and then taking the average of the three values.

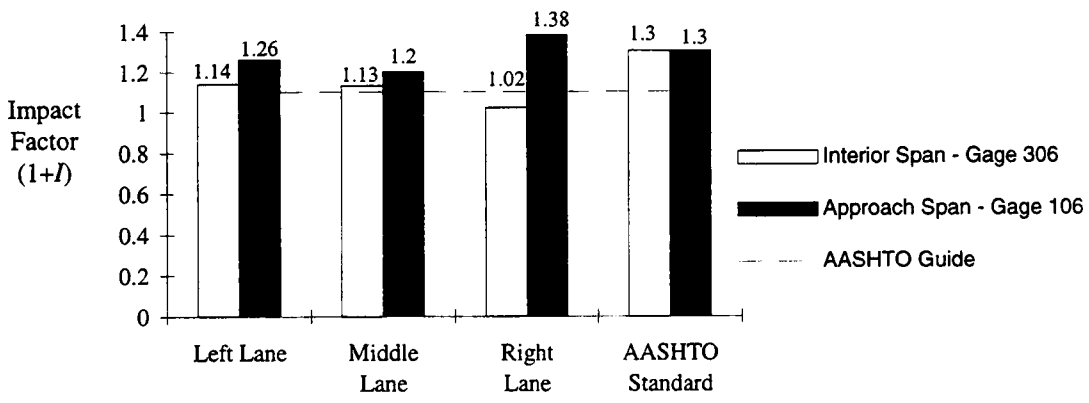
Schilling (1982) suggests that the impact factors for fatigue should be based on typical, or average, conditions and that these factors must account for the dynamic effects on the stress range rather than on the peak stress. The 1995 impact test was conducted

Fatigue Category E' Details



Main Bridge Member Gages

Fatigue Category E Details



Secondary Bridge Member Gages

Figure 3-10. Measured Impact Factors for Main and Secondary Steel Bridge Member Gages Located in the Approach (End) Span and in the Third Span

under typical or average bridge conditions (smooth surface condition and truck velocity of 50 mph); thus, the results of this test were used to determine impact factors for AASHTO fatigue stress categories A, B, E, and E' details. Test results of measured impact factors for main and secondary steel bridge members are shown in Tables 3-2 and 3-3, respectively.

Based on test results presented in Tables 3-2 and 3-3, the following observations were made. There is not a significant difference in peak and stress range impact factors for the Holston River Bridge. Schilling's (1982) results for a continuous welded plate girder bridge concur with this finding. Since there is not a significant difference between peak and stress range impact factors for a continuous steel girder bridge, the peak impact factor for this type of bridge is appropriate for fatigue design. For the same fatigue prone detail, fascia girders have a higher impact factor than interior girders. For example, fascia girder gage 58 has a 15% higher impact factor than interior girder gage 201 for the truck in the left lane. This finding agrees with Peterson and Kostem's (1973) nonfatigue design analytical results for bridge beam members. For each fatigue stress category, the impact factor increases with increase in the lateral distance between the main longitudinal girder gage and the loaded traffic lane. For secondary bridge member fatigue prone details, the highest impact factor occurs when the gage is under the loaded traffic lane. For the same fatigue prone detail in both the approach (end) span and the interior bridge spans, impact factors for gages in the approach (end) span are significantly larger than those in the interior spans. For instance, the impact factor for gage 135 is 30% larger than for gage 5.

Table 3-2. Impact Factors for Main Longitudinal Steel Bridge Members

Fatigue Category	Gage Number	Measured Impact Factor			AASHTO Impact Factor	
		Left Lane	Middle Lane	Right Lane	Standard	Guide
A	136	-	1.06 (1.06)	1.01 (1.02)	1.14	1.1
	303	-	-	1.06 (1.11)	1.17	1.1
B	*5	1.15 (1.10)	-	1.05 (1.01)	1.14	1.10 to 1.30
	*58	1.20 (1.24)	1.08 (1.10)	1.11 (1.00)	1.14	1.10 to 1.30
	*83	1.12 (1.08)	1.03 (1.00)	1.05 (1.09)	1.14	1.10 to 1.30
	135	1.49 (1.43)	1.18 (1.24)	1.22 (1.25)	1.19	1.1
	137	1.13 (1.12)	1.07 (1.12)	1.31 (1.18)	1.19	1.1
	138	1.14 (1.17)	1.21 (1.23)	1.04 (1.04)	1.19	1.1
	201	1.05 (1.06)	-	-	1.14	1.1
	202	1.05 (1.00)	1.00 (0.98)	0.96 (1.08)	1.14	1.1
E	126	1.02 (1.10)	1.04 (1.11)	1.02 (1.07)	1.14	1.1
	127	-	1.08 (1.16)	0.98 (1.01)	1.14	1.1
	128	1.08 (1.09)	1.08 (1.12)	0.95 (1.02)	1.14	1.1
	129	-	1.25 (1.11)	1.05 (1.00)	1.14	1.1
E'	73	1.00 (1.04)	1.02 (1.07)	0.92 (1.00)	1.14	1.1
	74	-	1.00 (1.02)	0.94 (1.00)	1.14	1.1
	75	-	1.04 (1.03)	0.91 (0.94)	1.14	1.1
	95	1.14 (1.09)	1.05 (1.04)	1.01 (1.02)	1.14	1.1
	96	-	1.11 (1.00)	0.98 (0.94)	1.14	1.1
	97	-	1.16 (1.07)	1.00 (0.96)	1.14	1.1
	*98	1.26 (1.15)	1.16 (1.05)	1.14 (1.10)	1.14	1.10 to 1.30
	107	1.17 (1.23)	1.09 (1.11)	1.62 (1.57)	1.19	1.1
	108	1.10 (1.17)	1.10 (1.16)	1.28 (1.32)	1.19	1.1
	109	1.15 (1.19)	1.11 (1.16)	1.32 (1.30)	1.19	1.1
	110	1.19 (1.21)	1.10 (1.16)	1.51 (1.50)	1.19	1.1
	133	1.57 (1.49)	1.23 (1.28)	1.24 (1.25)	1.19	1.1
	134	1.49 (1.39)	1.22 (1.26)	1.27 (1.26)	1.19	1.1
	307	1.00 (1.08)	0.92 (1.00)	1.06 (1.20)	1.17	1.1
	308	0.93 (0.93)	0.92 (1.00)	0.93 (1.05)	1.17	1.1

Note: Values in ( ) are measured stress-range impact factors

* = Measured values from the 1993 impact test

- = No data

Table 3-3. Impact Factors for Secondary Steel Bridge Members

Fatigue Category	Gage Number	Measured Impact Factor			AASHTO Impact Factor	
		Left Lane	Middle Lane	Right Lane	Standard	Guide
A	*89	-	1.03 (1.23)	-	1.3	1.10 to 1.30
B	*81	-	0.93 (1.09)	1.03 (0.96)	1.3	1.10 to 1.30
	*92	-	1.11 (1.09)	-	1.3	1.10 to 1.30
E	61	-	1.06 (1.06)	1.16 (1.17)	1.3	1.1
	*79	-	1.11 (1.23)	-	1.3	1.10 to 1.30
	*90	-	1.13 (1.19)	-	1.3	1.10 to 1.30
	105	0.87 (0.96)	1.29 (1.23)	1.02 (1.05)	1.3	1.1
	106	1.26 (1.34)	1.20 (1.26)	1.38 (1.41)	1.3	1.1
	120	1.39 (1.38)	1.13 (1.17)	2.03 (1.98)	1.3	1.1
	121	1.37 (1.36)	1.46 (1.38)	1.60 (1.63)	1.3	1.1
	305	0.89 (0.93)	1.02 (1.00)	1.12 (1.11)	1.3	1.1
	306	1.14 (1.15)	1.13 (0.940	1.02 (1.08)	1.3	1.1
	320	1.16 (1.17)	1.01 (0.99)	-	1.3	1.1
	321	1.11 (1.13)	1.01 91.11)	1.02 (1.26)	1.3	1.1
E'	317	-	0.99 (0.98)	-	1.3	1.1
	318	-	0.98 (0.98)	-	1.3	1.1

Note: Values in ( ) are measured stress-range impact factors
* = Measured values from the 1993 impact test
- = No data

The impact factor for gage 107 is 53% larger than for gage 307. Gage 106's impact factor is 35% larger than that of gage 306, whereas gage 121's impact factor is 57% larger than that of gage 321.

Schilling (1982) states that the impact factors given by the AASHTO *Standard* formula are representative of actual bridge loading and, therefore, appropriate for fatigue design. Nowak and Nassif (1995) stated that the AASHTO *Standard* formula is not representative of actual bridge impact factors and recommends an impact factor (1+*I*) of 1.30 for design and analysis. From Tables 3-2 and 3-3, it can be seen that the AASHTO *Guide*'s impact factor of 1.10 is less than the AASHTO *Standard*'s impact factor for all

gages. The *Guide*'s impact factor is 4% to 8% less for main members and 18% less for secondary members. Therefore, all comparisons will be made with regards to the AASHTO *Standard*'s impact factors. A comparison of Tables 3-2's (main members) measured impact factor to AASHTO *Standard*'s impact factor shows that for fatigue categories A and B, the AASHTO formula is very conservative. With the exception of gage 129, the AASHTO values compare well with the measured values for fatigue category E. The impact values measured for the interior span for category E' are consistently lower than AASHTO's values while the measured values for the approach (end) span are consistently much higher than AASHTO's values. Table 3-3's (secondary members) measured impact values for fatigue categories A, B, E, and E' are much lower than AASHTO's values for the case with the truck in the bridge interior spans. For fatigue category E, AASHTO's values are unconservative for the case when the truck is in the approach (end) span. Nowak and Nassif's impact value of 1.30 (1+*I*) is conservative for fatigue prone details located in the bridge interior spans and is unconservative for details located in the approach (end) spans.

The test results of this study suggest that neither a constant impact factor nor impact factors given by the AASHTO *Standard* formula are representative of actual bridge loading for fatigue prone details. Table 3-4 lists the means and standard deviations for each fatigue category. These values were obtained by first calculating the percent increase of the measured impact factor for each stress category to AASHTO *Standard*'s value listed in Tables 3-2 and 3-3. Then the mean and standard deviation of these percent increase values were calculated. Table 3-5 gives measured impact factors for AASHTO

Table 3-4. Measured Impact Factor Mean and Standard Deviation Values

AASHTO Fatigue Category	Measured Data	Main Member		Secondary Member	
		Interior Span	Approach Span	Interior Span	Approach Span
A	Mean	$0.907I_A$	-	$0.792I_A$	-
	Std. Dev.	$0.022I_A$	-	*	-
B	Mean	$0.939I_A$	$1.007I_A$	$0.787I_A$	-
	Std. Dev.	$0.058I_A$	$0.114I_A$	$0.069I_A$	-
E	Mean	$0.925I_A$	-	$0.825I_A$	$0.930I_A$
	Std. Dev.	$0.071I_A$	-	$0.058I_A$	$0.194I_A$
E'	Mean	$0.872I_A$	$1.063I_A$	$0.758I_A$	-
	Std. Dev.	$0.070I_A$	$0.144I_A$	$0.005I_A$	-

Note: I_A = Equation (3.1); - = No data; * = One data point

Table 3-5. Measured Impact Factors for AASHTO Fatigue Stress Categories

AASHTO Fatigue Category	Steel Bridge Impact Factor (I)			
	Main Longitudinal Members		Secondary Members	
	Interior Span	Approach (End) Span	Interior Span	Approach (End) Span
A	I_A	-	I_A	-
B	I_A	$1.25\ I_A$	I_A	-
E	$1.10\ I_A$	-	I_A	$1.35\ I_A$
E'	$1.10\ I_A$	$1.40\ I_A$	I_A	-

Note: $I_A = 50 / (L + 125)$; L= Bridge span length in feet for main members and L = span length of member center-to-center of supports for secondary members
- = No data

fatigue stress categories A, B, E, and E' details. These measured impact factors were obtained by summing the mean plus two standard deviations of the values listed in Table 3-4. Unlike AASHTO's formula, these measured values are not limited to 30%. It should be noted that the approach span in these tables refers to an end span with an expansion joint.

3.5 Conclusions

Bridge approach, surface condition, and truck velocity effects on impact factors for fatigue prone details in both main and secondary steel bridge members were examined. Rough surface condition increases impact factor by an average of 8%. Impact factors increase linearly with increase in truck velocity. The bridge approach increases impact factors by 20 to 60% depending on the type of fatigue prone detail. Of the three parameters, the bridge approach had the most influence on impact factor.

Measured impact factors for fatigue prone details varied depending on the location of the detail. Fatigue prone details located on a fascia girder had a higher impact factor than the same detail located on an interior girder. For a main longitudinal bridge girder fatigue detail, impact factor increased with increase in the lateral distance between the detail and the load. For secondary bridge member fatigue prone details, impact factor is maximum when the detail is directly under the load. Fatigue prone details located in the approach (end) span have a higher impact factor than the same detail located in an interior span.

A comparison of the measured impact factors with impact factors obtained using the AASHTO *Standard* formula revealed the following: AASHTO impact values were

conservative for fatigue categories A and B details. For fatigue categories E and E' details located in the bridge interior span, AASHTO impact values were conservative for secondary member details and 10% unconservative for main girder details. For the approach (end) span, AASHTO values were unconservative for categories B and E' main girder details by 25% and 40%, respectively; and they were 35% unconservative for category E secondary bridge member details.

CHAPTER 4

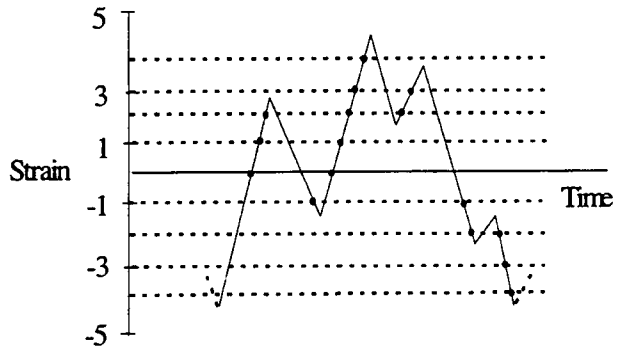
SENSITIVITY ANALYSIS

This chapter describes a sensitivity analysis addressing the effect of cycle counting methods, stress-range frequency-of-occurrence histogram construction, and field test duration on the effective stress range and the number of cycles per truck.

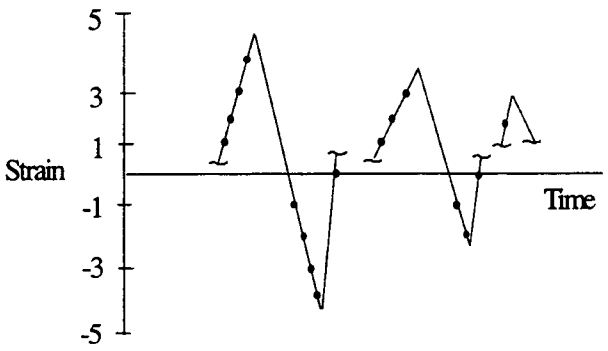
4.1 Literature Review

Cycle Counting Methods

There are several cycle counting methods available that can be used to determine stress ranges and number of cycles from a given strain-time history. Some of these include level-cross counting, peak counting, simple-range counting, mean-crossing-peak counting, and rainflow counting (SAE, 1988, Bannantine et al., 1990, Dowling, 1972, and Narayanan et al., 1991). In the level-crossing counting procedure, a count is recorded each time the strain history crosses predetermined strain levels. Only crossings with a positive slope are counted on the positive side of the datum and only negative crossings with a negative slope are counted on the negative side of the datum. Once the counts are determined, they are combined to form completed cycles. This is done by first forming the largest possible cycle, and then forming the next largest cycle from the remaining available counts, and so on, until all counts have been used, as shown in Figure 4-1. With the simple-range counting method the strain range between successive reversals is recorded. Each range is considered to form one half cycle, as shown in Figure 4-2. The peak counting technique involves the counting of all maximum (peak) and minimum (valley) strains in the strain-time history. Valleys on the positive side of the datum and

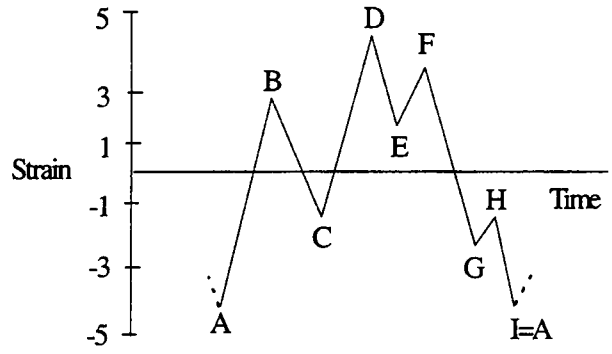


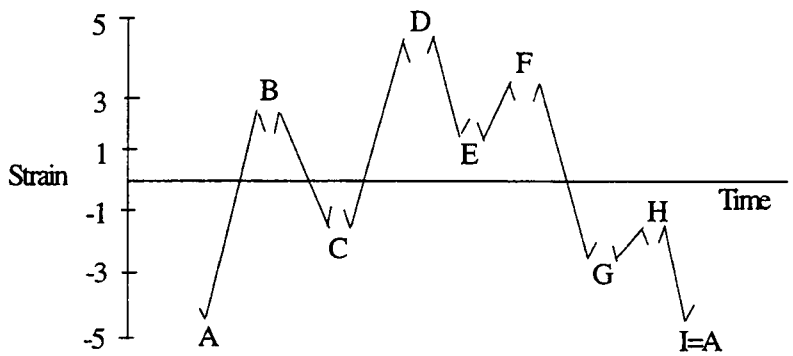
Level	Counts
4	1
3	2
2	3
1	2
0	2
-1	2
-2	2
-3	1
-4	1



Range Level	Cycle Counts
1	1
2	0
3	0
4	0
5	0
6	1
7	0
8	0
9	1
Total	3

Figure 4-1. Level-Crossing Counting (Bannantine et al., 1990)





Range Level	Cycle Counts
1	0.5
2	0.5
3	1
4	0.5
5	0
6	1
7	0.5
Total	4

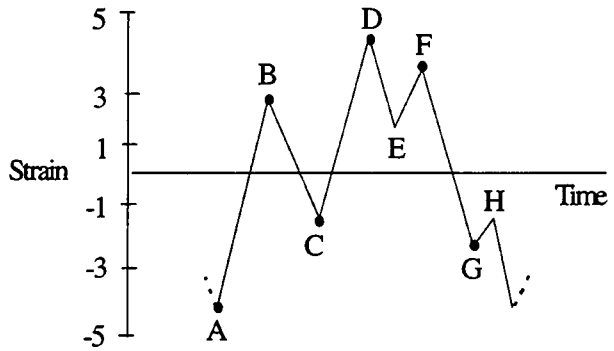
Figure 4-2. Simple-Range Counting (Bannantine et al., 1990)

peaks on the negative side of the datum are ignored. Complete cycles are formed by combining the largest peak with the largest valley, the second largest peak with the second largest valley, and so on, until all counts have been used, as shown in Figure 4-3.

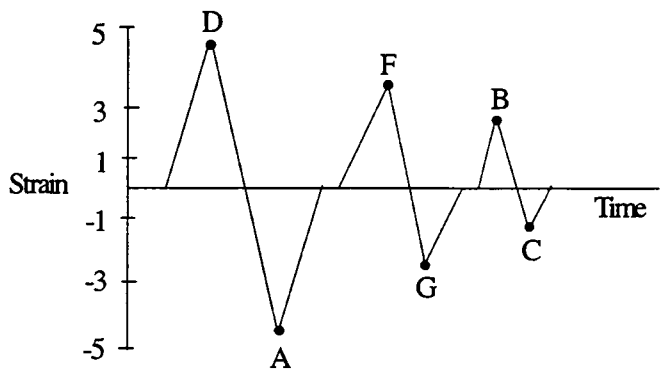
The mean-crossing-peak cycle counting method is a variation of the peak counting method. In this method, only the largest peak and valley between successive crossings of the mean (zero) axis is counted. For each crossing, the largest peak and valley form a cycle, as shown in Figure 4-4.

The rainflow counting method is a variation of the simple-range counting method. Instead of pairing adjacent peaks and valleys, this method pairs the peak and valley combinations which would define a closed stress-strain hysteresis loop. In the rainflow technique, the strain-time history is rotated so that the abscissa is vertical, with time increasing in the downward direction. An imaginary raindrop starts at the inside tip of each peak or valley and flows down the sloped 'roof'. The raindrop falls until it comes opposite a peak or valley greater than the one from which it started, or until it contacts the path of another raindrop started from a higher peak or valley. A half-cycle is counted for each raindrop. The strain range for a half-cycle is the difference between the strain at the starting point of a raindrop and the strain at the termination point. Full cycles are formed by combining half-cycles of the same strain range, but opposite flow direction. The rainflow counting method is illustrated in Figure 4-5.

From Figures 4-1 through 4-5, it can be seen that each counting method produces a different result for the same strain-time history. Unlike the level-crossing and the peak

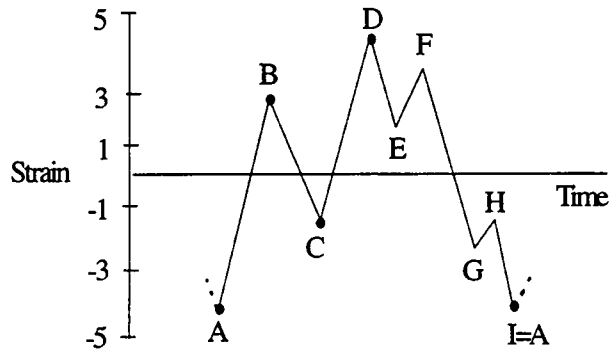


Peak	Counts
4	1
3	1
2	1
1	0
0	0
-1	1
-2	1
-3	0
-4	1

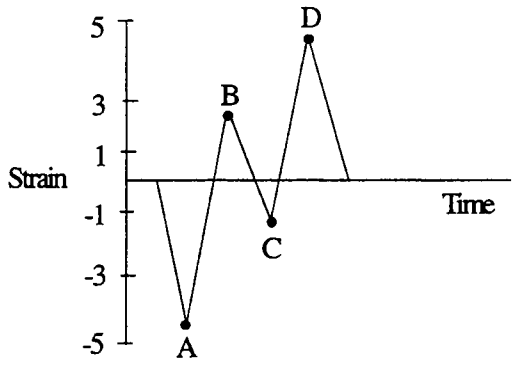


Range Level	Cycle Counts
1	0
2	0
3	0
4	1
5	0
6	1
7	0
8	0
9	1
Total	3

Figure 4-3. Peak Counting (Bannantine et al., 1990)

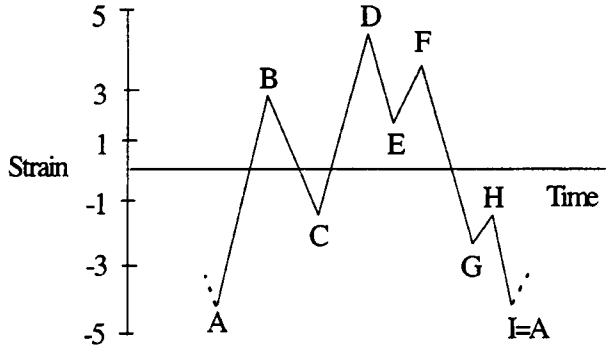


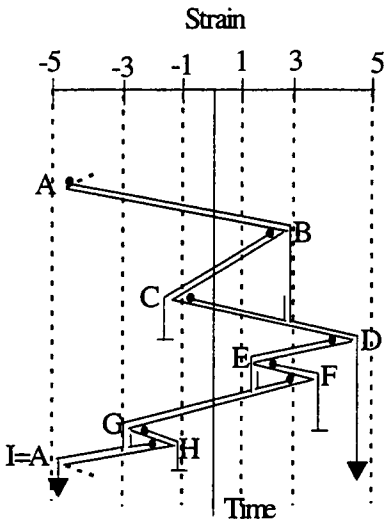
Peak	Counts
4	1
3	0
2	1
1	0
0	0
-1	1
-2	1
-3	0
-4	1



Range Level	Cycle Counts
1	0
2	0
3	0
4	0
5	0
6	1
7	1
Total	2

Figure 4-4. Mean-Crossing-Peak Counting





Range Level	Cycle Count
1	1
2	1
3	0
4	1
5	0
6	0
7	0
8	0
9	1
Total	4

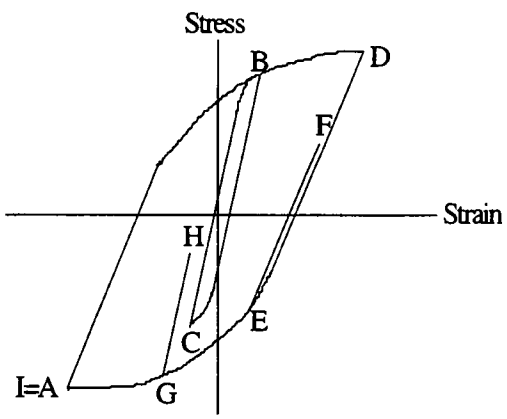


Figure 4-5. Rainflow Counting (Bannantine et al., 1990)

counting methods, the simple-range counting, the mean-crossing-peak, and the rainflow techniques count each cycle without altering the range of any cycles. Clearly, the level-crossing and the peak counting technique results predict more fatigue damage than the results of the other three methods. The simple-range counting method breaks up large ranges and counts them as several smaller ranges. This decreases the amount of predicted fatigue damage and can produce unconservative results. The mean-crossing-peak counting technique alters the strain-time history by ignoring reversals (ranges) that do not cross the mean axis. These small ranges do some fatigue damage that may be significant compared to the damage done by the large cycle on which they are superimposed. Rainflow counting technique treats the small reversals as interruptions of the larger ranges, and the damages for the large and small ranges are added.

Histogram Construction

The AASHTO *Standard* (1992) and *Guide* (1990) specifications do not provide any standards for construction of a stress-range frequency-of-occurrence histogram when obtained through field measurements. Histogram bar width and number of intervals has varied from researcher to researcher. Hanson et al. (1991) used a total of 19 stress range intervals each 500 psi wide ranging from 500 to 10,000 psi. This selection was made on the basis of a visual examination of the recorded data and a desire for four to eight intervals containing a significant number of cycles. King et al. (1976) used a total of 8 stress range intervals each 450 psi wide ranging from 895 to 4465 psi. Nowak et al. (1993) used a total of 16 stress range intervals each 300 psi wide ranging from 300 to 5550 psi. Post et al. (1988) used a total of 14 stress intervals each 380 psi wide ranging

from 570 psi to 5870 psi. Shaaban (1985) collected a total of 190 stress-range histograms from 34 highway steel bridges that were tested during the 1970s. The bar width of these histograms varied from 150 to 600 psi.

Test Duration

Neither the AASHTO *Standard* (1992) nor the AASHTO *Guide* (1990) provide any guidance for field measured test data duration. Fatigue test duration has varied from bridge to bridge and from researcher to researcher. For the Lehigh River and Canal bridges, 170 hours of strain data were acquired to assess the bridges (Fisher et al., 1984). For the Aguasabon River Bridge, a total of 32.5 hours of test data was recorded (King et al., 1976). For the Benicia-Martinez Bridge, a total of 297.7 hours of test data was recorded (Hanson et al., 1991). Moses et al. (1974) recorded 12 to 24 hours of strain data under normal traffic. Shaaban (1985) reported that test duration varied from 12 to 168 hours for the 34 steel bridges tested during the 1970s. Post et al. (1988) recommended that seven days (24 hours a day) of data be used in assessing a bridge. Yen et al. (1990) recommend that 48 hours of recorded data are sufficient to provide a realistic representation of the traffic pattern.

4.2 Cycle Counting Methods

The two most commonly used cycle counting methods for highway bridge variable amplitude loading are the mean-crossing-peak and the rainflow cycle counting techniques. The mean-crossing-peak method was used mostly during the seventies (Goodpasture, 1976). Fisher et al. (1983) conducted tests where a large percentage of the cycles fell below the fatigue limit and concluded that these cycles are damaging when

they are part of a variable amplitude history containing some cycles above the fatigue limit. A consensus has recently emerged that the best approach, when applying a linear damage model like the Palmgren-Miner rule, is to use the rainflow cycle counting procedure which accounts for all the cycles in a variable amplitude history (Dowling, 1993, Fisher et al., 1990, Narayanan, et al., 1991, Post et al., 1988, ASCE Committee, 1982). The effect of these two cycle counting methods on the effective stress range and the number of cycles per truck are evaluated.

Evaluation Procedure

The sensitivity of the effective stress range and the number of cycles per truck to the mean-crossing-peak and the rainflow cycle counting methods is examined by using field data taken under normal traffic. Table 4-1 provides a summary of the various fatigue prone details that were instrumented for this evaluation. This table lists the gage number, the applicable AASHTO fatigue stress category, the description of the detail, and the page number of the drawing in the Appendix that shows the gage location. The raw data was first reviewed for any erroneous readings and then reduced using a rainflow BASIC program and Mayhew's (1994) mean-crossing-peak BASIC program. The rainflow program incorporates the SAE's (1988) ppeak program and Downing and Socie's (1982) rainflow algorithm. For a given test duration and a histogram interval width of 500 psi, the stress ranges and the number of cycles were determined for both the rainflow and the mean-crossing-peak counting methods. Strain ranges below 500 psi were not included in this evaluation; these low level cycles are mostly the result of

Table 4-1. Summary of Cycle Counting Methods Fatigue Prone Details

Bridge Member	Fatigue Category	Gage No.	Detail Description	Drawing Page No.
	B	G31	Top of girder bottom flange near the web-to-flange weld	203
		G58, G59	"	206
		G82, G83	"	211
	E	G26	Girder web at end of retrofit plate longitudinal weld	201
M				
a	E'	G19	Girder horizontal web gap near the lateral gusset plate weld	200
i		G73	"	206
n		G95, G98	"	211
		G107,G110	"	193
		G20	Girder horizontal web gap near the transverse stiffener	200
		G74	"	206
		G96, G97	"	211
		G108,G109	"	193
		G115,G116	Girder web at end of lateral gusset plate longitudinal weld	193
	A	G10	Top flange of knee brace	198
		G11	Cross-frame top chord	198
		G67	"	205
		G88	"	210
		G14	Cross-frame truss diagonal	198
S		G63, G68	"	205
e		G84, G89	"	210
c				
o	B	G101	Cantilever bracket bottom flange near the web-to-flange weld	191
n		G104,G112	Floorbeam bottom flange near the web-to-flange weld	191
d		G111	Floorbeam top flange near the web-to-flange weld	191
a				
r	C	G60	Cross-frame bottom chord near gusset plate weld	205
y		G81	"	210
	E	G15, G16	Cross-frame bottom chord at end of gusset plate weld	198
		G61	"	205
		G79	"	210
		G71	Lateral X-bracing bottom flange at end of longitudinal weld	206
		G105,G106	Floorbeam web at flange termination weld	191
	E'	G117,G118	Floorbeam bottom flange at end of gusset plate weld	196

electronic noise (Hanson et al., 1991, Post et al., 1988). The effective stress range or the root-mean-cube (*RMC*) is determined by

$$RMC = \left(\frac{\sum n_i S_{ri}^3}{\sum n_i} \right)^{1/3} \tag{4.1}$$

in which S_{ri} is the midwidth of the ith interval in a frequency-of-occurrence histogram defining the variable amplitude spectrum and n_i is the number of cycles at stress range level S_{ri}. The number of cycles per truck, *CPT*, is given by

$$CPT = \frac{\left(\sum n_i\right)_{RF} \text{ or } \left(\sum n_i\right)_{MCP}}{T} \tag{4.2}$$

in which *RF* is the rainflow method, *MCP* is the mean-crossing-peak method, and T is the total number of trucks for a given test duration. Since T remains constant for either cycle counting method, the sensitivity of the *CPT* to the cycle counting methods is the same as the sensitivity of the total number of cycles to the cycle counting methods.

To determine which cycle counting method is more conservative, the fatigue damage based on Miner's Rule was calculated. The fatigue damage, D, is given by

$$D = \sum \frac{n_i}{N_i} \tag{4.3}$$

in which N_i is the number of cycles to failure under constant amplitude stress range S_{ri}. N_i is given by

$$N_i = \frac{A}{S_{ri}^3} \tag{4.4}$$

in which S_{ri} is in ksi and A is equal to 390,224,000, 1,024,000,000, 4,394,000,000, 11,664,000,000, and 27,648,000,000 for Categories E', E, C, B, and A details, respectively.

Since both the rainflow (*RF*) and the mean-crossing-peak (*MCP*) techniques have been used by researchers to determine stress ranges and number of cycles, it would be beneficial to know the relationship between the two methods. This relationship was determined in the form of a correlation coefficient. The correlation coefficient, r, is a measure of the degree of linear relationship between the two methods. This coefficient is defined as

$$r_{MCP,RF} = \frac{Cov(MCP, RF)}{\sigma_{MCP}\ \sigma_{RF}} \qquad -1 \le r_{MCP,RF} \le 1 \tag{4.5}$$

in which *Cov* is the covariance and σ is the standard deviation. A perfect positive correlation exists when r equals 1, a perfect negative correlation exists when r equals -1, and r equals to zero when there is no linear relationship between the two methods. Linear regression, using least-square fit, was used to determine the relationship between the two methods. That is

$$\begin{gathered} y = mx + b \\ or \\ RF = m * MCP + b \end{gathered} \tag{4.6}$$

in which m is the slope of the line and b is the intercept.

Evaluation Results and Discussion

The results of this evaluation are presented in Tables 4-2 and 4-3. These tables give the measured *RMC* value, the total number of cycles, and the damage for each gage

Table 4-2. Cycle Counting Sensitivity Results for Fatigue Prone Details in Bridge Main Members

Fatigue	Gage	Duration	Stress Range Starting at 500 psi						Stress Range Starting at 1000 psi					
Category	Number	(hrs)	RMC_{RF}	RMC_{MCP}	$Cycle_{RF}$	$Cycle_{MCP}$	D_{RF}	D_{MCP}	RMC_{RF}	RMC_{MCP}	$Cycle_{RF}$	$Cycle_{MCP}$	D_{RF}	D_{MCP}
B	G31	0.6	1229	1128	295	234	4.7E-8	2.9E-8	1773	1583	82	67	3.9E-8	2.3E-8
	G82	0.6	1448	1234	323	323	8.4E-8	5.2E-8	1814	1604	152	127	7.8E-8	4.5E-8
	G58	1.9	1381	1283	785	651	1.8E-7	1.2E-7	1735	1633	362	280	1.6E-7	1.0E-7
	G59	1.9	1413	1316	744	635	1.8E-7	1.2E-7	1729	1637	376	297	1.7E-7	1.1E-7
	G83	1.9	1450	1191	834	811	2.2E-7	1.2E-7	1799	1555	406	308	2.0E-7	9.9E-8
E	G26	1.2	999	856	202	159	2.0E-7	9.7E-8	1343	1287	58	19	1.4E-7	4.0E-8
E'	G19	0.6	966	939	585	598	1.4E-6	1.3E-6	1711	1530	61	77	7.8E-7	7.1E-7
	G20	0.6	1025	979	508	233	1.4E-6	5.6E-7	1637	1399	84	52	9.4E-7	3.6E-7
	G73	0.6	1494	1399	639	510	5.5E-6	3.6E-6	2166	1957	191	167	5.0E-6	3.2E-6
	G74	1.9	1574	1483	792	690	7.9E-6	5.8E-6	1905	1823	425	347	7.5E-6	5.4E-6
	G95	1.9	1813	1586	1739	1672	2.7E-5	1.7E-5	2546	2231	599	558	2.5E-5	1.6E-5
	G96	1.9	1297	1065	560	522	3.1E-6	1.6E-6	1575	1440	283	160	2.8E-6	1.2E-6
	G97	1.9	1355	1128	581	552	3.7E-6	2.0E-6	1628	1473	308	202	3.4E-6	1.7E-6
	G98	1.9	1549	1256	1646	1623	1.6E-5	8.2E-6	2176	1803	549	466	1.4E-5	7.0E-6
	G107	1.2	1452	1342	2404	1991	1.9E-5	1.2E-5	2240	2020	587	507	1.7E-5	1.1E-5
	G108	1.2	1210	1062	1510	1452	6.9E-6	4.5E-6	1785	1645	387	280	5.6E-6	3.2E-6
	G109	1.2	1185	1107	1318	1082	5.6E-6	3.8E-6	1771	1664	319	242	4.5E-6	2.9E-6
	G110	1.2	1634	1558	3469	2740	3.9E-5	2.7E-5	2656	2477	747	623	3.6E-5	2.4E-5
	G115	1.2	904	828	2042	1619	3.9E-6	2.4E-6	1568	1340	188	118	1.9E-6	7.3E-7
	G116	1.2	1186	1098	964	804	4.1E-6	2.7E-6	1774	1679	233	168	3.3E-6	2.0E-6

Note: *RF* = Rainflow cycle counting method

MCP = Mean-crossing-peak cycle counting method

Table 4-3. Cycle Counting Sensitivity Results for Fatigue Prone Details in Bridge Secondary Members

Fatigue	Gage	Duration	Stress Range Starting at 500 psi						Stress Range Starting at 1000 psi					
Category	Number	(hrs)	RMC_{RF}	RMC_{MCP}	$Cycle_{RF}$	$Cycle_{MCP}$	D_{RF}	D_{MCP}	RMC_{RF}	RMC_{MCP}	$Cycle_{RF}$	$Cycle_{MCP}$	D_{RF}	D_{MCP}
A	G10	0.6	883	796	177	130	4.4E-9	2.4E-9	1370	1250	22	7	2.0E-9	4.9E-10
	G11	0.6	1188	1178	208	131	1.3E-8	7.7E-9	1659	1506	63	53	1.0E-8	6.5E-9
	G14	0.6	918	816	98	63	2.7E-9	1.2E-9	1326	1250	18	5	1.5E-9	3.5E-10
	G63	1.9	1010	842	655	308	2.4E-8	6.7E-9	1539	1272	124	33	1.6E-8	2.5E-9
	G67	1.9	896	798	648	589	1.7E-8	1.1E-8	1414	1669	80	12	8.2E-9	2.0E-9
	G68	1.9	976	776	413	370	1.4E-8	6.3E-9	1381	1250	95	11	9.0E-9	7.8E-10
	G84	1.9	876	810	356	267	8.7E-9	5.1E-9	1276	1250	54	19	4.1E-9	1.3E-9
	G88	1.9	893	776	741	650	1.9E-8	1.1E-8	1400	1250	93	19	9.2E-9	1.3E-9
	G89	1.9	1063	817	532	488	2.3E-8	9.6E-9	1518	1290	135	35	1.7E-8	2.7E-9
B	G101	1.2	801	797	403	221	1.8E-8	9.6E-9	1282	1522	22	6	4.0E-9	1.8E-9
	G104	1.2	848	806	1393	845	7.3E-8	3.8E-8	1462	1309	97	47	2.6E-8	9.0E-9
	G111	1.2	1095	867	386	377	4.3E-8	2.1E-8	1583	1321	97	46	3.3E-8	9.1E-9
	G112	1.2	999	935	1239	1032	1.1E-7	7.2E-8	1683	1570	164	118	6.7E-8	3.9E-8
C	G60	1.9	959	867	1016	908	2.0E-7	1.3E-7	1342	1284	235	123	1.3E-7	5.9E-8
	G81	1.9	899	818	3117	3293	5.2E-7	4.1E-7	1461	1364	352	196	2.5E-7	1.1E-7
E	G15	0.6	887	840	279	162	1.9E-7	9.4E-8	1358	1250	37	18	9.0E-8	3.4E-8
	G16	0.6	918	864	825	658	6.2E-7	4.1E-7	1631	1458	74	55	3.1E-7	1.7E-7
	G61	1.9	1084	980	929	825	1.2E-6	7.6E-7	1477	1333	282	220	8.9E-7	5.1E-7
	G71	1.9	785	776	711	370	3.4E-7	1.7E-7	1308	1250	24	11	5.2E-8	2.1E-8
	G79	1.9	1087	1004	859	706	1.1E-6	7.0E-7	1448	1333	283	214	8.4E-7	4.9E-7
	G105	1.2	2305	2401	18775	10001	2.2E-4	1.4E-4	3180	2986	7002	5119	2.2E-4	1.3E-4
	G106	1.2	1118	1022	3267	2754	4.5E-6	2.9E-6	1813	1656	577	431	3.4E-6	1.9E-6
E'	G117	1.2	1248	1269	692	426	3.4E-6	2.2E-6	1817	1731	189	145	2.9E-6	1.9E-6
	G118	1.2	1278	1295	801	515	4.3E-6	2.9E-6	1968	1864	185	149	3.6E-6	2.5E-6

Note: *RF* = Rainflow cycle counting method

MCP = Mean-crossing-peak cycle counting method

listed in Table 4-1. These parameters are given for both the rainflow and the mean-crossing-peak counting methods with frequency-of-occurrence histograms starting at 500 psi and at 1000 psi.

Based on the results presented in these tables, the following observations were made. For both rainflow and mean-crossing-peak methods, as the stress-range frequency-of-occurrence histogram went from starting at 500 psi to starting at 1000 psi, the *RMC* value increased while the number of cycles and the fatigue damage decreased. For all fatigue prone details with stress-range histograms starting at 1000 psi, the rainflow method was more conservative than the mean-crossing-peak method, as illustrated in Figures 4-6 and 4-7. The averaged values shown in these figures were determined by taking the average of the data for each fatigue category listed in Tables 4-2 and 4-3.

Table 4-4 provides a summary of the percent increase in the rainflow results over the mean-crossing-peak results. The percent increase was determined by first calculating the percent increase for each gage and then taking an average of all the gages' percent increases for a given test duration.

Based on the results presented in Table 4-4, the following observations were made. With exception of the *RMC* value for Category E' secondary bridge member details, the rainflow method was more conservative than the mean-crossing-peak method. There was less of a difference between the two methods when the stress-range frequency-of-occurrence histogram started at 1000 psi rather than 500 psi. There was less of a difference in the number of cycles and the fatigue damage between the two methods when the stress-range histogram started at 500 psi. The difference in RMC values between the

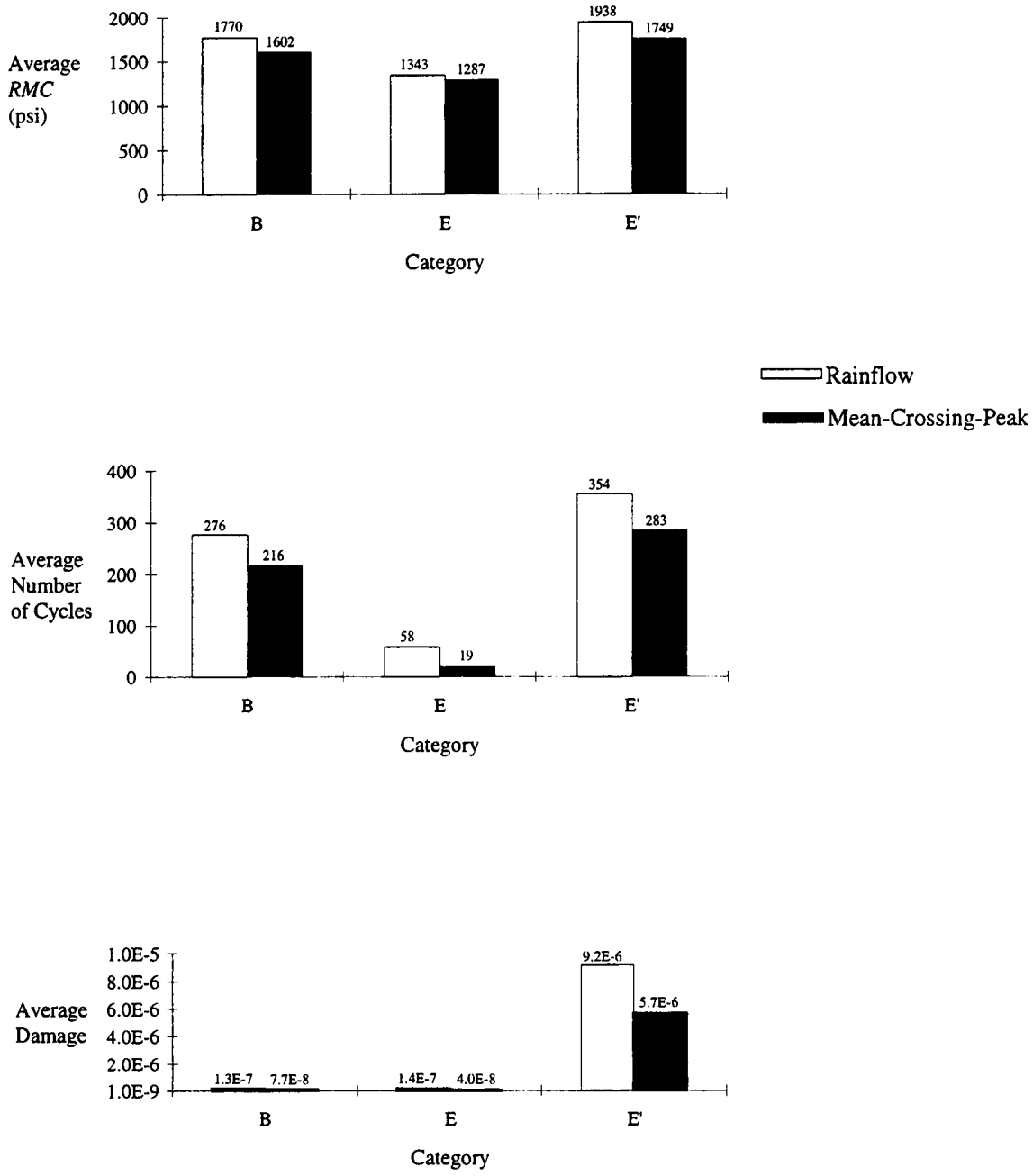


Figure 4-6. Main Bridge Member Rainflow and Mean-Crossing-Peak Average Values for Stress-Range Frequency-of-Occurrence Histogram Starting at 1000 psi

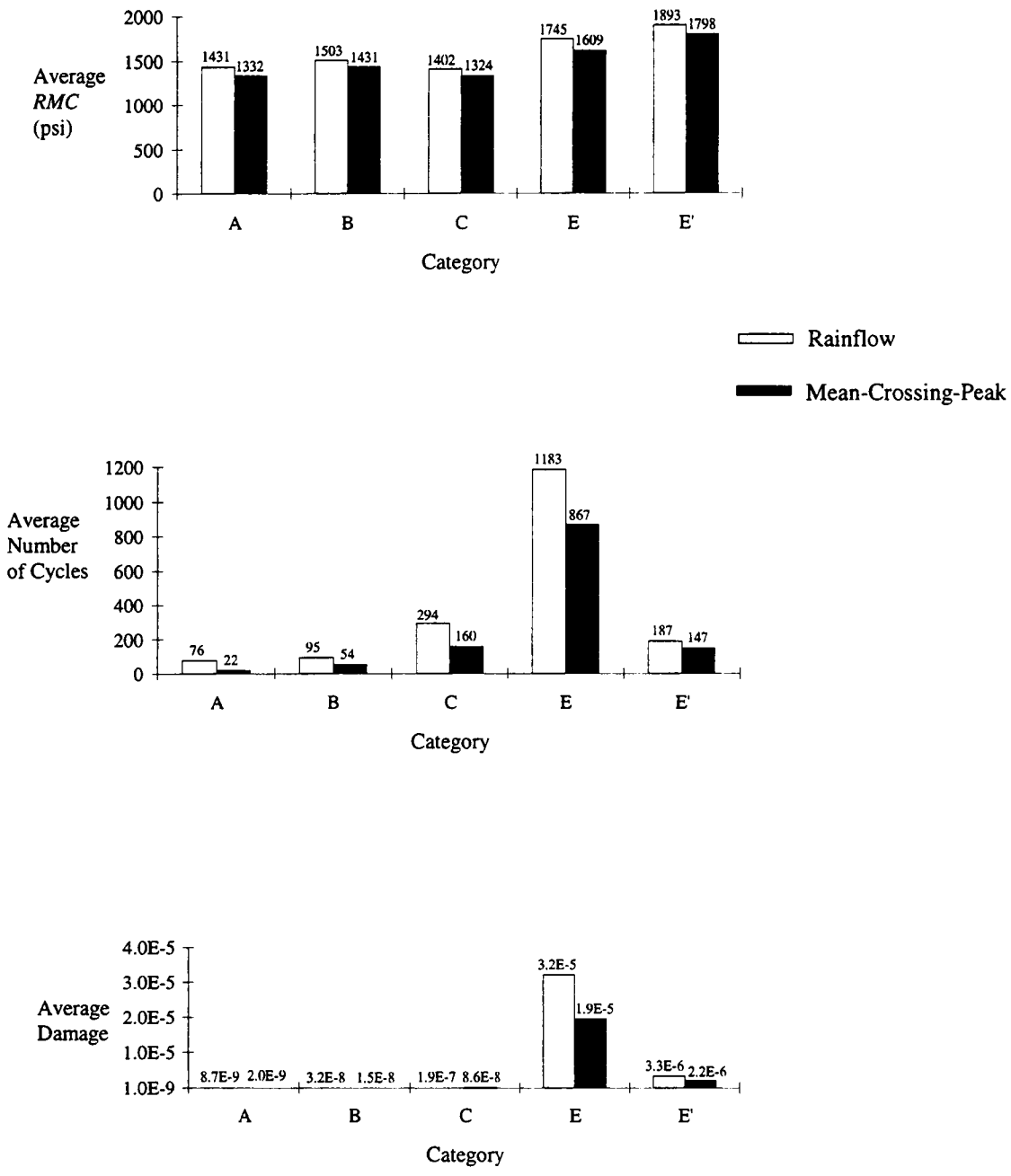


Figure 4-7. Secondary Bridge Member Rainflow and Mean-Crossing-Peak Average Values for Stress-Range Frequency-of-Occurrence Histogram Starting at 1000 psi

Table 4-4. Summary of Cycle Counting Sensitivity Analysis

Bridge Member	Category	Duration (hrs)	Average % Increase of Rainflow Over Mean-Crossing-Peak					
			SR Starting at 500 psi			SR Starting at 1000 psi		
			RMC	Cycles	Damage	RMC	Cycles	Damage
	B	0.6	13.1	13.0	62.3	12.5	21.0	72.5
		1.9	12.3	13.5	60.3	9.2	29.2	69.4
M	Average	1.4	12.6	13.3	61.1	10.5	26.0	70.7
a	E	1.2	16.7	27.0	101.9	4.4	205.3	246.9
i	E'	0.6	4.8	47.0	69.8	13.2	18.4	74.9
		1.2	8.5	19.9	52.9	9.3	34.0	76.7
n		1.9	17.1	6.5	71.8	11.8	35.4	88.7
	Average	1.3	10.8	20.9	63.3	11.0	31.1	80.6
	Average	1.3	11.6	19.3	64.7	10.6	38.5	86.4
	A	0.6	8.1	50.2	90.1	8.6	164.4	234.1
		1.9	18.6	31.8	121.2	8.0	410.9	542.3
	Average	1.5	15.1	37.9	110.8	8.2	328.7	439.6
S e c o n d a r y	B	1.2	9.7	42.4	82.5	5.7	130.7	160.2
	C	1.9	10.3	3.3	38.5	5.8	85.3	119.4
	E	0.6	5.9	48.8	76.6	10.3	70.1	126.0
		1.2	2.7	53.2	60.7	8.0	35.3	70.4
		1.9	6.7	42.1	68.6	8.0	59.5	98.0
	Average	1.3	5.3	47.2	68.6	8.7	55.6	98.1
	E'	1.2	-1.5	59.0	52.0	5.3	27.3	48.4
	Average	1.4	9.6	40.2	82.9	7.5	170.7	234.1

Note: SR = Stress range histogram

two methods was less for fatigue prone details located in secondary bridge members than those located in main bridge members. The difference in the number of cycles and the fatigue damage between the two methods was less for fatigue prone details located in main bridge members.

The relationship between the rainflow and mean-crossing-peak cycle counting methods is presented in Table 4-5 and illustrated in Figure 4-8. Table 4-5 gives the slope and intercept of equation (4.6) and the correlation coefficient of equation (4.5) for the data in each fatigue category and for the combined data in all the categories. Figure 4-8 is a plot showing the correlation between the rainflow and the mean-crossing-peak counting methods for all fatigue prone details located in both main and secondary bridge members with stress-range frequency-of-occurrence histogram starting at 1000 psi.

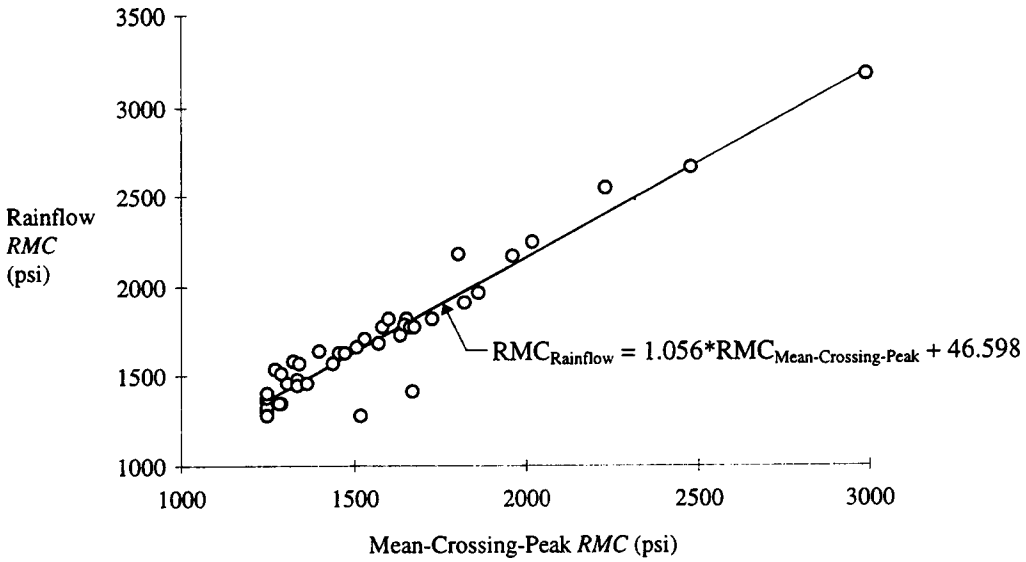
Based on the results presented in Table 4-5, the following observations were made. Main and secondary bridge member fatigue Categories C, E, and E' details have a nearly perfect positive correlation (i.e. r equals to 1.0) for both the *RMC* and the number of cycles. For fatigue Categories A and B details with stress-range histogram starting at 500 psi, there was a positive correlation (i.e. r is positive) for both the *RMC* and the number of cycles. Category B details with stress-range histogram starting at 1000 psi, have a negative correlation (i.e. r is negative) for the *RMC* value and a positive correlation for the number of cycles. For both the *RMC* and the number of cycles, fatigue Category A details have a higher degree of positive correlation for stress-range histograms that started at 500 psi than those that started at 1000 psi.

Table 4-5. Cycle Counting Regression Analysis Results

Bridge Member	AASHTO Fatigue Category	Stress Range Histogram Starting at 500 psi					
		RMC			Cycles		
		m	*b*	*r*	*m*	*b*	*r*
Main	B	0.715	504.865	0.583	1.067	29.716	0.979
	E'	1.078	35.242	0.955	1.192	-29.942	0.984
	ALL	1.059	66.392	0.948	1.186	-24.290	0.987
Secondary	A	0.683	389.699	0.822	1.010	89.260	0.908
	B	1.558	-390.252	0.734	1.308	46.110	0.933
	C	1.224	-102.633	1.000	0.881	216.122	1.000
	E	0.903	151.677	0.997	1.893	-521.767	0.995
	E'	1.154	-216.231	1.000	1.225	170.270	1.000
	ALL	0.860	212.811	0.978	1.797	-348.455	0.984
All	A	0.683	389.699	0.822	1.010	89.260	0.908
	B	1.117	-16.176	0.957	1.346	-30.430	0.943
	C	1.224	-102.633	1.000	0.881	216.122	1.000
	E	0.894	170.540	0.995	1.883	-450.108	0.995
	E'	1.050	50.891	0.932	1.158	33.354	0.981
	ALL	0.952	152.059	0.967	1.749	-409.793	0.978

Bridge Member	AASHTO Fatigue Category	Stress Range Histogram Starting at 1000 psi					
		RMC			Cycles		
		m	*b*	*r*	*m*	*b*	*r*
Main	B	-0.809	3066.950	-0.740	1.330	-11.470	0.999
	E'	1.057	89.526	0.975	1.084	47.129	0.984
	ALL	1.081	40.102	0.972	1.111	38.482	0.986
Secondary	A	0.311	1017.856	0.394	1.226	49.581	0.474
	B	0.020	1473.410	0.016	1.211	29.278	0.973
	C	1.488	-567.950	1.000	1.778	37.863	1.000
	E	1.050	54.861	0.999	1.368	-3.293	1.000
	E'	1.135	-148.271	1.000	-1.000	334.000	-1.000
	ALL	0.995	111.013	0.948	1.361	27.027	1.000
All	A	0.311	1017.856	0.394	1.226	49.581	0.474
	B	0.763	471.576	0.561	1.190	22.027	0.993
	C	1.488	-567.950	1.000	1.778	37.863	1.000
	E	1.058	35.348	0.998	1.367	2.031	1.000
	E'	1.052	86.702	0.970	1.094	42.141	0.985
	ALL	1.056	46.598	0.960	1.357	5.110	0.999

Note: m = Slope b = Intercept r = Correlation coefficient
ALL = The combined data for all the fatigue stress categories



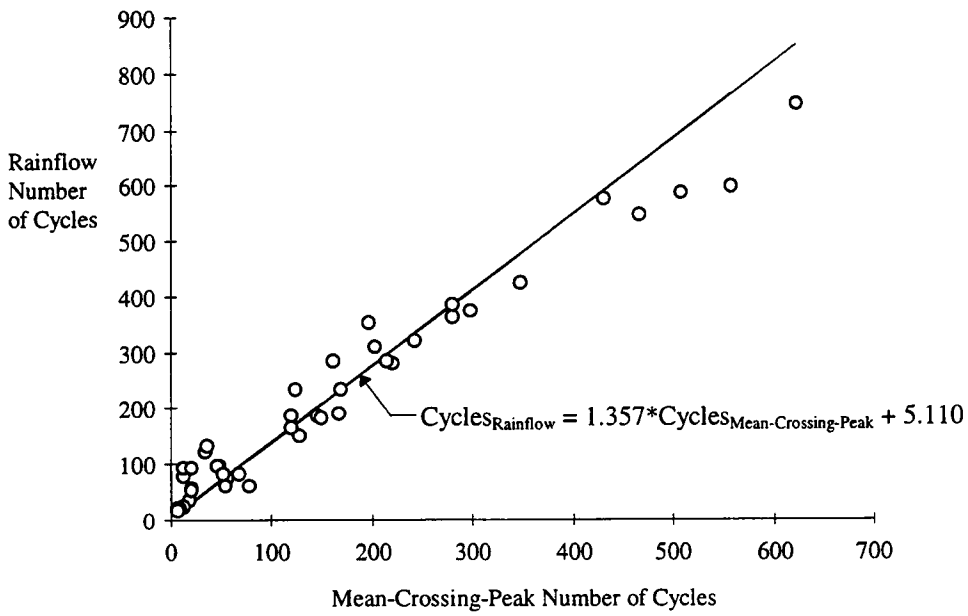


Figure 4-8. Plot Showing the Degree of Correlation Between Rainflow and Mean-Crossing-Peak Counting Methods for all Fatigue Prone Details with Stress-Range Frequency-of-Occurrence Histogram Starting at 1000 psi

4.3 Histogram Construction

The effects of various stress-range frequency of occurrence histogram construction on the effective stress range and the number of cycles per truck are evaluated in this section.

Evaluation Procedure

The sensitivity of the effective stress range and the number of cycles per truck to stress-range frequency of occurrence histogram construction are examined by first taking field data under normal traffic. Table 4-6 provides a summary of the various fatigue prone details that were instrumented for this evaluation. This table lists the gage number, the applicable AASHTO fatigue stress category, the description of the detail, and the page number of the drawing in the Appendix that shows the gage location. After reviewing the raw data for erroneous readings, the rainflow cycle counting method was used to reduce the data. Stress-range histograms with interval widths of 250, 350, 500, 600, and 1000 psi were then constructed. The histograms were constructed in two ways as shown in Figure 4-9. To compare various histogram construction with regards to the effective stress range (*RMC*), the number of cycles per truck, the total fatigue life, and the fatigue damage, the histograms were first constructed as shown in Figure 4-9 (A). Stress ranges from zero to the interval width were not included in the evaluation because these stresses are usually caused by electronic noise. To compare the effect of various histogram interval widths on the *RMC* value, the number of cycles per truck, the total fatigue life, and the fatigue damage, the histograms were then constructed as shown in Figure 4-9 (B).

Table 4-6. Summary of Histogram Construction Details

Bridge Member	Fatigue Category	Gage No.	Detail Description	Drawing Page No.
	A	G58C	Top of girder bottom flange near its edge	207
		G140	Bottom of girder bottom flange	207
		G143	Girder web	207
	B	G30	Top of girder bottom flange near the web-to-flange weld	203
		G83	"	211
M		G204	"	210
a				
i	C	G58B	Bottom of girder bottom flange at a change in flange thickness	207
n				
	E	G45, G47	Girder web above a drilled hole	200
		G46	Girder web below a drilled hole	200
	E'	G52	Girder horizontal web gap near the transverse stiffener	203
		G52A	Girder web at end of lateral gusset plate longitudinal weld	203
		G116	Girder web at end of lateral gusset plate longitudinal weld	193
S	A	G35, G41	Cross-frame truss diagonal	202
e		G37	Cross-frame top chord	202
c				
o	C	G32	Cross-frame bottom chord near gusset plate vertical weld	202
n				
d	E	G105,G120	Floorbeam web at flange termination weld	191
a		G305	"	213
r				
y	E'	G317,G318	Floorbeam bottom flange at end of gusset plate weld	213

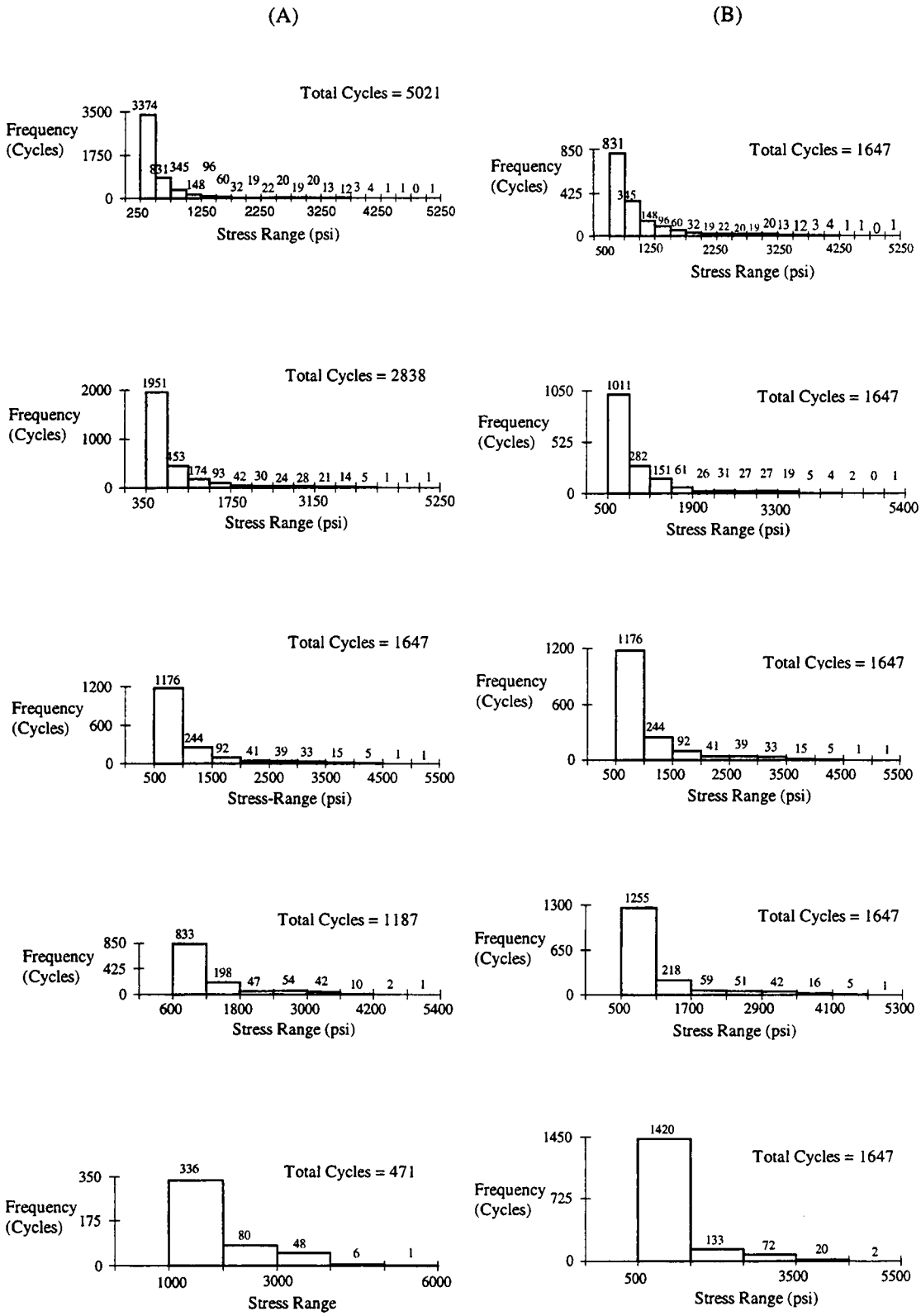


Figure 4-9. G105: Stress-Range Frequency-of-Occurrence Histograms, Interval Widths (from Top to Bottom) of 250, 350, 500, 600, & 1000 psi. Histograms (from top to Bottom) Start at (A) 250, 350, 500, 600, & 1000 psi and (B) 500 psi

Equations (4.1), (4.2), (4.3), and (4.4) were used to determine the *RMC* value, the number of cycles per truck, the fatigue damage, and the total fatigue life, respectively. Since the total number of trucks in equation (4.2) remains constant, the sensitivity of the number of cycles per truck to histogram construction is the same as the sensitivity of the total number of cycles to histogram construction. To compare histograms, the percent difference between the histograms was determined by

Width (psi)	Value
250	a
350	b
500	c
600	d
1000	e

Width (psi)	250	350	500	600	1000
250	(a-a)/a*100	(b-a)/b*100	(c-a)/c*100	(d-a)/d*100	(e-a)/e*100
350	(a-b)/a*100	(b-b)/b*100	(c-b)/c*100	(d-b)/d*100	(e-b)/e*100
500	(a-c)/a*100	(b-c)/b*100	(c-c)/c*100	(d-c)/d*100	(e-c)/e*100
600	(a-d)/a*100	(b-d)/b*100	(c-d)/c*100	(d-d)/d*100	(e-d)/e*100
1000	(a-e)/a*100	(b-e)/b*100	(c-e)/c*100	(d-e)/d*100	(e-e)/e*100

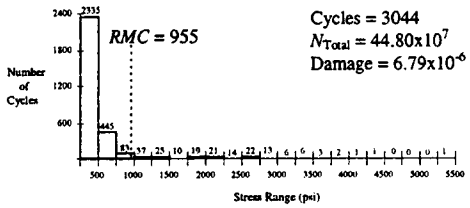
(4.7)

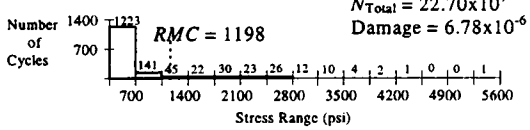
The percent difference was considered to be significant if the difference was greater than five percent.

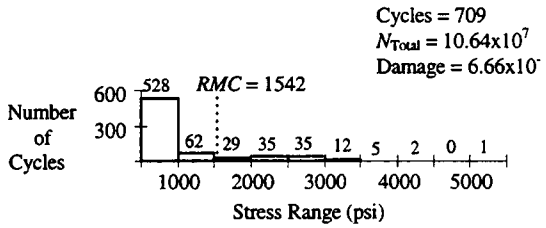
Evaluation Results and Discussion

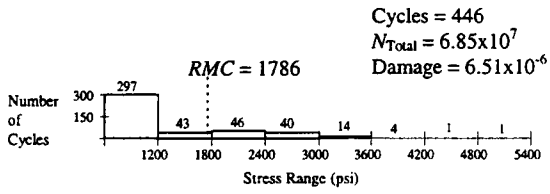
The effect of stress-range frequency-of-occurrence histogram construction on the *RMC* value, total number of cycles, total fatigue life, and fatigue damage is illustrated in Figure 4-10. Test results for both main and secondary bridge member details showed that as the interval width increased from 250 psi to 1000 psi, the *RMC* value increased while the number of intervals, the total number of cycles, and the total fatigue life decreased. For main member detail, the predicted fatigue damage decreased with increase in interval width. For secondary bridge member detail, interval width of 600 psi predicted the most damage while interval width of 1000 psi predicted the least amount of fatigue damage. The percent difference between the histograms of Figure 4-10 is shown in Table 4-7.

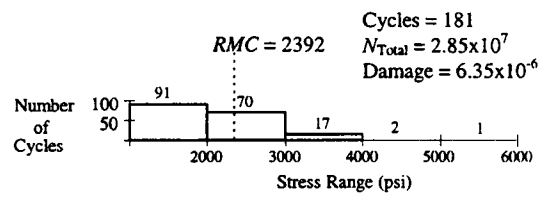
G52 - Main Bridge Member



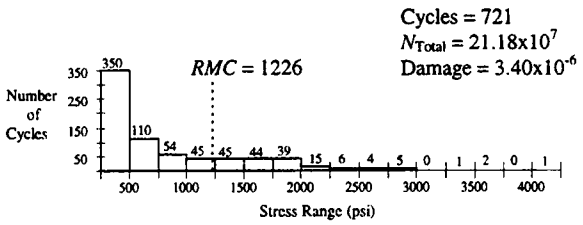


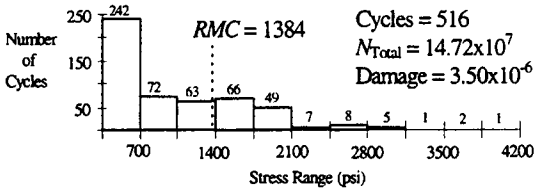


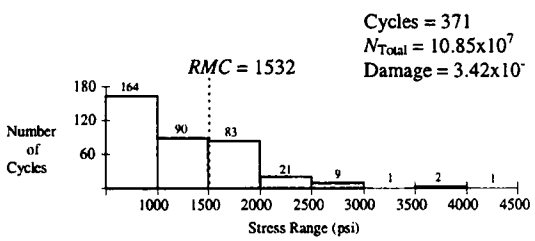


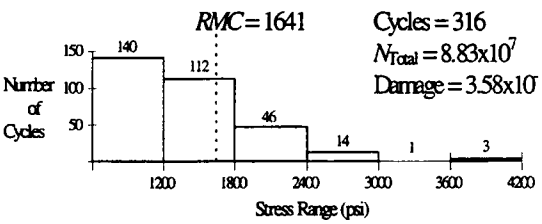


G318 - Secondary Bridge Member









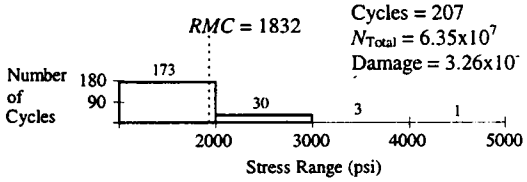


Figure 4-10. Category E' Detail Frequency-of-Occurrence Stress-Range Histogram for Histogram Interval Widths (from Top to Bottom) of 250 psi, 350 psi, 500 psi, 600 psi, and 1000 psi

Table 4-7. Percent Difference Results for Histograms of Gages G52 and G318

G52	Width (psi)	250	350	500	600	1000
RMC	250	0	20	38	47	60
	350	-25	0	22	33	50
	500	-61	-29	0	14	36
	600	-87	-49	-16	0	25
	1000	-150	-100	-55	-34	0
Cycles	250	0	-98	-329	-583	-1582
	350	49	0	-117	-245	-751
	500	77	54	0	-59	-292
	600	85	71	37	0	-146
	1000	94	88	74	59	0
N_{Total}	250	0	-97	-321	-554	-1472
	350	49	0	-113	-231	-696
	500	76	53	0	-55	-273
	600	85	70	36	0	-140
	1000	94	87	73	58	0
Damage	250	0	0	-2	-4	-7
	350	0	0	-2	-4	-7
	500	2	2	0	-2	-5
	600	4	4	2	0	-3
	1000	6	6	5	2	0

G318	Width (psi)	250	350	500	600	1000
RMC	250	0	11	20	25	33
	350	-13	0	10	16	24
	500	-25	-11	0	7	16
	600	-34	-19	-7	0	10
	1000	-49	-32	-20	-12	0
Cycles	250	0	-40	-94	-128	-248
	350	28	0	-39	-63	-149
	500	49	28	0	-17	-79
	600	56	39	15	0	-53
	1000	71	60	44	34	0
N_{Total}	250	0	-44	-95	-140	-234
	350	31	0	-36	-67	-132
	500	49	26	0	-23	-71
	600	58	40	19	0	-39
	1000	70	57	41	28	0
Damage	250	0	3	1	5	-4
	350	-3	0	-2	2	-7
	500	-1	2	0	4	-5
	600	-5	-2	-5	0	-10
	1000	4	7	5	9	0

Based on the results presented in Table 4-7, the following observations were made. The difference between the various histograms was greater for main bridge member details than for secondary bridge member details. For both main and secondary bridge member details, there was a significant difference between the various histograms in the *RMC* value, the total number of cycles, and the total fatigue life. With the exception of histograms with an interval width of 1000 psi, there was not a significant difference in fatigue damage between histograms for both main and secondary bridge member details. For all cases, histograms with an interval width of 1000 psi produced the greatest difference.

The main difference between the various histograms can be attributed to the first interval width. The stress range for this interval starts with a value equal to the interval width and ends with a value equal to twice the interval width, as shown in Figures 4-9 and 4-10. To eliminate this factor, two stress-range frequency-of-occurrence histograms were evaluated; one starting with 500 psi and the other with 1000 psi. The total number of cycles for histograms with interval widths of 250, 350, 500, 600, and 1000 psi was constant, as shown in Figure 4-9 (B). The results of this evaluation are presented in Tables 4-8 through 4-10. The *RMC* value and the total fatigue life for main and secondary bridge member details are presented in Tables 4-8 and 4-9, respectively. The fatigue damage for both main and secondary bridge member details is presented in Table 4-10.

Table 4-8. Histogram Construction Results for Bridge Main Member Details

			Stress Range Starting at 500 psi										
	Gage	Duration	Total	*RMC* (psi)					N_{Total} x 10^9 (Cycles)				
Category	No.	(hrs)	Cycles	250	350	500	600	1000	250	350	500	600	1000
A	G58C	1.081	362	1480	1496	1503	1501	1572	8.53	8.26	8.14	8.18	7.12
	G140	1.081	259	1525	1520	1532	1549	1591	7.8	7.87	7.69	7.44	6.87
	G143	1.081	197	1205	1193	1214	1234	1279	15.8	16.28	15.45	14.71	13.21
B	G30	1.029	6334	779	800	844	886	1056	24.7	22.78	19.4	16.77	9.91
	G83	1.029	1531	942	954	991	1030	1144	13.95	13.43	11.98	10.67	7.79
	G204	1.029	7201	713	744	804	847	1026	32.18	28.32	22.44	19.19	10.8
C	G58B	1.081	363	1662	1662	1680	1697	1712	0.957	0.957	0.927	0.899	0.876
E	G45	1.029	125	1211	1223	1233	1258	1250	0.287	0.291	0.279	0.282	0.247
	G46	1.029	549	1273	1292	1287	1314	1371	0.119	0.118	0.118	0.117	0.109
	G47	1.029	281	1456	1462	1468	1498	1548	0.347	0.342	0.338	0.324	0.294
E'	G52	1.029	709	1528	1521	1542	1537	1607	0.109	0.111	0.106	0.107	0.094
	G52A	1.029	493	2051	2053	2053	2058	2108	0.045	0.045	0.045	0.045	0.042
	G116	1.029	609	1434	1442	1447	1468	1515	0.132	0.13	0.129	0.123	0.112

			Stress Range Starting at 1000 psi										
	Gage	Duration	Total	*RMC* (psi)					N_{Total} x 10^9 (Cycles)				
Category	No.	(hrs)	Cycles	250	350	500	600	1000	250	350	500	600	1000
A	G58C	1.081	153	1929	1938	1953	1959	1979	3.85	3.8	3.71	3.68	3.57
	G140	1.081	135	1863	1871	1867	1860	1899	4.28	4.22	4.25	4.3	4.04
	G143	1.081	92	1484	1504	1497	1497	1575	8.46	8.13	8.24	8.24	7.08
B	G30	1.029	175	1897	1882	1908	1905	1925	1.71	1.75	1.69	1.69	1.64
	G83	1.029	146	1836	1855	1837	1867	1898	1.88	1.83	1.79	1.79	1.71
	G204	1.029	197	1569	1575	1586	1612	1660	3.02	2.99	2.78	2.78	2.55
C	G58B	1.081	165	2131	2146	2149	2146	2206	0.454	0.445	0.445	0.445	0.409
E	G45	1.029	69	1413	1432	1451	1453	1575	0.078	0.078	0.078	0.078	0.075
	G46	1.029	145	1907	1904	1904	1907	1956	0.046	0.047	0.046	0.047	0.046
	G47	1.029	108	1956	1950	1963	1959	1980	0.123	0.124	0.121	0.123	0.114
E'	G52	1.029	181	2355	2358	2359	2355	2392	0.03	0.03	0.03	0.03	0.028
	G52A	1.029	188	2803	2796	2803	2800	2802	0.018	0.018	0.018	0.018	0.018
	G116	1.029	198	2028	2020	2037	2027	2077	0.047	0.044	0.046	0.044	0.044

Table 4-9. Histogram Construction Results for Bridge Secondary Member Details

			Stress Range Starting at 500 psi										
	Gage	Duration	Total	*RMC* (psi)					N_{Total} x 10^9 (Cycles)				
Category	No.	(hrs)	Cycles	250	350	500	600	1000	250	350	500	600	1000
A	G35	1.029	139	904	898	973	922	1017	37.42	38.17	30.01	35.27	26.28
	G37	1.029	531	1704	1716	1710	1727	1753	5.59	5.47	5.53	5.37	5.13
	G41	1.029	307	897	915	952	957	1103	38.31	36.09	32.04	32.04	20.6
C	G32	1.028	127	752	758	784	811	1000	10.33	10.09	9.12	8.24	4.39
E	G105	1.029	1647	1458	1457	1477	1487	1535	0.33	0.331	0.318	0.311	0.283
	G120	1.029	2321	2637	2644	2641	2651	2663	0.056	0.055	0.056	0.055	0.054
	G305	1.029	4335	1187	1191	1218	1235	1331	0.207	0.203	0.205	0.199	0.19
E'	G317	1.019	201	1290	1284	1314	1291	1417	0.182	0.184	0.172	0.181	0.137
	G318	1.019	371	1523	1517	1532	1538	1610	0.11	0.112	0.109	0.107	0.094

			Stress Range Starting at 1000 psi										
	Gage	Duration	Total	*RMC* (psi)					N_{Total} x 10^9 (Cycles)				
Category	No.	(hrs)	Cycles	250	350	500	600	1000	250	350	500	600	1000
A	G35	1.029	43	1156	1186	1267	1321	1500	17.9	16.57	13.59	11.99	8.19
	G37	1.029	202	2319	2315	2318	2341	2360	2.22	2.23	2.22	2.16	2.1
	G41	1.029	43	1470	1488	1527	1484	1617	8.7	8.39	7.77	8.46	6.54
C	G32	1.028	5	1125	1175	1250	1300	1500	3.09	2.71	2.25	2	1.3
E	G105	1.029	471	2149	2163	2169	2173	2220	0.103	0.101	0.1	0.1	0.094
	G120	1.029	897	3604	3538	3615	3609	3638	0.022	0.021	0.022	0.022	0.021
	G305	1.029	291	2756	2764	2760	2755	2787	0.082	0.083	0.082	0.08	0.078
E'	G317	1.019	113	1519	1509	1548	1520	1547	0.111	0.114	0.105	0.111	0.105
	G318	1.019	207	1819	1830	1828	1852	1832	0.065	0.064	0.064	0.061	0.064

Table 4-10. Histogram Construction Fatigue Damage Results

Bridge Member	Category	Gage Number	Damage x 10^{-9} with SR Starting at 500 psi					Damage x 10^{-9} with SR Starting at 1000 psi				
			250	350	500	600	1000	250	350	500	600	1000
M	A	G58C	4.2	4.4	4.4	4.4	5.1	4.0	4.0	4.1	4.2	4.3
		G140	3.3	3.3	3.4	3.5	3.8	3.2	3.2	3.2	3.1	3.3
a		G143	1.2	1.2	1.3	1.3	1.5	1.1	1.1	1.1	1.1	1.3
i	B	G30	25.6	27.8	32.6	37.8	63.9	10.2	10.0	10.4	10.4	10.7
		G83	11.0	11.4	12.8	14.3	19.7	7.8	8.0	8.2	8.2	8.5
n		G204	22.4	25.4	32.1	37.5	66.7	6.5	6.6	7.1	7.1	7.7
	C	G58B	37.9	37.9	39.2	40.4	41.4	36.3	37.1	37.1	37.1	40.3
	E	G45	43.6	43.0	44.8	44.3	50.6	88.5	88.5	88.5	88.5	92.0
		G46	461.3	465.3	465.3	469.2	503.7	315.2	308.5	315.2	308.5	315.2
		G47	81.0	82.2	83.1	86.7	95.6	87.8	87.1	89.3	87.8	94.7
	E'	G52	650.5	638.7	668.9	662.6	754.3	603.3	603.3	603.3	603.3	646.4
		G52A	1095.6	1095.6	1095.6	1095.6	1173.8	1044.4	1044.4	1044.4	1044.4	1044.4
		G116	461.4	468.5	472.1	495.1	543.8	421.3	450.0	430.4	450.0	450.0
S	A	G35	0.4	0.4	0.5	0.4	0.5	0.2	0.3	0.3	0.4	0.5
e		G37	9.5	9.7	9.6	9.9	10.4	9.1	9.1	9.1	9.4	9.6
c		G41	0.8	0.9	1.0	1.0	1.5	0.5	0.5	0.6	0.5	0.7
o												
n	C	G32	1.2	1.3	1.4	1.5	2.9	0.2	0.2	0.2	0.3	0.4
d												
a	E	G105	499.1	497.6	517.9	529.6	582.0	457.3	466.3	471.0	471.0	501.1
r		G120	4144.6	4220.0	4144.6	4220.0	4298.1	4077.3	4271.4	4077.3	4077.3	4271.4
y		G305	2094.2	2135.5	2114.6	2178.4	2281.6	354.9	350.6	354.9	363.8	373.1
	E'	G317	110.4	109.2	116.9	111.0	146.7	101.8	99.1	107.6	101.8	107.6
		G318	337.3	331.3	340.4	346.7	394.7	318.5	323.4	323.4	339.3	323.4

Note: SR = Stress range histogram

Based on the results presented in Tables 4-8 through 4-10, the following observations were made. For fatigue Category A through E' details located in both main and secondary bridge members, the *RMC* value and the fatigue damage increased with increase in interval width, while the total fatigue life decreased with increase in interval width. The percent difference between the histograms of Tables 4-8 through 4-10 are presented in Tables 4-11 through 4-14. For main bridge member Category A details, there was not a significant difference in the *RMC* value for the various histograms. And, there was only a significant difference in the total fatigue life and damage for those

Table 4-11. Percent Difference Between Histograms for Bridge Main Member Details

Category	Gage Number	Width	RMC SR at 500 psi					N_{Total} SR at 500 psi					RMC SR at 1000 psi					N_{Total} SR at 1000 psi				
			250	350	500	600	1000	250	350	500	600	1000	250	350	500	600	1000	250	350	500	600	1000
A	G58C	250	0	-1	-2	-1	-6	0	3	5	4	20	0	0	-1	-2	-3	0	1	4	5	8
		350	1	0	0	0	-5	-3	0	1	1	16	0	0	-1	-1	-2	-1	0	2	3	6
		500	2	0	0	0	-4	-5	-2	0	0	14	1	1	0	0	-1	-4	-2	0	1	4
		600	1	0	0	0	-5	-4	-1	0	0	15	2	1	0	0	-1	-5	-3	-1	0	3
		1000	6	5	5	5	0	-17	-14	-13	-13	0	3	2	1	1	0	-7	-6	-4	-3	0
	G140	250	0	0	0	-2	-4	0	-1	1	5	14	0	0	0	0	-2	0	1	1	0	6
		350	0	0	-1	-2	-4	1	0	2	6	15	0	0	0	1	-2	-1	0	-1	-2	4
		500	0	1	0	-1	-4	-1	-2	0	3	12	0	0	0	0	-2	-1	1	0	-1	5
		600	2	2	1	0	-3	-5	-6	-3	0	8	0	-1	0	0	-2	0	2	1	0	6
		1000	4	5	4	3	0	-12	-13	-11	-8	0	2	2	2	2	0	-6	-4	-5	-6	0
	G143	250	0	1	-1	-2	-6	0	-3	2	7	20	0	-1	-1	-1	6	0	4	-3	3	20
		350	-1	0	-2	-3	-7	3	0	5	11	23	1	0	0	0	-5	-4	0	-1	-1	15
		500	0	2	0	-2	-5	-2	-5	0	5	17	1	0	0	0	-5	-3	1	0	0	17
		600	2	3	2	0	-4	-7	-10	-5	0	11	1	0	0	0	-5	-3	1	0	0	17
		1000	6	7	5	4	0	-16	-19	-15	-10	0	6	5	5	5	0	-16	-13	-14	-14	0
B	G30	250	0	-3	-8	-12	-26	0	8	27	47	149	0	1	-1	0	-2	0	2	2	1	5
		350	3	0	-5	-10	-24	-8	0	17	36	130	-1	0	-1	-1	-2	2	0	4	4	7
		500	8	6	0	-5	-20	-21	-15	0	16	96	1	1	0	0	-1	-2	-4	0	0	3
		600	14	11	5	0	-16	-32	-26	-14	0	69	0	1	0	0	-1	-1	-4	0	0	3
		1000	36	32	25	19	0	-60	-57	-49	-41	0	2	2	1	1	0	-4	-7	-3	-3	0
	G83	250	0	-1	-5	-9	-18	0	4	16	31	79	0	-1	0	-2	-3	0	30	0	5	11
		350	1	0	-4	-7	-17	-4	0	12	26	72	1	0	1	-1	-2	-3	0	-3	2	7
		500	5	4	0	-4	-13	-14	-11	0	12	54	0	-1	0	-2	-3	0	3	0	5	10
		600	9	8	4	0	-10	-24	-21	-11	0	37	2	1	2	0	-2	-5	-2	-5	0	5
		1000	21	20	15	11	0	-44	-42	-35	-27	0	3	2	3	2	0	-10	-7	-10	-5	0
	G204	250	0	-4	-11	-16	-31	0	14	43	68	198	0	0	-1	-3	-5	0	1	3	8	18
		350	4	0	-7	-12	-27	-12	0	26	48	162	0	0	-1	-2	-5	-1	0	2	7	17
		500	13	8	0	-5	-22	-30	-21	0	17	108	1	1	0	-2	-4	-3	-2	0	5	15
		600	19	14	5	0	-17	-40	-32	-14	0	78	3	2	2	0	-3	-8	-7	-5	0	9
		1000	44	38	28	21	0	-66	-62	-52	-44	0	6	5	5	3	0	-16	-15	-13	-8	0
C	G58B	250	0	0	0	-2	-4	0	0	3	6	9	0	0	0	0	-2	0	2	3	2	11
		350	0	0	-1	-2	-4	0	0	3	6	9	0	0	0	1	-2	-2	0	0	0	9
		500	0	1	0	-1	-4	-4	-3	0	3	6	0	0	0	0	-2	3	0	0	0	8
		600	2	2	1	0	-3	-6	-6	-3	0	3	0	-1	0	0	-2	-2	0	0	0	9
		1000	4	5	4	3	0	-9	-9	-6	-3	0	2	2	2	2	0	-10	-8	-8	-8	0

Note: SR = Stress-range frequency-of-occurrence histogram

Table 4-11. Continued

Category	Gage Number	Width	RMC SR at 500 psi					N_{Total} SR at 500 psi					RMC SR at 1000 psi					N_{Total} SR at 1000 psi				
			250	350	500	600	1000	250	350	500	600	1000	250	350	500	600	1000	250	350	500	600	1000
E	G45	250	0	-1	-2	-4	-3	0	-1	3	2	16	0	-1	-3	-3	-10	0	0	1	0	5
		350	1	0	-1	-3	-2	1	0	4	3	18	1	0	-1	-2	-9	0	0	0	0	4
		500	2	1	0	-2	-1	-3	-4	0	-1	13	3	1	0	0	-8	-1	0	0	-1	4
		600	4	3	2	0	1	-2	-3	1	0	14	3	2	0	0	-8	0	0	1	0	5
		1000	3	2	1	-1	0	-14	-15	-12	-13	0	12	10	9	8	0	-5	-4	-4	-5	0
	G46	250	0	-2	-1	-3	-7	0	0	0	1	9	0	0	0	0	-3	0	-1	0	0	0
		350	2	0	0	-2	-6	0	0	0	1	8	0	0	0	0	-3	1	0	1	0	1
		500	1	0	0	-2	-6	0	0	0	1	8	0	0	0	0	-3	0	-1	0	0	0
		600	3	2	2	0	-4	-1	-1	-1	0	7	0	0	0	0	-3	0	0	0	0	0
		1000	8	6	7	4	0	-8	-8	-8	-7	0	3	3	3	3	0	0	-1	0	0	0
	G47	250	0	0	-1	-3	-6	0	2	3	7	18	0	0	0	0	-1	0	-1	1	0	7
		350	0	0	0	-2	-6	-2	0	1	6	16	0	0	-1	0	-2	1	0	3	1	9
		500	1	0	0	-2	-5	-3	-1	0	4	15	0	1	0	0	-1	-1	-2	0	-1	6
		600	3	3	2	0	-3	-8	-5	4	0	10	0	0	0	0	-1	0	-1	1	0	8
		1000	6	6	5	3	0	-15	-14	-13	-9	0	1	2	1	1	0	-7	-8	-6	-7	0
E'	G52	250	0	0	-1	-1	-5	0	-1	3	2	16	0	0	0	0	-2	0	0	1	0	5
		350	0	0	-1	-1	-5	1	0	4	3	18	0	0	0	0	-1	0	0	0	0	4
		500	1	1	0	0	-4	-3	-4	0	-1	13	0	0	0	0	-1	-1	0	0	-1	4
		600	1	1	0	0	-4	-2	-3	1	0	14	0	0	0	0	-2	0	0	1	0	5
		1000	5	6	4	5	0	-14	-15	-12	-13	0	2	1	1	2	0	-5	-4	-4	-5	0
	G52A	250	0	0	0	0	-3	0	0	0	1	9	0	0	0	0	0	0	-1	0	0	0
		350	0	0	0	0	-3	0	0	0	1	8	0	0	0	0	0	1	0	1	0	1
		500	0	0	0	0	-3	0	0	0	1	8	0	0	0	0	0	0	-1	0	0	0
		600	0	0	0	0	-2	-1	-1	-1	0	7	0	0	0	0	0	0	0	0	0	0
		1000	3	3	3	2	0	-8	-8	-8	-7	0	0	0	0	0	0	0	-1	0	0	0
	G116	250	0	-1	-1	-2	-5	0	2	3	7	18	0	0	0	0	-2	0	-1	1	0	7
		350	1	0	0	-2	-5	-2	0	1	6	16	0	0	-1	0	-3	1	0	3	1	9
		500	1	0	0	-1	-5	-3	-1	0	4	15	0	1	0	0	-2	-1	-2	0	-1	6
		600	2	2	1	0	-3	-7	-5	-4	0	10	0	0	0	0	-2	0	-1	1	0	8
		1000	6	5	5	3	0	-15	-14	-13	9	0	2	3	2	2	0	-7	-8	-6	-7	0

Note: SR = Stress-range frequency-of-occurrence histogram

Table 4-12. Percent Difference Between Histograms for Secondary Member Details

	Gage		RMC SR at 500 psi					N_{Total} SR at 500 psi					RMC SR at 1000 psi					N_{Total} SR at 1000 psi				
Category	Number	Width	250	350	500	600	1000	250	350	500	600	1000	250	350	500	600	1000	250	350	500	600	1000
A	G35	250	0	1	-7	-2	-11	0	-2	25	6	42	0	4	-9	-12	-23	0	8	32	49	118
		350	-1	0	-8	-3	-12	2	0	27	8	45	-3	0	-12	-16	-26	-7	0	22	38	102
		500	8	8	0	6	-4	-20	-21	0	-15	14	10	14	0	-4	-16	-24	-18	0	13	66
		600	2	3	-5	0	-9	-6	-8	18	0	34	14	18	4	0	-12	-33	-28	-12	0	46
		1000	13	13	5	10	0	-30	-31	-12	-25	0	30	34	18	14	0	-54	-51	-40	-32	0
	G37	250	0	-1	0	-1	-3	0	2	1	4	9	0	0	0	-1	-2	0	-1	-1	3	5
		350	1	0	0	-1	-3	-2	0	-1	2	7	0	0	0	-1	-2	1	0	-1	3	6
		500	0	0	0	-1	-3	-1	1	0	3	8	0	0	0	-1	-2	1	1	0	4	6
		600	1	1	1	0	-2	-4	-2	-3	0	5	1	1	1	0	-1	-3	-3	-4	0	2
		1000	3	2	3	2	0	-8	-6	-7	-4	0	2	2	2	1	0	-5	-6	-6	-2	0
	G41	250	0	-2	-6	-6	-19	0	6	20	21	86	0	-1	-4	-1	-9	0	4	12	3	33
		350	2	0	-6	-6	-19	-6	0	13	14	75	1	0	-3	0	-8	-4	0	8	-1	28
		500	6	4	0	-1	-14	-16	-11	0	2	56	4	3	0	3	-6	-11	-7	0	-8	19
		600	7	5	1	0	-13	-18	-13	-2	0	53	1	0	-3	0	-8	-3	1	9	0	29
		1000	23	21	16	15	0	-46	-43	-36	-35	0	10	9	6	9	0	-25	-22	-16	-23	0
C	G32	250	0	-1	-4	-7	-25	0	2	13	25	135	0	-4	-10	-13	-25	0	14	37	54	137
		350	1	0	-4	-7	-25	-2	0	11	22	130	4	0	-6	-10	-22	-12	0	20	35	108
		500	4	3	0	-3	-22	-12	-10	0	11	108	11	6	0	-4	-17	-27	-17	0	12	73
		600	8	7	3	0	-19	-20	-18	-10	0	87	16	11	4	0	-13	-35	-26	-11	0	54
		1000	33	32	28	23	0	-57	-56	-52	-47	0	33	28	20	15	0	-58	-52	-42	-35	0
E	G105	250	0	0	-1	-2	-5	0	0	4	6	17	0	-1	-1	-1	-3	0	2	3	3	10
		350	0	0	-1	-2	-5	0	0	4	6	17	1	0	0	0	-3	-2	0	1	1	8
		500	1	1	0	-1	-4	-4	-4	0	2	12	1	0	0	0	-2	-3	-1	0	1	7
		600	2	2	1	0	-3	-6	-6	-2	0	10	1	0	0	0	-2	-3	-1	-1	0	7
		1000	5	5	4	3	0	-14	-14	-11	-9	0	3	3	2	2	0	-9	-8	-7	-6	0
	G120	250	0	0	0	-1	-1	0	1	0	2	3	0	2	0	0	-1	0	-5	1	0	3
		350	0	0	0	0	-1	-1	0	0	1	2	-2	0	-2	-2	-3	6	0	7	6	9
		500	0	0	0	0	-1	0	0	0	1	3	0	2	0	0	-1	-1	-6	0	0	2
		600	1	0	0	0	0	-2	-1	-1	0	1	0	2	0	0	-1	0	-6	0	0	2
		1000	1	1	1	0	0	-3	-2	-2	-1	0	1	3	1	1	0	-3	-8	-2	-2	0
	G305	250	0	-1	0	-1	-3	0	2	1	4	9	0	0	0	-1	-2	0	-1	0	3	5
		350	1	0	0	-1	2	-2	0	1	2	7	0	0	0	-1	-2	1	0	0	3	6
		500	0	0	0	-1	-3	-1	1	0	3	8	0	0	0	-1	-2	0	0	0	3	6
		600	1	1	1	0	-2	-4	-2	-3	0	5	0	1	1	0	-1	-3	-3	-3	0	2
		1000	3	2	3	2	0	0	-6	-7	-4	0	2	2	2	1	0	-5	-6	-5	-2	0
E'	G317	250	0	0	-2	0	-9	0	-1	6	0	33	0	1	-2	0	-2	0	-2	6	0	6
		350	0	0	-2	-1	-9	1	0	7	2	34	-1	0	-3	-1	-3	2	0	8	2	8
		500	2	2	0	2	-7	-5	-7	0	-5	25	2	3	0	2	0	-6	-7	0	-5	0
		600	0	1	-2	0	-9	0	-2	5	0	32	0	1	-2	0	-2	0	-2	6	0	5
		1000	10	10	8	10	0	-25	-26	-20	-24	0	2	3	0	2	0	-5	-7	0	-5	0
	G318	250	0	0	-1	-1	-5	0	-1	2	3	18	0	-1	-1	-2	-1	0	2	2	6	2
		350	0	0	-1	-1	-6	1	0	3	4	20	1	0	0	-1	0	-2	0	0	4	0
		500	1	1	0	0	-5	-2	-3	0	1	16	1	0	0	-1	0	-2	0	0	4	1
		600	1	1	0	0	-4	-3	-4	-1	0	15	2	1	1	0	1	-5	-4	-4	0	-3
		1000	6	6	5	5	0	-15	-16	-14	-13	0	1	0	0	-1	0	-2	0	-1	3	0

Note: SR = Stress-range frequency-of-occurrence histogram

Table 4-13. Percent Difference Between Histograms for Fatigue Damage of Bridge Main Member Details

Fatigue	Gage		Damage SR at 500 psi					Damage SR at 1000 psi				
Category	Number	Width	250	350	500	600	1000	250	350	500	600	1000
A	G58C	250	0	3	5	4	17	0	1	4	4	7
		350	-3	0	1	1	14	-1	0	2	3	6
		500	-5	-1	0	0	13	-4	-2	0	1	4
		600	-4	-1	0	0	13	-5	-3	-1	0	3
		1000	-20	-16	-14	-15	0	-8	-6	-4	-3	0
	G140	250	0	-1	1	5	12	0	1	1	0	6
		350	1	0	2	5	13	-1	0	-1	-2	4
		500	-1	-2	0	3	11	-1	1	0	-1	5
		600	-5	-6	-3	0	8	0	2	1	0	6
		1000	-14	-15	-12	-8	0	-6	-4	-5	-6	0
	G143	250	0	-3	2	7	16	0	4	3	3	16
		350	3	0	5	10	19	-4	0	-1	-1	13
		500	-2	-5	0	5	14	-3	1	0	0	14
		600	-7	-11	-5	0	10	-3	1	0	0	14
		1000	-20	-23	-17	-11	0	-19	-15	-16	-16	0
B	G30	250	0	8	21	32	60	0	-2	1	1	4
		350	-8	0	15	26	56	2	0	3	3	6
		500	-27	-17	0	14	49	-1	-4	0	0	3
		600	-47	-36	-16	0	41	-1	-4	0	0	3
		1000	-149	-130	-96	-69	0	-4	-7	-3	-3	0
	G83	250	0	4	14	24	44	0	3	5	5	9
		350	-4	0	11	21	42	-3	0	2	2	7
		500	-16	-12	0	11	35	-5	-2	0	0	4
		600	-31	-26	-12	0	27	-5	-2	0	0	4
		1000	-79	-72	-54	-37	0	-10	-7	-5	-5	0
	G204	250	0	12	30	40	66	0	1	8	8	16
		350	-14	0	21	32	62	-1	0	7	7	15
		500	-43	-26	0	14	52	-9	-8	0	0	8
		600	-68	-48	-17	0	44	-9	-8	0	0	8
		1000	-198	-162	-108	-78	0	-18	-17	-9	-9	0
C	G58B	250	0	0	3	6	8	0	2	2	2	10
		350	0	0	3	6	8	-2	0	0	0	8
		500	-3	-3	0	3	6	-2	0	0	0	8
		600	-6	-6	-3	0	3	-2	0	0	0	8
		1000	-9	-9	-6	-3	0	-11	-9	-9	-9	0

Note: SR = Stress-range frequency-of-occurrence histogram

Table 4-13. Continued

Fatigue Category	Gage Number	Width	Damage SR at 500 psi					Damage SR at 1000 psi				
			250	350	500	600	1000	250	350	500	600	1000
E	G45	250	0	-1	3	2	14	0	0	0	0	4
		350	1	0	4	3	15	0	0	0	0	4
		500	-3	-4	0	-1	11	0	0	0	0	4
		600	-2	-3	1	0	12	0	0	0	0	4
		1000	-16	-18	-13	-14	0	-4	-4	-4	-4	0
	G46	250	0	1	1	2	8	0	-2	0	-2	0
		350	-1	0	0	1	8	2	0	2	0	2
		500	-1	0	0	1	8	0	-2	0	-2	0
		600	-2	-1	-1	0	7	2	0	2	0	2
		1000	-9	-8	-8	-7	0	0	-2	0	-2	0
	G47	250	0	1	3	7	15	0	-1	2	0	7
		350	-1	0	1	5	14	1	0	2	1	8
		500	-3	-1	0	4	13	-2	-2	0	-2	6
		600	-7	-6	-4	0	9	0	-1	2	0	7
		1000	-18	-16	-15	-10	0	-8	-9	-6	-8	0
E'	G52	250	0	-2	3	2	14	0	0	0	0	7
		350	2	0	5	4	15	0	0	0	0	7
		500	-3	-5	0	-1	11	0	0	0	0	7
		600	-2	-4	1	0	12	0	0	0	0	7
		1000	-16	-18	-13	-14	0	-7	-7	-7	-7	0
	G52A	250	0	0	0	0	7	0	0	0	0	0
		350	0	0	0	0	7	0	0	0	0	0
		500	0	0	0	0	7	0	0	0	0	0
		600	0	0	0	0	7	0	0	0	0	0
		1000	-7	-7	-7	-7	0	0	0	0	0	0
	G116	250	0	2	2	7	15	0	6	2	6	6
		350	-2	0	1	5	14	-7	0	-5	0	0
		500	-2	-1	0	5	13	-2	4	0	4	4
		600	-7	-6	-5	0	9	-7	0	-5	0	0
		1000	-18	-16	-15	-10	0	-7	0	-5	0	0

Note: SR = Stress-range frequency-of-occurrence histogram

Table 4-14. Percent Difference Between Histograms for Fatigue Damage of Bridge Secondary Member Details

Fatigue	Gage		Damage SR at 500 psi					Damage SR at 1000 psi				
Category	Number	Width	250	350	500	600	1000	250	350	500	600	1000
A	G35	250	0	-2	20	6	30	0	7	24	33	54
		350	2	0	21	8	31	-8	0	18	28	51
		500	-25	-27	0	-18	12	-32	-22	0	12	40
		600	-6	-8	15	0	25	-49	-38	-13	0	32
		1000	-42	-45	-14	-34	0	-119	-102	-66	-46	0
	G37	250	0	2	1	4	8	0	0	0	3	5
		350	-2	0	-1	2	6	0	0	0	3	6
		500	-1	1	0	3	7	0	0	0	3	5
		600	-4	-2	-3	0	4	-3	-3	-3	0	3
		1000	-9	-7	-8	-5	0	-6	-6	-6	-3	0
	G41	250	0	6	16	16	46	0	4	11	3	25
		350	-6	0	11	11	43	-4	0	7	-1	22
		500	-20	-13	0	0	36	-12	-8	0	-9	16
		600	-20	-13	0	0	36	-3	1	8	0	23
		1000	-86	-75	-56	-56	0	-33	-28	-19	-29	0
C	G32	250	0	2	12	20	58	0	12	27	35	58
		350	-2	0	10	18	56	-14	0	17	26	52
		500	-13	-11	0	10	52	-37	-20	0	11	42
		600	-25	-22	-11	0	47	-55	-36	-13	0	35
		1000	-135	-130	-108	-88	0	-138	-108	-73	-54	0
E	G105	250	0	0	4	6	14	0	2	3	3	9
		350	0	0	4	6	15	-2	0	1	1	7
		500	-4	-4	0	2	11	-3	-1	0	0	6
		600	-6	-6	-2	0	9	-3	-1	0	0	6
		1000	-17	-17	-12	-10	0	-10	-7	-6	-6	0
	G120	250	0	2	0	2	4	0	5	0	0	5
		350	-2	0	-2	0	2	-5	0	-5	-5	0
		500	0	2	0	2	4	0	5	0	0	5
		600	-2	0	-2	0	2	0	5	0	0	5
		1000	-4	-2	-4	-2	0	-5	0	-5	-5	0
	G305	250	0	2	1	4	8	0	-1	0	2	5
		350	-2	0	-1	2	6	1	0	1	4	6
		500	-1	1	0	3	7	0	-1	0	2	5
		600	-4	-2	-3	0	5	-3	-4	-3	0	3
		1000	-9	-7	-8	-5	0	-5	-6	-5	-3	0
E'	G317	250	0	-1	5	1	25	0	-3	5	0	5
		350	1	0	7	2	26	3	0	8	3	8
		500	-6	-7	0	-5	20	-6	-9	0	-6	0
		600	-1	-2	5	0	24	0	-3	5	0	5
		1000	-33	-34	-26	-32	0	-6	-9	0	-6	0
	G318	250	0	-2	1	3	15	0	2	2	6	2
		350	2	0	3	4	16	-2	0	0	5	0
		500	-1	-3	0	2	14	-2	0	0	5	0
		600	-3	-5	-2	0	12	-7	-5	-5	0	-5
		1000	-17	-19	-16	-14	0	-2	0	0	5	0

Note: SR = Stress-range frequency-of-occurrence histogram

histograms with an interval width of 1000 psi. For main bridge member Category B details, there was a significant difference in the *RMC* value, the total fatigue life, and the fatigue damage for histograms with various interval widths that started at 500 psi. There was a significant difference in the total fatigue life and damage for those histograms that started at 1000 psi, while there was not a significant difference in its *RMC* values. For all histograms, with exception of those with interval width of 1000 psi, there was not a significant difference in the *RMC* value, the total fatigue life, and the fatigue damage for main member fatigue Categories C, E, and E' details. For all secondary bridge member details and histograms, with exception of those histograms with an interval width of 1000 psi and *RMC* values less than 1000 psi, there was not a significant difference in the *RMC* value, the total fatigue life, and the fatigue damage between the various histogram interval widths.

4.4 Test Duration

Fatigue field test duration should be long enough to incorporate the effect of truck traffic flow on the effective stress range (*RMC*) and the number of cycles per truck (*CPT*). While collecting field data, most researchers (Fisher et al., 1984; King et al., 1976; Moses et al., 1974; Hanson et al., 1991; Shaaban, 1985; Yen et al., 1990; Chen, 1992) considered the *CPT* to be equal to one and therefore were only concerned with collecting enough data to provide a realistic representation of traffic flow with regards to the *RMC* value. Fatigue life is not only dependent on the effective stress range but also on the number of cycles per truck. The effect of field test duration on the effective stress range and the number of cycles per truck are evaluated.

Evaluation Procedure

The sensitivity of the effective stress range and the number of cycles per truck to test duration is examined by using field data taken under normal traffic. Table 4-15 provides a summary of the various bridge details that were instrumented for this evaluation. Included in this table is the page number of the drawing in the Appendix that shows the gage location. The data for each strain gage was collected in one-hour segments. The raw data was reviewed for any erroneous readings and then reduced using the rainflow cycle counting method. A stress-range frequency-of-occurrence histogram starting at 1000 psi with an interval width of 500 psi was constructed for each hour of recorded strain gage data. In addition to the strain gage data collection, tallies of truck traffic data were also collected for each test. Equation (4.1) was used to determine the *RMC* value. The number of cycles per truck, *CPT*, is given by

$$\text{CPT} = \frac{n_t}{T} \tag{4.8}$$

in which, for a given test duration, n_t is the total number of cycles and T is the one-way total number of trucks (excluding 2-axle/6-wheel trucks). The total fatigue life based on AASHTO *Guide* (1990) specifications was also calculated. The total fatigue life, Y_t, is given by

$$Y_t = \frac{(K)\left(10^6\right)}{T_a\, C\left(R_s\, S_r\right)^3} \tag{4.9}$$

in which T_a is the estimated lifetime average daily truck volume (*ADTT*) in the outer lane, C is the number of cycles per truck (*CPT*), R_s is a reliability factor, S_r is the effective

Table 4-15. Summary of Test Duration Details

Bridge Member	Fatigue Category	Gage No.	Detail Description	Drawing Page No.
Main	A	G58D	Top of girder bottom flange near flange edge	207
	B	G5	Top of girder bottom flange near the web-to-flange weld	199
		G58	"	207
	C	G58B	Bottom of girder bottom flange at a change in flange thickness	207
	E	G47	Above drilled hole for a six inch tear in girder web	200
	E'	G51	Girder horizontal web gap near the lateral gusset plate weld	204
		G73	"	206
		G110	"	193
		G116	Girder web at end of lateral gusset plate weld	193
Secondary	A	G35	Cross frame truss diagonal	202
	B	G2	Bottom flange of cantilever bracket near the web-to-flange weld	199
	C	G32	Cross-frame bottom chord near gusset plate vertical weld	202
	E	G34	Cross-frame bottom chord at end of gusset plate weld	202
		G105	End of floorbeam flange termination weld	191
		G305	"	213
	E'	G117	Floorbeam bottom flange at end of gusset plate weld	196
		G317	"	213

stress range (*RMC*), and K is a detail constant. For this evaluation, T_a was taken as 5600, R_s as 1.1475, and K as 68, 33, 12, 2.9, and 1.1 for Categories A, B, C, E, and E' details, respectively.

Two evaluation procedures were employed in determining the sufficient length of time required for field testing of fatigue prone details. In the first procedure, the effective stress range (*RMC*), the number of cycles per truck (*CPT*), and the total fatigue life (Y_t) were calculated for each test segment, as shown in Table 4-16. In addition, the percent difference for the *RMC*, the *CPT*, and total life were calculated. The percent difference is given by

$$\%\ Diff. = \frac{Data\ Value\ (RMC, CPT, or\ Life) - Corresponding\ Total\ Test\ Duration\ Value}{Corresponding\ Total\ Test\ Duration\ Value} \times 100\% \qquad (4.10)$$

Table 4-16. Test Duration Example Calculation for Gage 58D

Stress Range	Test Duration Segments													
	One Hour						Two Hour			Three Hour		Four Hour	Five Hour	Total
(psi)	A	B	C	D	E	F	A+B	C+D	E+F	A+B+C	D+E+F	A+B+C+D	A+B+C+D+E	A+B+C+D+E+F
1000 - 1500	62	57	61	47	56	51	119	108	107	180	154	227	283	334
1500 - 2000	43	35	39	44	50	54	78	83	104	117	148	161	211	265
2000 - 2500	28	20	27	23	27	31	48	50	58	75	81	98	125	156
2500 - 3000	14	21	18	18	11	13	35	36	24	53	42	71	82	95
3000 - 3500	0	6	6	4	1	8	6	10	9	12	13	16	17	25
3500 - 4000	1	1	1	1	0	2	2	2	2	3	3	4	4	6
4000 - 4500		1	1	1	1	1	1	2	2	2	3	3	4	5
4500 - 5000				0				0			0	0	0	0
5000 - 5500				1				1			1	1	1	1
Time (hrs)	1.081	1.081	1.081	1.072	1.061	1.066	2.162	2.153	2.128	3.244	3.200	4.316	5.377	6.443
No. Cycles	148	141	153	139	146	160	289	292	306	442	445	581	727	887
Total Trucks	442	411	446	415	441	452	853	861	893	1299	1308	1714	2155	2607
RMC (psi)	1900	2096	2064	2147	1915	2094	2000	2104	2012	2023	2056	2054	2027	2040
CPT	0.335	0.343	0.343	0.335	0.331	0.354	0.339	0.339	0.343	0.340	0.340	0.339	0.337	0.340
Life (yrs)	3497	2544	2665	2424	3457	2472	2963	2545	2877	2855	2720	2736	2863	2784
%Diff. RMC	7	-3	-1	-5	6	-3	2	-3	1	1	-1	-1	1	0
%Diff. CPT	2	-1	-1	1	3	-4	0	0	-1	0	0	0	1	0
%Diff. Life	-26	9	4	13	-24	11	-6	9	-3	-3	2	2	-3	0

Plots of test duration versus *RMC*, *CPT*, and life were made to determine the sufficient length of time required for field testing of fatigue prone details. Sufficient length of time was defined as the test duration in which the scatter in the data converges to a single value. It was assumed that the total test duration was long enough for the scatter in the data to converge, that is, it was long enough to sufficiently incorporate the effect of the variation in truck traffic flow on the *RMC* value and the *CPT* value. Also, based on equation (4.10), plots of the percent difference in the *RMC*, *CPT*, and life versus test duration were made. A percent difference greater than 5% was considered to be significant. The required field test duration was determined to be the duration at which the data was within $\pm$ 5% of the total test duration's value.

The second evaluation procedure tests the hypothesis that for a linearly elastic system, as the one-hour truck count approaches the average hourly truck traffic volume (*AHTT*), then its corresponding one-hour *RMC* and *CPT* values approach the total test duration's *RMC* and *CPT* values. If the hypothesis is true, then one hour of field test duration is sufficient as long as the data is collected at a time of day when the one-hour truck count approaches the *AHTT*. This hypothesis was tested by plotting the individual one hour test duration's *RMC* value, *CPT*, and truck count versus the time of day in which the data was recorded. Along with these individual test data points, the total test duration's *RMC*, *CPT*, and *AHTT* was also be plotted. The *AHTT* was obtained by dividing the average daily truck traffic volume (*ADTT*) by 24. The *ADTT* was obtained from tallies of truck traffic recorded during testing.

Evaluation Results and Discussion

The effect of test duration on the effective stress range, the number of cycles per truck, and the total fatigue life for bridge main member fatigue prone details is illustrated in Figures 4-11 through 4-20. Based on the results presented in these figures, the following observations were made. The scatter in the data decreased with increase in test duration, that is, the data converged to a single value as test duration was increased. For all fatigue prone details, the *RMC* values converged at a faster rate than the *CPT* and fatigue life values. With exception of fatigue Category B gages G5 and G58 and Category E' gage G110, the *RMC* value for all other gages converged to within 5% of their total test duration's *RMC* value at a test duration of two hours. Gages G5 and G58 are identical details located on the eastbound and westbound fascia girders, respectively. Figures 4-12 and 4-13 show that gages G5 and G58's *RMC* values converged to within 5% of their total test duration's *RMC* value after 3 and 15 hours of testing, respectively. It took longer for gage G58's data points to converge due to the presence of an outlier data point (*RMC* value of 2100 psi). Once this data point was removed, the remaining data points converge at a faster rate, as shown in Figure 4-14. At a test duration of 2 hours and 5 hours, the *RMC* values were within 7% and 5% of the total test duration's *RMC* value, respectively. Gages G51, G73, and G110 are identical web gap details located in the eastbound second span, westbound second span, and eastbound first span, respectively. At a test duration of 2 hours, gages G51 and G73's RMC values were within 5% of their total test duration's *RMC* value, as shown in Figures 4-17 and 4-18. Figure 4-19 shows that at a test duration of 6 hours and 10 hours, gage G110's *RMC*

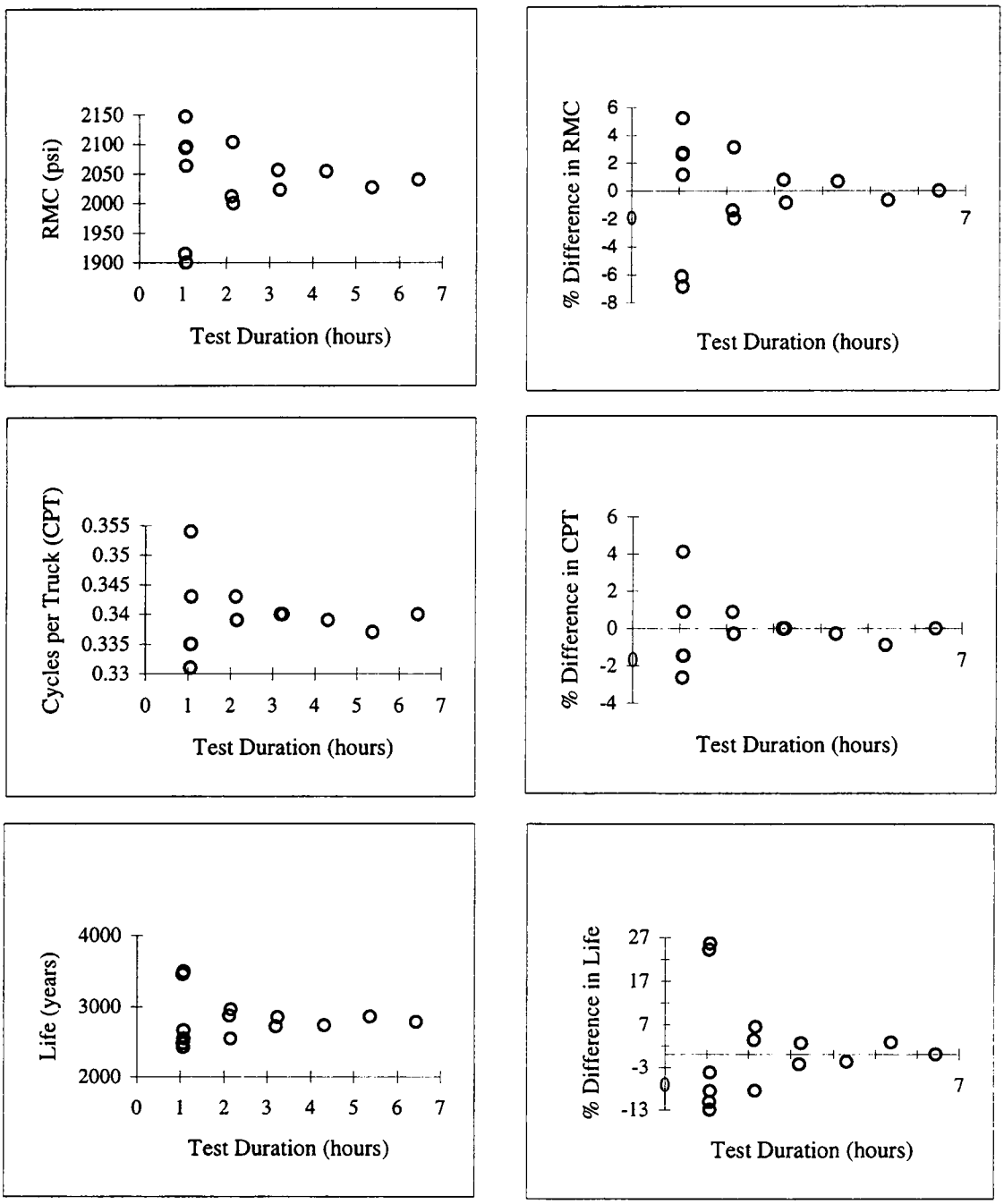


Figure 4-11. The Effect of Field Test Duration on the Effective Stress Range (RMC), the Number of Cycles Per Truck (CPT), and the Total Fatigue Life for Category A Main Bridge Member Detail, Gage G58D

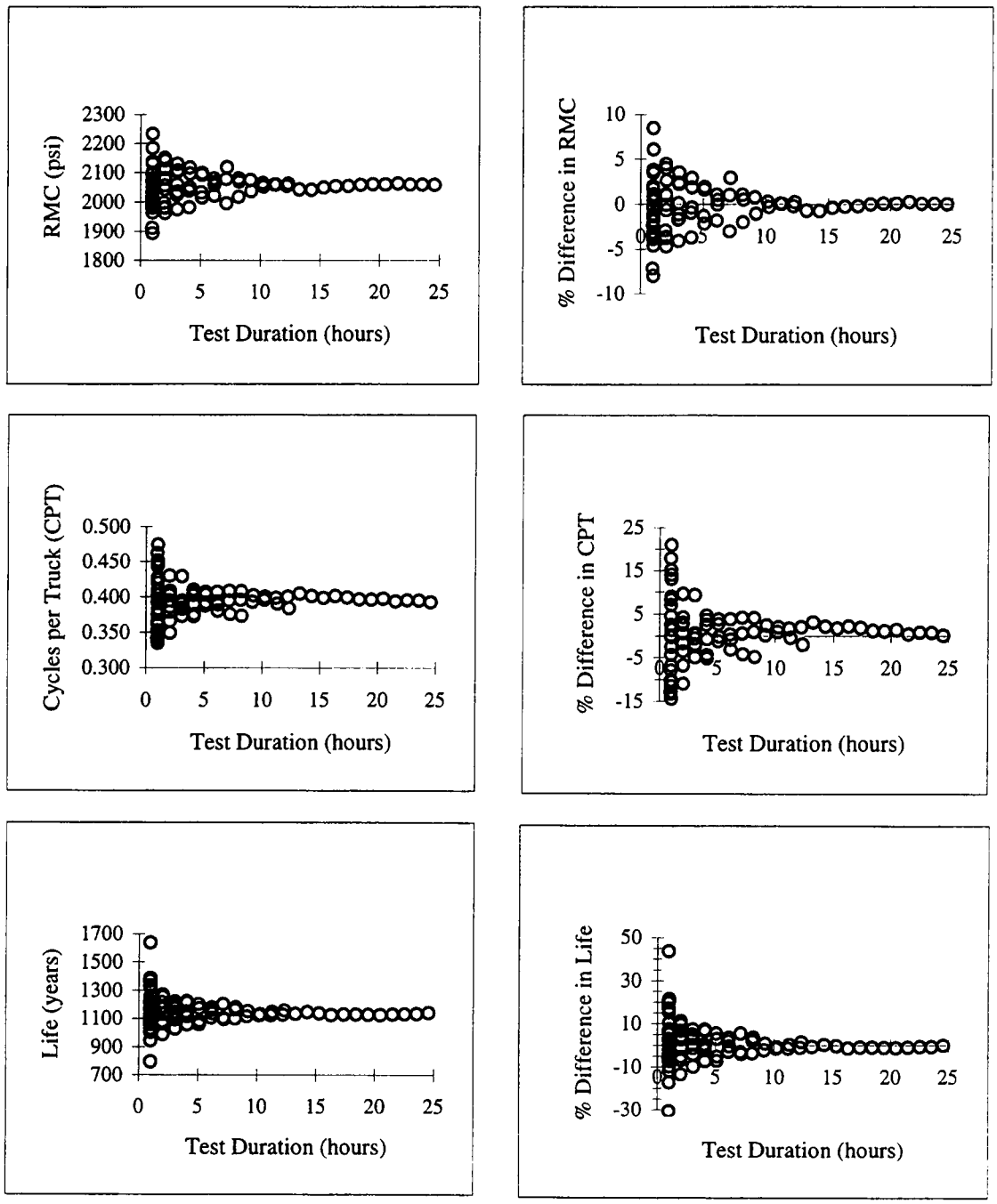


Figure 4-12. The Effect of Field Test Duration on the Effective Stress Range (RMC), the Number of Cycles Per Truck (CPT), and the Total Fatigue Life for Category B Main Bridge Member Detail, Gage G5

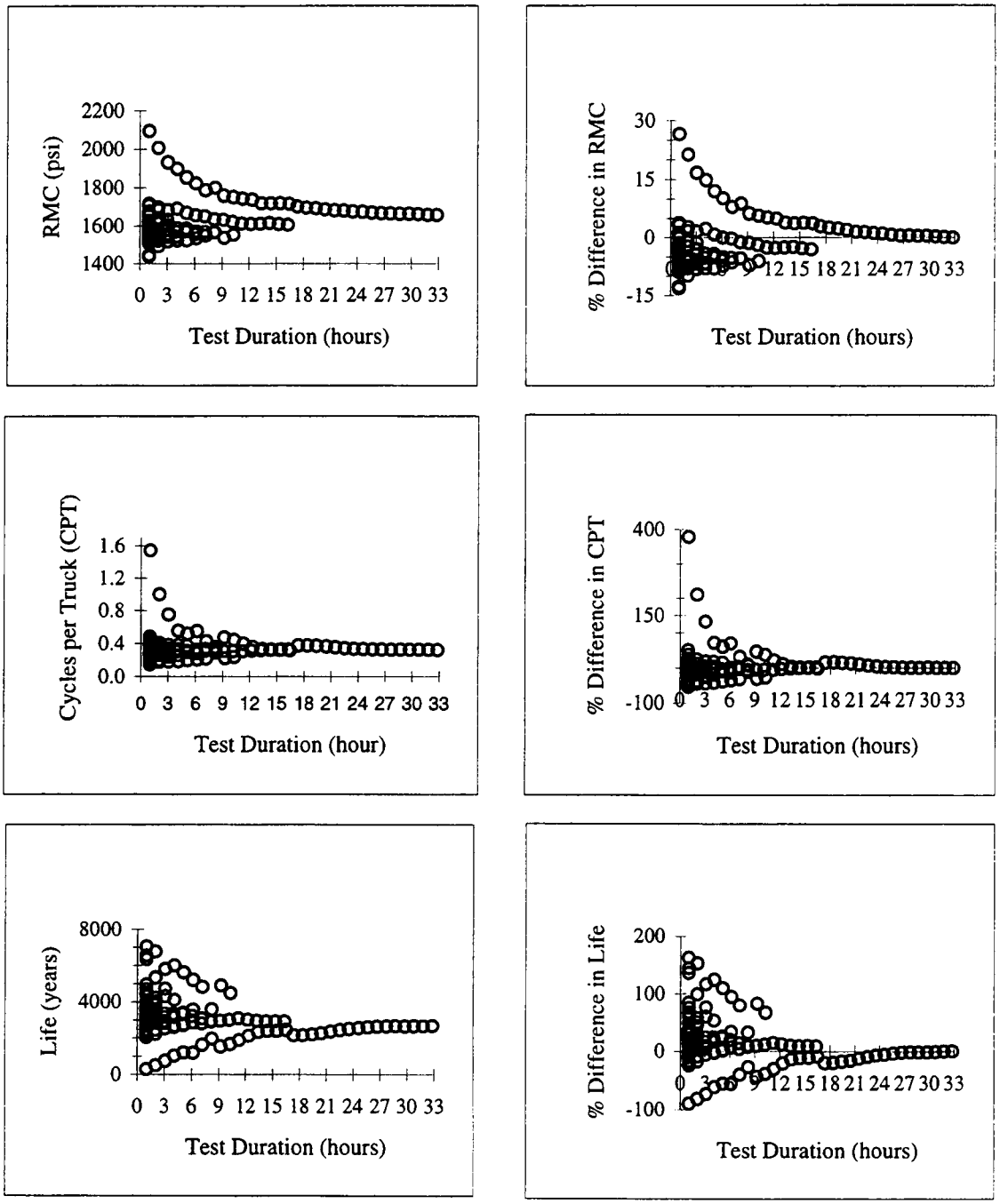


Figure 4-13. The Effect of Field Test Duration on the Effective Stress Range (RMC), the Number of Cycles Per Truck (CPT), and the Total Fatigue Life for Category B Main Bridge Member Detail, Gage G58

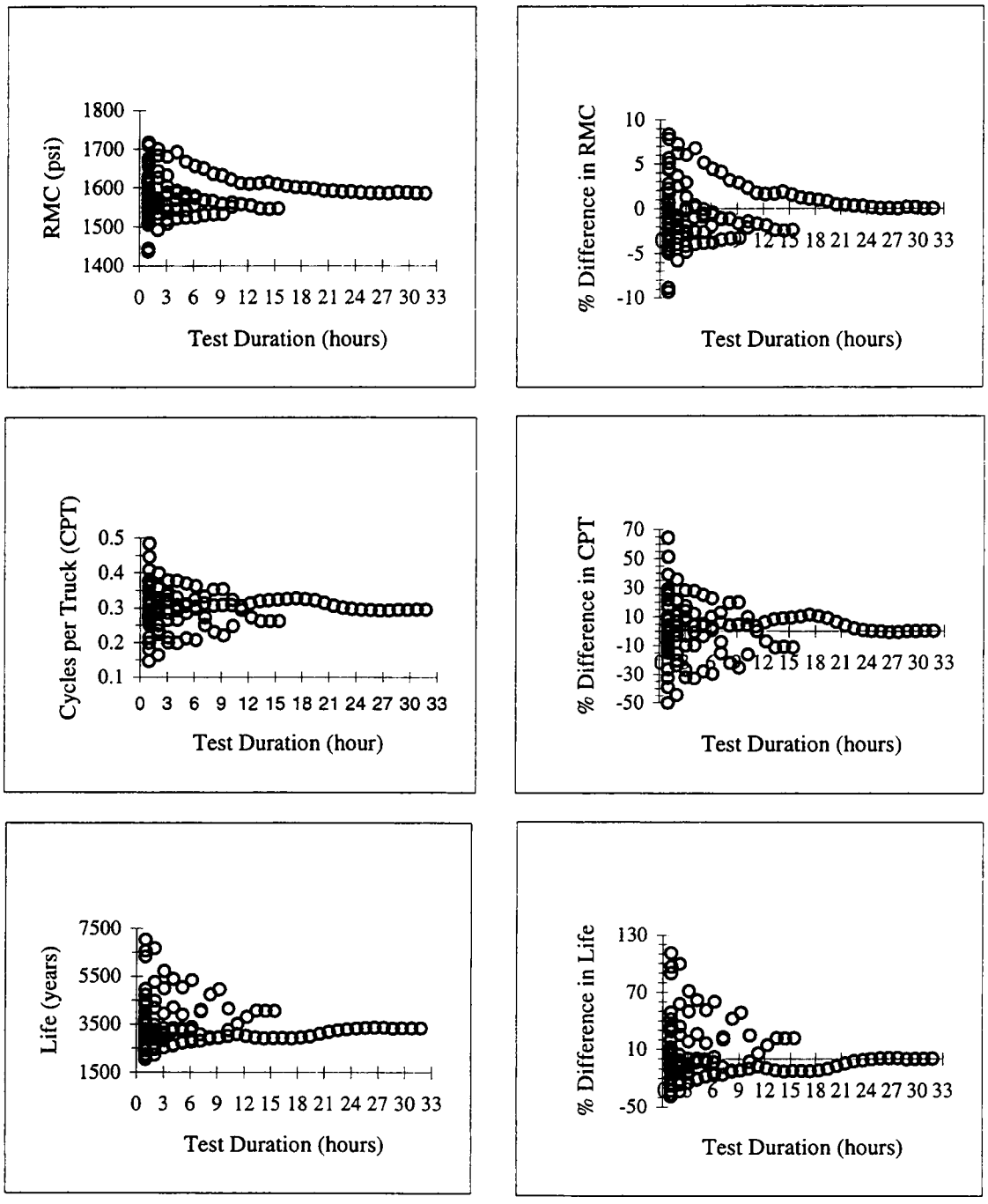


Figure 4-14. The Effect of Field Test Duration on the Effective Stress Range (RMC), the Number of Cycles Per Truck (CPT), and the Total Fatigue Life for Category B Main Bridge Member Detail, Gage G58 (Without Outlier Data Point)

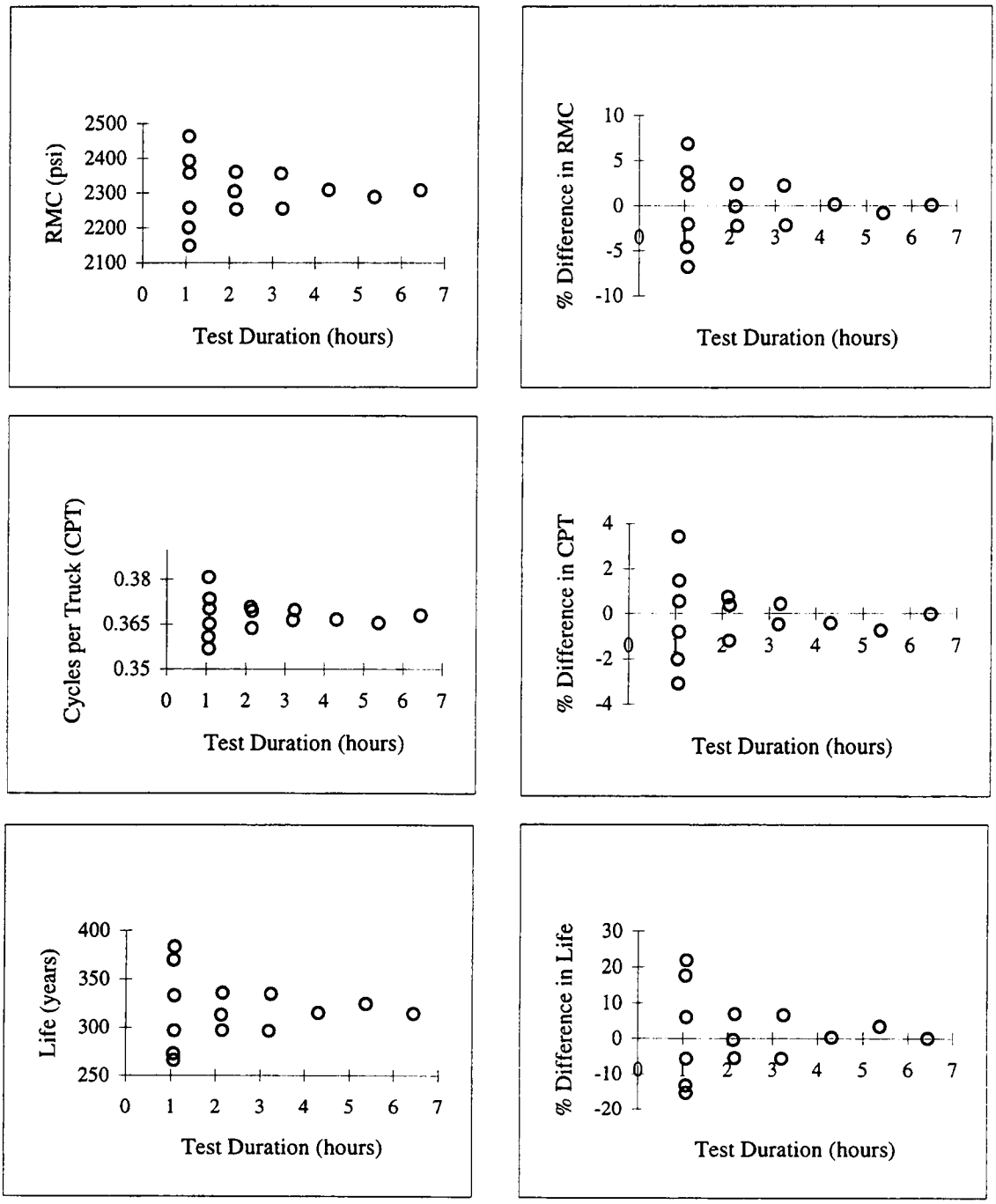


Figure 4-15. The Effect of Field Test Duration on the Effective Stress Range (RMC), the Number of Cycles Per Truck (CPT), and the Total Fatigue Life for Category C Main Bridge Member Detail, G58B

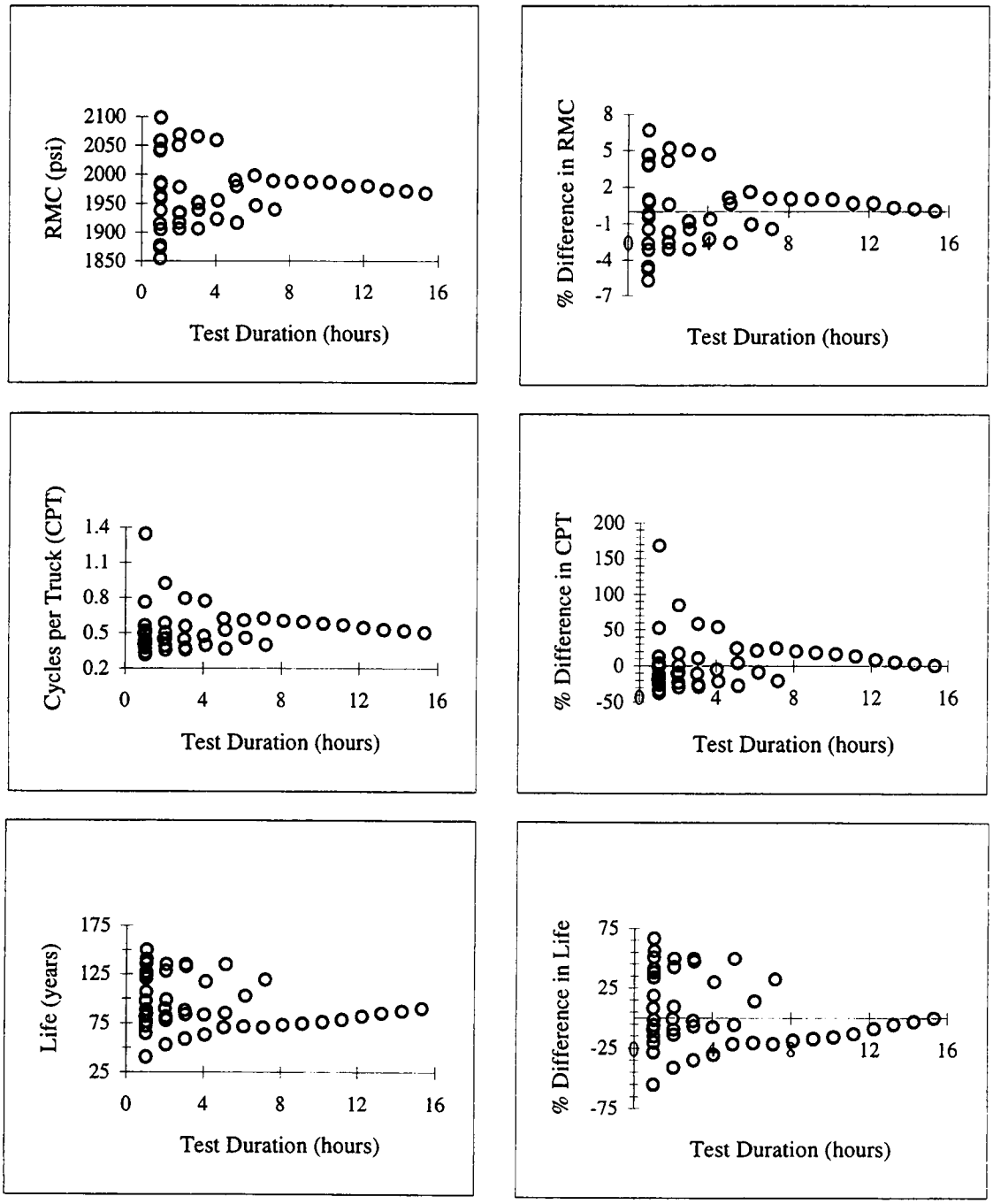


Figure 4-16. The Effect of Field Test Duration on the Effective Stress Range (RMC), the Number of Cycles Per Truck (CPT), and the Total Fatigue Life for Category E Main Bridge Member Detail, Gage G47

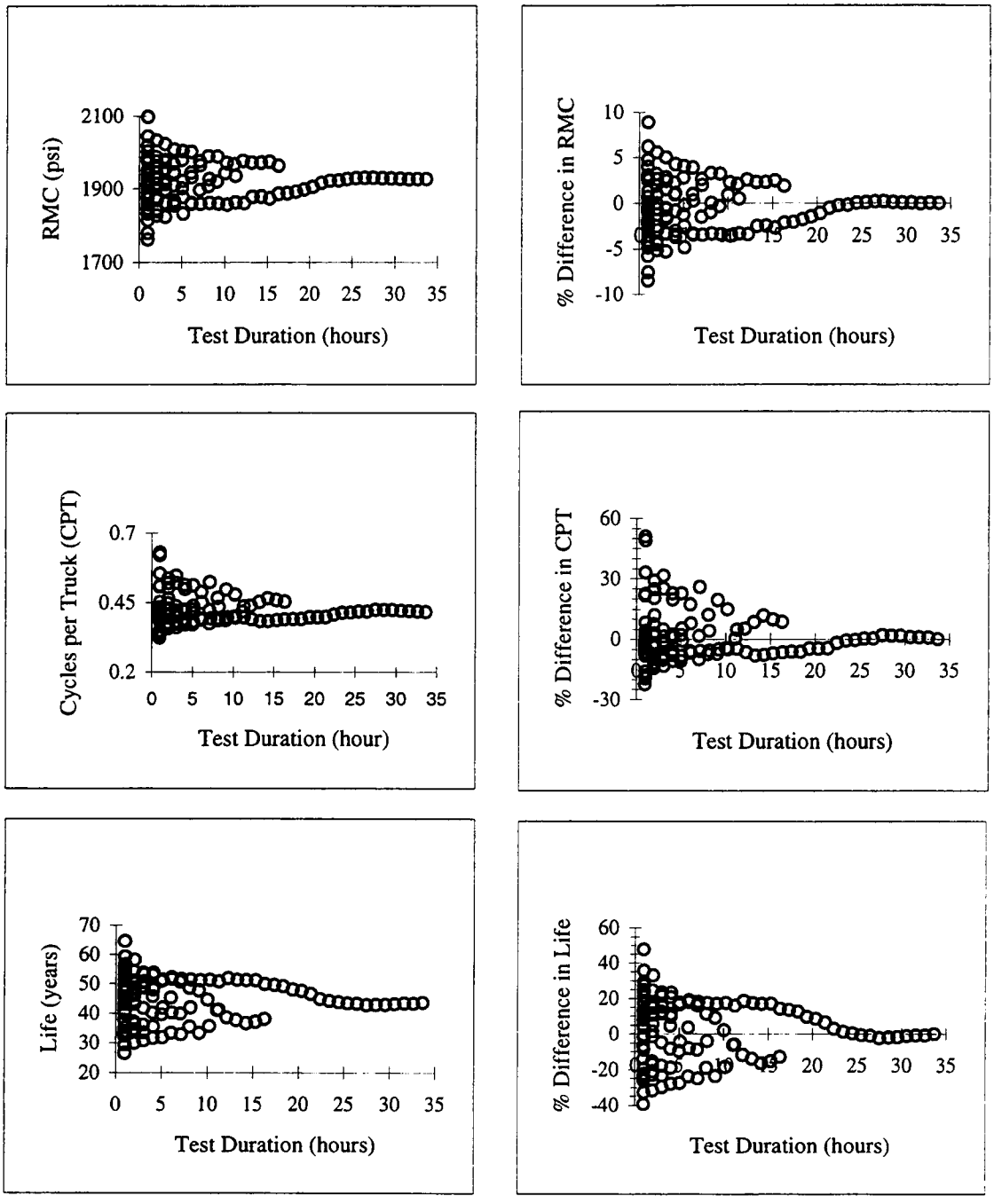


Figure 4-17. The Effect of Field Test Duration on the Effective Stress Range (RMC), the Number of Cycles Per Truck (CPT), and the Total Fatigue Life for Category E' Main Bridge Member Detail, Gage G51

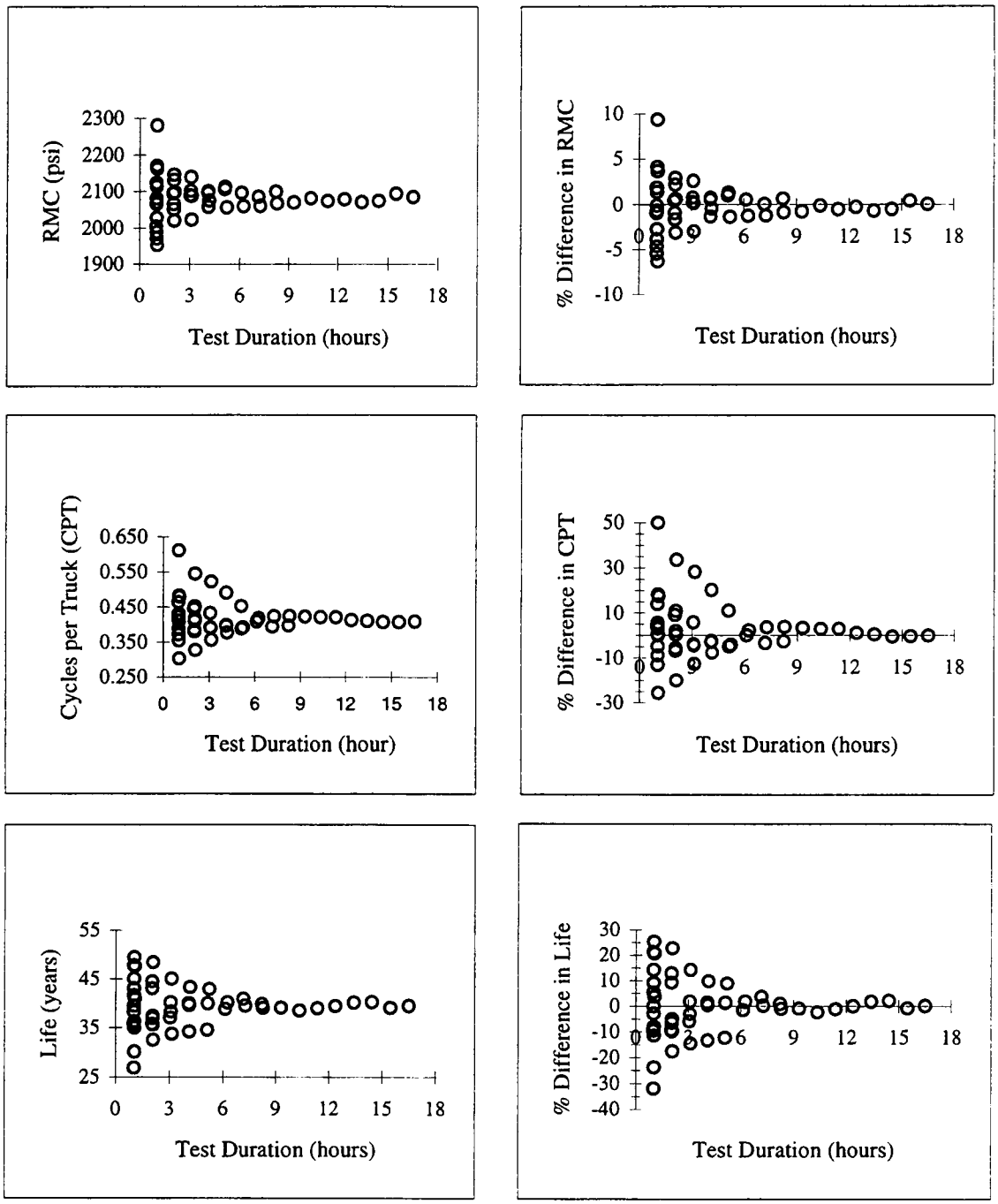


Figure 4-18. The Effect of Field Test Duration on the Effective Stress Range (RMC), the Number of Cycles Per Truck (CPT), and the Total Fatigue Life for Category E' Main Bridge Member Detail, Gage G73

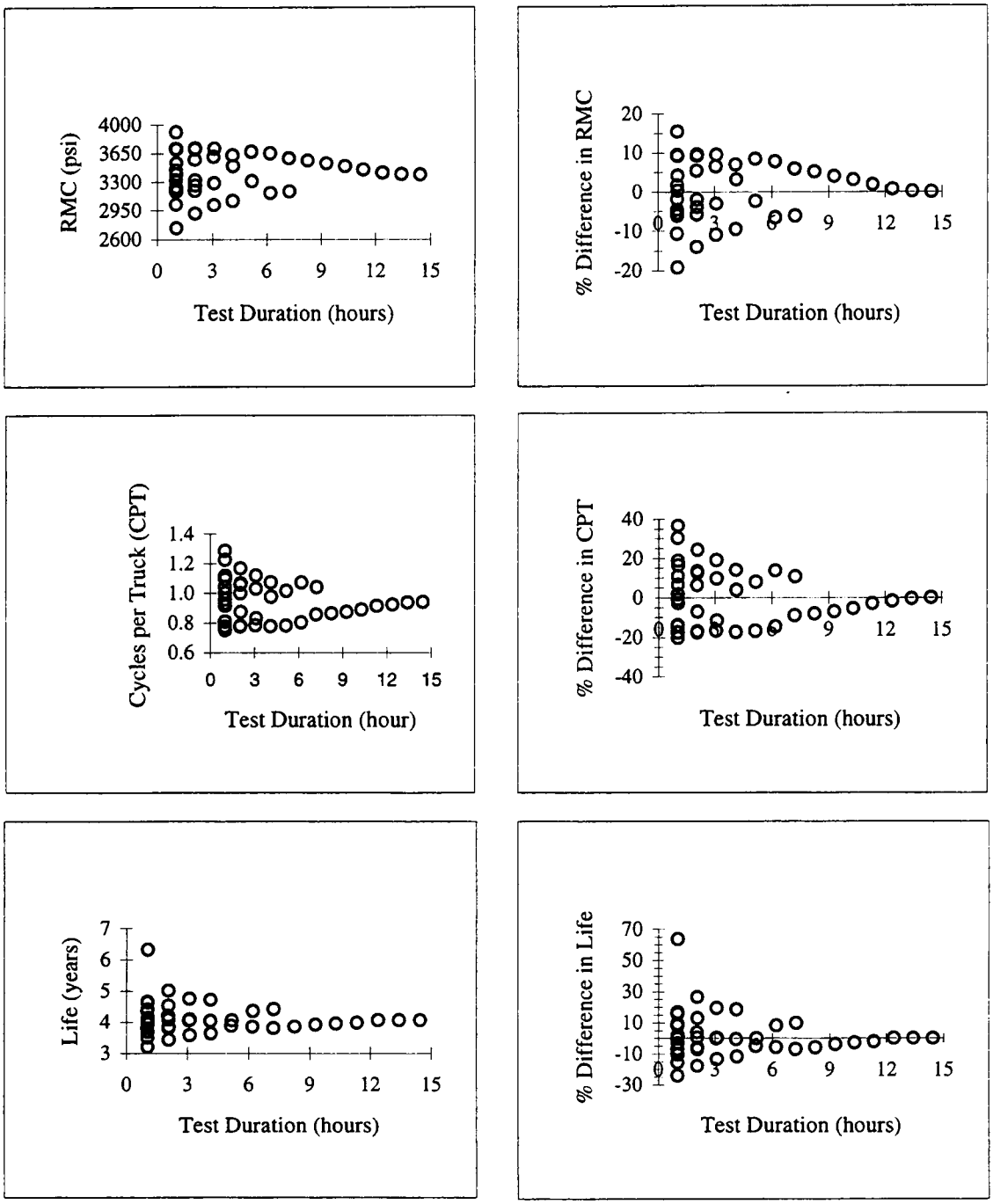


Figure 4-19. The Effect of Field Test Duration on the Effective Stress Range (RMC), the Number of Cycles Per Truck (CPT), and the Total Fatigue Life for Category E' Main Bridge Member Detail, Gage G110

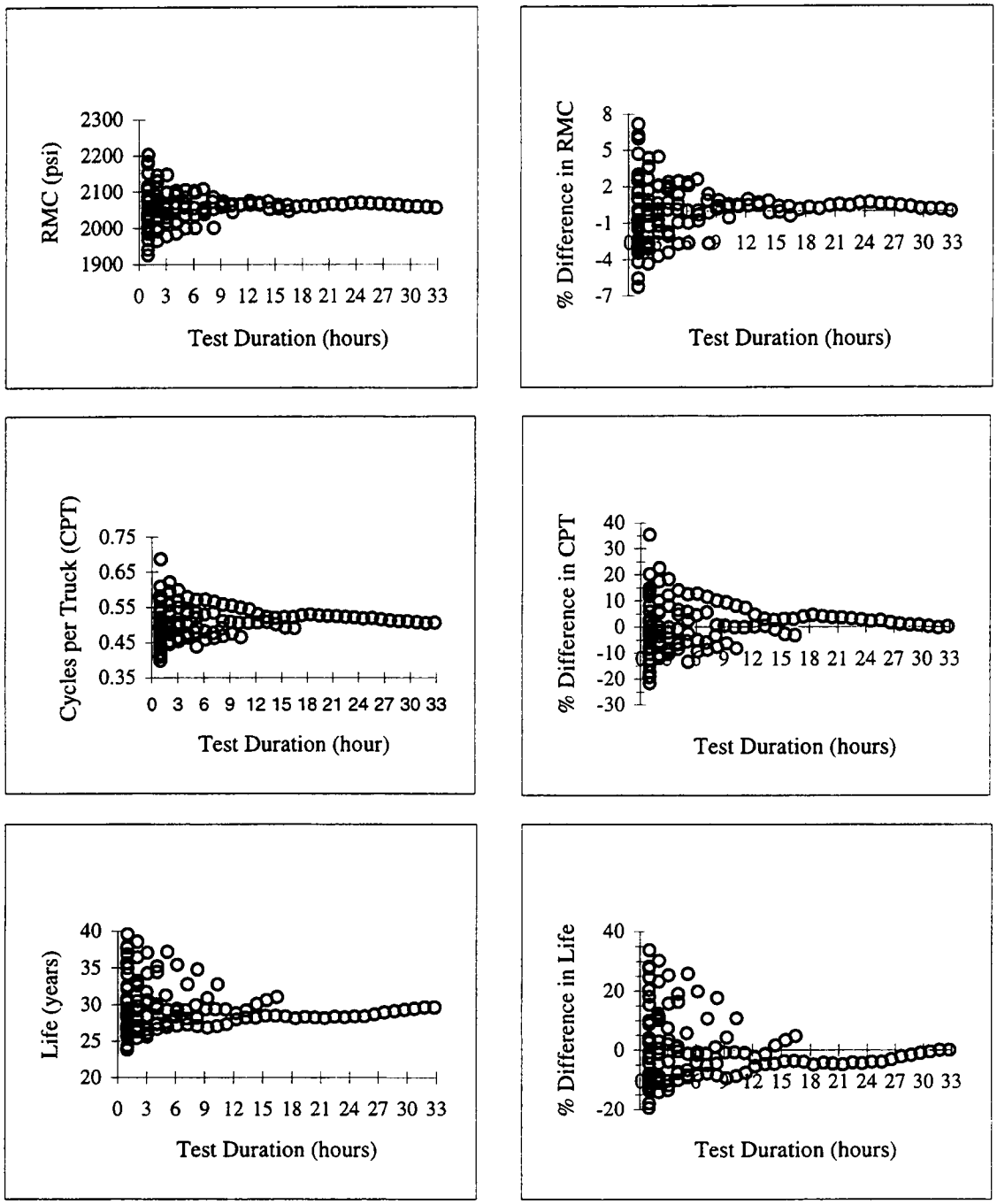


Figure 4-20. The Effect of Field Test Duration on the Effective Stress Range (RMC), the Number of Cycles Per Truck (CPT), and the Total Fatigue Life for Category E' Main Bridge Member Detail, Gage G116

values were within 10% and 5% of its total test duration *RMC* value, respectively. The difference in the required test duration between the second span (G51 and G73) and first span (G110) gages can be attributed to the scatter in the data. The variation in the individual one hour *RMC* values for G110 was greater than those for gages G51 and G73, thus causing G110's values to converge at a slower rate. This variation in the data was due to the difference in the bridge's dynamics between the first and second spans. The first span is an approach span which has a higher dynamic amplification factor than the second span, an interior span.

With exception of gages G58B and G58D, the dispersion in the *CPT* data was greater than that for the *RMC* data, as shown in Figures 4-11 through 4-20. The large variation in the individual one-hour test segment's *CPT* values caused the data to converge at a slower rate than the *RMC* data. The *CPT* data for gages 58B and 58D converged to within 5% of their total test duration's *CPT* value after one hour of testing. The *CPT* data for all other gages took between 3 to 21 hours of testing to converge within 5% of their total test duration's *CPT* value.

The variation in the *RMC* and the *CPT* data contribute to the variation in the total life data. In equation (4.9), if C (*CPT*) is constant, then the *RMC* value has the greatest effect on the variation in the total life data. If S_r (*RMC*) is constant, then the *CPT* value has the greatest effect on the variation in the total life data. Figures 4-11 through 4-20 illustrates the combined effect of the variation in the *RMC* and the *CPT* data on the variation in the total life data. The variation in the total life data was always greater than the variation in the *RMC* data. Where as, the variation in the total life data was greater

than or equal to the variation in the *CPT* data. Therefore, the total life data and the *CPT* data converged to within 5% of their respective total test duration's values at the same test duration.

The effect of test duration on the effective stress range, the number of cycles per truck, and the total fatigue life for secondary bridge member fatigue prone details is illustrated in Figures 4-21 through 4-28. Based on the results presented in these figures, the following observations were made. The scatter in the data decreased with increase in test duration. For all fatigue prone details, the *RMC* data converged at a faster rate than the *CPT* and total life data. For gages G32, G34, G35 and G317, their individual one-hour *RMC* values were not significantly different than their corresponding total test duration's *RMC* value. Gages G2 and G117's *RMC* values converged to within 5% of their total test duration's *RMC* value at a test duration of two hours, while gages G305 and G105 converged at 3 and 7 hours, respectively. The behavior of the approach span gages (G2, G105, and G117) and the interior span gages (G32, G34, G35, G305, and G317) were similar to that of the main member gages. That is, the data for a given detail located in the approach span converged at a slower rate than the data for the same detail located in an interior span. This is due to the difference in the bridge's dynamics between these spans. The effect of test duration on *CPT* and total fatigue life for secondary bridge member details was the same as that for main member details. Table 4-17 summarizes the results of the first evaluation procedure.

The second evaluation procedure tested the hypothesis that as the one-hour test segment's truck traffic count approaches the average hourly truck traffic volume (*AHTT*),

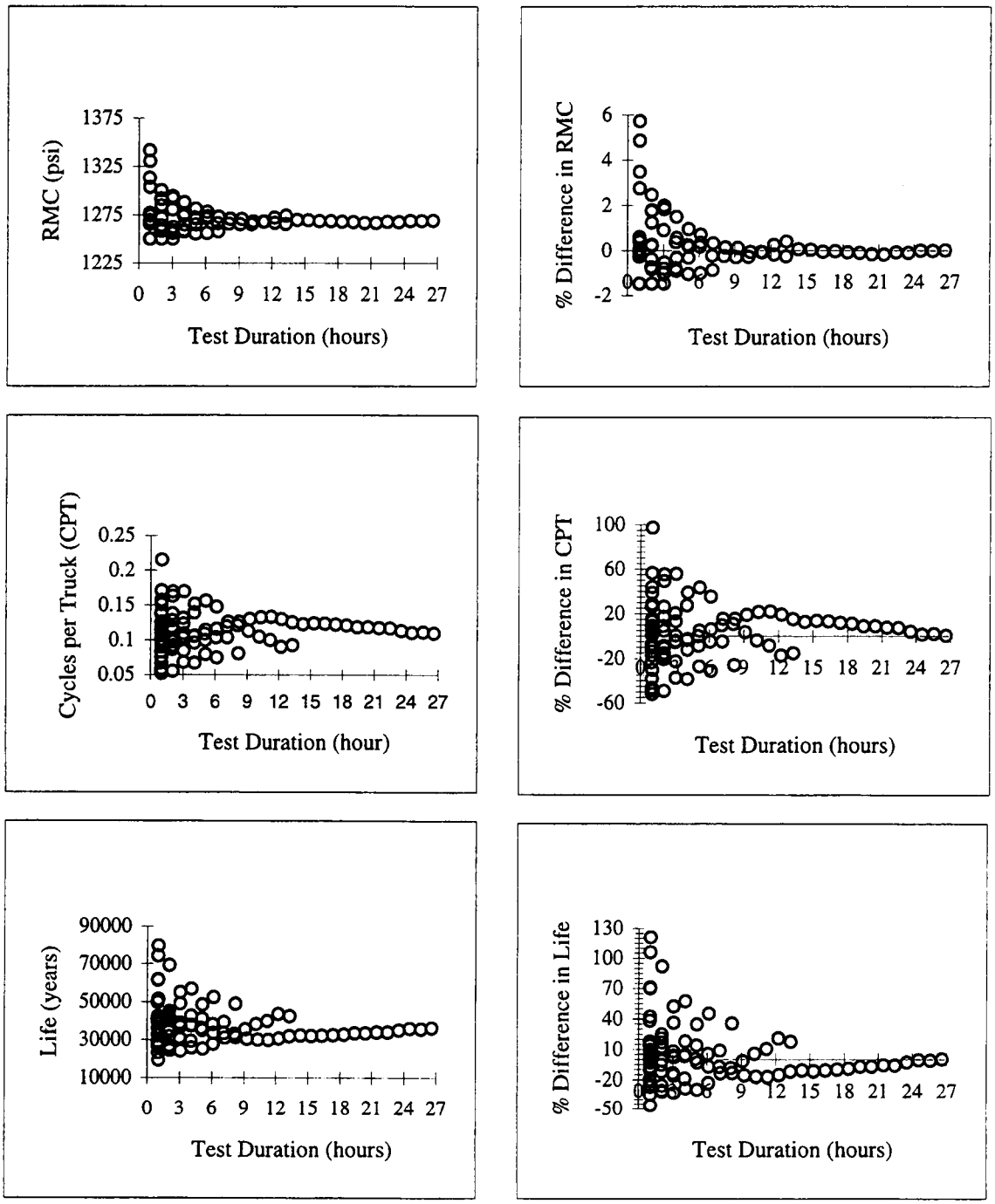


Figure 4-21. The Effect of Field Test Duration on the Effective Stress Range (RMC), the Number of Cycles Per Truck (CPT), and the Total Fatigue Life for Category A Secondary Bridge Member Detail, Gage G35

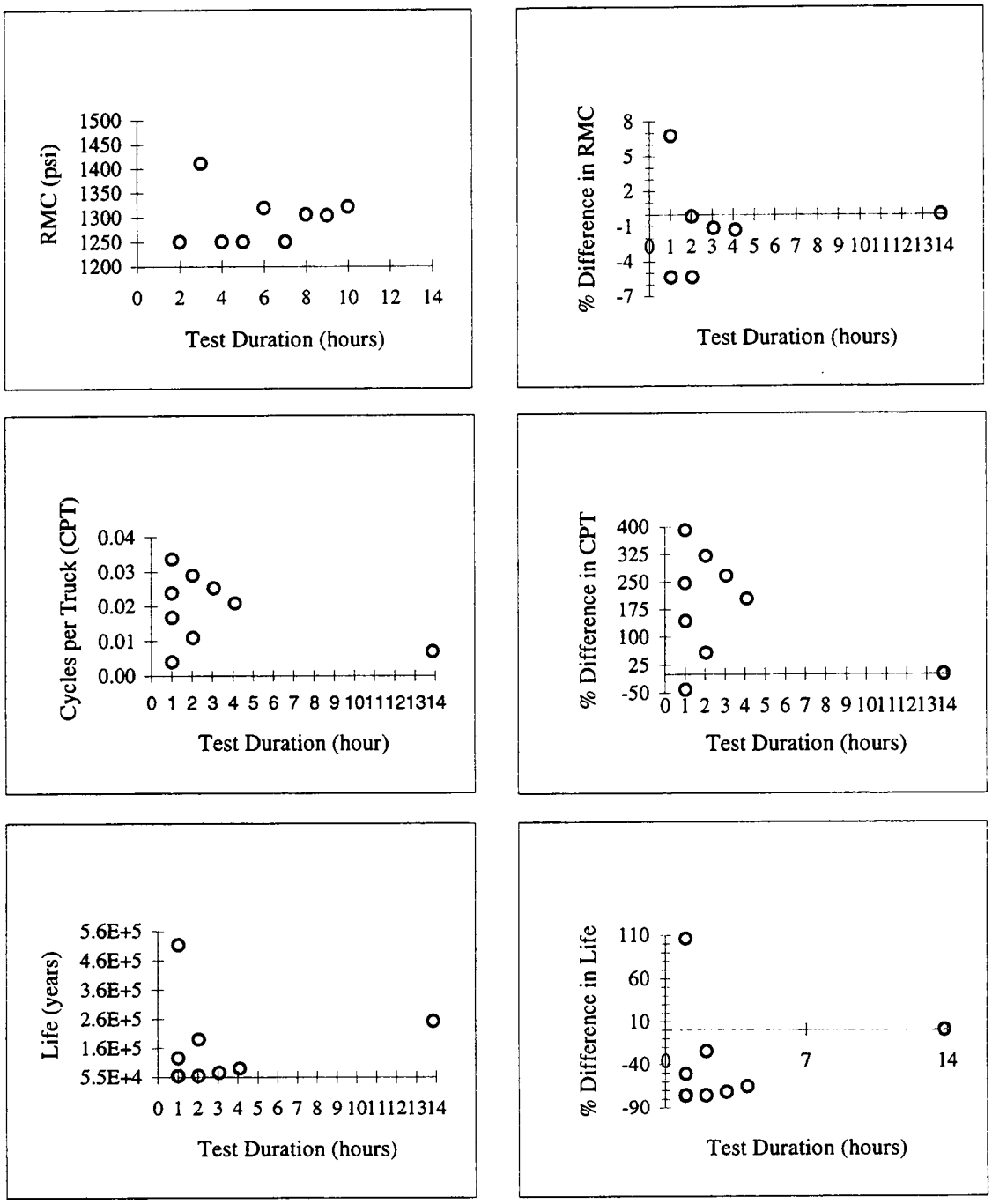


Figure 4-22. The Effect of Field Test Duration on the Effective Stress Range (RMC), the Number of Cycles Per Truck (CPT), and the Total Fatigue Life for Category B Secondary Bridge Member Detail, Gage G2

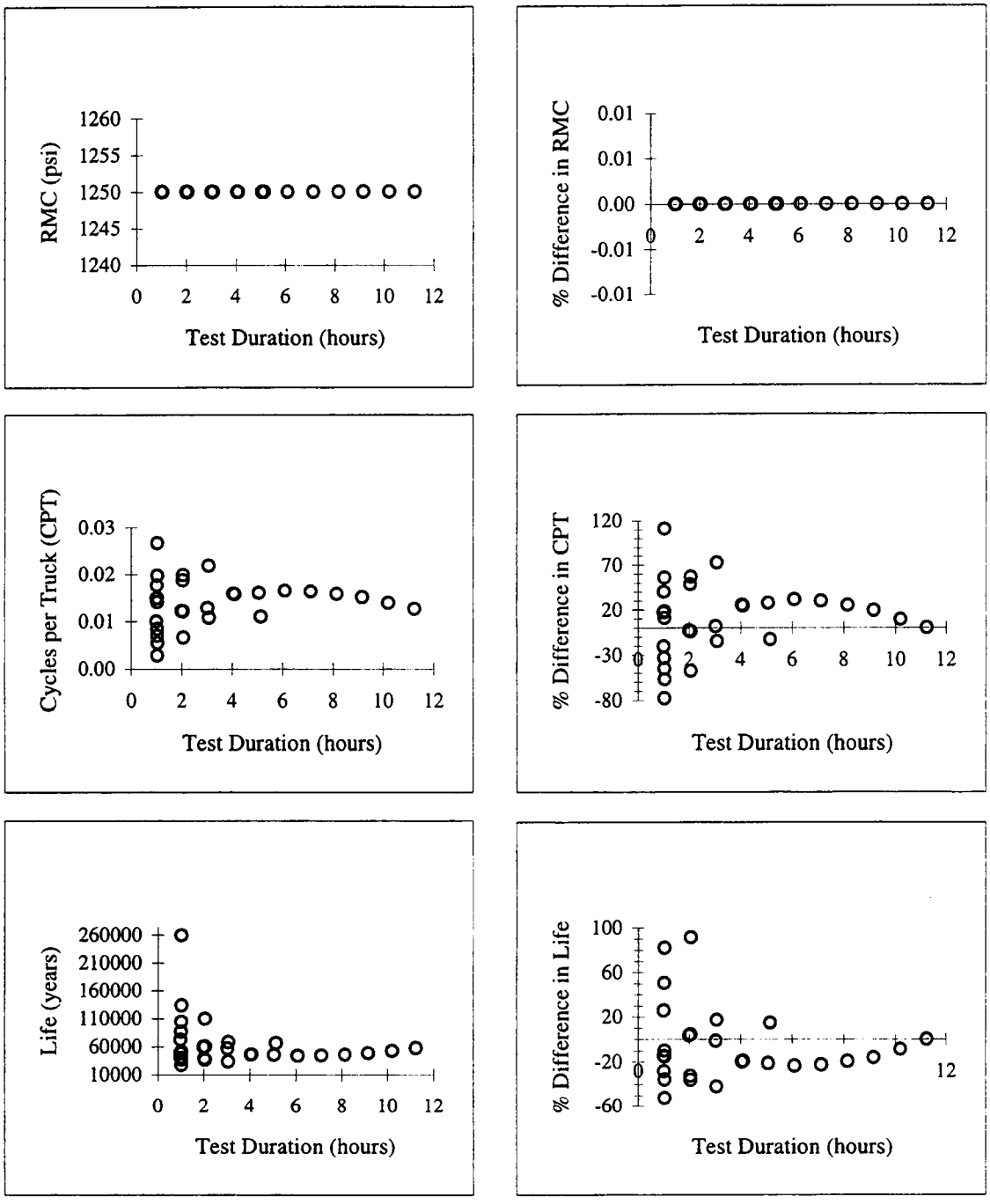


Figure 4-23. The Effect of Field Test Duration on the Effective Stress Range (RMC), the Number of Cycles Per Truck (CPT), and the Total Fatigue Life for Category C Secondary Bridge Member Detail, Gage G32

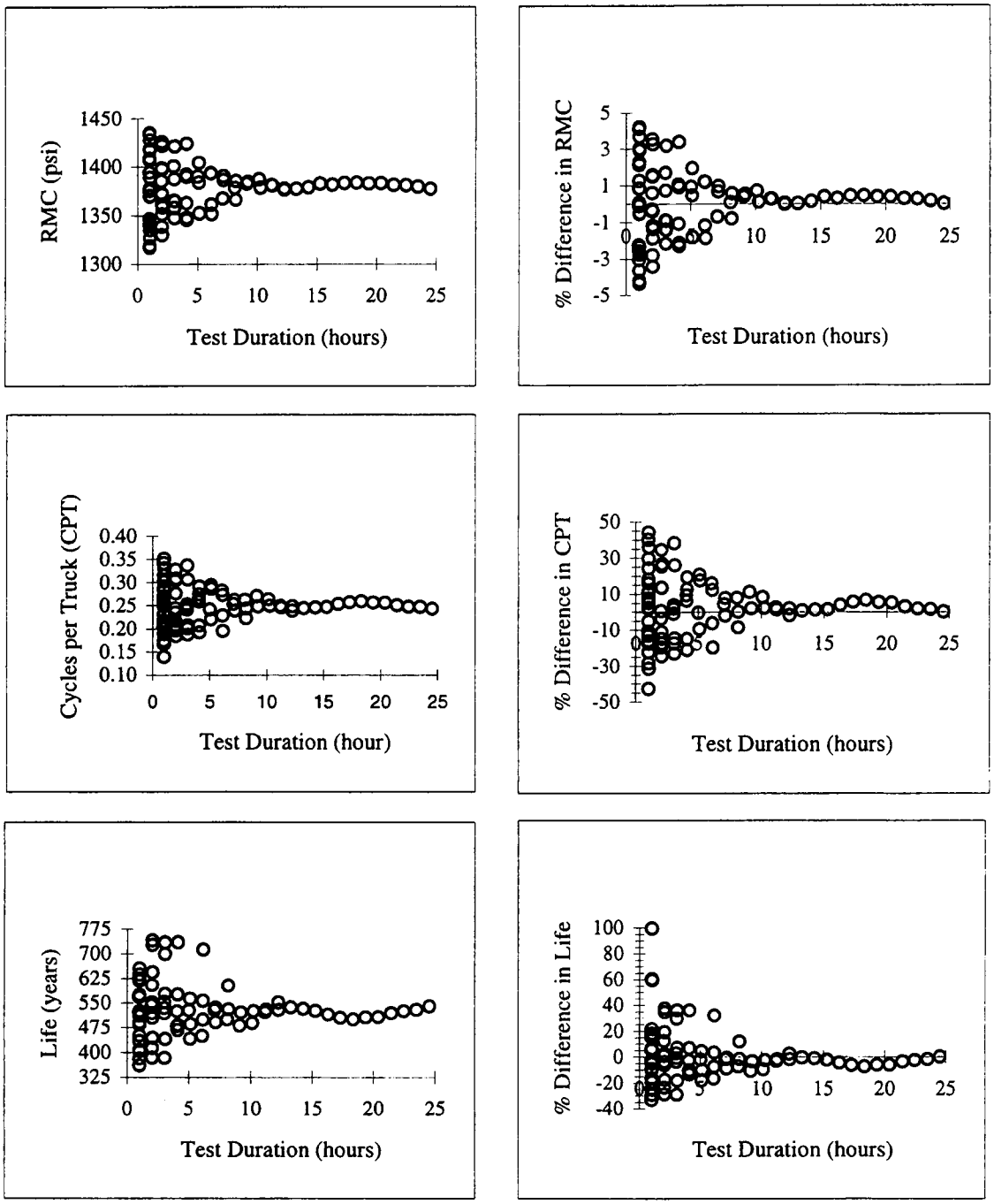


Figure 4-24. The Effect of Field Test Duration on the Effective Stress Range (RMC), the Number of Cycles Per Truck (CPT), and the Total Fatigue Life for Category E Secondary Bridge Member Detail, Gage G34

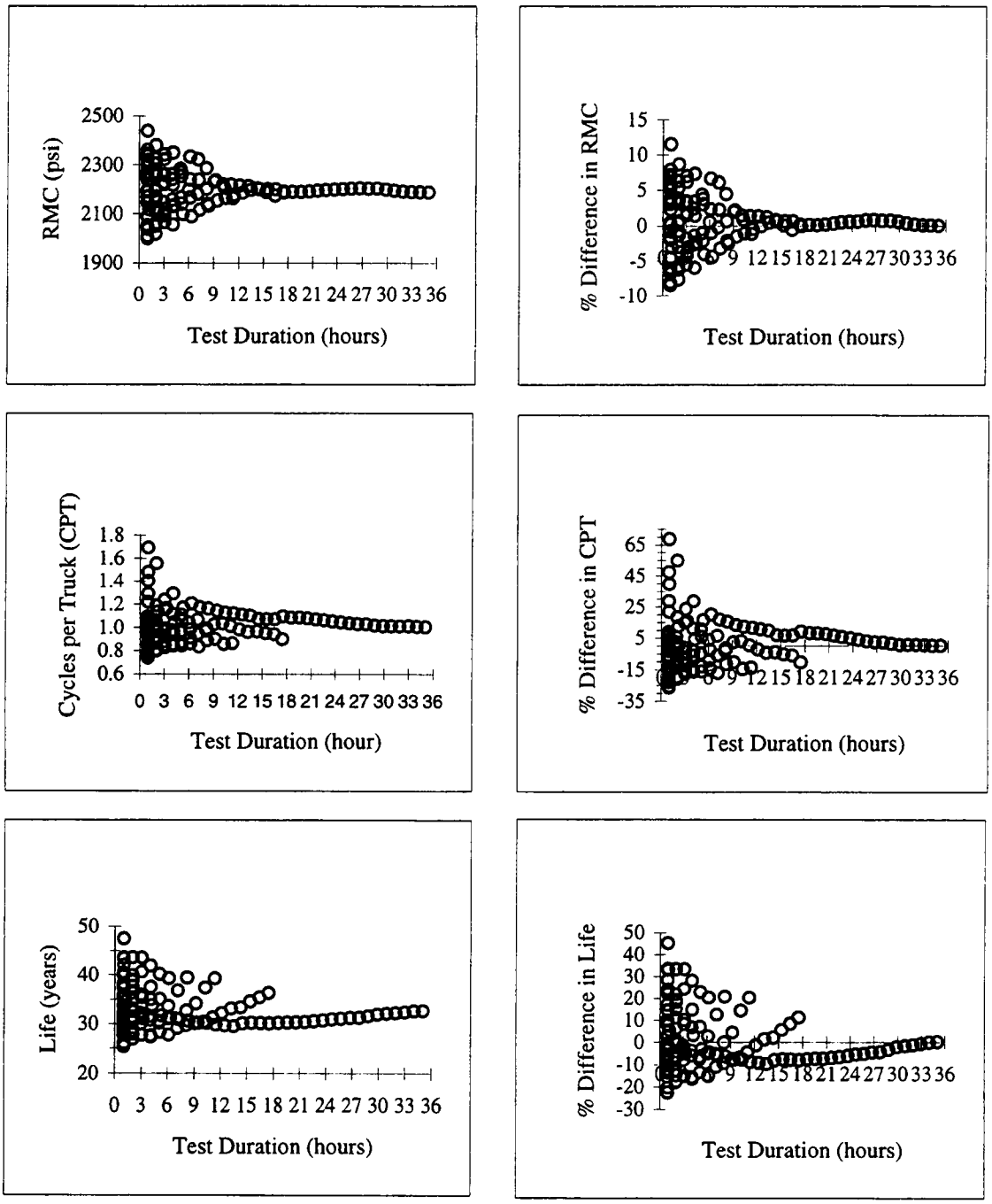


Figure 4-25. The Effect of Field Test Duration on the Effective Stress Range (RMC), the Number of Cycles Per Truck (CPT), and the Total Fatigue Life for Category E Secondary Bridge Member Detail, Gage G105

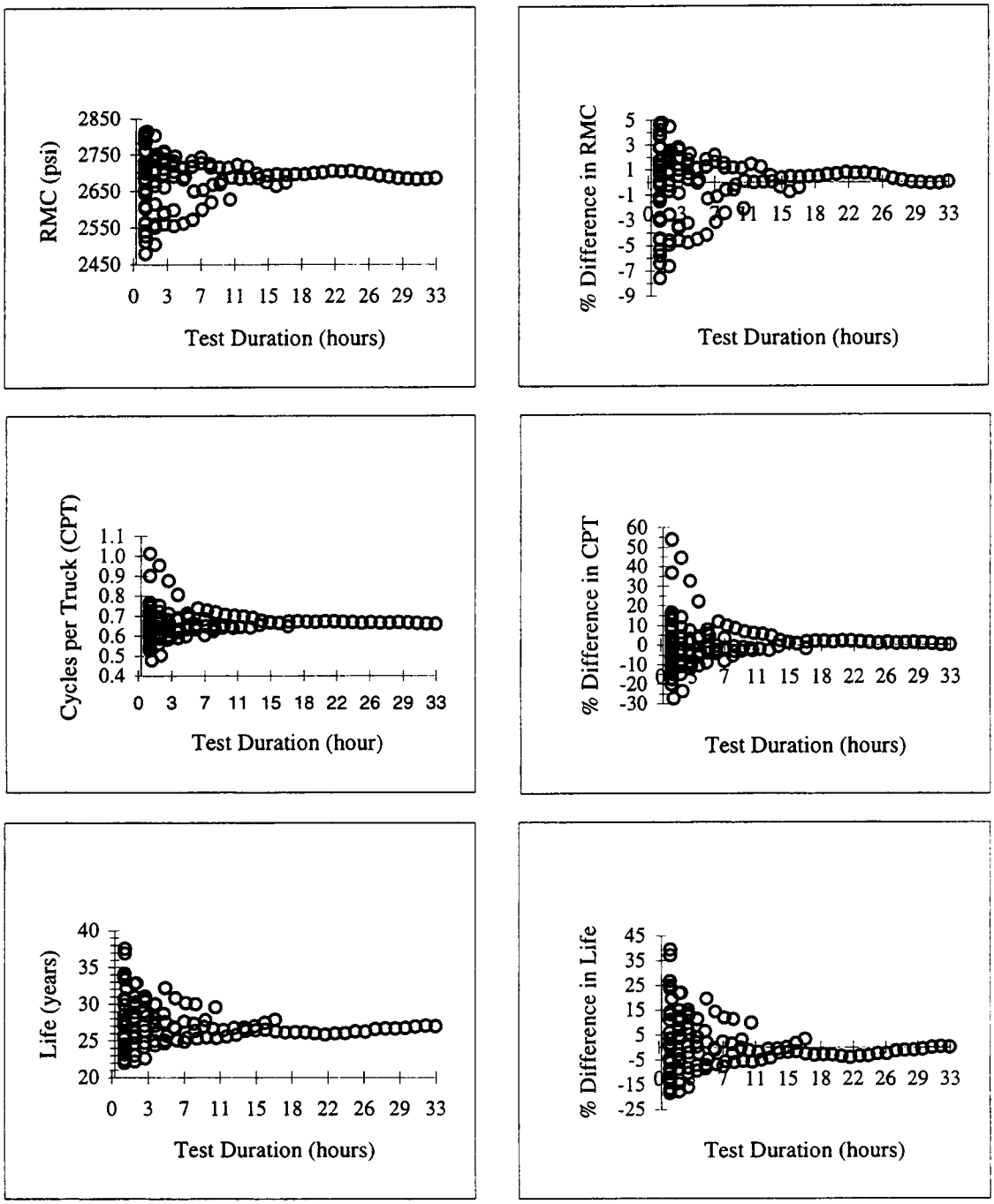


Figure 4-26. The Effect of Field Test Duration on the Effective Stress Range (RMC), the Number of Cycles Per Truck (CPT), and the Total Fatigue Life for Category E Secondary Bridge Member Detail, Gage G305

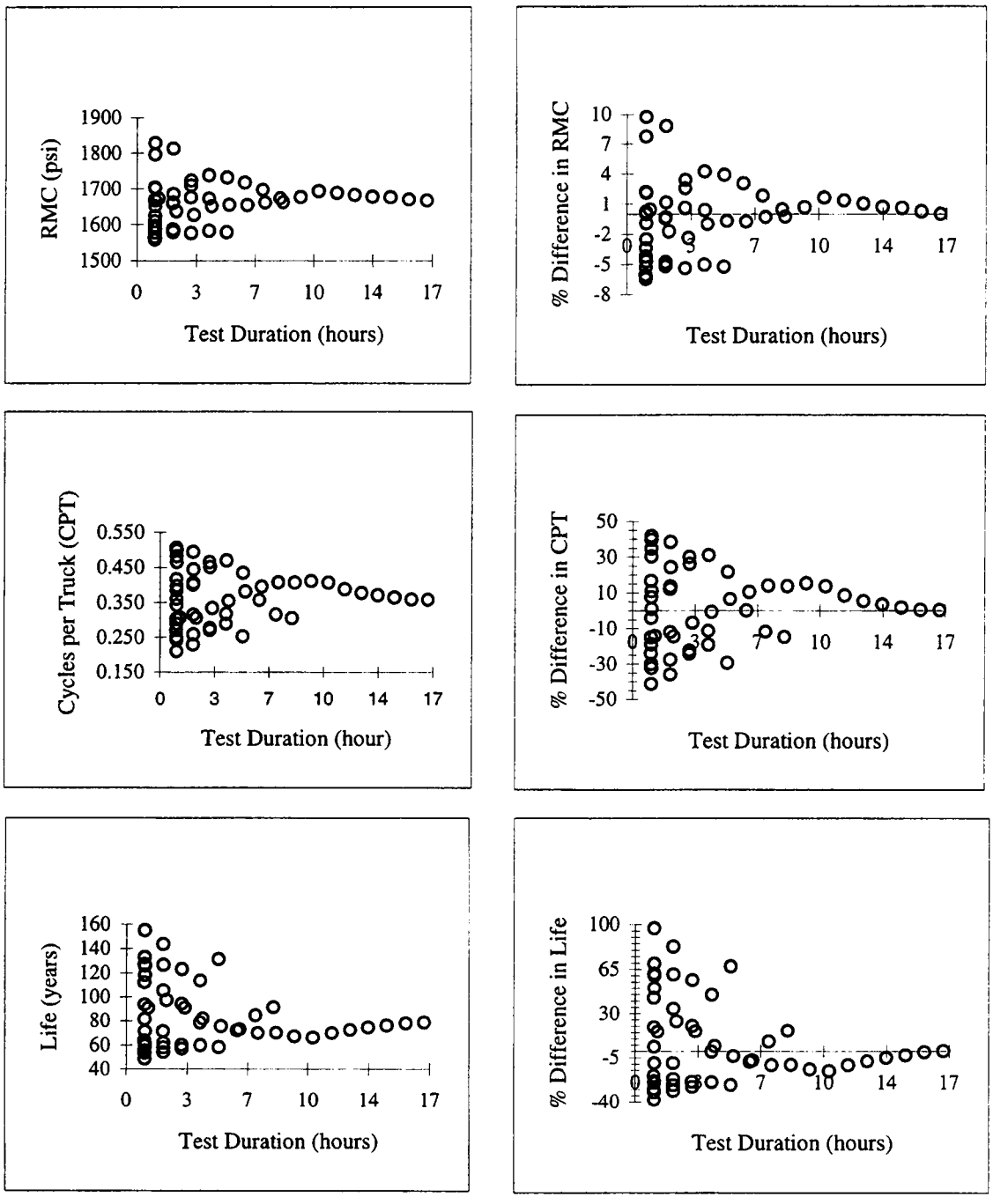


Figure 4-27. The Effect of Field Test Duration on the Effective Stress Range (RMC), the Number of Cycles Per Truck (CPT), and the Total Fatigue Life for Category E' Secondary Bridge Member Detail, Gage G117

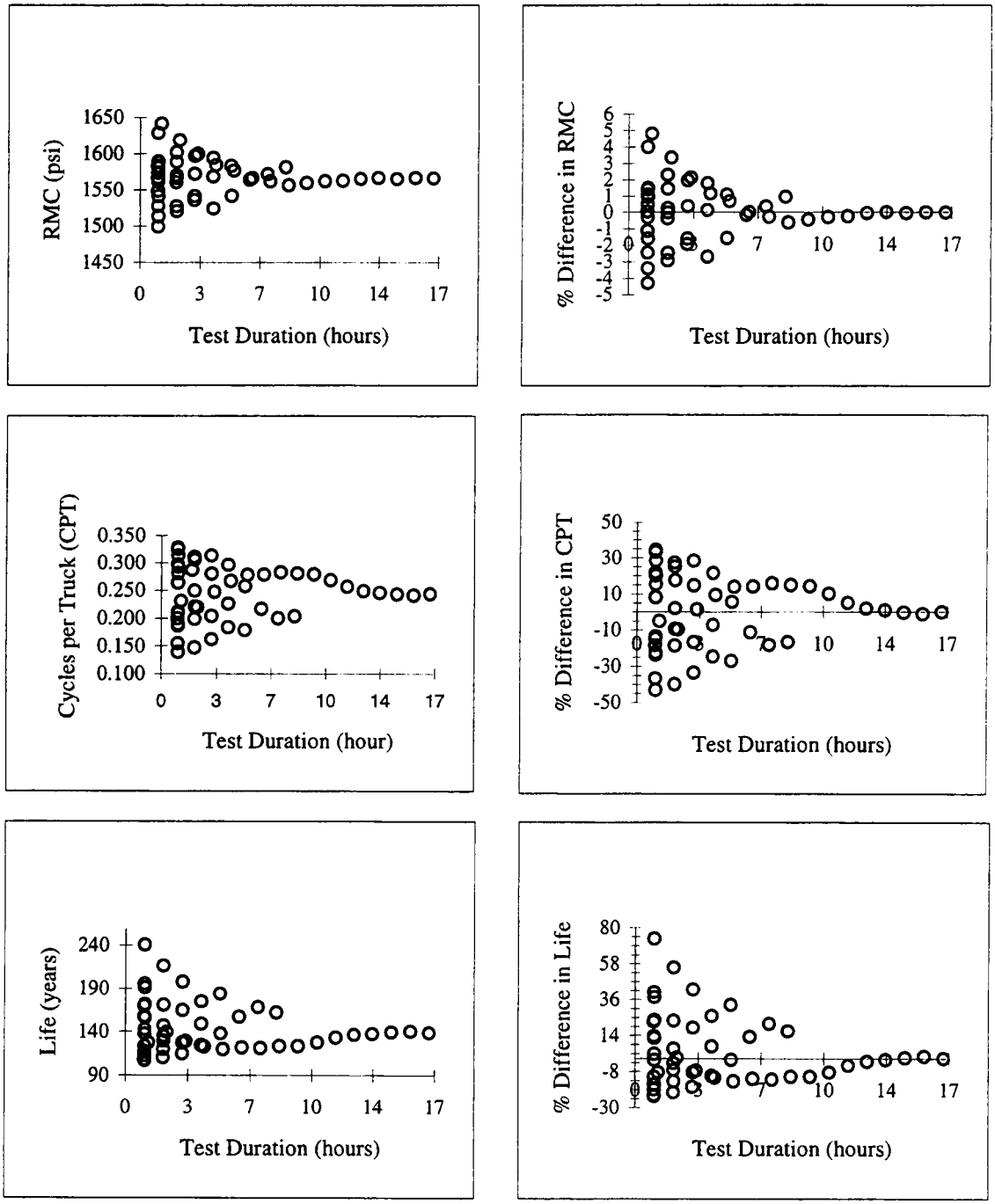


Figure 4-28. The Effect of Field Test Duration on the Effective Stress Range (RMC), the Number of Cycles Per Truck (CPT), and the Total Fatigue Life for Category E' Secondary Bridge Member Detail, Gage G317

Table 4-17. Summary of Test Duration Results

Bridge Member	Fatigue Category	Gage Number	Gage Location	Total Test Duration (hrs)	Required Test Duration (hours)		
					RMC	CPT	Life
	A	G58D	Span 2	6.44	2	1	3
	B	G5	"	24.6	3	3	8
		G58	"	32.84	15	21	21
M		*	"	31.8	5	21	21
a	C	G58B	"	6.44	2	1	3
i	E	G47	"	15.31	2	12	12
n	E'	G51	"	33.68	2	20	20
		G73	"	16.51	2	9	8
		G110	Span 1	14.45	10	10	10
		G116	Span 1	32.82	2	18	18
S	A	G35	Span 2	26.61	1	21	21
e	B	G2	Span 1	13.86	2	13	13
c	C	G32	Span 2	11.24	1	10	10
o	E	G34	"	24.52	1	10	12
n		G105	Span 1	35.06	7	23	25
d		G305	Span 3	32.98	3	12	12
a	E'	G117	Span 1	16.69	2	13	13
ry		G317	Span 3	16.69	1	12	12

Note: * = G58 without outlier data point

then its corresponding *RMC* and *CPT* values approach the total test duration's *RMC* and *CPT* values. The results of this evaluation for bridge main member fatigue prone details are presented in Figures 4-29 through 4-37. In each figure, the top graph is a plot of the individual one-hour test segment's *RMC* values and truck traffic count versus the time of day. The bottom graph is a plot of the individual test segment's *CPT* values and truck traffic count versus the time of day. The total test duration's *RMC* and *CPT* values and the *AHTT* are indicated by solid lines. Based on the results presented in theses figures, the following observations were made. For all gages, with exception of gages G58 and G110, the majority of the *RMC* values fell within ± 5% of their total test duration's *RMC*

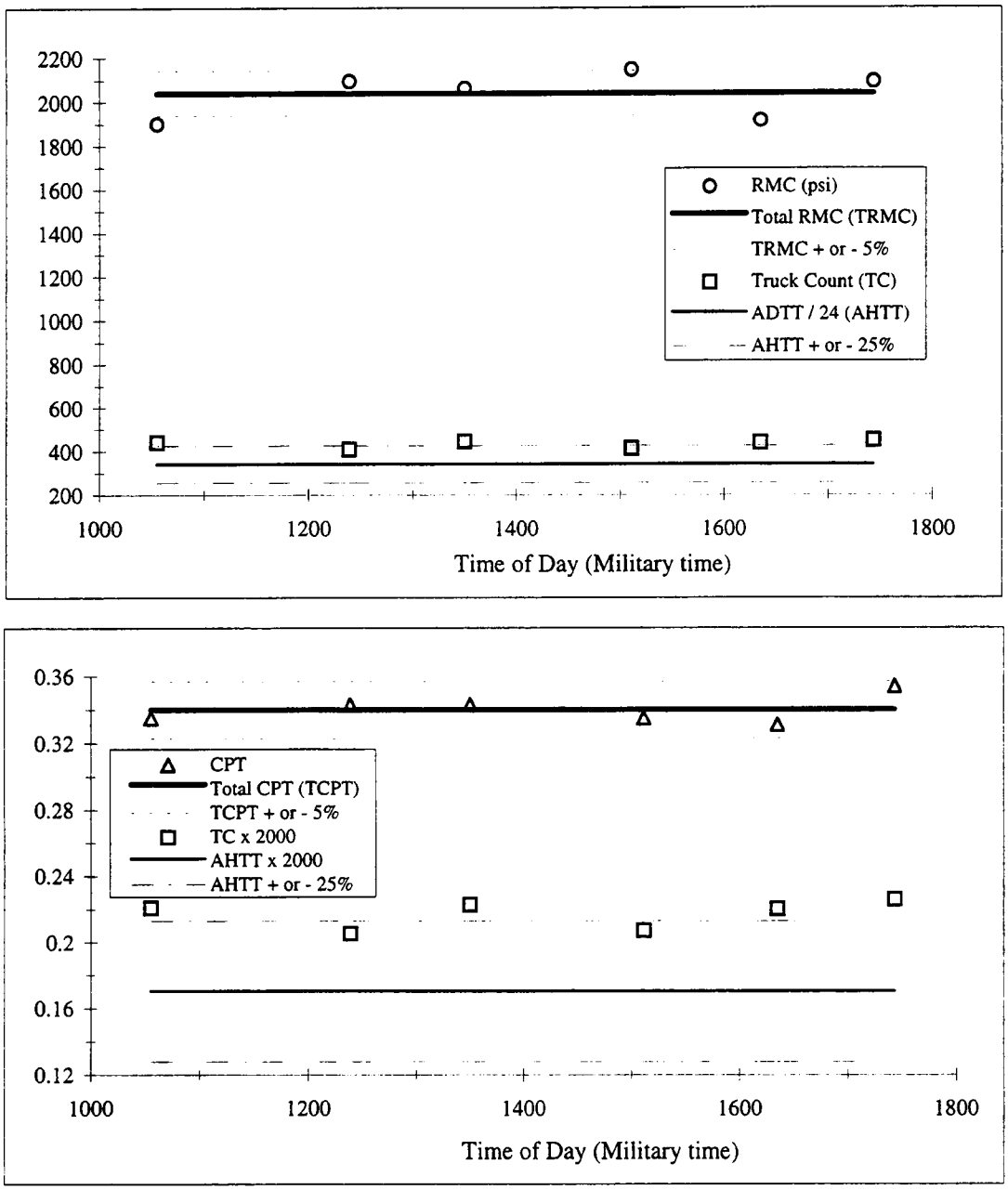


Figure 4-29. Top Plot Showing the Relationship Between RMC and Truck Count and Bottom Plot Showing the Relationship Between CPT and Truck Count for Category A Main Bridge Member Detail, G58D

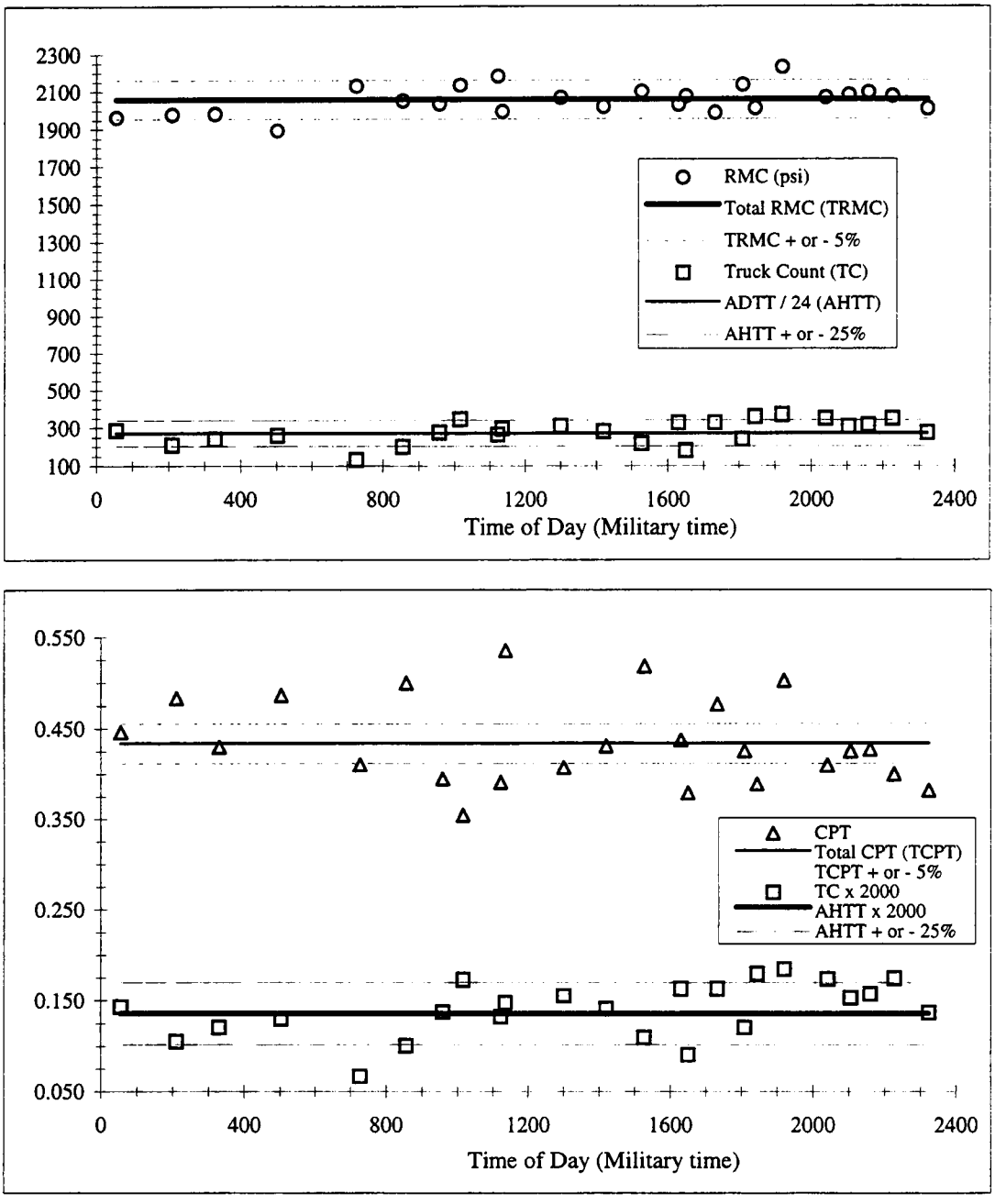


Figure 4-30. Top Plot Showing the Relationship Between RMC and Truck Count and Bottom Plot Showing the Relationship Between CPT and Truck Count for Category B Main Bridge Member Detail, G5

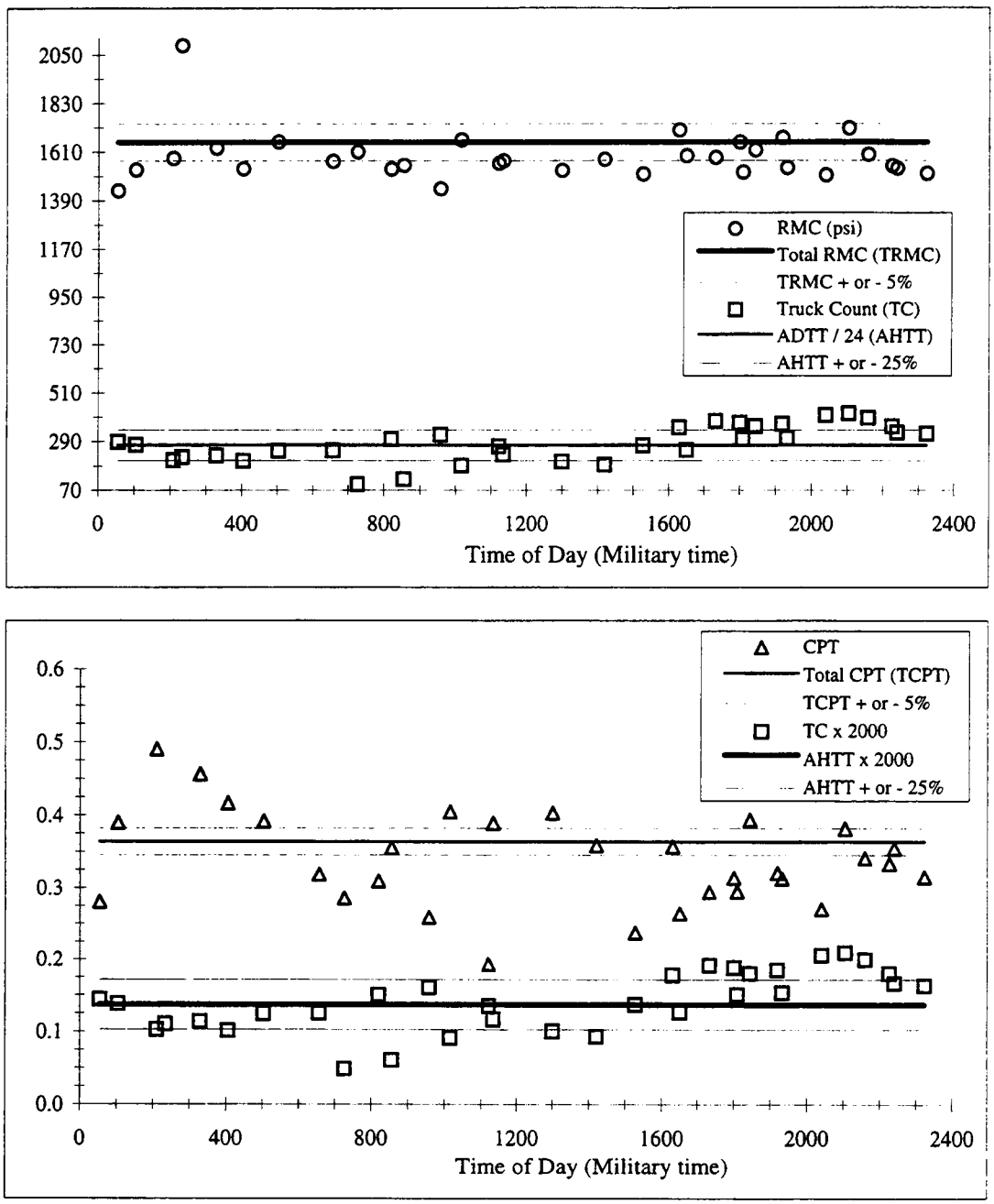


Figure 4-31. Top Plot Showing the Relationship Between RMC and Truck Count and Bottom Plot Showing the Relationship Between CPT and Truck Count for Category B Main Bridge Member Detail, G58

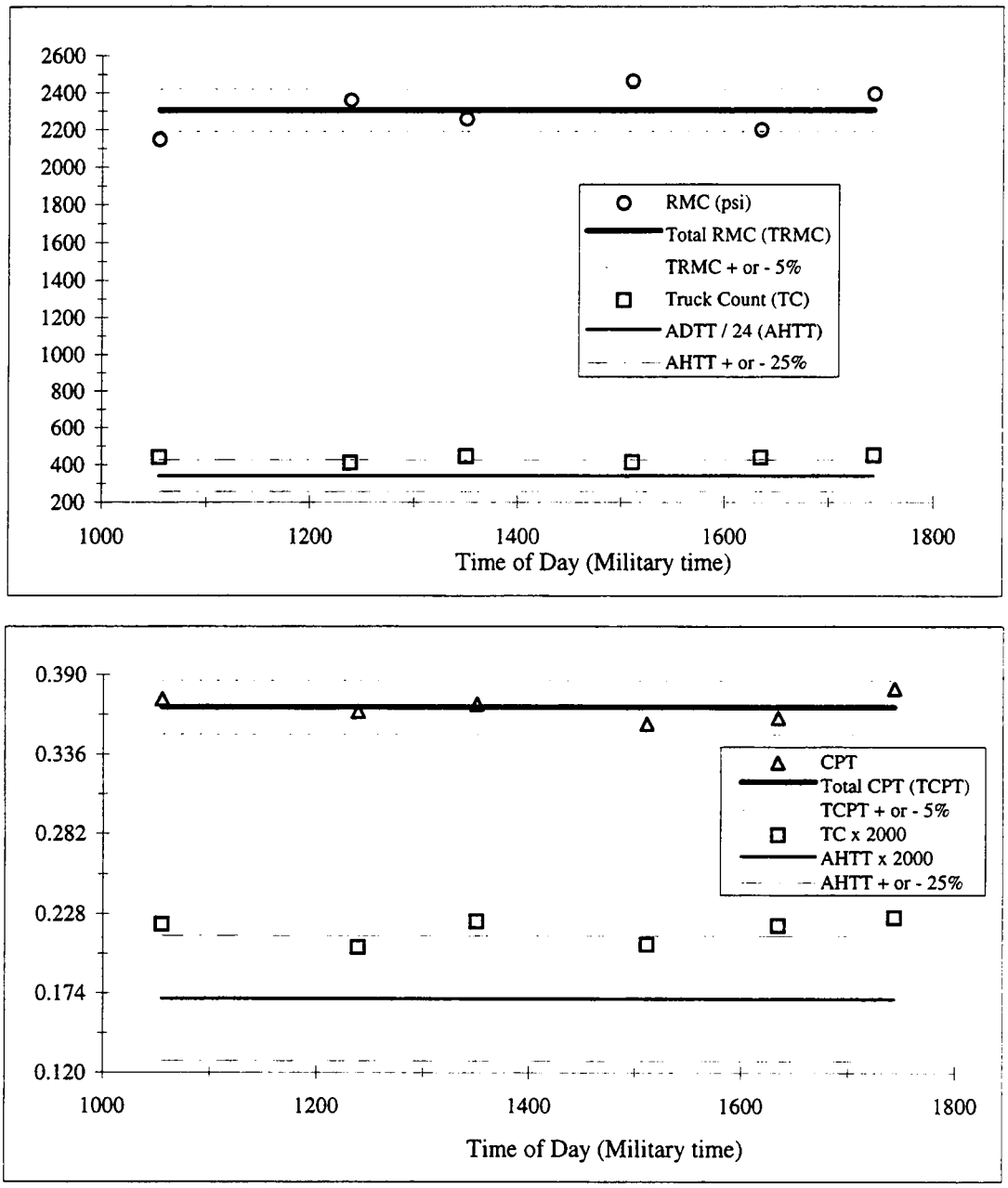


Figure 4-32. Top Plot Showing the Relationship Between RMC and Truck Count and Bottom Plot Showing the Relationship Between CPT and Truck Count for Category C Main Bridge Member Detail, G58B

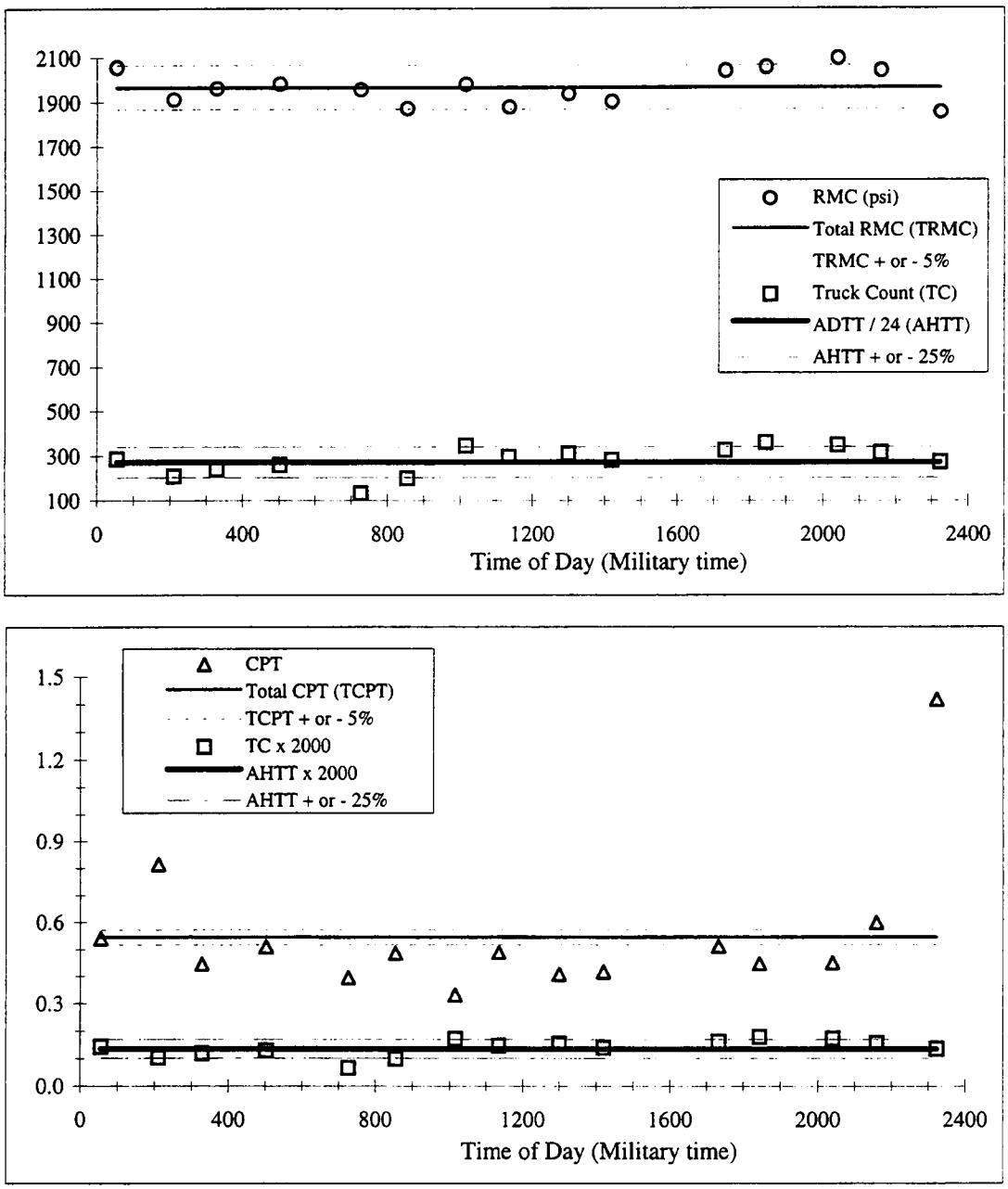


Figure 4-33. Top Plot Showing the Relationship Between RMC and Truck Count and Bottom Plot Showing the Relationship Between CPT and Truck Count for Category E Main Bridge Member Detail, G47

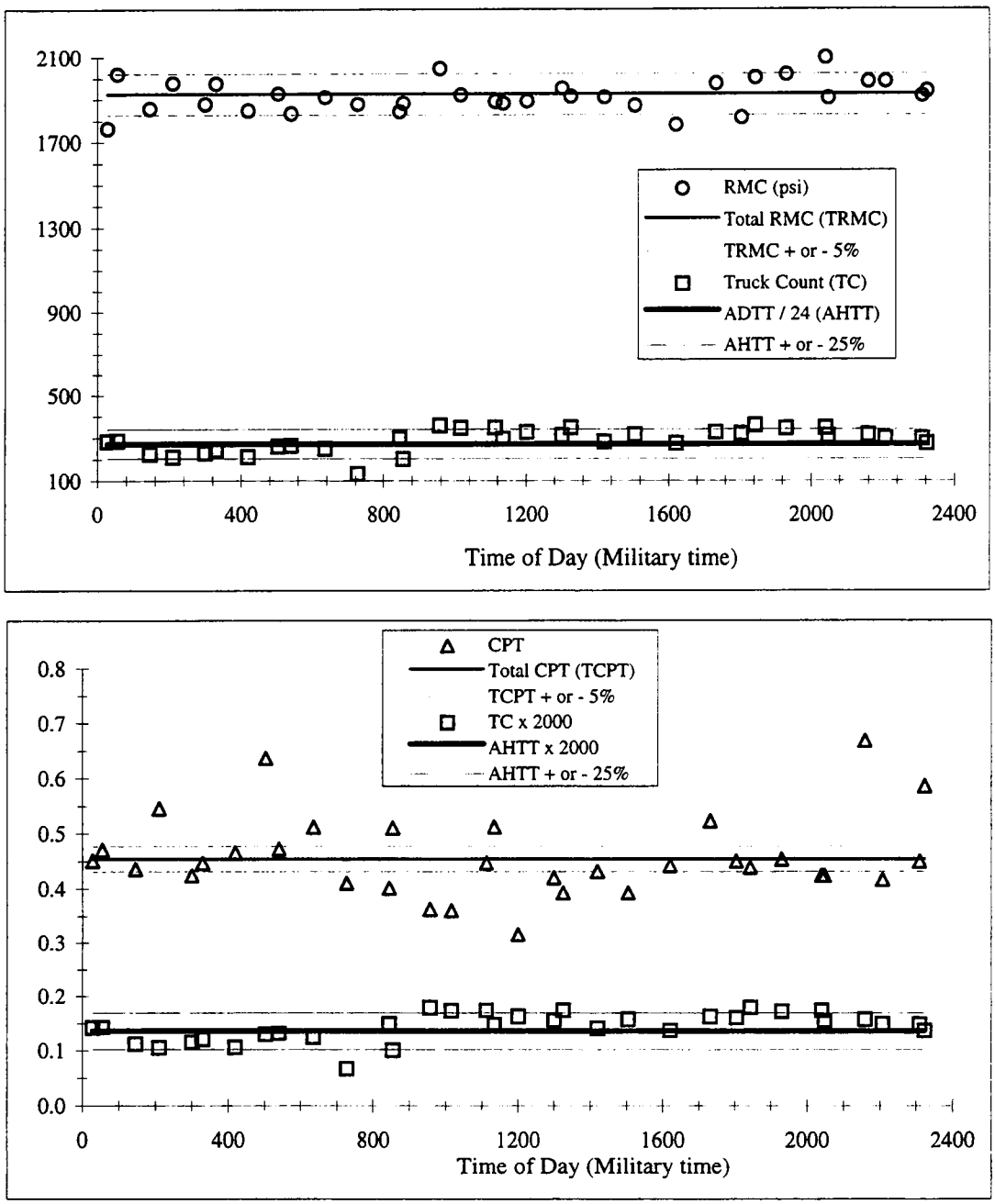


Figure 4-34. Top Plot Showing the Relationship Between RMC and Truck Count and Bottom Plot Showing the Relationship Between CPT and Truck Count for Category E' Main Bridge Member Detail, G51

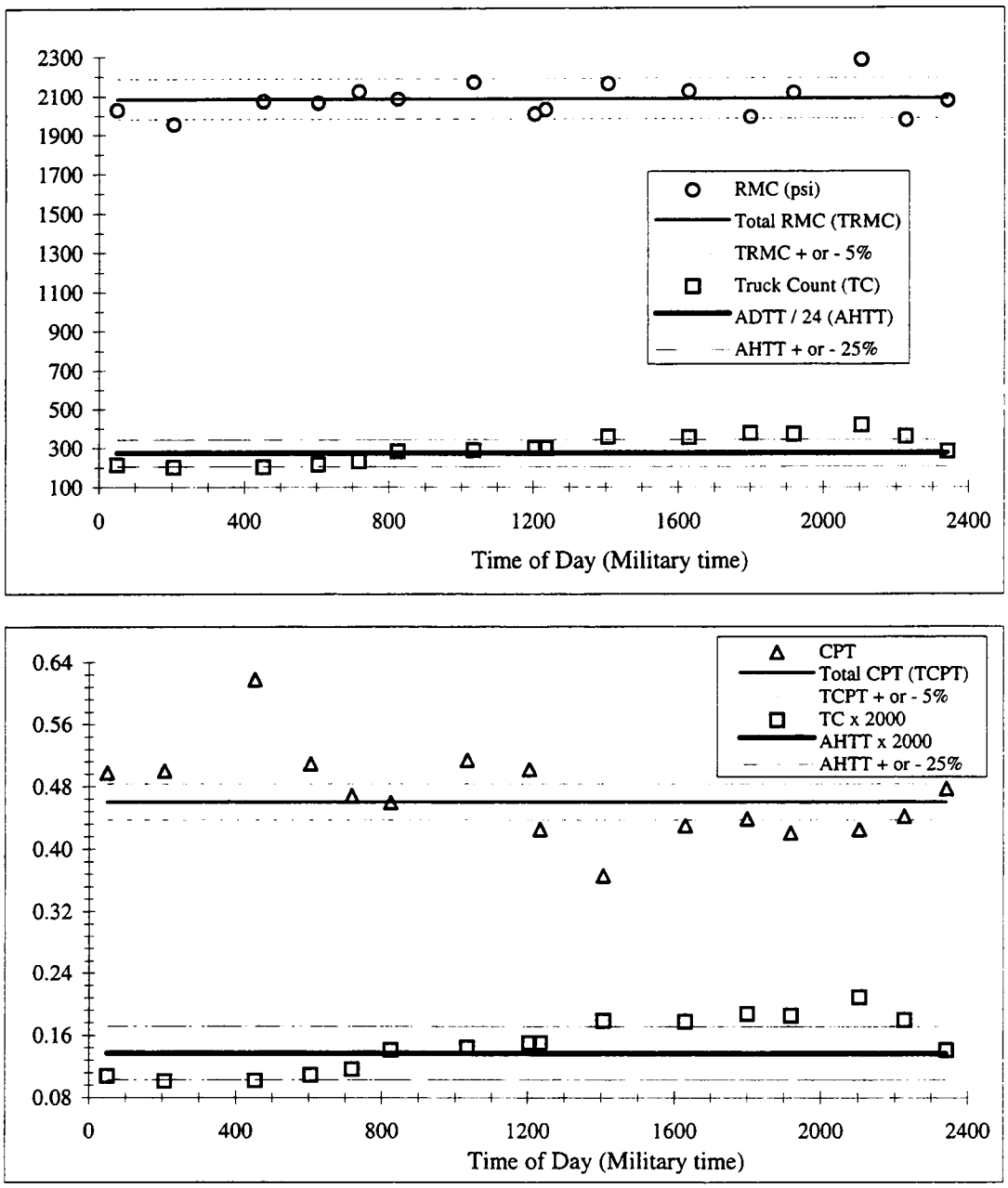


Figure 4-35. Top Plot Showing the Relationship Between RMC and Truck Count and Bottom Plot Showing the Relationship Between CPT and Truck Count for Category E' Main Bridge Member Detail, G73

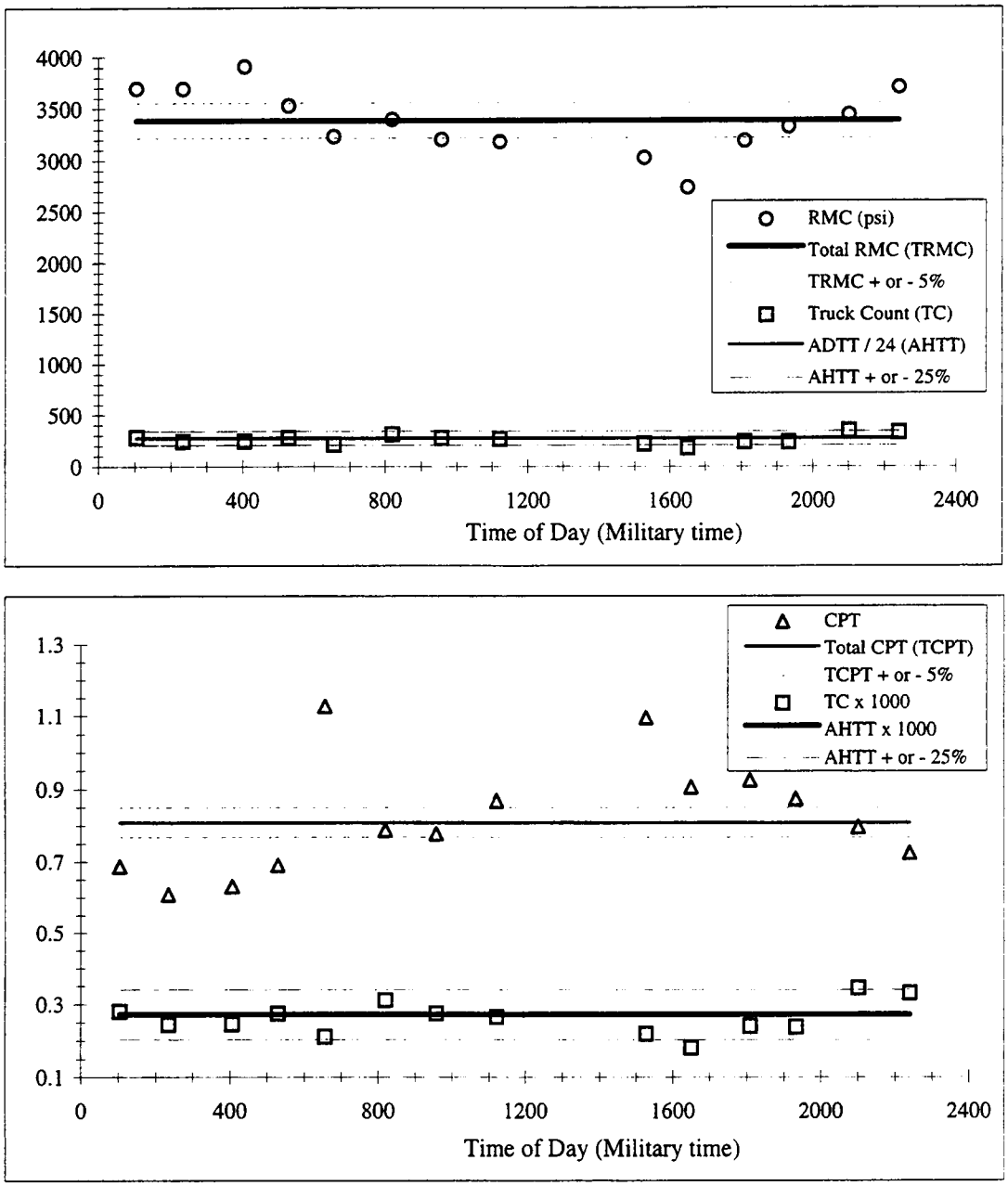


Figure 4-36. Top Plot Showing the Relationship Between RMC and Truck Count and Bottom Plot Showing the Relationship Between CPT and Truck Count for Category E' Main Bridge Member Detail, G110

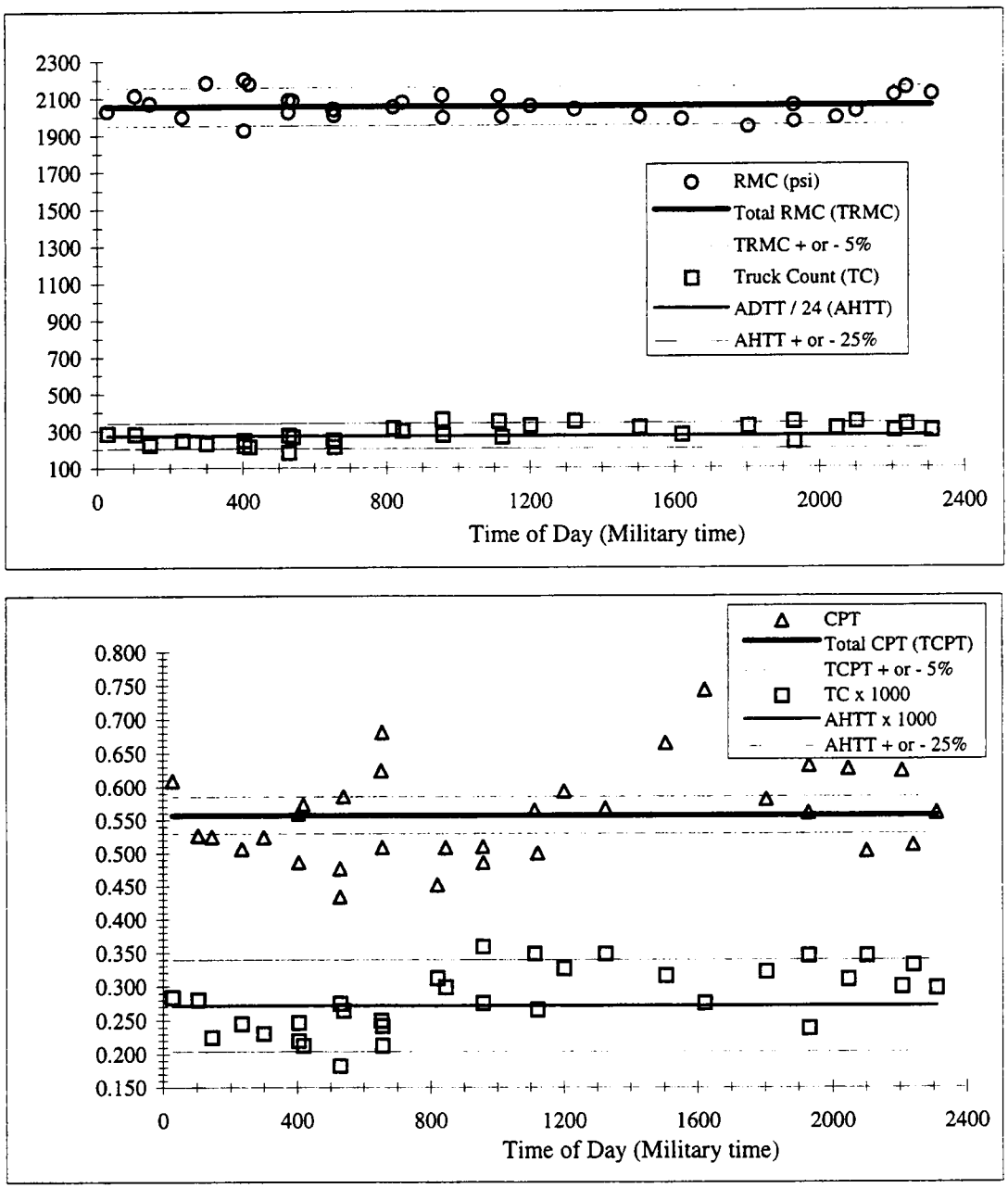


Figure 4-37. Top Plot Showing the Relationship Between RMC and Truck Count and Bottom Plot Showing the Relationship Between CPT and Truck Count for Category E' Main Bridge Member Detail, G116

value. For all gages, with exception of gages G58B and G58D, the majority of the *CPT* values did not fall within ± 5% of the total test duration's *CPT* value. The majority of the truck counts fell within ± 25% of the *AHTT*. The only other trend in the data was with regards to the *RMC* values. From 4:00 AM to noon, when the *RMC* data points were within ± 5% of their total test duration's *RMC* value, their corresponding truck counts were within ± 25% of the *AHTT*. However, there was not a direct relationship between a test's *RMC* value and its corresponding truck count nor between a test's *CPT* value and its corresponding truck count. This is due to variables that were not specifically considered in the individual one-hour test's truck count. These variables include the variation in the truck weight and configuration, the variation in bridge lane truck traffic flow, and the variation in truck traffic flow due to the time of day, the day of the week, and the month of the year. The best correlation between the *RMC* values and its corresponding truck count occurred between 4:00 AM and 8:00 AM. During this time period, when the RMC values were at or below the total test duration's RMC value, its corresponding truck counts were at or below the *AHTT* volume.

The results of the second evaluation procedure for secondary bridge member fatigue prone details are presented in Figures 4-38 through 4-45. Based on the results presented in these figures, the following observations were made. The majority of the *RMC* values for all gages fell within ± 5% of the total test duration's *RMC* value. The majority of the *CPT* values for all gages did not fall within ± 5% of the total test duration's *CPT* value. The majority of the truck counts fell within ± 25% of the *AHTT*.

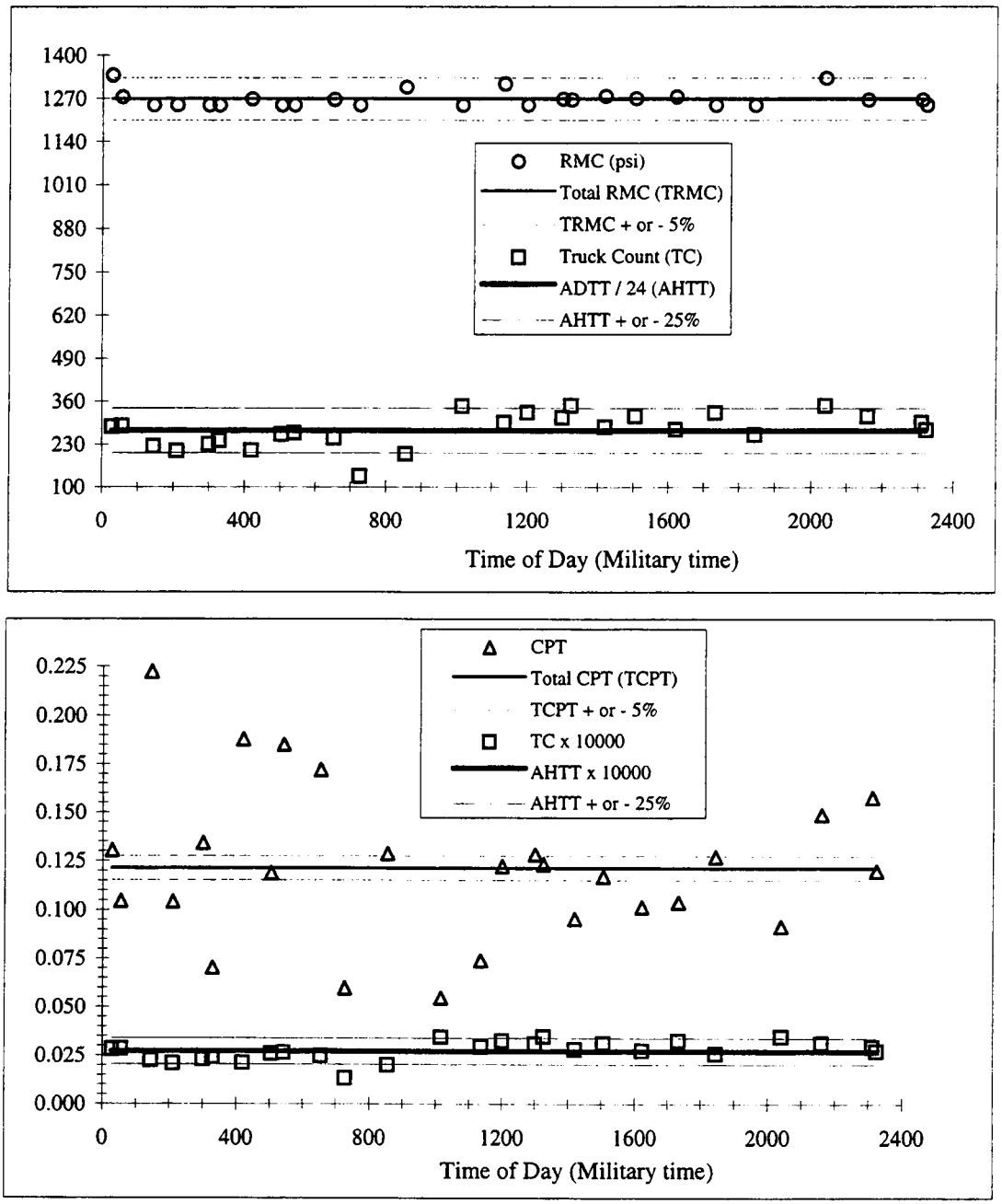


Figure 4-38. Top Plot Showing the Relationship Between RMC and Truck Count and Bottom Plot Showing the Relationship Between CPT and Truck Count for Category A Secondary Bridge Member Detail, G35

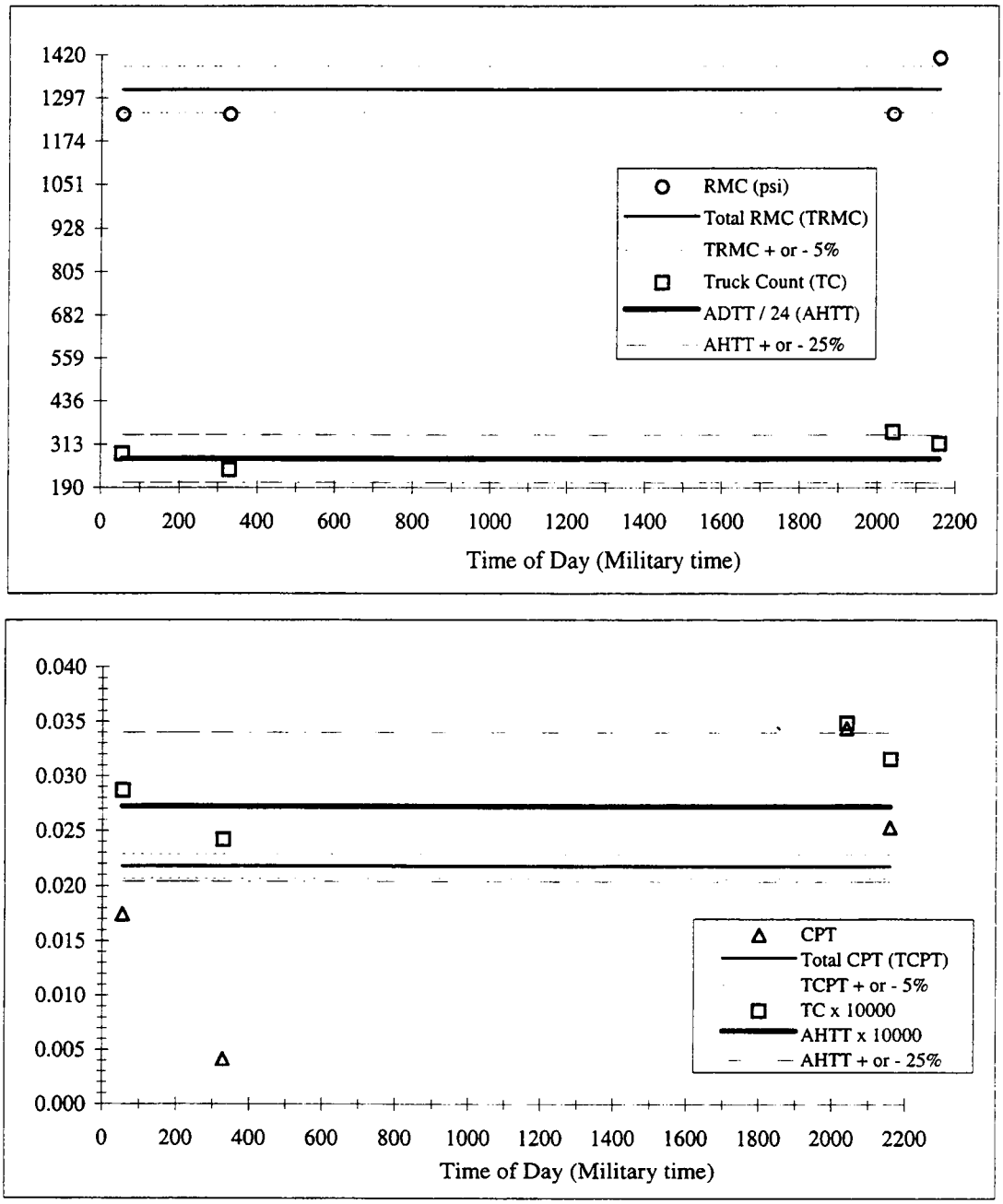


Figure 4-39. Top Plot Showing the Relationship Between RMC and Truck Count and Bottom Plot Showing the Relationship Between CPT and Truck Count for Category B Secondary Bridge Member Detail, G2

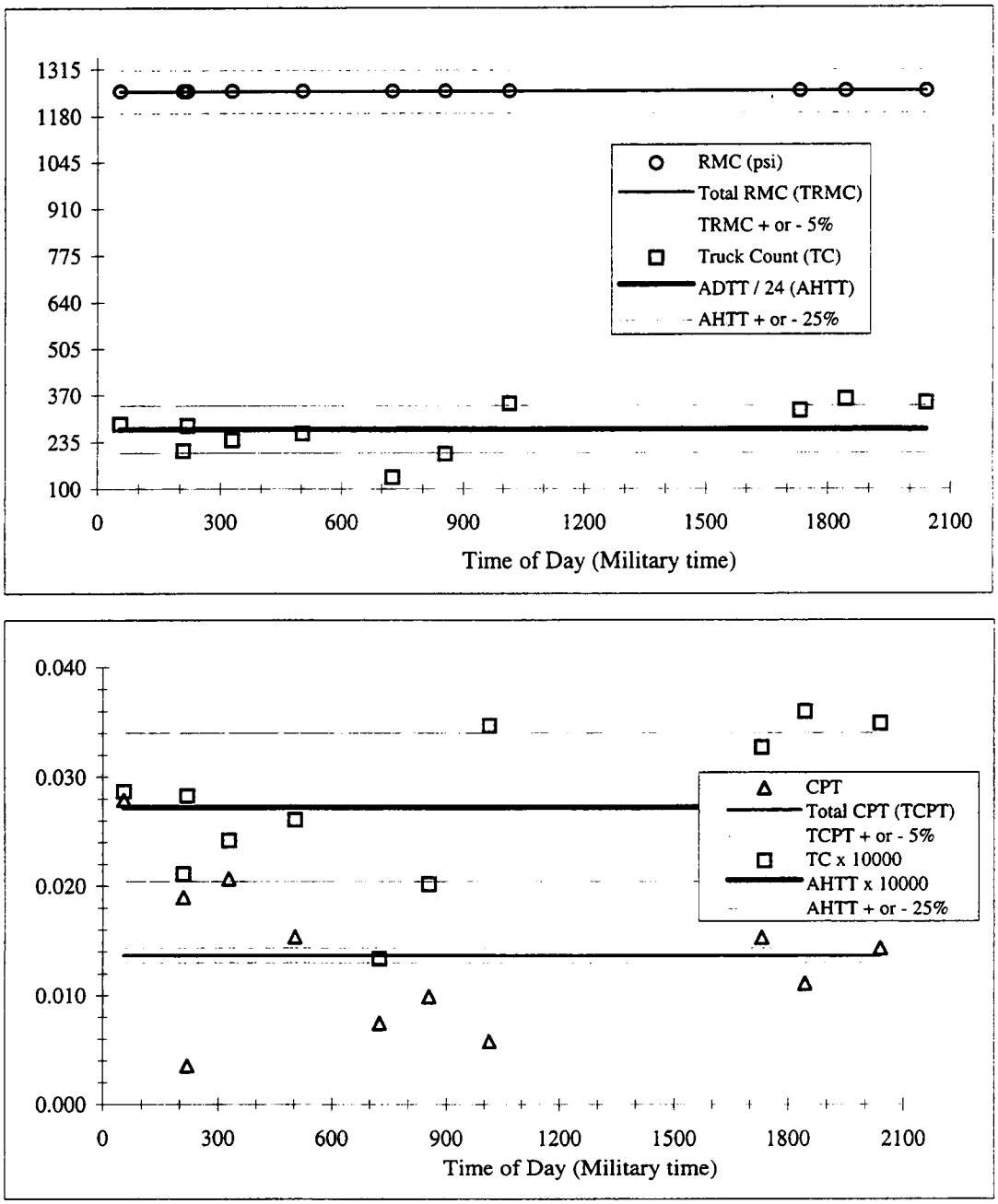


Figure 4-40. Top Plot Showing the Relationship Between RMC and Truck Count and Bottom Plot Showing the Relationship Between CPT and Truck Count for Category C Secondary Bridge Member Detail, G32

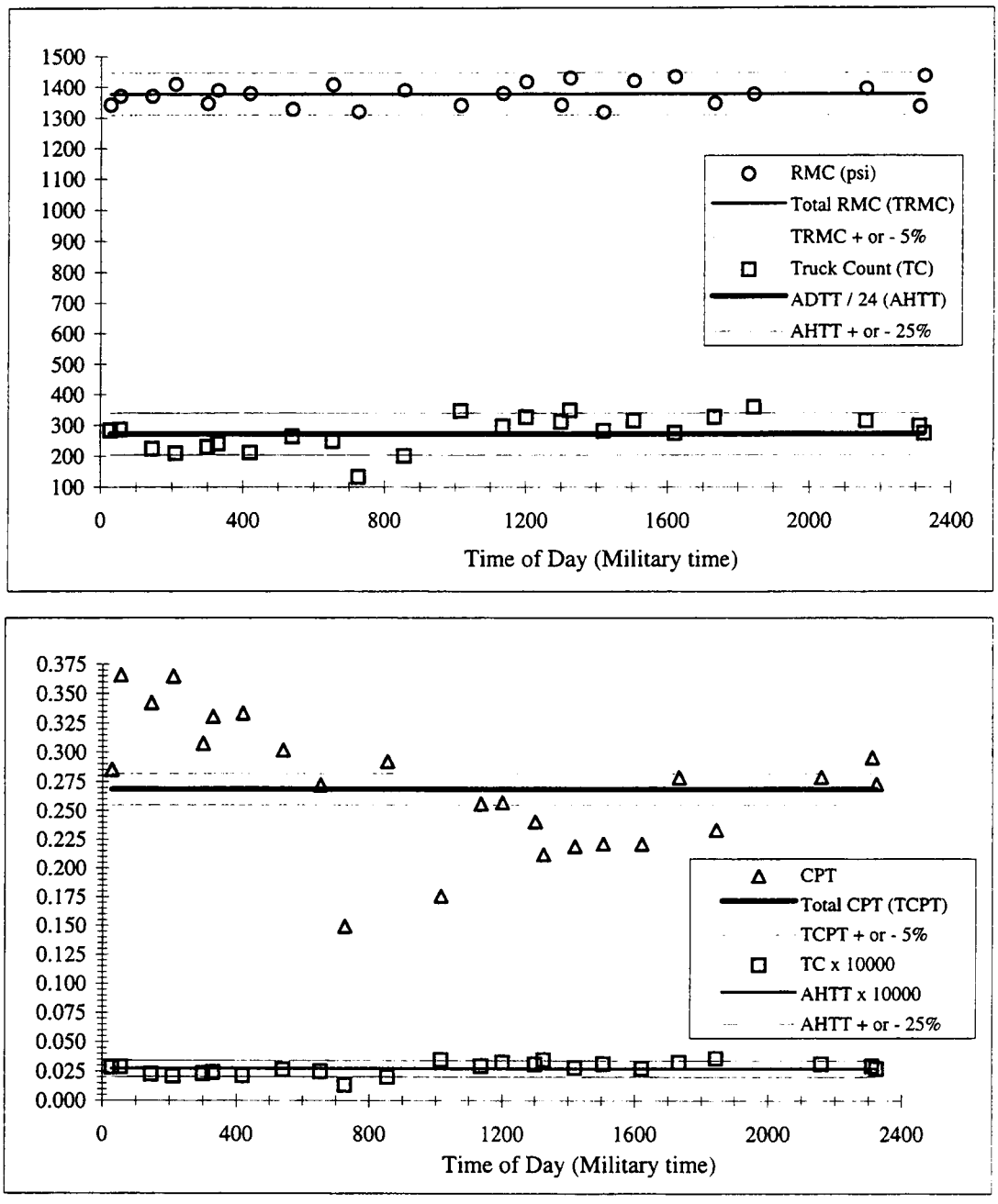


Figure 4-41. Top Plot Showing the Relationship Between RMC and Truck Count and Bottom Plot Showing the Relationship Between CPT and Truck Count for Category E Secondary Bridge Member Detail, G34

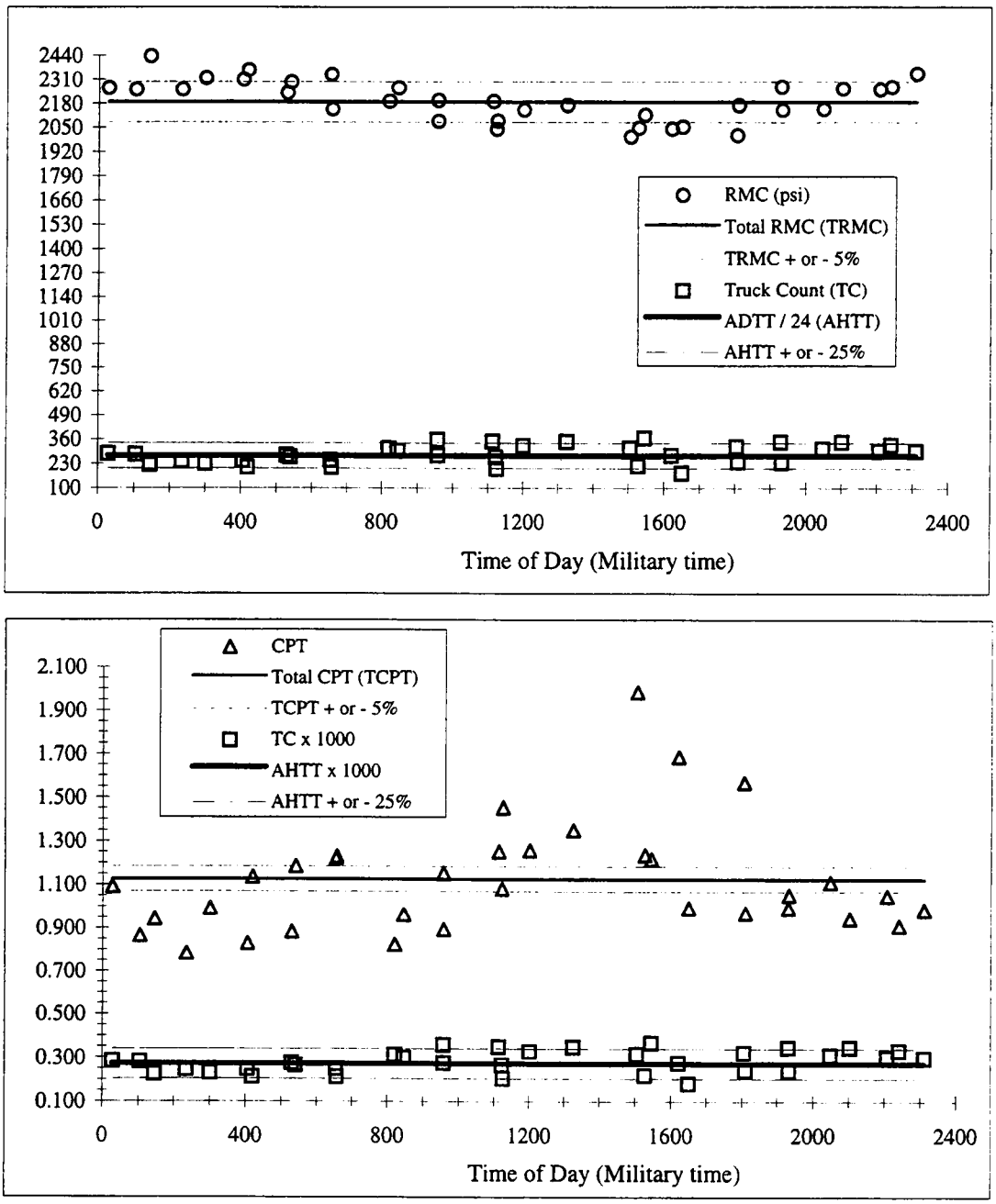


Figure 4-42. Top Plot Showing the Relationship Between RMC and Truck Count and Bottom Plot Showing the Relationship Between CPT and Truck Count for Category E Secondary Bridge Member Detail, G105

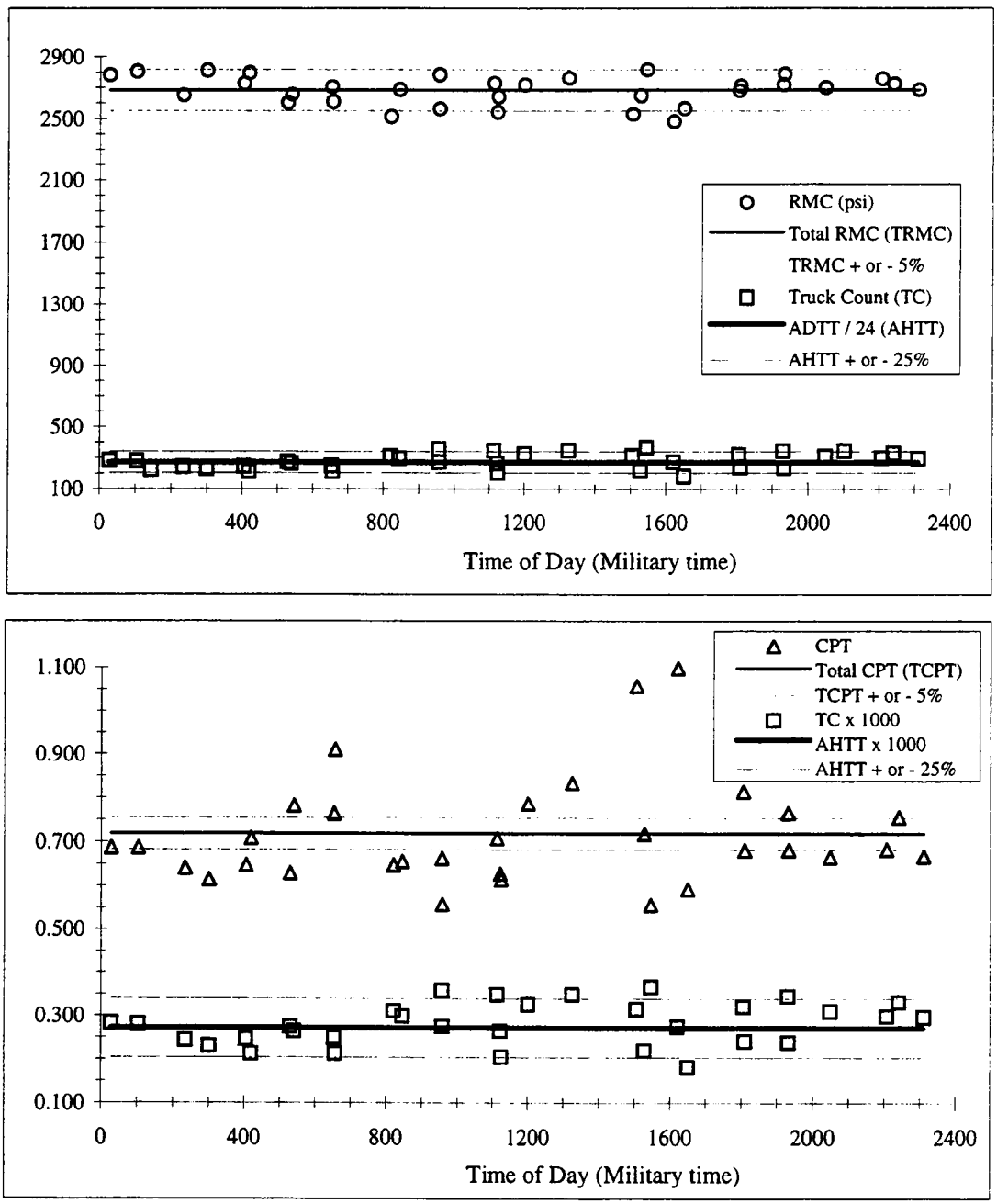


Figure 4-43. Top Plot Showing the Relationship Between RMC and Truck Count and Bottom Plot Showing the Relationship Between CPT and Truck Count for Category E Secondary Bridge Member Detail, G305

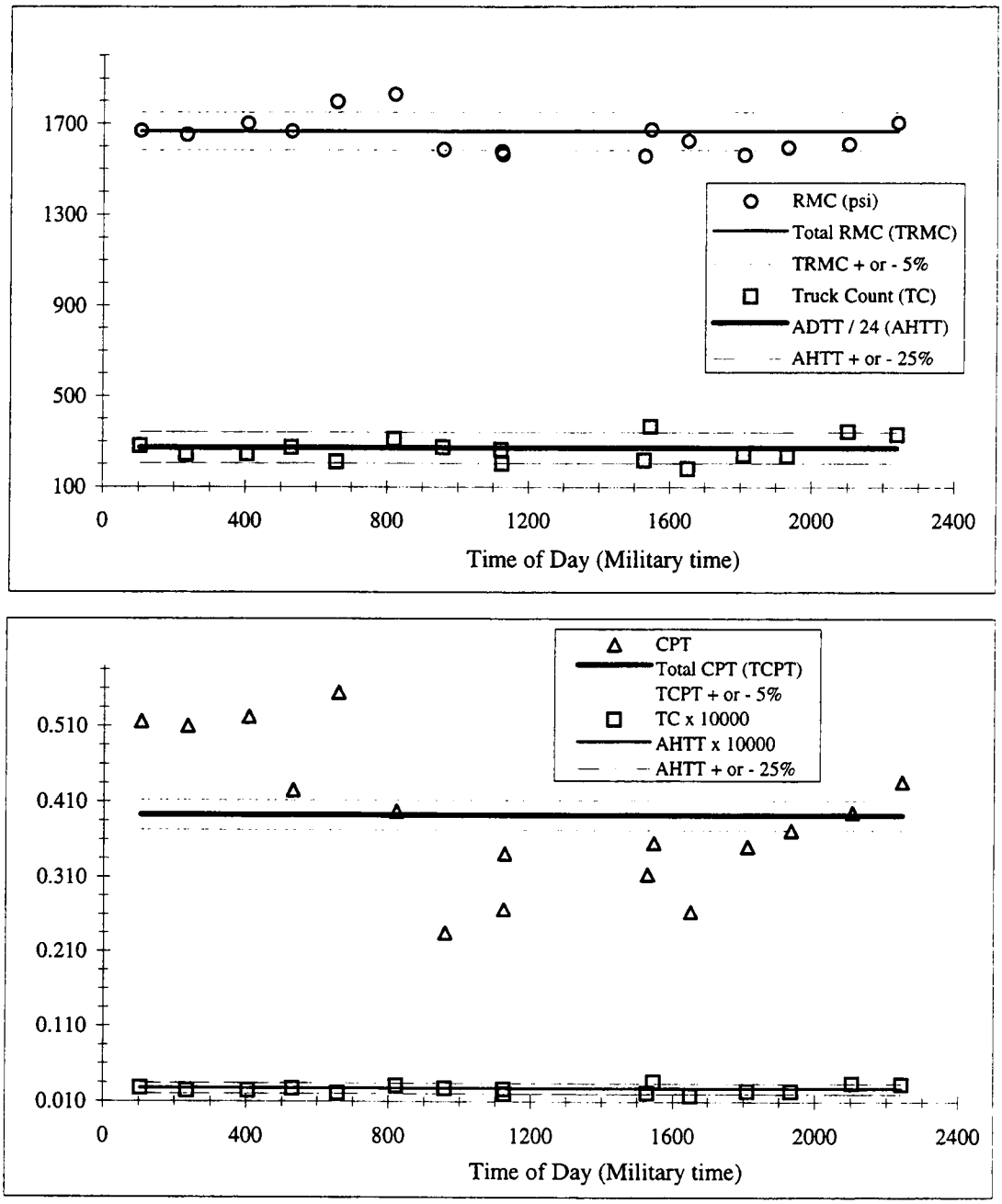


Figure 4-44. Top Plot Showing the Relationship Between RMC and Truck Count and Bottom Plot Showing the Relationship Between CPT and Truck Count for Category E' Secondary Bridge Member Detail, G117

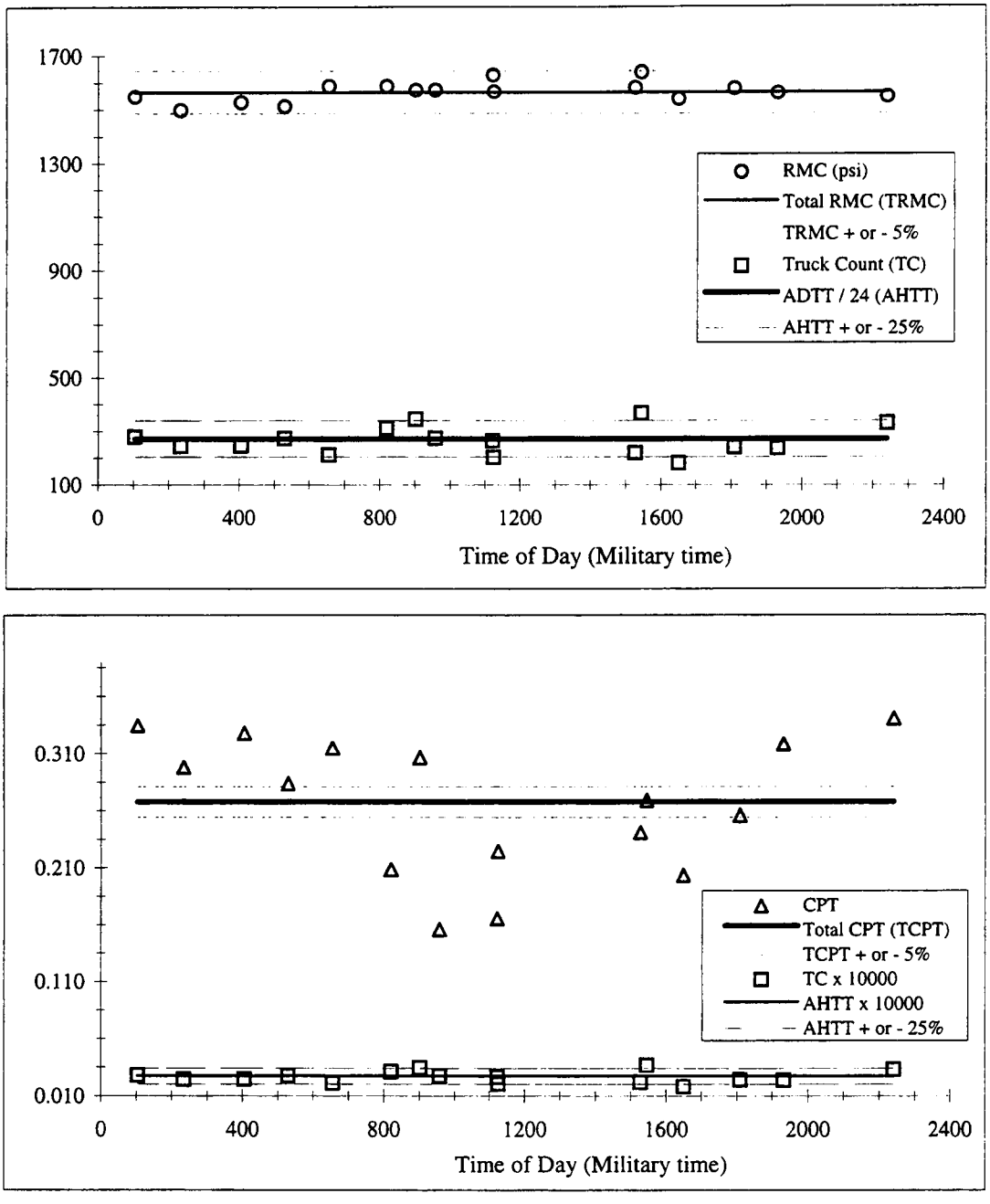


Figure 4-45. Top Plot Showing the Relationship Between RMC and Truck Count and Bottom Plot Showing the Relationship Between CPT and Truck Count for Category E' Secondary Bridge Member Detail, G317

There were no other trends in the data.

The results of these two evaluation procedures show that test duration has a greater effect on the number of cycles per truck than it does on the effective stress range. The results of the second evaluation procedure suggested that there was no direct relationship between the *RMC* and the truck count nor between the *CPT* and the truck count. Thus, the results of the second evaluation procedure validates the results of the first evaluation procedure as was shown in Table 4-17. However, the results presented in this table indicate that some of the less critical fatigue prone details require a longer test duration than some of the more critical fatigue prone details. Therefore, the criticality of the fatigue prone detail in addition to the results given in Table 4-17 should be taken into consideration in determining the minimum required field test duration. Criticality of a detail in this case is based on the detail's total fatigue life. Generally fatigue categories A, B, and C details, in accordance with the AASHTO *Guide* (1990) provisions, have an infinite fatigue life due to their low *RMC* and *CPT* values. Therefore, although the *RMC* data of G58 converged after five hours of testing, two hours of testing is sufficient since its fatigue life is so long. The maximum *CPT* value for all gages, with the exception of gages G47, G110, G105, and G305, was below one. The maximum *CPT* values for Categories A, B, and C main bridge member details were 0.36, 0.55, and 0.5, respectively. For secondary bridge members, the maximum *CPT* values for categories A, B, and C were 0.225, 0.035, and 0.03, respectively. Thus, a test duration of five hours is sufficient in providing a realistic representation of truck traffic flow. Table 4-18 gives recommended duration for field testing of fatigue prone details. These values are based

on the results presented in Figures 4-11 through 4-45, Table 4-17, and the fatigue criticality of the detail. These test duration are considered to be long enough to provide a realistic representation of truck traffic flow.

Table 4-18. Field Test Duration for AASHTO Fatigue Stress Categories

AASHTO Fatigue Category	Field Test Duration (hours)							
	Bridge Main Longitudinal Members				Bridge Secondary Members			
	Interior Span		Approach Span		Interior Span		Approach Span	
	RMC	CPT	RMC	CPT	RMC	CPT	RMC	CPT
A	2	3	-	-	1	3	-	-
B	2	5	-	-	-	-	2	5
C	2	5	-	-	1	5	-	-
E	2	12	-	-	3	12	7	23
E'	2	18	10	18	1	12	2	13

Note: - = No Data

4.5 Conclusions

A sensitivity analysis examining the effect of cycle counting methods on the effective stress range and the number of cycles per truck revealed the following:

1. A comparison of five cycle counting methods, level-cross counting, peak counting, simple-range counting, mean-crossing-peak counting, and rainflow counting, using a simple variable amplitude strain-time history showed that both the stress range and the number of cycles are sensitive to cycle counting methods.
2. Two of the most commonly used cycle counting techniques for highway bridge variable amplitude loading are the mean-crossing-peak and the rainflow cycle counting methods. A comparison of the two methods using field data

taken under normal traffic showed that the rainflow cycle counting method is more conservative than the mean-crossing-peak method.

3. The relationship between mean-crossing-peak and rainflow cycle counting methods was determined in the form of a correlation coefficient and a linear regression line. It was determined that there is a nearly perfect positive correlation between the two methods.

A sensitivity analysis examining the effect of stress-range frequency-of-occurrence histogram construction on the effective stress range and the number of cycles per truck revealed the following:

1. For histograms starting at 250, 350, 500, 600, and 1000 psi with interval widths of 250, 350, 500, 600, and 1000 psi, respectively:
    - Both the effective stress range and the number of cycles per truck are sensitive to histogram construction;
    - The effective stress range increased with increase in interval width while the number of cycles decreased with increase in interval width.
    - For main bridge member details, the fatigue damage decreased with increase in interval width;
    - For secondary bridge member details, interval width of 600 psi caused the most damage while interval width of 1000 psi caused the least fatigue damage; and

- With exception of histograms with interval width of 1000 psi, there was no significant difference in fatigue damage between the various histograms.

2. For histograms starting at 500 psi with interval widths of 250, 350, 500, 600, and 1000 psi:
    - The effective stress range was sensitive to histogram construction, while the number of cycles per truck was not sensitive to histogram construction;
    - The effective stress range and fatigue damage increased with increase in interval width;
    - For Category A and B details with an effective stress range less than 1000 psi, there was a significant difference in fatigue damage between the histograms; and
    - For Category A, C, E, and E' details, with exception of histograms with an interval width of 1000 psi and those histograms with an effective stress range less than 1000 psi, there was no significant difference in fatigue damage between the various histograms.
3. For histograms starting at 1000 psi with interval width of 250, 350, 500, 600, and 1000 psi:
    - For both main and secondary bridge member details, the effective stress range, the total fatigue life, and the fatigue damage slightly increased with increase in interval width; and

- With exception of Category A and C secondary bridge member details and those histograms with an interval width of 1000 psi, there was not a significant difference in the effective stress range, the total fatigue life, and the fatigue damage between the various histograms.

A sensitivity analysis examining the effect of fatigue field test duration on the effective stress range (*RMC*) and the number of cycles per truck (*CPT*) revealed the following:

1. With increase in test duration, the *RMC* and the *CPT* data converged to a single value for fatigue categories A, B, C, E, and E' details;
    - The RMC data converged at a faster rate than the *CPT* data;
    - The data for the bridge's interior span details converged at a faster rate than that for its approach span details; and
    - The data for the bridge's secondary member details converged at a faster rate than that for its main member details.
2. For fatigue categories A, B, C, E, and E' details, the *CPT* data was more sensitive to test duration than the *RMC* data. The field test duration required to realistically represent the effect of truck traffic flow was much less for the effective stress range than it was for the number of cycles per truck.
    - The required field test duration with regards to the *RMC* data for main and secondary bridge member fatigue prone details located in an interior span were 2 hours and 1 hour, respectively;

- The required field test duration with regards to the *RMC* data for secondary bridge member fatigue categories B, E, and E' details located in an approach span were 2, 7, and 2 hours, respectively;
- The required field test duration with regards to the *RMC* data for main bridge member fatigue category E' details located in an approach span was 10 hours;
- The required field test duration with regards to the *CPT* data for main bridge member fatigue categories A, B, C, E, and E' details located in an interior span were 3, 5, 5, 12, and 18 hours, respectively. Where as, for category E' main bridge member detail located in an approach span, the required test duration was 18 hours; and
- The required field test duration with regards to the *CPT* data for secondary bridge member fatigue categories A, C, E, and E' details located in an interior span were 3, 5, 12, and 12 hours, respectively. Where as, for categories B, E, and E' secondary bridge member details located in an approach span, the required test duration were 5, 23, and 13 hours, respectively.

3. As part of this sensitivity analysis, the relationship between a given one-hour test segment's truck count and its corresponding *RMC* value was evaluated. It was determined that the *RMC* value was not very sensitive to the truck count. As long as the hourly truck count was within ± 25% of the average hourly truck traffic volume, then its corresponding *RMC* value was within ± 5% of

the total test duration's *RMC* value. Also, the relationship between a given one-hour test segment's truck count and its corresponding *CPT* value was evaluated. It was determined that the *CPT* value was very sensitive to the truck count. However, there was no direct correlation between the *RMC* and the truck count nor between the *CPT* and the truck count.

CHAPTER 5

REMAINING FATIGUE LIFE ESTIMATION

This chapter presents a more refined remaining fatigue life calculation procedure than AASHTO *Guide*'s (1990) procedure. The number of cycles per truck for various fatigue stress category details and a formula for the present truck volume are also developed in this chapter. Finally, a comparison of the remaining fatigue life calculation results based on the refined procedure and the AASHTO *Guide*'s procedure is presented.

5.1 Literature Review

Stress Cycles per Truck

Highway steel bridge main member fatigue life is controlled by the passages of trucks across the bridge. An important parameter for each truck passage is the equivalent number of stress cycles. The AASHTO *Guide*'s provision for the number of stress cycles per truck , C, is dependent upon the bridge type and length, as shown in Table 5-1.

Table 5-1. AASHTO Guide's Number of Stress Cycle per Truck Passage

Bridge Member	Bridge Type	Span Length	C (cycle / truck)
Longitudinal	Simple-Span Girders	Above 40-ft	1.0
		Below 40-ft	1.8
	Continuous-Span Girders	Above 80-ft	1 + (Span-80)/400
	(within 0.1 of the span on each	40-ft < Span < 80-ft	1.0
	side of an interior support)	Below 40-ft	1.5
	Continuous-Span Girders	Above 40-ft	1.0
	(Elsewhere)	Below 40-ft	1.5
	Cantilever (Suspended Span) Girders	Any Span Length	2.0
	Trusses	Any Span Length	1.0
Transverse	Any Bridge Type	Above 20-ft	1.0
		Below 20-ft	2.0

As an alternative, the number of stress cycles per passage of a fatigue truck across a given span can be calculated by

$$N_e = 1 + \sum \left(\frac{S_{ri}}{S_{rp}} \right)^3 \tag{5.1}$$

in which N_e is the equivalent number of primary cycles for a complex cycle, S_{ri} is the stress range for a higher order cycle, and S_{rp} is the stress range for the primary cycle. The *Guide* allows the shape of the complex cycle to either be calculated for a given span by using an influence line or obtained from a field measured stress-time plot of a typical truck passage.

The AASHTO *Guide*'s provisions were adopted from the work done by Schilling (1984), in which analytical methods were used to develop design values for the number of stress cycles caused by the passage of a fatigue truck across various lengths of simple and continuous span steel bridges. Many investigators have since assumed the number of stress cycles per truck for main members to be 1.0 regardless of bridge type and span length. They include Keating et al. (1990), Yen et al. (1990), Hanson et al. (1991), Chen (1992), and Zuraski (1993). Post et al. (1988), through field measurements, obtained a value of 0.09 stress cycles per truck for a Category E' detail. Nowak et al. (1993), through field testing of a continuous steel bridge with typical spans of 62-ft, observed that about one-half of the trucks crossing the bridge produced a measured stress cycle.

Remaining Life

Section 3 of the AASHTO *Guide* (1990) outlines a procedure for estimating the remaining fatigue life of an existing steel bridge. This procedure is limited to uncracked

and unrepaired members subjected to primary stresses that are normally calculated in design. Outlined in this procedure are remaining life estimation criteria for when the effective stress range is calculated and when it is obtained through field measurements while the bridge is under normal traffic. The discussion herein will be limited to when the effective stress range is obtained through field measurements. The first step in this procedure is to calculate the effective stress range or the root-mean-cube (*RMC*) value from stress-range histograms obtained through field measurements. The *RMC*, S_r, is given by

$$S_r = \left(\sum f_i S_{ri}^3\right)^{1/3} \tag{5.2}$$

in which f_i is the fraction of stress range within an interval and S_{ri} is the midwidth of the interval. The next step in the procedure is to ascertain if the remaining fatigue life is infinite or finite. The criteria for infinite remaining life is

$$R_s S_r \langle S_{FL} \tag{5.3}$$

in which R_s, a reliability factor, is 1.15 and S_{FL} is the limiting stress range for infinite life, as shown in Table 5-2. If this criteria is met, than no further fatigue calculations are required. If this criteria is not met, than the finite remaining fatigue life for an estimated lifetime average daily truck volume is calculated by

$$Y_f = \frac{f K \times 10^6}{T_a C(R_s S_r)^3} - a \tag{5.4}$$

Table 5-2. Detail Constant, K, and Limiting Stress Range, S_{FL}, Values

	$N = 2 \times 10^6$ Cycles			$N > 2 \times 10^6$ Cycles	
Detail Category	F_{sr} (ksi)	$A = N(F_{sr})^3$	$K = A / 356 \times 10^6$	F_{sr} (ksi)	$S_{FL} = F_{sr} / 2.75$ (ksi)
A	24.0	2.50×10^{10}	68.0	24.0	8.8
B	18.0	1.19×10^{10}	33.0	16.0	5.9
C	13.0	4.39×10^{9}	12.0	10.0	3.7
D	10.0	2.19×10^{9}	6.0	7.0	2.6
E	8.0	1.06×10^{9}	2.9	4.5	1.6
E'	5.8	3.90×10^{8}	1.1	2.6	0.9

Note: F_{sr} = AASHTO *Standard* (1992) constant-amplitude fatigue limit or allowable stress range

in which Y_f is the remaining fatigue life in years, K is the detail constant (see Table 5-2), T_a is the estimated average daily truck volume (*ADTT*) in the outer lane, C is the number of stress cycles per truck passage (see Table 5-1), S_r is the *RMC* value in ksi, R_s is a reliability factor (1.35 x 0.85), a is the present age of the bridge in years, and f is 1.0 for calculating safe life and 2.0 for calculating mean life. The *Guide*'s mean life is the best possible estimate of the actual life; there is a 50% probability that the actual life will exceed the mean life. The *Guide*'s safe life provides a much higher degree of safety; the probability that the actual life will exceed the safe life is 97.7%.

The lifetime *ADTT* in the outer lane is estimated from the present *ADTT* in the outer lane, T, the present age of the bridge, a, and the annual growth rate, g. The present *ADTT*, T, is calculated by

$$T = (ADT) F_T F_L \tag{5.5}$$

in which *ADT* is the present average daily traffic volume (both directions) on the bridge. F_T is the fraction of trucks (excluding panel, pickup, and 2-axle/4-wheel trucks) in the traffic; F_T is 0.20 for rural interstate highways, 0.15 for other rural highways and urban interstate highways, and 0.10 for other urban highways. F_L is the fraction of trucks in the outer lane. For two-way traffic, F_L is 0.60, 0.50, 0.45, 0.45, 0.40 for number of bridge lanes equal to 2, 3, 4, 5, and 6 or more, respectively. For one-way traffic, F_L is 1.00, 0.85, and 0.80, for number of bridge lanes equal to 1, 2, and 3 or more, respectively.

A widely accepted method of calculating the remaining fatigue life of existing steel bridges (AISC 1986, Yen et al. 1990, Hanson et al. 1991) is by comparing the cycles to date, N_p, with the total fatigue life, N_t. The difference between these two values is the remaining fatigue life, N_r, as shown in Figure 5-1.

$$N_r = N_t - N_p \tag{5.6}$$

For a given effective stress range or root-mean-cube (*RMC*) value, S_r, the total fatigue life is given by

$$N_t = A S_r^{-3} \tag{5.7}$$

in which *A*, a coefficient with values as listed in Table 5-2, is the intercept for AASHTO Standard design curves at *N* equal to 2,000,000 cycles. The number of cycles to date, N_p, is the area under a time versus one-way *ADTT* plot starting from year zero to present, as shown in Figure 5-2. The remaining life in years, Y_r, is taken as

$$Y_r = \frac{N_r}{ADTT_p \times CPT \times 365} \tag{5.8}$$

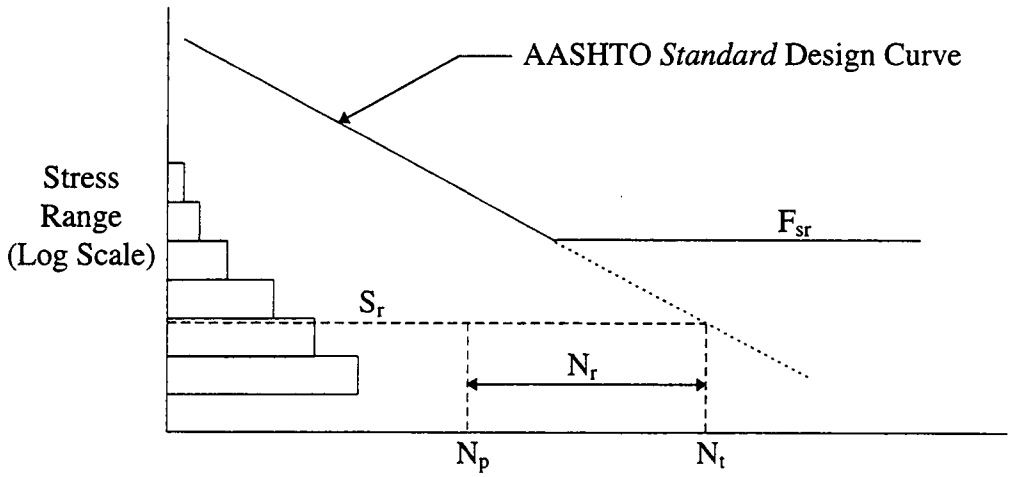


Figure 5-1. Estimation of Remaining Fatigue Life

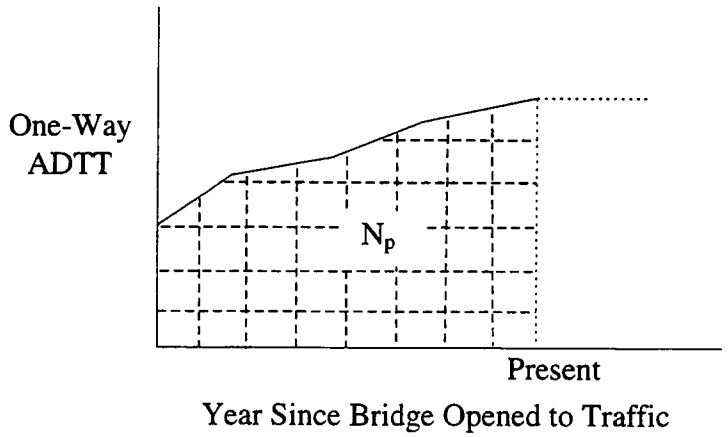


Figure 5-2. Average Daily Truck Traffic Volume (*ADTT*) Variation with Time

in which $ADTT_p$ is the present *ADTT* and *CPT* is the number of stress cycles per truck passage (usually taken as 1.0).

5.2 Fatigue Testing Procedure

Fatigue testing of the Holston River Bridge was conducted under normal traffic. Electrical resistance foil strain gages were used to measure dynamic strain during testing. Strain gages were installed in areas of high stress that would be susceptible to fatigue damage. The gage locations were all within the first three spans of the bridge, as shown in the Appendix. Table A-1 is a listing of all the gages; this table lists the gage number, the gage sample location, the applicable AASHTO fatigue stress category, and the gage detail description.

The data collection procedure was as follows. The cargo van equipped with the data acquisition system was parked off the shoulder approximately 75 ft from the west end of the bridge, so as not to disrupt normal truck traffic flow. Gages were balanced prior to each set of tests and the data for the prebalanced and the balanced conditions were recorded. In addition to the strain gage data collection, tallies of truck traffic were also collected for each test. For each truck passage, this manual record included traffic direction, lane of traffic, and time relative to the beginning of the test. After each test, the recorded gage data were reviewed in conjunction with the manual truck traffic record to determine what load condition caused a specific reading at a specific gage location. Recorded gage data that contained unexplainable spikes and/or numerous shifts were discarded. The data for each gage was generally recorded in one-hour segments. The

total test duration for each gage varied; some gages were tested as little as half an hour and some as much as sixty-seven hours.

After reviewing the raw data for any erroneous readings, it was then reduced using the rainflow cycle counting method. A stress-range frequency-of-occurrence histogram starting at 1000 psi with interval width of 500 psi was constructed for each hour of recorded strain data. The histograms for each gage's one-hour test segment was added to obtain the gage's total test duration frequency-of-occurrence histogram.

5.3 Present Truck Volume

During data collection under normal traffic, strain traces were observed as trucks crossed the bridge. The correlation between gage and truck location in producing a measurable strain range was noted. Figure 5-3 illustrates the truck traffic position that produced a measurable strain range reading for gages located on Girder 4 and gage locations 1 and 2. Based on field observations, the effect of lane truck traffic on each gage varied depending on the location of the gage. For a given gage location, Table 5-3 gives the percentage of truck traffic in each lane that produced a measurable strain range reading.

Based on the results presented in Table 5-3, the present truck volume, T, can be expressed as

$$T_I = (\, P_{ML} + P_{RL} \,) ADTT$$

or

$$T_{II} = (\, 0.15\, P_{LL} + P_{ML} + 0.15\, P_{RL} \,) ADTT \qquad (5.9)$$

or

$$T_{III} = [\, (P_{LL} + P_{ML} + 0.15\, P_{RL}) ADTT \,]_1 + (P_{LL}\, ADTT)_2$$

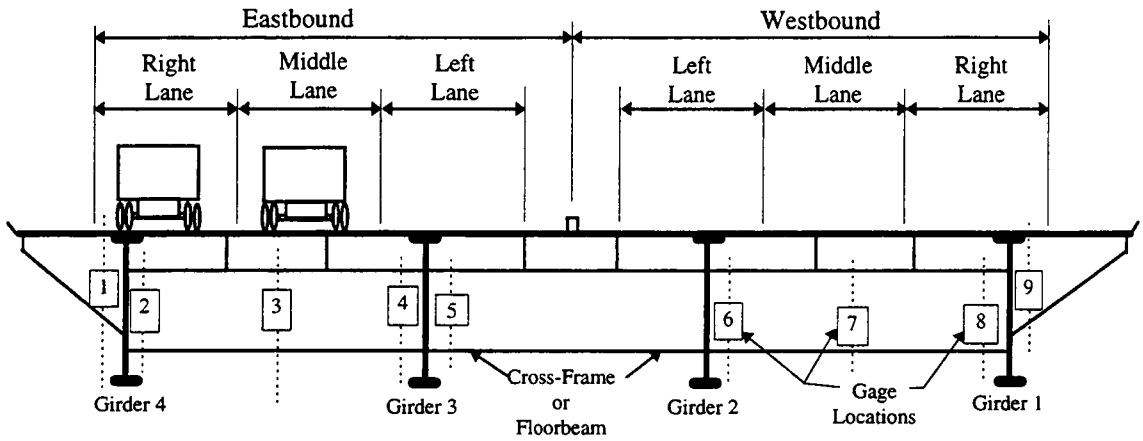


Figure 5-3. Typical Gage Locations Throughout the First Three Spans

Table 5-3. Percentage of Trucks Producing a Measurable Strain Range Reading

Gage Location	% of Truck Traffic in Each Lane					
	Eastbound Traffic			Westbound Traffic		
	Right Lane	Middle Lane	Left Lane	Left Lane	Middle Lane	Right Lane
9	0	0	0	0	100	100
Girder 1	0	0	0	0	100	100
8	0	0	0	0	100	100
7	0	0	0	15	100	15
6	0	0	100	100	100	15
Girder 2	0	0	100	100	100	15
5	15	100	100	100	0	0
Girder 3	15	100	100	100	0	0
4	15	100	100	100	0	0
3	15	100	15	0	0	0
2	100	100	0	0	0	0
Girder 4	100	100	0	0	0	0
1	100	100	0	0	0	0

Note: See Figure 5-3 for gage location

in which T_I is the present truck volume for gages located on a main longitudinal fascia girder or at the end of any secondary member that is attached to the fascia girder, such as gage locations 1, 2, 8, and 9 of Figure 5-3, T_{II} is the present truck volume for gages located at the midlength of a transverse member that is between a fascia girder and an interior girder, and T_{III} is the present truck volume for gages located on an interior girder or at the end of a secondary member that is attached to an interior girder, such as gage locations 4, 5, and 6 of Figure 5-3; *ADTT* is the one-way average daily truck traffic volume (excluding panel, pickup, and 2-axle/4 or 6-wheel trucks) on the bridge; *P* is the percentage of the *ADTT* in each lane; the subscripts *1* and *2* represents the two traffic directions while the subscripts *LL*, *ML*, and *RL* represents the bridge's left, middle, and right lanes, respectively.

The average daily truck traffic volume was obtained from the truck tallies recorded during testing. The truck traffic data was collected around the clock to account for the variation in traffic. The Holston River Bridge's truck traffic characteristics, lane distribution, and percentage of the average daily traffic volume (*ADT*) are shown in Table 5-4. The *ADT* was obtained from traffic flow maps (TNDOT, 1994). Based on equations (5.5) and (5.9), the present truck volume for the Holston River Bridge is given in Table 5-5. The *Guide*'s *ADTT* equal to 15% of *ADT* is unconservative for the Holston River Bridge when compared to actual recorded truck traffic. The actual recorded truck traffic shows that the *ADTT* is 27.31% and 28.94% of *ADT* for the eastbound and westbound traffic, respectively. The *Guide*'s requirement of using the *ADTT* in the outer lane is also

Table 5-4 Holston River Bridge Truck Traffic Characteristics

	Eastbound	Westbound
Total Recorded Traffic Duration (hours)	67.94	67.94
*Total Number of Trucks	18536	18769
*Average Number of Trucks per Hour (AHTT)	273	276
*Average Daily Truck Traffic Volume (ADTT)	6552	6624
Average Daily Traffic Volume (ADT)	23990	22890
Percentage of ADT = ADTT	27.31	28.94
Percentage of Trucks in the Left Lane	14	10
Percentage of Trucks in the Middle Lane	60	56
Percentage of Trucks in the Right Lane	26	34
Percentage of Trucks 3D (3-Axle Trucks)	1.38	1.88
Percentage of Trucks 4D (4-Axle Trucks)	0.15	0.2
Percentage of Trucks 2S1 (3-Axle Semitrailer Trucks)	1.02	2.04
Percentage of Trucks 2S2 (4-Axle Semitrailer Trucks)	2.04	2.71
Percentage of Trucks 3S2 (5-Axle Semitrailer Trucks)	87.24	84.08
Percentage of Trucks 3S3 (6-Axle Semitrailer Trucks)	0.31	0.24
Percentage of Trucks DT (Double/Twin Trailer Trucks)	7.47	8.35
*Percentage of Trucks Other	0.39	0.5

Note: * = Excluding panel, pickup, and 2-axle/4 or 6-wheel trucks

Table 5-5 Present Truck Volume Based on Equations (5.5) and (5.9)

		Eastbound		Westbound	
		Expression	Value	Expression	Value
Eq. (5.5)	ADT		23990		22890
AASHTO	F_T (% of ADT = ADTT)	0.15 ADT	3599	0.15 ADT	3434
Guide	F_L (% of Trucks in RL)	80%	0.8	80%	0.8
Values	$T = (ADT) F_T F_L$	0.12 ADT	2879	0.12 ADT	2747
Actual	F_T (% of ADT = ADTT)	0.2731 ADT	6552	0.2894 ADT	6624
Values	F_L (% of Trucks in RL)	26%	0.26	34%	0.34
	$T = (ADT) F_T F_L$	0.071ADT	1703	0.098 ADT	2252
Eq. (5.9)	ADTT	0.2731 ADT	6552	0.2894 ADT	6624
	$T_I = (P_{ML} + P_{RL})$ ADTT	0.235 ADT	5638	0.260 ADT	5951
	$T_{II} = (0.15$ ADTT $(P_{LL} + P_{RL}))$ + ADTT P_{ML}	0.180 ADT	4318	0.181 ADT	4143
	$T_{III} = [(P_{LL} + P_{ML} + 0.15 P_{RL})$ ADTT$]_1$ + $(P_{LL}$ ADTT$)_2$	0.213 ADT_E + 0.029 ADT_W	5766	0.206 ADT_W + 0.038 ADT_E	5627

unconservative for this bridge. The present truck volume based on the *Guide*'s requirements, equation (5.5), is about 50% of the actual present truck volume (equation 5.9). Also, using the one-way *ADTT* for the present truck traffic volume as is suggested in equation (5.8) would be conservative for this bridge. The actual present truck volume based on equation (5.9) varies from 62.5% to 90% of the one-way *ADTT* depending on the gage location. The values for T_I, T_{II}, and T_{III} can conservatively be taken as 90%, 70%, and 90% of the one-way *ADTT*, respectively. A better estimate of the *ADTT* would be 25% of the *ADT* rather than the *Guide*'s 15% for this bridge.

5.4 Stress Cycles per Truck

The evaluation procedure for determining the number of stress cycles per truck under normal traffic was as follows. For each gage, the total test duration's number of cycles and truck traffic count was used to calculate the number of stress cycles per truck (*CPT*). The total truck count corresponding to the total number of cycles was calculated using equation (5.9); instead of *ADTT*, the total test duration's truck count was used. The *CPT* is given by

$$CPT = \frac{Total\ Cycles}{T_I} = \frac{Total\ Cycles}{(P_{ML} + P_{RL})TC}$$

or

$$CPT = \frac{Total\ Cycles}{T_{II}} = \frac{Total\ Cycles}{(0.15P_{LL} + P_{ML} + 0.15P_{RL})TC} \qquad (5.10)$$

or

$$CPT = \frac{Total\ Cycles}{T_{III}} = \frac{Total\ Cycles}{\left[(P_{LL} + P_{ML} + 0.15P_{RL})TC\right]_1 + \left(P_{LL}\,TC\right)_2}$$

in which *TC* is the one-way total test duration's recorded truck count (excluding panel, pickup, and 2-axle/4 or 6-wheel trucks). This evaluation is limited to gages that have a total test duration greater than five hours and a total number of stress cycles greater than twenty. Test durations of less than five hours were not considered long enough to incorporate the effect of truck traffic variation on the number of cycles per truck. Number of stress cycles less than twenty results in unrealistically low *CPT* values. The results of this evaluation are presented in Table 5-6.

Based on the results presented in Table 5-6, the following observations were made. All *CPT* values, with the exception of those for gages 126, 128, 105, and 120, were less than one. Nowak et al.'s (1993) observation of a continuous steel bridge concur with this finding. *CPT* values varied depending on the location and the severity of the fatigue prone detail. For main member category A details, the *CPT* values for gages located on the girder bottom flange (58C, 58D, 140, 141, and 154) were almost twice the *CPT* values for gages located on the girder web (136, 143, 152, and 155). For the same main member web gap fatigue prone detail, approach span gages (107, 108,109, and 110) have larger *CPT* values than interior span gages (19, 20, 51, 52, 53, 73 to 76, and 95 to 98). Category E' gages at the end of main member web longitudinal weld (124, 126, and 128) have a larger *CPT* value than main member category E' web gap gages. For main member fatigue prone details, *CPT* values tend to increase with increase in the severity of the detail. For the same secondary bridge member categories E and E' details, the approach span gages (105, 117, and 118) have a larger *CPT* value than the interior span gages (305, 317, and 318). Secondary bridge member category E floorbeam flange

Table 5-6. Measured Stress Cycles per Truck Values

Main Bridge Member									Secondary Bridge Member								
	Gage	Dur.	TC			Total	Total			Gage	Dur.	TC			Total	Total	
FC	No.	(hrs)	EB	WB	T	Trucks	Cycle	CPT	FC	No.	(hrs)	EB	WB	T	Trucks	Cycle	CPT
A_2	58C	6.4		2316	I	2084	916	0.4395	A_2	35	26.6	7287		I	6267	866	0.1382
	58D	6.4		2316	I	2084	887	0.4255		41	26.6	7287		II	4809	817	0.1699
	136	7.4		2675	I	2408	312	0.1296		63	20.3		6070	I	5463	800	0.1464
	140	6.4		2316	I	2084	793	0.3804		64	5.14		948	I	853	120	0.1406
	141	6.4		2316	I	2084	775	0.3718		68	19.3		5260	II	3293	571	0.1734
	143	6.4		2316	I	2084	550	0.2639		84	19.5		5594	I	5035	425	0.0844
	152	6.4		2316	I	2084	469	0.225		88	19.5		5594	II	3502	377	0.1077
	154	6.4	1569	2316	III	1866	839	0.4495		89	19.5		5594	II	3502	895	0.2556
	155	6.4	1569	2316	III	1866	554	0.2968		150	6.44		2316	II	1450	196	0.1352
B_2	5	27	7420		I	6381	3286	0.515		151	6.44		2316	I	2084	469	0.225
	30	12	3414		I	2936	1172	0.3992	B_2	2	13.9	3874		I	3332	29	0.0087
	58	35		9774	I	8797	3662	0.4163		78	34		9500	I	8550	22	0.0026
	83	67		18612	I	16751	7485	0.4468	C_2	32	11.2	3020		I	2597	41	0.0158
	201	26	6934	7456	III	6147	668	0.1087	E_1	105	35.4	9693	10195	III	8570	11026	1.2865
	202	31	8198	8544	III	7223	2232	0.309		106	16.9	4902	5131	III	4332	1380	0.3186
	203	14	3700	3906	III	3273	1043	0.3187		120	34.4	9370	9752	III	8274	19247	2.3261
	204	45	12702	13349	III	11269	4555	0.4042		121	8.07	2506	2461	III	2198	1821	0.8284
C_2	58B	6.4		2316	I	2084	959	0.4601	E_2	34	24.5	6684		I	5748	1778	0.3093
E_2	45	15	4238		I	3645	1270	0.3485		42	15.3	4238		II	2797	1249	0.4465
	46	15	4238		I	3645	2797	0.7674		43	9.24	2400		II	1584	828	0.5227
	47	15	4238		I	3645	2288	0.6278		50	22.5	6190		I	5323	1122	0.2108
	48	14	3923		I	3374	2024	0.5999		61	20.4		6043	I	5439	2296	0.4222
	49	14	3984		I	3426	1902	0.5551		69	17.6		4968	II	3110	1233	0.3965
E'_1	107	15	3779	4001	III	3344	2952	0.8828		70	17.6		4968	II	3110	1357	0.4363
	108	15	3779	4001	III	3344	2166	0.6477		79	17.4		4920	I	4428	1411	0.3187
	109	15	3779	4001	III	3344	2348	0.7022		90	17.6		4968	II	3110	1643	0.5283
	110	15	3779	4001	III	3344	3129	0.9357		91	17.6		4968	II	3110	1460	0.4695
	116	33	9062	9440	III	8003	5010	0.626	E_3	305	33.3	9122	9631	III	8069	6567	0.8138
E'_2	19	15	4062		I	3493	1782	0.5101	E'_1	117	17	4331		II	2858	1726	0.6038
	20	15	4047		I	3480	1647	0.4732		118	17	4331		II	2858	1644	0.5751
	26	14	3396		I	2921	813	0.2784	E'_3	317	17	4331		II	2858	1177	0.4118
	51	34	9600		I	8256	4355	0.5275		318	6.68	1854		II	1224	618	0.5051
	52	32	8907		I	7660	5410	0.7063									
	52A	18	5362		I	4611	2907	0.6304									
	53	32	9023		I	7760	4028	0.5191									
	54A	18	5362		I	4611	2651	0.5749									
	73	17		5034	I	4531	2380	0.5253									
	74	9.9		3479	I	3131	1248	0.3986									
	75	20		5594	I	5035	2260	0.4489									
	76	16		5017	I	4515	2169	0.4804									
	95	16		4884	I	4396	2718	0.6183									
	96	20		5594	I	5035	1673	0.3323									
	97	20		5594	I	5035	1800	0.3575									
	98	15		4723	I	4251	2434	0.5726									
	124	18	5362		I	4611	4494	0.9746									
	126	8		2853	I	2568	3273	1.2747									
	128	8		2853	I	2567.7	2596	1.011									

Note: FC = Fatigue Category; Subscripts 1, 2, 3 = Bridge spans 1, 2, and 3; See eq. (5.10) for T & Total Trucks

termination details have the largest *CPT* values of any main and secondary fatigue prone details. These details consistently measured more than one stress cycle per truck passage; sometimes, each truck axle crossing produced a stress cycle.

The results of this evaluation suggests that the constant *CPT* value of one given by the AASHTO *Guide* (1990) for this type of bridge is not representative of actual conditions on the bridge. Table 5-7 gives measured *CPT* values for AASHTO fatigue stress categories A, B, C, E, and E' details.

Table 5-7. Measured *CPT* Values for AASHTO Fatigue Stress Categories

Steel Bridge Member	AASHTO Fatigue Category	Stress Cycle per Truck (CPT) Values							
		Interior Span				Approach (End) Span			
		Maximum	Minimum	Average	s	Maximum	Minimum	Average	s
Main	A	0.450	0.130	0.331	0.110	-	-	-	-
	B	0.515	0.109	0.365	0.123	-	-	-	-
	C	0.460	0.460	0.460	-	-	-	-	-
	E	0.767	0.348	0.580	0.152	-	-	-	-
	E'	1.275	0.278	0.590	0.251	0.883	0.626	0.759	0.141
Secondary	A	0.256	0.084	0.158	0.051	-	-	-	-
	B	0.009	0.003	0.006	0.004	-	-	-	-
	C	0.016	0.016	0.016	-	-	-	-	-
	E	0.814	0.211	0.443	0.155	2.326	0.319	1.190	0.854
	E'	0.505	0.412	0.458	0.066	0.604	0.575	0.589	0.020

Note: Average = The average value of all gages for a given fatigue category
s = The sample standard deviation
- = No data

5.5 Remaining Fatigue Life Procedure

Refined Procedure

A more refined calculation procedure than the AASHTO *Guide*'s (1990) procedure, equation (5.4), for estimating the remaining fatigue life of existing steel

bridges is presented. This procedure is based on equation (5.6), that is, comparing the number of cycles to date, N_p, with the total number of cycles to failure, N_t. The difference between these two values is the remaining fatigue life, N_r, as was shown in Figure 5-1. In order to estimate the remaining life of a detail, it is assumed that the detail's frequency-of-occurrence stress range histogram and its associated effective stress range or root-mean-cube (*RMC*) value, S_r, and the number of stress cycles per truck passage do not vary over time. Based on this assumption, the remaining fatigue life of steel bridges can be estimated using the following procedure:

1. Estimate the *RMC* value either through analytical methods or from stress range histograms obtained through field measurements and equation (5.2).
2. Estimate the number of stress cycles per truck passage (*CPT*) from Table 5-7 or calculate the *CPT* using measured data and equation (5.10).
3. Estimate the present one-way *ADTT*, *T*, using site specific data and equation (5.9) or conservatively assume that the present one-way truck traffic is 90%, 70%, and 90% of the total one-way *ADTT* for T_I, T_{II}, and T_{III}, respectively. Use the present estimated one-way *ADTT* percentages to estimate the *ADTT* for each year since the opening of the bridge.
4. Estimate the total number of cycles to date, N_p:

$$ADTT_{sum} = \sum_{j=1}^{p} T_j \left(\frac{W_j}{W_p} \right) \tag{5.11}$$

$$N_p = ADTT_{sum} \times CPT \times 365 \tag{5.12}$$

in which p is number of years since the opening of the bridge to traffic and by inference the present year, T_j is the estimated average daily truck volume in year j for each detail, W_j is the legal gross weight of trucks in year j, *CPT* is the estimated number of stress cycles per truck, and *365* is the number of days in a year.

5. Estimate the total number of cycles to failure, N_t, using equation (5.7) and the present estimated *RMC* value.
6. Calculate the remaining number of cycles, N_r, using equation (5.6).
7. Estimate the total number of trucks, T_r, corresponding to N_r:

$$T_r = \frac{N_r}{CPT} \tag{5.13}$$

8. Estimate the future yearly truck volume, T_i:

$$T_i = T \times (1+g)^i \times \left(\frac{W_i}{W_p}\right)^3 \times 365 \leq T_{\max} \tag{5.14}$$

in which i is the number of years in the future, p is the present, T is the estimated present *ADTT*, g is the annual growth rate, W is the legal gross weight of trucks, *365* is the number of days in a year, and T_{max} is the maximum practical truck traffic volume.

9. Finally, estimate the remaining fatigue life, Y_r, in years:

$$Y_r = i \quad when \quad \sum_{j=1}^{i} T_j \leq T_r \tag{5.15}$$

in which i is the number of years in the future.

Comparison of Remaining Life Calculation Results

Remaining fatigue life calculations based on the AASHTO *Guide* procedure and the refined procedure are presented. For both procedures, three remaining fatigue life calculations were performed for various fatigue prone details located in both main and secondary bridge members. The first set of calculations was conducted using the AASHTO *Guide*'s parameters for estimating the present truck volume, T, and the number of stress cycles per truck, C or CPT. The second set of calculations was conducted using the refined parameters for T and CPT. The third set of calculations was conducted using the actual measured values for these parameters. Since measured parameters reflect actual conditions on the bridge, the best estimate of the actual remaining fatigue life is one where the measured parameters are used.

The results of the remaining fatigue life estimation based on the AASHTO *Guide* procedure, equation (5.4), are presented in Table 5-8. This procedure uses an estimated lifetime average daily truck volume ($ADTT$) in the outer lane, T_a, to estimate the remaining fatigue life of a detail. Also included in Table 5-8 is a remaining fatigue life calculation using equation (5.4) with the actual truck traffic flow, equation (5.9), instead of the $ADTT$ in the outer lane.

The results of the remaining fatigue life estimation based on the refined procedure are presented in Table 5-9, Figure 5-4, and Table 5-10. Table 5-9 lists the $ADTT$ and the T values for each gage. Figure 5-4 is a plot of the Holston River Bridge's average daily traffic volume (ADT) versus time. Table 5-10 shows the refined procedure's remaining fatigue life estimation. Since 1974, the maximum legal gross weight of trucks on

Table 5-8. AASHTO Guide's Remaining Fatigue Life Estimates, Equation (5.4)

	Bridge Member	Main					Secondary				
	Fatigue Category	A	B	C	E	E'	A	B	C	E	E'
	Gage Number	140	5	58B	47	124	89	78	32	105	317
AASHTO Guide's Parameters	K (Table 5-2)	68	33	12	2.9	1.1	68	33	12	2.9	1.1
	Two-Way ADT	46880	46880	46880	46880	46880	46880	46880	46880	46880	46880
	F_T	0.15	0.15	0.15	0.15	0.15	0.15	0.15	0.15	0.15	0.15
	F_L	0.4	0.4	0.4	0.4	0.4	0.4	0.4	0.4	0.4	0.4
	T (Eq. 5.5)	2812.8	2812.8	2812.8	2812.8	2812.8	2812.8	2812.8	2812.8	2812.8	2812.8
	g (%)	4.5	4.5	4.5	4.5	4.5	4.5	4.5	4.5	4.5	4.5
	T_a / T	1.46	1.46	1.46	1.46	1.46	1.46	1.46	1.46	1.46	1.46
	$T_a = T \times (T_a / T)$	4106.7	4106.7	4106.7	4106.7	4106.7	4106.7	4106.7	4106.7	4106.7	4106.7
	C (Table 5-1)	1	1	1	1	1	1	1	1	1	1
	$R_s = 0.85 \times 1.35$	1.1475	1.1475	1.1475	1.1475	1.1475	1.1475	1.1475	1.1475	1.1475	1.1475
	S_r (ksi)	1.993	2.046	2.306	1.967	3.612	1.494	1.336	1.25	2.187	1.566
	a (years)	21	21	21	4	4	21	21	21	21	21
	Y_f (years); f = 1	1363.3	599.94	136.71	57.409	-0.238	3265.3	2209.2	969.15	23.679	25.16
	Y_f (years); f = 2	2747.6	1220.9	294.42	118.82	3.5237	6551.6	4439.4	1959.3	68.358	71.32
Refined Parameters	One-Way ADT	23440	23440	23440	23440	23440	23440	23440	23440	23440	23440
	F_T	0.25	0.25	0.25	0.25	0.25	0.25	0.25	0.25	0.25	0.25
	F_L	0.9	0.9	0.9	0.9	0.9	0.7	0.9	0.9	0.9	0.7
	T (Eq. 5.5)	5274	5274	5274	5274	5274	4102	5274	5274	5274	4102
	g (%)	4.5	4.5	4.5	4.5	4.5	4.5	4.5	4.5	4.5	4.5
	T_a / T	1.46	1.46	1.46	1.46	1.46	1.46	1.46	1.46	1.46	1.46
	$T_a = T \times (T_a / T)$	7700	7700	7700	7700	7700	5988.9	7700	7700	7700	5988.9
	C (Table 5-7)	0.331	0.365	0.46	0.58	0.59	0.158	0.006	0.016	1.19	0.458
	Y_f (years); f = 1	2209.5	886.3	161.85	52.468	-0.599	14241	198219	32984	-0.976	48.111
	Y_f (years); f = 2	4440.1	1793.6	344.7	108.94	2.8011	28504	396460	65989	19.048	117.22
Measured Parameters	One-Way ADT	22890	23990	22890	23990	23990	22890	22890	23990	23990	23990
	F_T (Table 5-4)	0.2894	0.2731	0.2894	0.2731	0.2731	0.2894	0.2894	0.2731	0.2731	0.2731
	F_L (Table 5-4)	0.34	0.26	0.34	0.26	0.26	0.34	0.34	0.26	0.26	0.26
	*F_L (Eq. 5.9)	0.9	0.86	0.9	0.86	0.86	0.626	0.9	0.86	0.9	0.651
	T (Eq. 5.5)	2252.3	1703.4	2252.3	1703.4	1703.4	2252.3	2252.3	1703.4	1703.4	1703.4
	*T (Eq. 5.5)	5961.9	5634.4	5961.9	5634.4	5634.4	4146.9	5961.9	5634.4	5896.5	4265.1
	g (%)	4.5	4.5	4.5	4.5	4.5	4.5	4.5	4.5	4.5	4.5
	T_a / T	1.46	1.46	1.46	1.46	1.46	1.46	1.46	1.46	1.46	1.46
	$T_a = T \times (T_a / T)$	3288.3	2487	3288.3	2487	2487	3288.3	3288.3	2487	2487	2487
	*T_a = *T x (T_a /T)	8704.4	8226.3	8704.4	8226.3	8226.3	6054.4	8704.4	8226.3	8608.9	6227.1
	C (Table 5-6)	0.3804	0.515	0.4601	0.6278	0.9746	0.2556	0.0026	0.0158	1.2865	0.4118
	Y_f (years); f = 1	4523.8	1969.9	407.07	157.52	2.3736	16036	1E+06	103459	36.346	164.1
	Y_f (years); f = 2	9068.5	3960.8	835.14	319.04	8.7473	32093	2E+06	206940	93.693	349.19
	*Y_f (years); f = 1	1695.9	580.91	140.72	44.832	-2.073	8700	404670	31264	-4.433	52.924
	*Y_f (years); f = 2	3412.8	1182.8	302.43	93.663	-0.146	17421	809361	62549	12.133	126.85

Note: K= Detail constant, ADT = Average daily traffic (Table 5-4), F_T = Fraction of trucks in traffic, F_L = Fraction of trucks in outer lane, T = Present Avg. daily truck volume (ADTT), T_a = Estimated lifetime ADTT in outer lane, g = Annual growth rate, a = Present age of bridge, T_a / T (from Figure 3.5A of AASHTO Guide, 1990), C = Cycles per truck, R_s = Reliability factor, S_r = Measured stress range or RMC (Eq. 5.2), f = 1 for calculating safe life and 2 for calculating mean life, Y_f = Remaining fatigue life (Eq. 5.4), * = Based on Eq. 5.9

Table 5-9. Estimations of the ADTT and the T Parameters

Gage Number	ADTT			T		
	Guide	Refind	Measured	Guide	Refind	Measured
140	0.15 DT_W	0.25 DT_W	0.2894 DT_W	0.8 TT_W	0.9 TT_W	0.90 TT_W
5	0.15 DT_E	0.25 DT_E	0.2731 DT_E	0.8 TT_E	0.9 TT_E	0.86 TT_E
58B	0.15 DT_W	0.25 DT_W	0.2894 DT_W	0.8 TT_W	0.9 TT_W	0.90 TT_W
47	0.15 DT_E	0.25 DT_E	0.2731 DT_E	0.8 TT_E	0.9 TT_E	0.86 TT_E
124	0.15 DT_E	0.25 DT_E	0.2731 DT_E	0.8 TT_E	0.9 TT_E	0.86 TT_E
89	0.15 DT_W	0.25 DT_W	0.2894 DT_W	0.8 TT_W	0.7 TT_W	0.626 TT_W
78	0.15 DT_W	0.25 DT_W	0.2894 DT_W	0.8 TT_W	0.9 TT_W	0.90 TT_W
32	0.15 DT_E	0.25 DT_E	0.2731 DT_E	0.8 TT_E	0.9 TT_E	0.86 TT_E
105	0.15 DT_E	0.25 DT_E	0.2731DT_E + 0.2894DT_W	0.8 TT_E	0.9 TT_E	0.779 TT_E + 0.10 TT_W
317	0.15 DT_E	0.25 DT_E	0.2731 DT_E	0.8 TT_E	0.7 TT_E	0.66 TT_E

Note: ADTT = Average daily truck volume, T = Present ADTT (Guide = Eq. 5.5, Measured = Eq. 5.9), DT = Average daily traffic volume (ADT), TT = ADTT, E = Eastbound traffic, and W = Westbound traffic

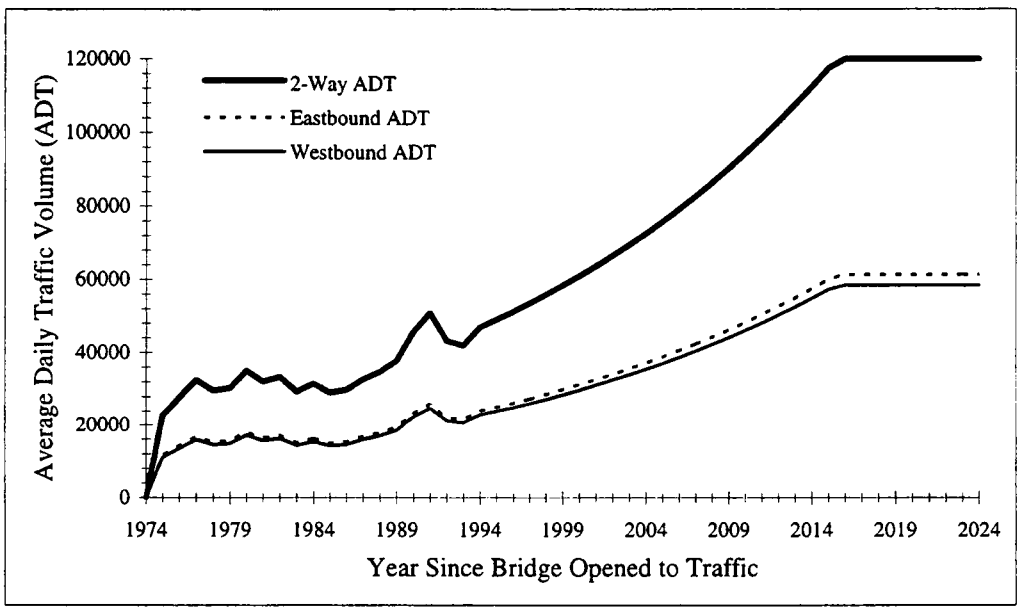


Figure 5-4. The Yearly ADT for the Holston River Bridge

Table 5-10. Refined Procedure's Remaining Fatigue Life Estimates

	Bridge Member	Main					Secondary				
	Fatigue Category	A	B	C	E	E'	A	B	C	E	E'
	Gage Number	140	5	58B	47	124	89	78	32	105	317
AASHTO Guide's Parameters	RMC (ksi)	1.993	2.046	2.306	1.967	3.612	1.494	1.336	1.25	2.187	1.566
	CPT (Table 5-1)	1	1	1	1	1	1	1	1	1	1
	One-Way ADT	22890	23990	22890	23990	23990	22890	22890	23990	23990	23990
	T (Eq. 5.5)	2746.8	2878.8	2746.8	2878.8	2878.8	2746.8	2746.8	2878.8	2878.8	2878.8
	$ADTT_{sum}$ (Eq. 5.11)	43654	45752	43654	11118	11118	43654	43654	45752	45752	45752
	N_p (Eq. 5.12)	2E+07	2E+07	2E+07	4E+06	4E+06	2E+07	2E+07	2E+07	2E+07	2E+07
	(A (Table 5-2))$_{safe}$	3E+10	1E+10	4E+09	1E+09	4E+08	3E+10	1E+10	4E+09	1E+09	4E+08
	(N_t (Eq. 5.7))$_{safe}$	3E+09	1E+09	4E+08	1E+08	8E+06	8E+09	5E+09	2E+09	1E+08	1E+08
	(N_r (Eq. 5.6))$_{safe}$	3E+09	1E+09	3E+08	1E+08	4E+06	8E+09	5E+09	2E+09	8E+07	8E+07
	(T_r (Eq. 5.13))$_{safe}$	3E+09	1E+09	3E+08	1E+08	4E+06	8E+09	5E+09	2E+09	8E+07	8E+07
	$(A)_{mean}$	8E+10	2E+10	9E+09	2E+09	7E+08	8E+10	2E+10	9E+09	2E+09	7E+08
	(N_t (Eq. 5.7))$_{mean}$	1E+10	3E+09	8E+08	2E+08	2E+07	2E+10	1E+10	5E+09	2E+08	2E+08
	(N_r (Eq. 5.6))$_{mean}$	1E+10	3E+09	8E+08	2E+08	1E+07	2E+10	1E+10	5E+09	1E+08	2E+08
	(T_r (Eq. 5.13))$_{mean}$	1E+10	3E+09	8E+08	2E+08	1E+07	2E+10	1E+10	5E+09	1E+08	2E+08
	(Y_r (Eq. 5.15))$_{safe}$	1364	510	140	55.1	3.384	3235	1910	837	36.85	38.23
	(Y_r (Eq. 5.15))$_{mean}$	3897	1016	300	85	8.605	9261	3815	1796	58.6	72.6
Refined Parameters	CPT (Table 5-7)	0.331	0.365	0.46	0.58	0.59	0.158	0.006	0.016	1.19	0.458
	One-Way ADTT	5722.5	5997.5	5722.5	5997.5	5997.5	5722.5	5722.5	5997.5	5997.5	5997.5
	T	5150.3	5397.8	5150.3	5397.8	5397.8	4005.8	5150.3	5397.8	5397.8	4198.3
	$ADTT_{sum}$ (Eq. 5.11)	81852	85785	81852	20846	20846	63663	81852	85785	85785	66722
	N_p (Eq. 5.12)	1E+07	1E+07	1E+07	4E+06	4E+06	4E+06	179256	500987	4E+07	1E+07
	(N_r (Eq. 5.6))$_{safe}$	3E+09	1E+09	3E+08	1E+08	4E+06	8E+09	5E+09	2E+09	6E+07	9E+07
	(T_r (Eq. 5.13))$_{safe}$	1E+10	4E+09	7E+08	2E+08	6E+06	5E+10	8E+11	1E+11	5E+07	2E+08
	(N_r (Eq. 5.6))$_{mean}$	1E+10	3E+09	8E+08	2E+08	1E+07	2E+10	1E+10	5E+09	1E+08	2E+08
	(T_r (Eq. 5.13))$_{mean}$	3E+10	7E+09	2E+09	4E+08	2E+07	2E+11	2E+12	3E+11	1E+08	4E+08
	(Y_r (Eq. 5.15))$_{safe}$	2199	741	162.4	51.18	2.864	14047	169486	28064	15.512	57.27
	(Y_r (Eq. 5.15))$_{mean}$	6293	1480	348	78.94	7.658	40218	339796	59988	26.594	108.51
Measured Parameters	CPT (Table 5-6)	0.3804	0.515	0.4601	0.6278	0.9746	0.2556	0.0026	0.0158	1.2865	0.4118
	One-Way ADTT	6624.4	6551.7	6624.4	6551.7	6551.7	6624.4	6624.4	6551.7	6551.7	6551.7
	T (Eq. 5.9)	5961.9	5634.4	5961.9	5634.4	5634.4	4146.9	5961.9	5634.4	5766.2	4324.1
	$ADTT_{sum}$ (Eq. 5.11)	94747	89552	94747	21761	21761	65902	94747	89552	91645	68726
	N_p (Eq. 5.12)	1E+07	2E+07	2E+07	5E+06	8E+06	6E+06	89915	516444	4E+07	1E+07
	(N_r (Eq. 5.6))$_{safe}$	3E+09	1E+09	3E+08	1E+08	539864	8E+09	5E+09	2E+09	5E+07	9E+07
	(T_r (Eq. 5.13))$_{safe}$	9E+09	3E+09	7E+08	2E+08	553934	3E+10	2E+12	1E+11	4E+07	2E+08
	(N_r (Eq. 5.6))$_{mean}$	1E+10	3E+09	8E+08	2E+08	8E+06	2E+10	1E+10	5E+09	1E+08	2E+08
	(T_r (Eq. 5.13))$_{mean}$	3E+10	5E+09	2E+09	3E+08	8E+06	9E+10	4E+12	3E+11	9E+07	4E+08
	(Y_r (Eq. 5.15))$_{safe}$	1650	503	140.3	45.89	2.387	8382	338432	27088	13.813	61.73
	(Y_r (Eq. 5.15))$_{mean}$	4737	1006	302	70.39	3.475	23999	675961	58241	23.078	116.93

Note: RMC = Measured stress range (Eq. 5.2), CPT = cycles per truck, ADT = Avgerage daily traffic volume (Table 5-4), ADTT = Average daily truck volume, T = Present ADTT, ADTTsum = ADTT from year 0 to present, N_p = Total number of cycles to date, A = The intercept of AASHTO design curves at 2,000,000 cycles, N_t = Total number of cycles to failure, N_r = Remaining number of cycles, T_r = Total number of trucks corresponding to N_r, Y_r = Estimated remaining fatigue life (yrs), mean = Mean life, safe = Safe life

Interstate highways has been 80,000 pounds (TRB Committee, 1990). Therefore, no adjustments for change in legal truck weights were made in equations (5.11) and (5.14).

Based on the results presented in Table 5-8, the following observations were made. For the case of measured parameters, the remaining fatigue life estimates based on the AASHTO *Guide*'s requirement of trucks in the outer lane are extremely uncoservative and unrealistic when compared with the remaining life estimates based on observed truck traffic position on the bridge in producing a measurable strain range readings. The AASHTO *Guide* westbound and eastbound values for T_a are 3288.3 and 2487, respectively. The observed westbound and eastbound values for T_a are 8704.4 and 8226.3, respectively. Henceforth, all comparisons will be made with regards to the observed estimates. For both main and secondary bridge member fatigue stress categories A, B, and C details, the remaining fatigue life estimates using the AASHTO *Guide*'s parameters were more conservative than those using the refined and measured parameters. For both main and secondary bridge member category E details, the remaining fatigue life estimation using the AASHTO *Guide*'s parameters were unconservative when compared with the remaining life estimation using the refined and the measured parameters. Category E' detail's remaining life estimates using the AASHTO *Guide*'s parameters were unconservative for main member details and conservative for secondary member details as compared with the results of remaining life estimates using the refined and measured parameters. With exception of fatigue categories A, B, and C main member details, there was less of a difference in remaining fatigue life estimates between using the refined and the measured parameters than there

was between using the AASHTO *Guide*'s parameters and the measured parameters. Fatigue stress categories A, B, and C details are not as prone to fatigue failure as fatigue stress categories E and E' details. The remaining fatigue lives of categories A, B, and C details can be considered infinite regardless of the parameters used in the estimation. For categories E and E' details, the refined parameters reflect actual conditions on the bridge better than the AASHTO *Guide*'s parameters.

Based on the results presented in Table 5-10, the following observations were made. For all practical purposes, fatigue categories A, B, and C details have infinite fatigue life regardless of the parameters used to estimate the remaining life. For category E main and secondary member details and category E' main member details, remaining life estimates using either the refined parameters or the AASHTO *Guide*'s parameters were unconservative when compared to the remaining life estimate using the measured parameters. For category E' secondary member details, remaining life estimates using either the refined parameters or the AASHTO *Guide*'s parameters were conservative when compared to the remaining life estimates using the measured parameters. For fatigue stress categories E and E' details, there is less of a difference in remaining fatigue life estimates between using the refined parameters and the measured parameters than there is between using the AASHTO *Guide*'s parameter and the measured parameters. Therefore for categories E and E' details, the refined parameters reflect actual conditions on the bridge better than the AASHTO *Guide*'s parameters.

Based on a comparison of the results presented in Tables 5-8 and 5-10, the following observations were made. Regardless of the parameters used in estimating the

remaining life of fatigue prone details, both the AASHTO *Guide* procedure and the refined procedure predict an infinite remaining fatigue life for categories A, B, and C details. With exception of category E main member details, the remaining fatigue life estimates for categories E and E' details when using the refined procedure is greater than that when using the AASHTO *Guide* procedure.

The estimated remaining safe and mean lives of gage 124 when using measured parameters are negative for the AASHTO *Guide* procedure and positive for the refined procedure. The negative sign indicates that the remaining fatigue life is exhausted and that a visible fatigue crack should be present. The results of the refined procedure suggests that 53% of gage 124's mean fatigue life is remaining and that 47% of its mean fatigue life has been used, while 63% of its safe fatigue life has been used. The AASHTO *Guide* procedure indicates that 37% of gage 105's mean fatigue life is remaining and that 63% of its mean fatigue life has been used, while its safe fatigue life has been exhausted. The refined procedure suggests that 52% of gage 105's mean fatigue life is remaining and that 48% of its mean fatigue life has been used, while 60% of its safe fatigue life has been used.

Zheng et al. (1994) conducted fatigue testing on butt welded details and determined that visible cracks occur at 70% of the total fatigue life. Harland et al. (1986) reported that visible cracks occur at 80% of the total fatigue life. Fisher et al. (1990) and Yazdani (1984) found that visible cracks occur at 80% to 90% of the total fatigue life. Bannantine et al. (1990) suggests that up to 90% of total fatigue life may be taken up in

initiating a crack. Keating et al. (1990) states that visible fatigue cracks occur between 85% to 95% of the total fatigue life.

A visual inspection of gages 105 and 124's details showed that there were no visible fatigue cracks present, suggesting that 70% to 95% of their total fatigue life has not yet been used. Therefore, the refined procedure gives a better estimate of the remaining fatigue life than the AASHTO *Guide* procedure. The refined parameters reflect actual conditions on the bridge better than the AASHTO *Guide*'s parameters.

5.6 Conclusions

The present truck volume and the number of stress cycles per truck passage affects the remaining fatigue life estimation of existing steel bridges. Based on field observations of truck traffic position on the bridge in producing a measurable stress range reading, the present truck volume for fatigue prone details varied depending on the location of the detail. For details located on main longitudinal fascia girder or at the end of any secondary member that is attached to the fascia girder, the present truck volume was 90% of the one-way average daily truck volume (*ADTT*). For details located at the midlength of a transverse member that spans between a fascia and an interior girder, the present truck volume was 70% of the one-way *ADTT*. For details located on an interior girder or on a transverse member that spans between two interior girders, the present truck volume was 90% of the one-way *ADTT*. The AASHTO *Guide*'s estimation of the *ADTT* as 15% of the average daily traffic volume (*ADT*) was unconservative for the Holston River Bridge. The AASHTO *Guide*'s requirement of using the *ADTT* in the outer lane for fatigue life estimation was also unconservative for this bridge. The

AASHTO *Guide*'s estimation of the present truck volume was 50% of the observed present truck volume.

Measured stress cycles per truck passage (*CPT*) for fatigue prone details varied depending on the location of the detail. For the same location along a main girder, the *CPT* values for category A bottom flange details were twice the *CPT* values for category A web details. Fatigue category E' main girder web gap details located in the approach (end) span have a larger *CPT* value than the same detail located in an interior span. For the same location along a main girder, category E' longitudinal attachment end weld details have a larger *CPT* value than category E' web gap details. Fatigue categories E and E' secondary bridge member details located in the approach span have a larger *CPT* value than the same detail located in an interior span. Category E secondary member flange termination details have the largest *CPT* values of any main or secondary fatigue prone details. The average measured *CPT* values for interior span categories A, B, C, E, and E' main member details were 0.331, 0.365, 0.460, 0.580, and 0.590, respectively. The average measured *CPT* values for approach span category E' main member details was 0.759. The average measured *CPT* values for interior span categories A, B, C, E, and E' secondary member details were 0.158, 0.006, 0.016, 0.443, and 0.458, respectively. The average measured *CPT* values for approach span categories E and E' secondary member details were 1.190 and 0.589, respectively. The AASHTO *Guide*'s *CPT* value for this type of bridge was one. With exception of approach span category E secondary bridge member details, the AASHTO *Guide*'s value was very conservative.

A refined remaining fatigue life estimation procedure, based on the widely accepted method of comparing the number of cycles to date with the number of cycles to failure, was developed. A comparison of the refined procedure's remaining life estimates with the remaining life estimates using the AASHTO Guide procedure revealed the following. Both procedures predicted an infinite remaining fatigue life for fatigue stress categories A, B, and C details. For fatigue categories E and E' details, the refined procedure's remaining fatigue life estimates were greater than the AASHTO *Guide*'s remaining life estimates. For a category E' main member detail, the AASHTO Guide procedure predicted that the fatigue life of the detail had been exhausted while the refined procedure predicted that only 47% of its fatigue life had been used. The consensus among researchers is that visible fatigue cracks occur at 70% to 95% of the total fatigue life. A visual inspection of this detail showed that there were no fatigue cracks present and thus the total fatigue life had not yet been used. Therefore, the refined procedure gave a more accurate estimate of the actual remaining fatigue life than the AASHTO *Guide* procedure.

CHAPTER 6

CONCLUSIONS AND RECOMMENDATIONS

6.1 Summary of Research Findings

The detail type, the truck traffic volume, the number of stress cycles per truck, and the effective stress range are the most important parameters in fatigue life evaluation of steel bridges. The uncertainties in predicting fatigue life can be attributed to any one of these parameters. Field testing of a six lane long span continuous girder bridge revealed that the provisions of the AASHTO *Guide* with respect to these parameters do not reflect actual conditions on a bridge.

- In regards to truck traffic volume, remaining fatigue life estimation using the *Guide*'s requirement of the average daily truck volume for the outer lane (T_a) was unconservative. A better estimate of T_a would be to limit it to a fraction of the one-way average daily truck volume (*ADTT*) instead of limiting it to the outer lane. The measured estimate of T_a for the test bridge was 90% of the one-way *ADTT*. Also, the *Guide*'s assignment of fixed values for the fraction of trucks in traffic (F_T) was unconservative. Assigning fixed values for F_T is too rigid and can easily become outdated as traffic characteristics change. A better estimate of F_T would be to obtain actual values from the state Department of Transportation (DOT). For most Interstate highway bridges, the DOT's bridge section has gathered these data. The test bridge's measured eastbound and westbound F_T were 0.273 and 0.289, respectively. The DOT's F_T for this bridge was 0.26, where as the *Guide*'s value for F_T was 0.15.

- In regards to the number of stress cycles per truck passage, the *Guide*'s value of 1.0 for the test bridge was very conservative for all fatigue prone details with the exception of category E secondary member details. A better estimate of the number of cycles per truck passage (*CPT*) would be to base the *Guide*'s provision on field measured data rather than on analytical models as it is now. For the test bridge, field measured *CPT* values varied depending on the location and severity of the fatigue prone detail. A measured estimate of the test bridge's *CPT* value for fatigue prone details located in an interior span was 0.60. A measured estimates of the test bridge's *CPT* values for approach span main and secondary member fatigue prone details were 0.80 and 1.20, respectively.
- In regards to the calculated effective stress range, the *Guide*'s impact factor is solely a function of surface roughness with values ranging between 10 to 30%. The AASHTO *Standard*'s formula for calculating impact factor is strictly a function of span length with a maximum value of 30%. Test results showed that surface roughness, truck velocity, and bridge approach affect the impact factor. Rough surface condition increases the impact factor by an average of 8%. Impact factors increase linearly with increase in truck velocity. The bridge approach increases impact factors by 20 to 60% depending on the type of fatigue prone detail. Of the three parameters, the bridge approach has the most influence on impact factor. Measured impact factors for fatigue prone details varied depending on the location of the detail. The *Guide*'s impact

factor for the test bridge was 8% and 18% less than the *Standard*'s impact factor for gages located in the main and secondary members, respectively. Thus, all comparisons will be made with regards to the AASHTO *Standard*'s impact factors. AASHTO impact values were conservative for fatigue categories A and B details. For fatigue categories E and E' details located in the bridge interior span, AASHTO impact values were conservative for secondary member details and 10% unconservative for main girder details. For the approach (end) span, AASHTO values were unconservative for categories B and E' main girder details by 25% and 40%, respectively; and they were 35% unconservative for category E secondary bridge member details.

- In regards to field measured effective stress range, the *Guide* has no provisions for cycle counting methods, stress-range frequency of occurrence histogram construction, and field test duration. Field test results showed that all these parameters have a significant affect on the effective stress range and the number of stress cycles per truck passage. In the interest of uniformity and as a means of upgrading the *Guide*'s specifications, the *Guide* should provide provisions for these parameters. A sensitivity analysis examining the effect of these parameters on the effective stress range and the number of cycles per truck revealed that the rainflow cycle counting method was the best technique to use for highway variable amplitude loading. Stress-range frequency of occurrence histograms starting at 1000 psi with an interval width of 500 psi

produced the most conservative results. With this histogram construction, all 2-axle/4 or 6-wheel trucks were excluded since fatigue damage under normal traffic is primarily caused by 4 and 5-axle trucks. For fatigue categories A, B, C, E, and E' details, the number of cycles per truck data was more sensitive to test duration than the effective stress range data. The field test duration required to realistically represent the effect of truck traffic flow was much less for the effective stress range than it was for the number of cycles per truck. Test duration for fatigue prone details varied depending on the location of the detail. The required field test duration with regards to the effective stress range for details located in an interior span and in an approach (end) span were 2 and 10 hours, respectively. The required field test duration with regards to the number of cycles per truck passage for main member details was 18 hours. The required field test duration with regards to the number of cycles per truck passage for secondary member details located in an interior span and in an approach span were 12 and 23 hours, respectively.

For a category E' main member test bridge detail, either using the *Guide* parameters or the measured parameters, the AASHTO *Guide* procedure predicted that the fatigue life of the detail had been exhausted. The consensus among researchers is that visible fatigue cracks occur at 70% to 95% of the total fatigue life. A visual inspection of this detail showed that there were no fatigue cracks present and thus the total fatigue life had not yet been used. A refined remaining fatigue life estimation procedure, based on

the widely accepted method of comparing the number of cycles to date with the number of cycles to failure, was developed to better reflect actual conditions on a bridge. A comparison of the refined procedure's remaining life estimates with the remaining life estimates using the *Guide* procedure revealed the following. Both procedures predicted an infinite remaining fatigue life for fatigue stress categories A, B, and C details. For fatigue categories E and E' details, the refined procedure's remaining fatigue life estimates were greater than the *Guide*'s remaining life estimates. For the same category E' main member detail that the *Guide* procedure predicted that its fatigue life had been exhausted, the refined procedure predicted that only 47% of its fatigue life had been used. Thus, the refined procedure gave a more accurate estimate of the actual remaining fatigue life than the AASHTO *Guide* procedure.

6.2 Recommendations for Further Research

This research study revealed some deficiencies in the AASHTO *Guide*'s remaining fatigue life estimation procedure in reflecting actual conditions in steel bridges. One such deficiency not addressed in this research is the detail constant, a parameter that affects fatigue life estimation. The AASHTO design curves from which this constant is obtained are based on 30 year old laboratory investigations. Updating these design curves to reflect actual conditions in steel bridges would be an enormous improvement in fatigue life prediction of steel bridges. Field testing of other types of highway steel bridge fatigue prone details under normal traffic are needed to further refine the *Guide*'s parameters with regard to truck traffic volume, the number of stress cycles per truck passage, and the effective stress range. Both the *Guide* procedure and the refined procedure developed in

this research apply to uncracked and unrepaired steel members subjected to primary stresses. Development of a fatigue life prediction procedure that applies to retrofitted steel bridge members would be beneficial. Perhaps a simplified fracture mechanics approach procedure would be appropriate.

REFERENCES

REFERENCES

American Association of State Highway and Transportation Officials, AASHTO, (1992). *Standard Specification for Highway Bridges.*

American Association of State Highway and Transportation Officials (1990). *Guide Specifications for Fatigue Evaluation of Existing Steel Bridges.*

American Institute of Steel Construction, AISC, (1986). *Highway Structures Design Handbook Volume I,* United States Steel Corporation.

American Railway Engineering Association, AREA, (1990). *Manual for Railway Engineering, Volume II.*

Society of Automotive Engineering, SAE, (1988). *Fatigue Design Handbook.*

Ontario Highway Bridge Design Code. (1983). Ministry of Transportation and Communication, Downsview, Ontario, Canada.

ASCE Committee on Fatigue and Fracture Reliability of the Committee on Structural Safety and Reliability of the Structural Division (1982). "Fatigue Reliability: Variable Amplitude Loading," *Journal of the Structural Division*, ASCE, Vol. 108, No. ST1, pp. 47-69.

Tennessee Department of Transportation, TNDOT, Bureau of Planning and Development (1994). "Traffic Flow Maps Tennessee Roads and Streets."

TRB Committee for the Truck Weight Study (1990). "Truck Weight Limits Issues and Options," TRB National Research Council, *Special Report 225.*

Albrecht, P. (1983). "S-N Fatigue Reliability Analysis of Highway Bridges," *Probabilistic Fracture Mechanics and Fatigue Methods: Applications for Structural Design and Maintenance*, ASTM STP 798, pp. 184-204.

Bannantine, J.A., Comer, J.J., and Handrock, J.L. (1990). *Fundamentals of Metal Fatigue Analysis,* New Jersey: Prentice Hall, Inc.

Biggs, J.M. (1964). *Introduction to Structural Dynamics,* New York: McGraw-Hill, Inc.

Chen, X. (1992). "Application of Fracture Mechanics to Highway Bridges," Ph.D. Dissertation, The University of Maryland.

Deatherage, J.H., Sanders, M.D., Goodpasture, D.W., and Burdette, E.G. (1995). "Controlled Load Tests on a Four Girder Steel Bridge," *Transportation Research Record 1476*, pp. 106-116.

Dowling, N.E. (1972). "Fatigue Failure Predictions for Complicated Stress-Strain Histories," *Journal of Materials*, JMLSA, Vol. 7, No. 1, pp. 71-87.

Dowling, N.E. (1993). *Mechanical Behavior of Materials*, New Jersey: Prentice-Hall,Inc.

Downing, S.D. and Socie, D.F. (1982). "Simple Rainflow Counting Algorithms," *International Journal of Fatigue,* Vol. 4, No. 1, pp. 31-40.

Fisher, J.W. (1977). "Bridge Fatigue Guide Design and Details," American Institute of Steel Construction.

Fisher, J.W. (1984). *Fatigue and Fracture in Steel Bridges, Case Studies*, New York: John Wiley and Sons.

Fisher, J.W., Albrecht, P.A., Yen, B.T., Klingerman, D.J., and McNamee, B.M. (1974). "Fatigue Strength of Steel Beams with Welded Stiffeners and Attachments," *NCHRP Report 147*, Transportation Research Board.

Fisher, J.W., Barthelemy, B.M., Mertz, D.R., and Edinger, J.A. (1980). "Fatigue Behavior of Full-Scale Welded Bridge Attachments," *NCHRP Report 227*, Transportation Research Board.

Fisher, J.W., Frank, K.H., Hirt, M.A., and McNamee, B.M. (1970). "Effect of Weldments on the Fatigue Strength of Steel Beams," *NCHRP Report 102*, Transportation Research Board.

Fisher, J.W., Hausammann, H., Sullivan, M.D., and Pense, A.W. (1979). "Detection and Repair of Fatigue Damage in Welded Highway Bridges," *NCHRP Report 206*, Transportation Research Board.

Fisher, J.W., Mertz, D.R., and Zhong, A. (1983). "Steel Bridge Members Under Variable Amplitude Long Life Fatigue Loading," *NCHRP Report 267*, Transportation Research Board.

Fisher, J.W., Yen, B.T., and Wang, D. (1990). "Fatigue Cracking of Steel Bridge Structures. Volume II: A Commentary and Guide for Design, Evaluation, and Investigation of Cracking," *FHWA-RD-89-167.*

Ghosn, M., Moses, F., and Gobieski, J. (1986). "Evaluation of Steel Bridges Using In-Service Testing," *Transportation Research Record 1072*, pp. 71-78.

Goodpasture, D.W. (1976). "Stress History of Highway Bridges-II," Department of Civil Engineering, The University of Tennessee at Knoxville, TN.

Hanson, J.M., Koob, M.J., and Fisher, J.W. (1991). "Evaluation of Fatigue Life and Retrofitting on the Benicia-Martinez Bridge," *Transportation Research Record 1290*, Vol. 1, pp. 227-242.

Harland, J.W., Purvis, R.I., Graber, D.R., Albrecht, P., and Flournoy, T.S. (1986). "Inspection of Fracture Critical Bridge Members," *Report FHWA-IP-86-26.*

Keating, P.B. and Fisher, J.W. (1986). "Evaluation of Fatigue Tests and Design Criteria on Welded Details," *NCHRP Report 286*, Transportation Research Board.

Keating, P.B., Kulick, J.M., Mertz, D.R., and Hess, C.R. (1990). "Economical and Fatigue Resistant Steel Bridge Details," *Report FHWA-HI-90-043.*

King, J.P.C., Csagoly, P.F., and Fisher, J.W. (1976). "Field Testing of Aguasabon River Bridge in Ontario," *Transportation Research Record No. 579*, pp. 48-60.

Mayhew, M.D. (1994). "Measured Stress Ranges and Cross Frame Analysis of the Holston River Bridge," M.S. Thesis, The University of Tennessee, Knoxville, TN.

Moses, F., Goble, G., and Pavia, A. (1974). "Truck Loading Model for Bridge Fatigue," *Specialty Conference on Metal Bridges*, ASCE, pp. 333-356.

Moses, F., Schilling, C.G., and Raju, K.S. (1987). "Fatigue Evaluation Procedure for Steel Bridges," *NCHRP report 299*, Transportation Research Board.

Moses, F. and Verma, D. (1987). "Load Capacity Evaluation of Existing Bridges," *NCHRP report 301*, Transportation Research Board.

Narayanan, R. and Roberts, T.M. (1991). *Structures Subjected to Repeated Loading*, London: Elsevier Science Publisher LTD.

Nowak, A.S, Hong, Y-K., and Hwang, E-S. (1991). "Modeling Live Load and Dynamic Load," *Transportation Research Record 1290*, pp. 110-118.

Nowak, A.S. and Nassif, H.H. (1995). "Dynamic Load Spectra for Girder Bridges," *Transportation Research Board, Conference Paper 951126.*

Nowak, A.S., Nassif, H.H., and Frank, K.H. (1993). "Fatigue Load Spectra for Steel Girder Bridge," *Transportation Research Board, Conference Paper 930786.*

Peterson, W.S. and Kostem, C.N. (1973). "Dynamic Analysis of Beam-Slab Highway Bridges," *Highway Research Record 428*, pp. 57-63.

Post, G.J., Frank, K.H., and Tahmassebi, B. (1988). "Estimating Residual Fatigue Life of Bridges," *Research Report 464-1F*, Center for Transportation Research, The University of Texas at Austin, TX.

Schilling, C.G. (1982). "Impact Factors for Fatigue Design," *Journal of the Structural Division*, ASCE, Vol. 108, No. ST9, pp. 2034-2044.

Schilling, C.G. (1984). "Stress Cycles for Fatigue Design of Steel Bridges," *Journal of Structural Engineering*, Vol. 110, No. 6, pp. 1222-1233.

Schilling, C.G., Klippstein, K.H., Barsom, J.M., and Blake, G.T. (1978). "Fatigue of Welded Steel Bridge Members Under Variable-Amplitude Loadings," *NCHRP Report 188*, Transportation Research Board.

Shaaban, H.A. (1985). "Fatigue Rating of Steel Highway Bridges," Ph.D. Dissertation, The University of Maryland.

Yang, Y-B., Liao, S-S., and Lin, B-H. (1995). "Impact Formulas for Moving Vehicles Moving Over Simple and Continuous Beam," *Journal of Structural Engineering*, Vol. 121, No. 11, pp. 1644-1650.

Yazdani, N. (1984). "Risk Analysis of Extending Bridge Service Life," Ph.D. Dissertation, The University of Maryland.

Yen, B.T., Hung, T., Lai, L-Y., and Fisher, J.W. (1990). "Manual for Inspecting Bridges for Fatigue Damage Conditions," *Fritz Engineering Laboratory Report No. 511.1*, Lehigh University, Bethlehem, Pennsylvania.

Zhao, Z., Haldar, A., and Breen, F.L. (1994). "Fatigue-Reliability Evaluation of Steel Bridges," *Journal of Structural Engineering*, Vol. 120, No. 5, pp. 1608-1623.

Zheng, X., Lu, B., Cui, T., and Lin, C. (1994). "Fatigue Tests and Life Prediction of 16 Mn Steel Butt Welds Without Crack-Like Defect," *International Journal of Fracture*, Vol. 68, No. 3, pp. 275-285.

Zuraski, P.D. (1993). "Service Performance of Steel Bridges Compared to Fatigue-Life Predictions," *Journal of Structural Engineering*, Vol. 119, No. 10, pp. 3056-3068.

APPENDIX

Table A-1 Strain Gage Information

GAGE NUMBER	GAGE LOCATION	FATIGUE CATEGORY	DETAIL DESCRIPTION
1	1A	B	Top flange of cantilever bracket
2	1A	B	Bottom flange of cantilver bracket
3	1A	B	Top flange of girder #4
4	1A	B	Top of thick bottom flange of girder #4 on eastside
5	1A	B	Top of thin bottom flange of girder #4 on westside
6	1A	C	Gusset plate at end of bottom chord of cross frame
7	1A	E	Bottom gage cross frame bottom chord at first diagonal
8	1A	E	Top gage cross frame bottom chord at first diagonal
9	1A	A	First truss diagonal of cross frame
10	1A	A	Top flange of knee brace
11	1A	A	Horizontal Rosette - cross frame top chord
12	1A	A	45 Degree Rosette - cross frame top chord
13	1A	A	Vertical Rosette - cross frame top chord
13A	1A	A	Vertical gage cross frame top chord opposite gage 13
14	1A	A	Cross frame second truss diagonal
15	1A	E	End of gusset plate at cross frame 2nd truss diagonal
16	1A	E	End of gusset plate at cross frame 3rd truss diagonal
17	1A	E	Flange of lateral X-bracing at gusset plate on eastside
18	1A	E	Flange of lateral X-bracing at gusset plate on westside
19	1A	E'	Web gap near lateral gusset plate on eastside
20	1A	E'	Web gap near transverse stiffener on eastside
23	4	E'	Vertical gage at end of retrofit plate on east side
24	4	E'	Horizontal gage at end of retrofit plate on east side
25	4	E'	Vertical gage at end of retrofit plate on west side
26	4	E'	Horizontal gage at end of retrofit plate on east side
27	1B	B	Top flange of cantilever bracket
28	1B	B	Bottom flange of cantilver bracket
29	1B	B	Top flange of girder #4
30	1B	B	Top of thick bottom flange of girder #4 on eastside
31	1B	B	Top of thin bottom flange of girder #4 on westside
32	1B	C	Gusset plate at end of cross frame bottom chord
33	1B	E	Bottom gage cross frame bottom chord at first diagonal
34	1B	E	Top gage cross frame bottom chord at first diagonal
35	1B	A	First truss diagonal of cross frame
36	1B	A	Top flange of knee brace
37	1B	A	Horizontal Rosette - cross frame top chord
41	1B	A	Second truss diagonal of cross frame
42	1B	E	End of gusset plate at cross frame 2nd truss diagonal

Table A-1 Strain Gage Information

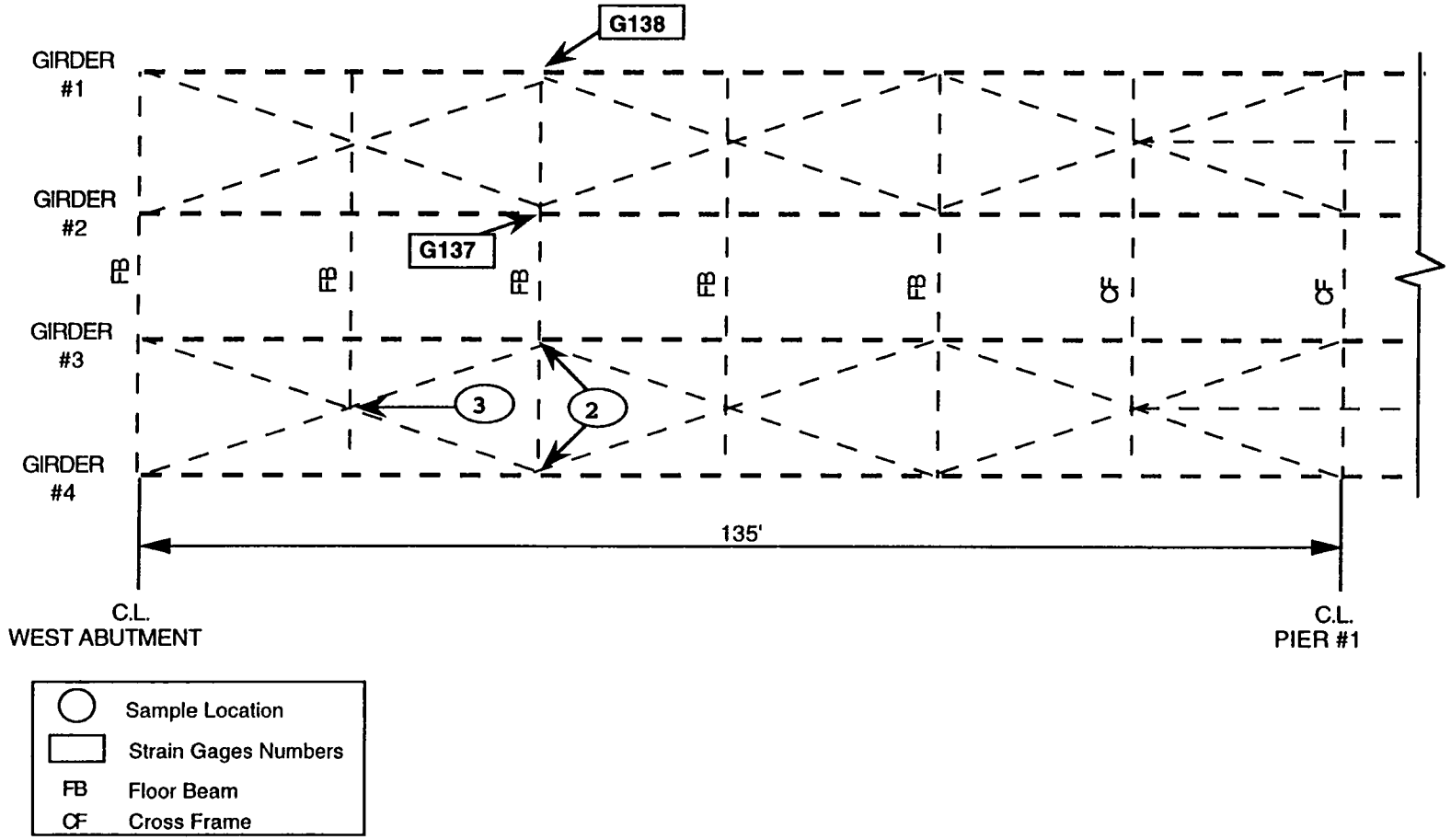
GAGE NUMBER	GAGE LOCATION	FATIGUE CATEGORY	DETAIL DESCRIPTION
43	1B	E	End of gusset plate at cross frame 3rd truss diagonal
44	1B	E	Flange of lateral X-bracing at gusset plate on eastside
45	5	E	End of lateral gusset above 2" tear on eastside
46	5	E	End of lateral gusset below 2" tear on eastside
47	5	E	End of lateral gusset above 6" tear on westside
48	5	E	End of lateral gusset across 6" tear on westside
49	5	E	End of lateral gusset below 6" tear on westside
50	1B	E	Flange of lateral X-bracing at gusset plate on westside
51	1B	E'	Web gap near lateral gusset plate on eastside
51A	6	E'	Vertical gage at end of lateral gusset plate on eastside
52	1B	E'	Web gap near transverse stiffener on eastside
52A	6	E'	Horizontal gage at end of lateral gusset plate on eastside
53	1B	E'	Web gap near transverse stiffener on westside
53A	6	E'	Vertical gage at end of lateral gusset plate on westside
54	1B	E'	Web gap near lateral gusset plate on westside
54A	6	E'	Horizontal gage at end of lateral gusset plate on westside
55	1C	A	Top flange of cantilever bracket
56	1C	B	Bottom flange of cantilver bracket
57	1C	B	Top flange of girder #1
58	1C	B	Top of thin bottom flange of girder #1 on westside
58B	1C	C	Bottom of thin bottom flange of girder #1 opposite 58
58C	1C	A	Top of thin bottom flange of girder #1 14" west of 58
58D	1C	A	Top of thin bottom flange of girder #1 opposite 58C
59	1C	B	Top of thick bottom flange of girder #1 on eastside
60	1C	C	Gusset plate at end of cross frame bottom chord
61	1C	E	Top gage cross frame bottom chord at first diagonal
62	1C	E	Bottom gage cross frame bottom chord at first diagonal
63	1C	A	First truss diagonal of cross frame
64	1C	A	Top flange of knee brace
67	1C	A	Horizontal Rosette - cross frame top chord
68	1C	A	Second truss diagonal of cross frame
69	1C	E	End of gusset plate at cross frame 2nd truss diagonal
70	1C	E	End of gusset plate at cross frame 3rd truss diagonal
71	1C	E	Flange of lateral X-bracing at gusset plate on westside
72	1C	E	Flange of lateral X-bracing at gusset plate on eastside
73	1C	E'	Web gap near lateral gusset plate on westside
74	1C	E'	Web gap near transverse stiffener on westside
75	1C	E'	Web gap near transverse stiffener on eastside
76	1C	E'	Web gap near lateral gusset plate on eastside
78	1D	B	Top flange of cantilever bracket
79	1D	E	Top gage cross frame bottom chord at first diagonal

Table A-1 Strain Gage Information (Con't)

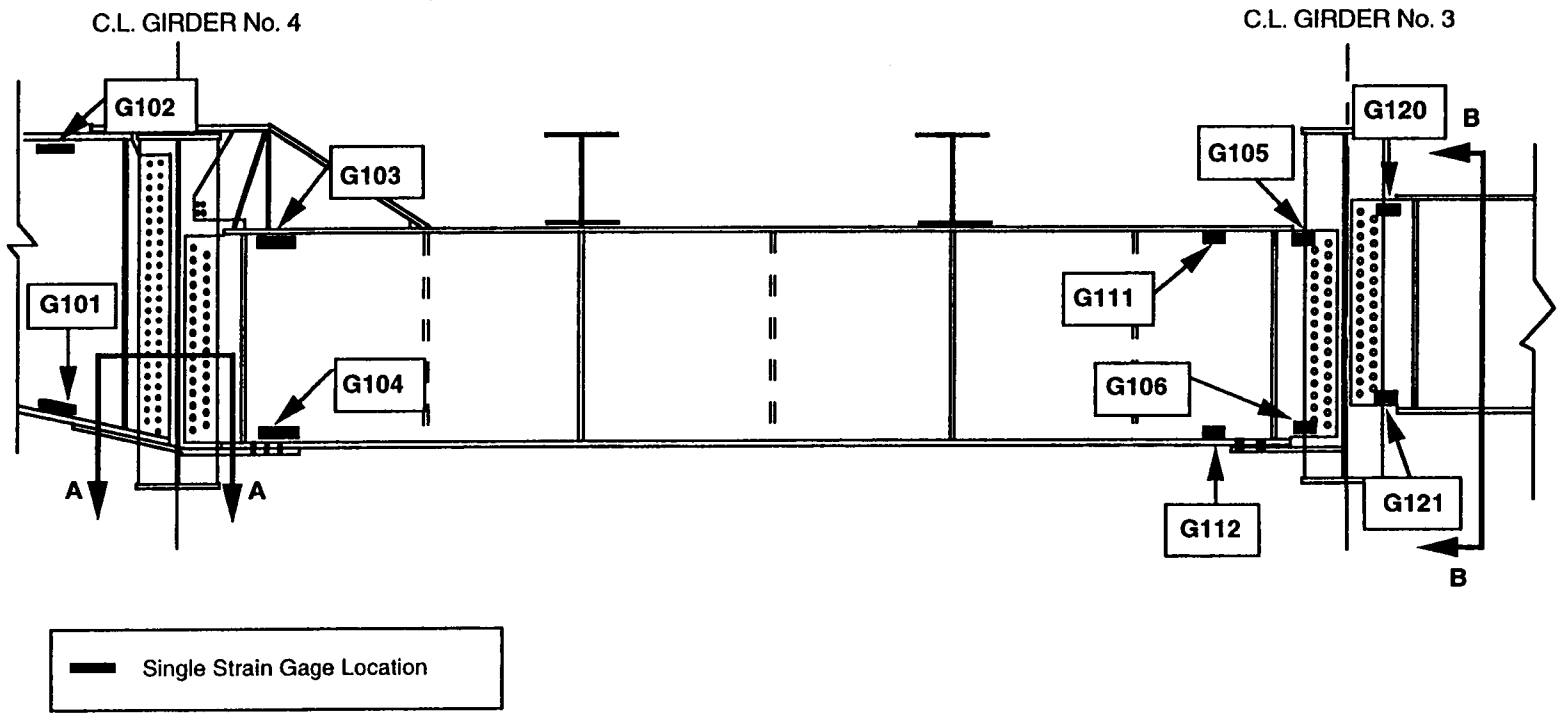
GAGE NUMBER	GAGE LOCATION	FATIGUE CATEGORY	DETAIL DESCRIPTION
80	1D	E	Bottom gage cross frame bottom chord at first diagonal
81	1D	C	Gusset plate at end of bottom chord of cross frame
82	1D	B	Top of thick bottom flange of girder #1 on eastside
83	1D	B	Top of thin bottom flange of girder #1 on westside
84	1D	A	First truss diagonal of cross frame
85	1D	A	Top flange of knee brace
86	1D	A	Vertical Rosette - cross frame top chord
87	1D	A	45 Degree Rosette - cross frame top chord
88	1D	A	Horizontal Rosette - cross frame top chord
89	1D	A	Second truss diagonal of cross frame
90	1D	E	End of gusset plate at cross frame 2nd truss diagonal
91	1D	E	End of gusset plate at cross frame 3rd truss diagonal
92	1D	A	Vertical gage cross frame top chord opposite gage 88
93	1D	E	Flange of lateral X-bracing at gusset plate on westside
94	1D	E	Flange of lateral X-bracing at gusset plate on eastside
95	1D	E'	Web gap near lateral gusset plate on westside
96	1D	E'	Web gap near transverse stiffener on westside
97	1D	E'	Web gap near transverse stiffener on eastside
98	1D	E'	Web gap near lateral gusset plate on eastside
99	1D	B	Bottom flange of cantilver bracket
100	1D	B	Top flange of girder #1
101	2	B	Bottom flange of cantilver bracket
102	2	B	Top flange of cantilver bracket
103	2	B	Floor beam top flange at girder #4
104	2	B	Floor beam bottom flange at girder #4
105	2	E	Floor beam web at top flange termination south side of girder #3
106	2	E	Floor beam web at bottom flange termination south side of girder #3
107	2	E'	Web gap near lateral gusset plate on eastside at girder #3
108	2	E'	Web gap near transverse stiffener on eastside at girder #3
109	2	E'	Web gap near transverse stiffener on westside at girder #3
110	2	E'	Web gap near lateral gusset plate on westside at girder #3
111	2	B	Floor beam top flange at girder #3 north side
112	2	B	Floor beam bottom flange at girder #3 north side
113	2	E'	Vertical Rosette on girder #3 web at end of lateral gusset plate
114	2	E'	45 degree Rosette on girder #3 web at end of lateral gusset plate
115	2	E'	Horizontal Rosette on girder #3 web at end of lateral gusset plate
116	2	E'	Horizontal gage adjacent to and below gage 115
117	3	E'	Floor beam bottom flange at end of gusset plate for X-bracing south
118	3	E'	Floor beam bottom flange at end of gusset plate for X-bracing north
120	2	E	Floor beam web at top flange termination north side of girder #3
121	2	E	Floor beam web at bottom flange termination north side of girder #3
122	6	E'	Horizontal gage at end of retrofit plate eastside
123	6	E'	Vertical gage at end of retrofit plate eastside
124	6	E'	Horizontal gage at end of retrofit plate westside

Table A-1 Strain Gage Information (Con't)

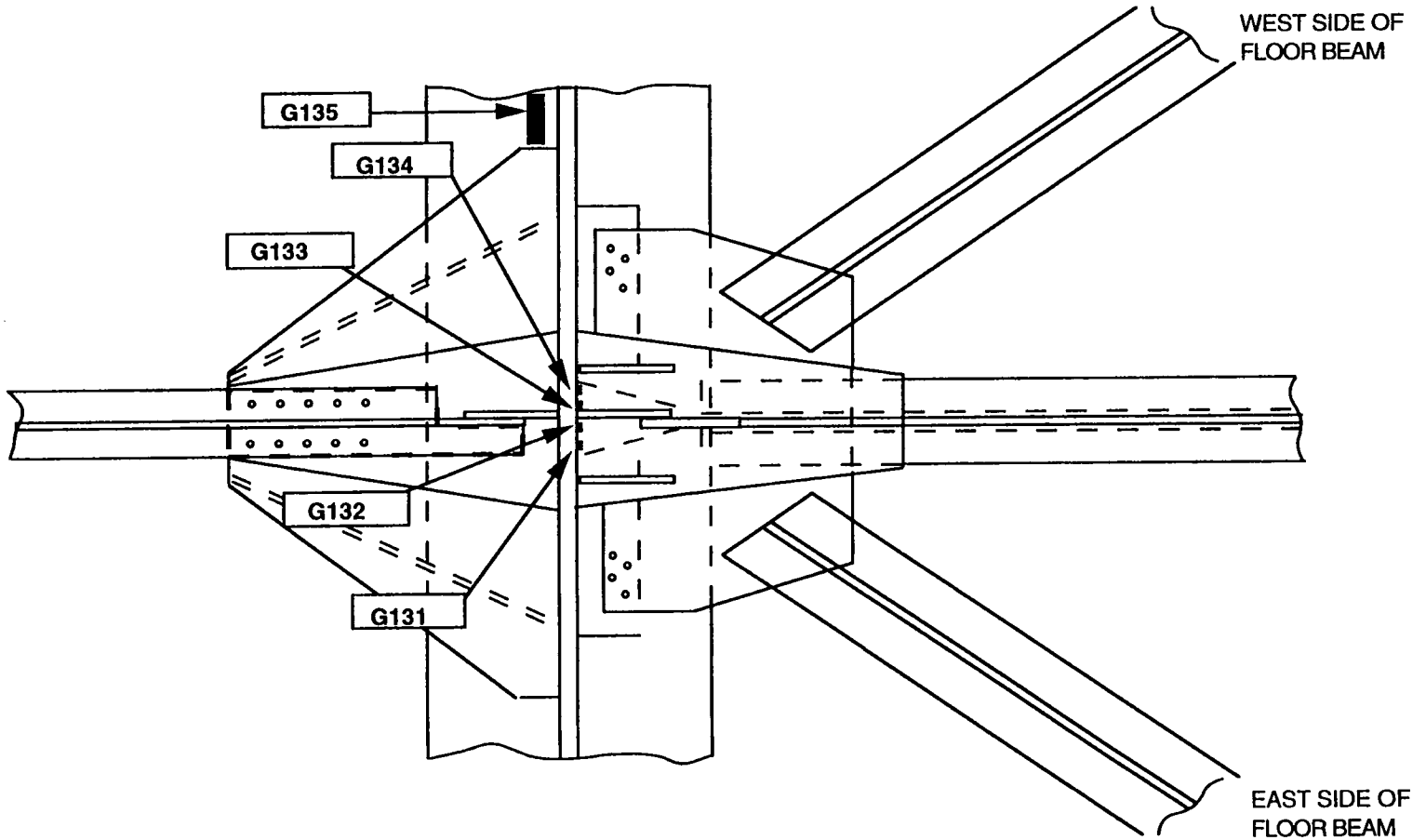
GAGE NUMBER	GAGE LOCATION	FATIGUE CATEGORY	DETAIL DESCRIPTION
125	6	E'	Vertical gage at end of retrofit plate west
126	1C	E'	Horizontal gage at end of retrofit plate westside
127	1C	E'	Vertical gage at end of retrofit plate westside
128	1C	E'	Horizontal gage at end of retrofit plate eastside
129	1C	E'	Vertical gage at end of retrofit plate eastside
130	2	A	Bottom of bottom flange of girder #3
131	2	E'	Web gap near lateral gusset plate on eastside at girder #4
132	2	E'	Web gap near transverse stiffener on eastside at girder #4
133	2	E'	Web gap near transverse stiffener on westside at girder #4
134	2	E'	Web gap near lateral gusset plate on westside at girder #4
135	2	B	Top of bottom flange of girder #4
136	1C	A	Girder #1 web at 42" from top of bottom flange in line with 58
137	137	B	Top of bottom flange of girder #2
138	138	B	Top of bottom flange of girder #1
140	1C	A	Bottom of bottom flange of girder #1, 66" west of 1C
141	1C	A	Top of bottom flange of girder #1, 66" west of 1C
143	1C	A	Girder #1 web 23" from top of bottom flange, 66" west of 1C
144	1C	A	Girder #1 web 45" from top of bottom flange, 66" west of 1C
145	1C	A	Girder #1web 58" from top of bottom flange, 66" west of 1C
147	1C	A	Girder #1 web 2" from bottom of top flange, 66" west of 1C
150	1C	A	Cross frame top chord at mid-length of chord
151	1C	A	Cross frame bottom chord at 1/4 - length of chord
152	1C	A	4" below gage 136 at buckled area
153	1C	A	Vertical gage above gage 152 at buckled area
154	1C	B	Top of bottom flange of girder #2, 66" west of 1C
155	1C	A	Girder #2 web same location as gage 143
156	1C	A	Girder #2 web same location as gage 144
157	1C	A	Girder #2 web same location as gage 145
201	201	B	Top of bottom flange of girder #3
202	202	B	Top of bottom flange of girder #2
203	203	B	Top of bottom flange of girder #3
204	204	B	Top of bottom flange of girder #2
303	7	A	Bottom of bottom flange of girder #3
305	7	E	Floor beam web at top flange termination southside of girder #3
306	7	E	Floor beam web at bottom flange termination southside of girder #3
307	7	E'	Web gap near lateral gusset plate eastside
308	7	E'	Web gap near transverse stiffener eastside
317	7	E'	Floor beam bottom flange at end of X-bracing gusset plate south
318	7	E'	Floor beam bottom flange at end of X-bracing gusset plate north
320	7	E	Floor beam web at top flange termination northside of girder #3
321	7	E	Floor beam web at bottom flange termination northside of girder #3



Plan View of Span 1 (Approach Span)

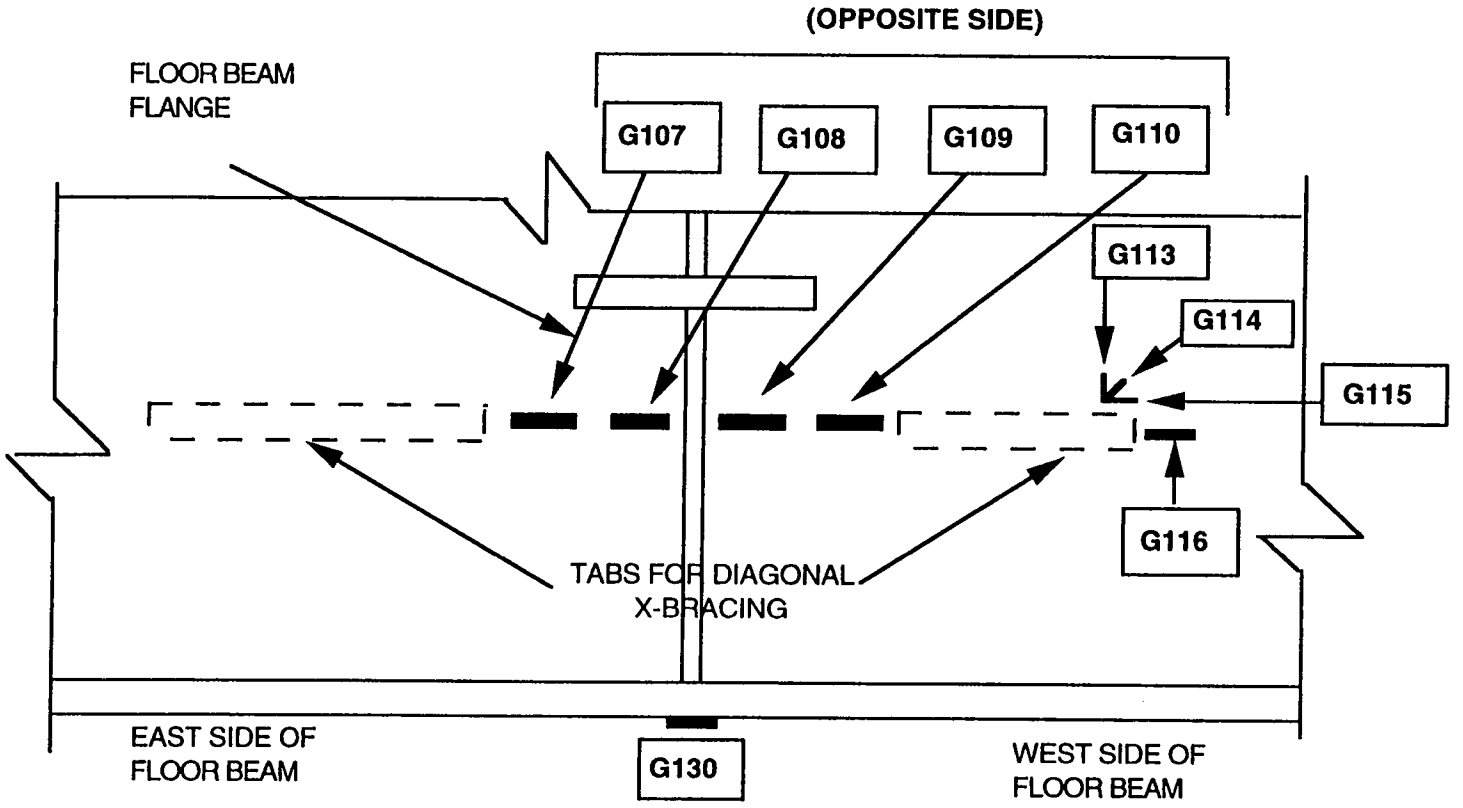


2 SAMPLE LOCATION #2



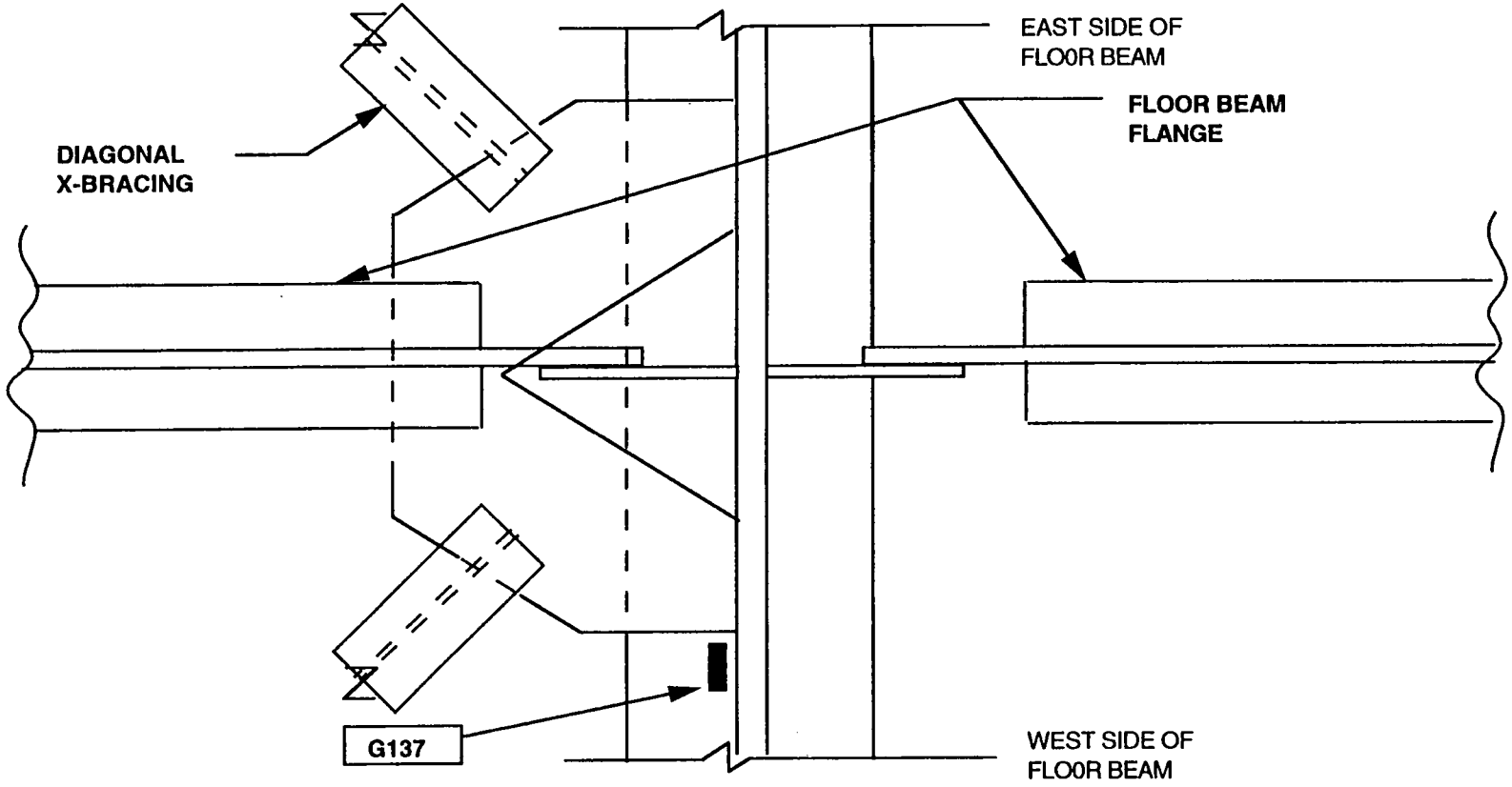
2 **SAMPLE LOCATION #2**

SECTION A-A



2 SAMPLE LOCATION #2

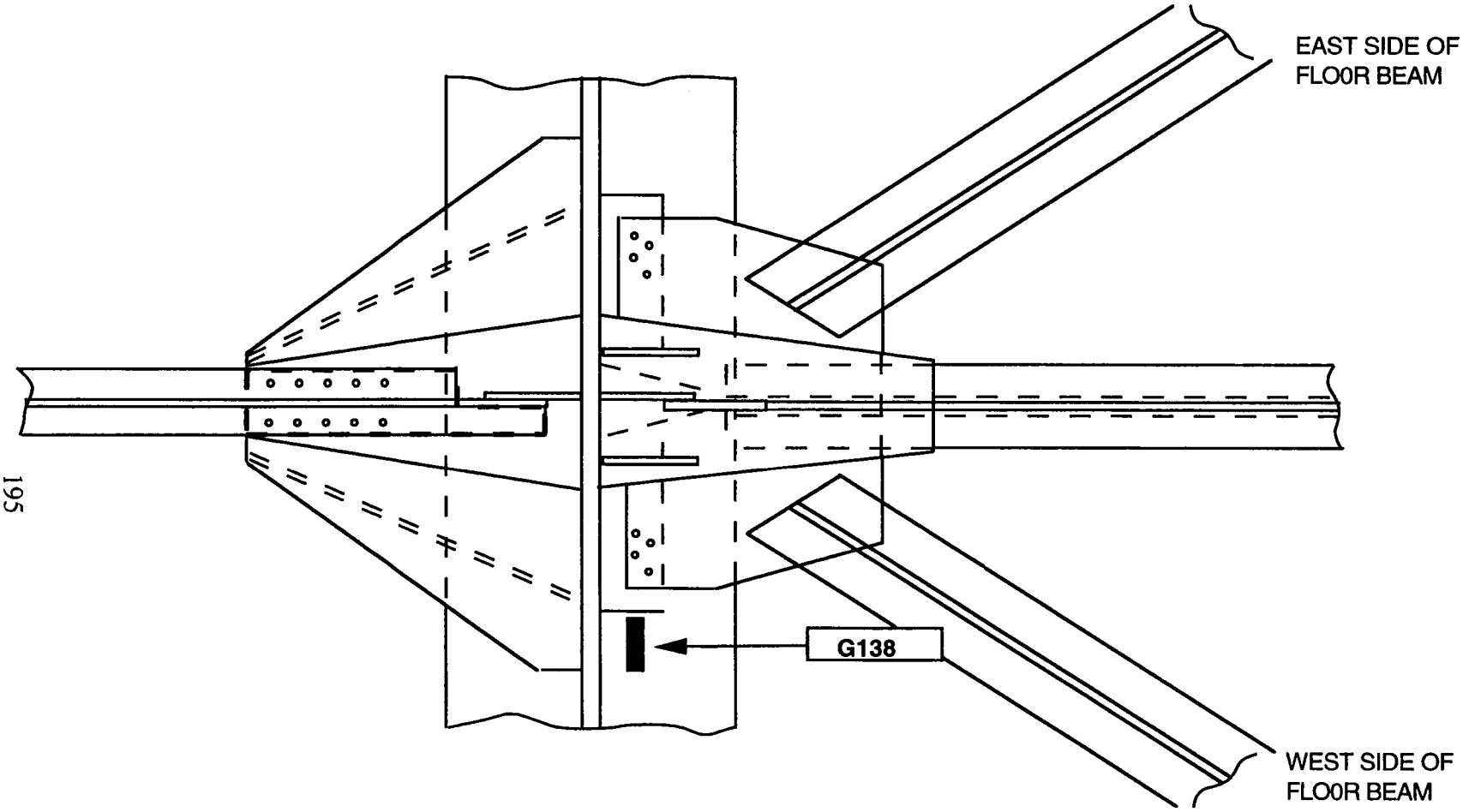
SECTION B-B



G137

SAMPLE LOCATION G137

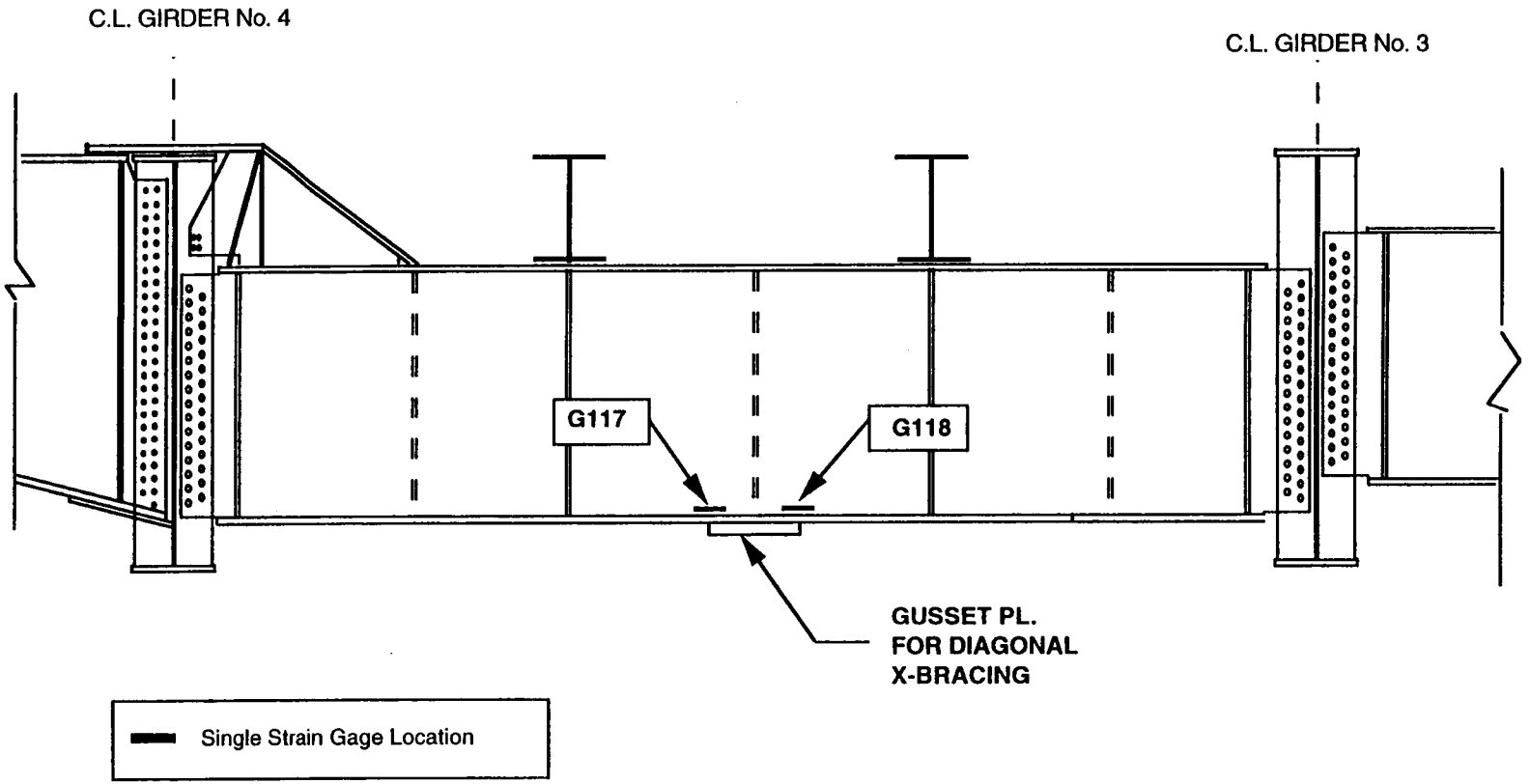
GIRDER #2 1ST SPAN ADJACENT TO SAMPLE LOCATION 2



G138

SAMPLE LOCATION G138

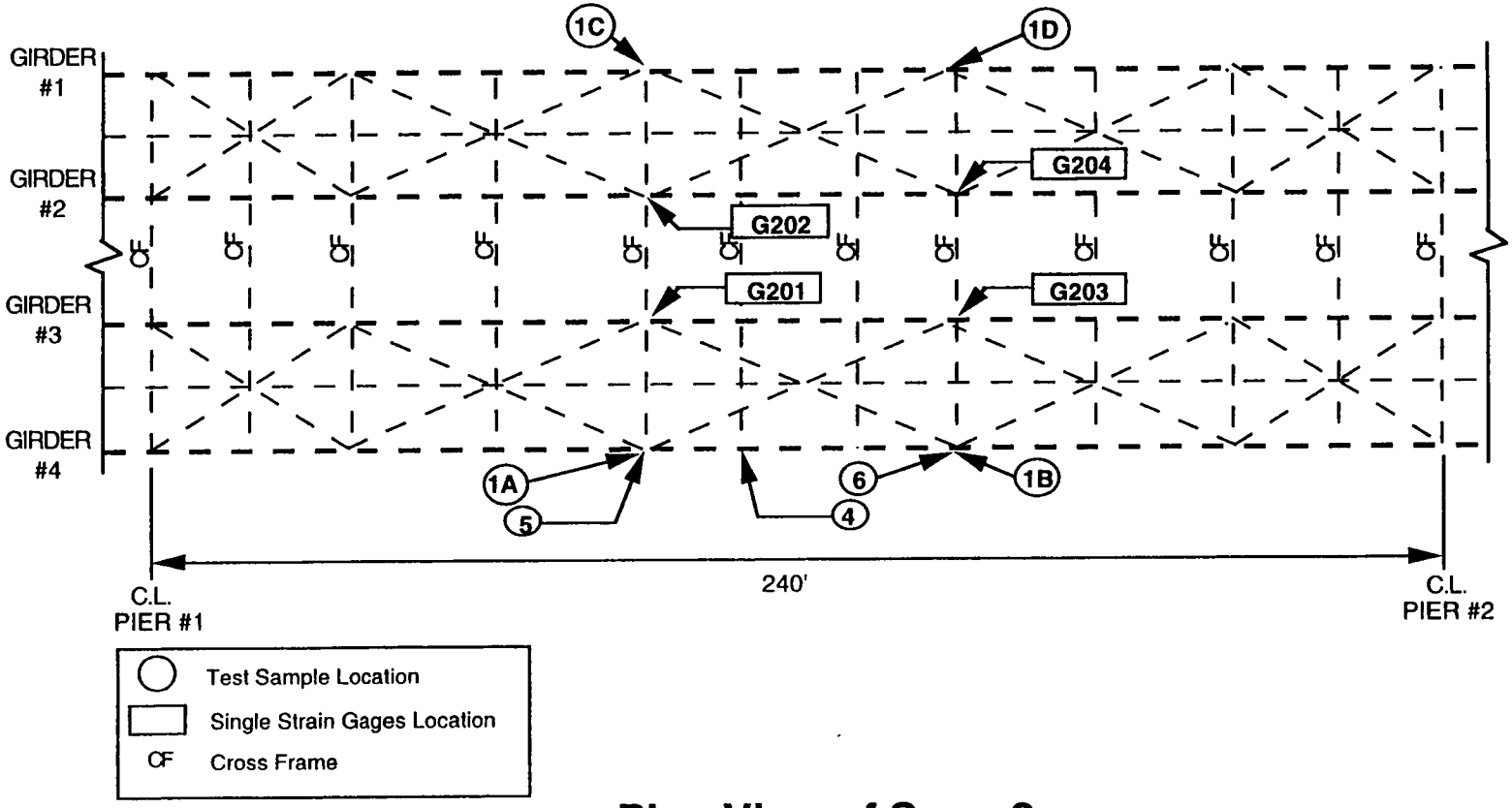
GIRDER #1 1ST SPAN ADJACENT TO SAMPLE LOCATION 2



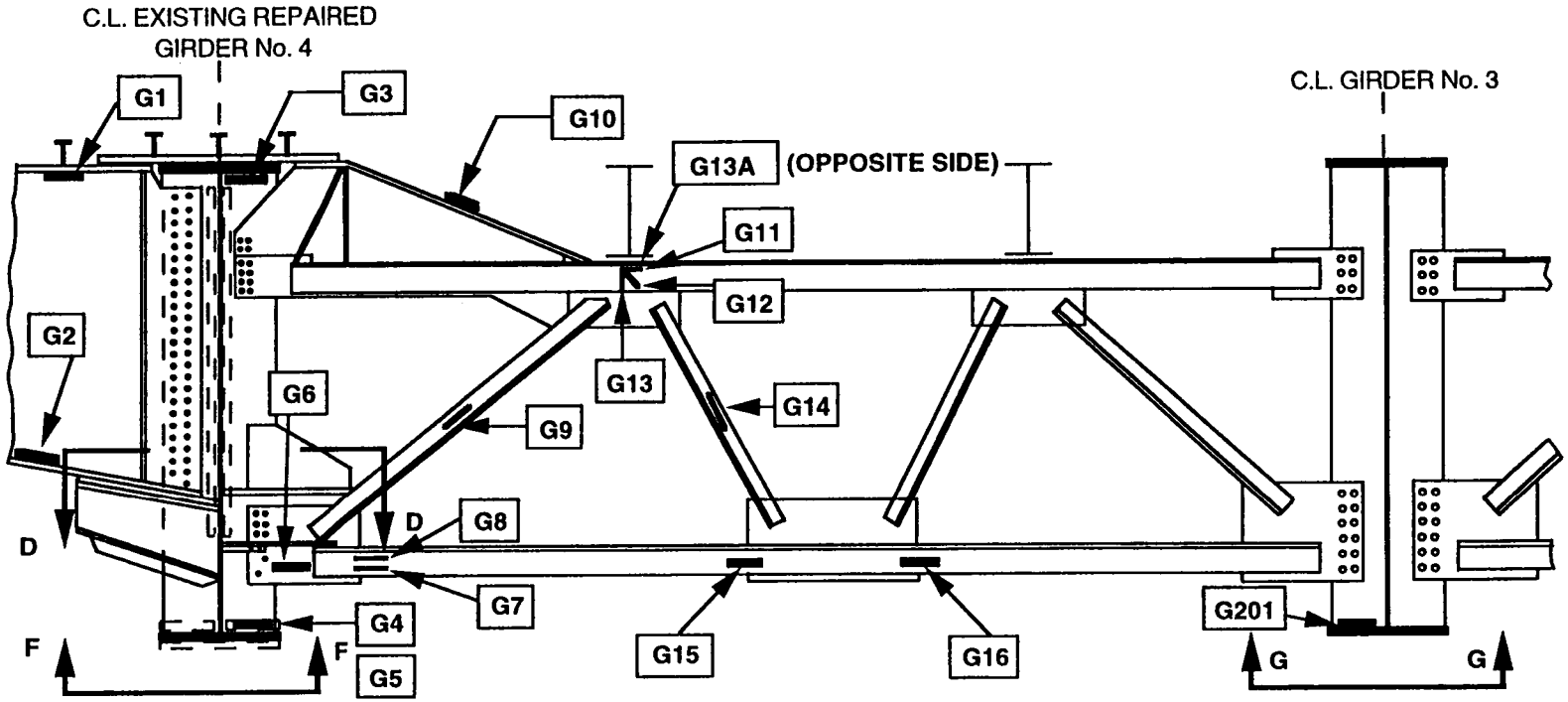
3

SAMPLE LOCATION #3

FLOOR BEAM WEST OF SAMPLE LOCATION 2



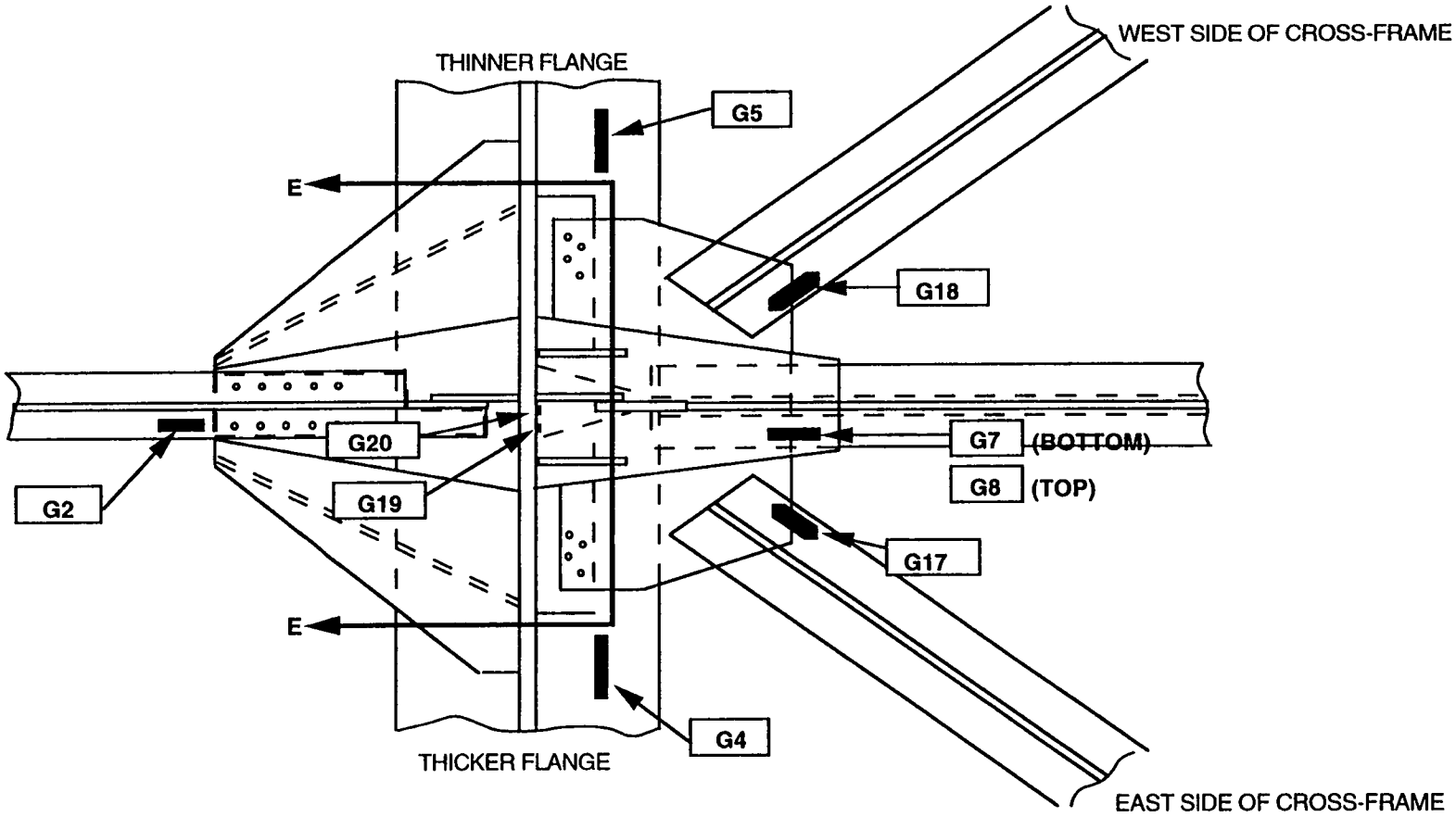
Plan View of Span 2
(FAILURE LOCATION At 1A)



1A

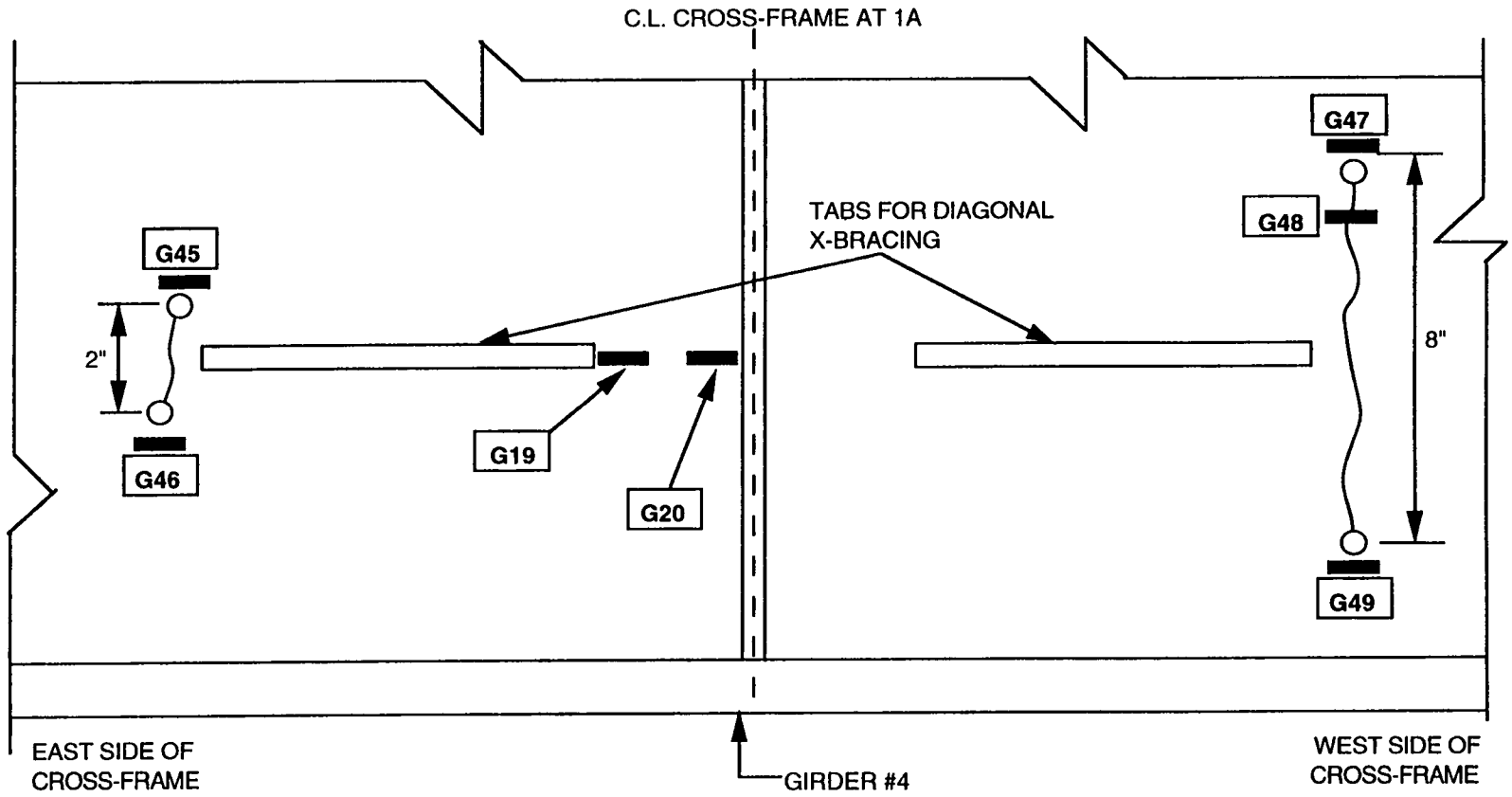
SAMPLE LOCATION #1A

CROSS-FRAME AT FAILURE LOCATION



1A **SAMPLE LOCATION #1A**

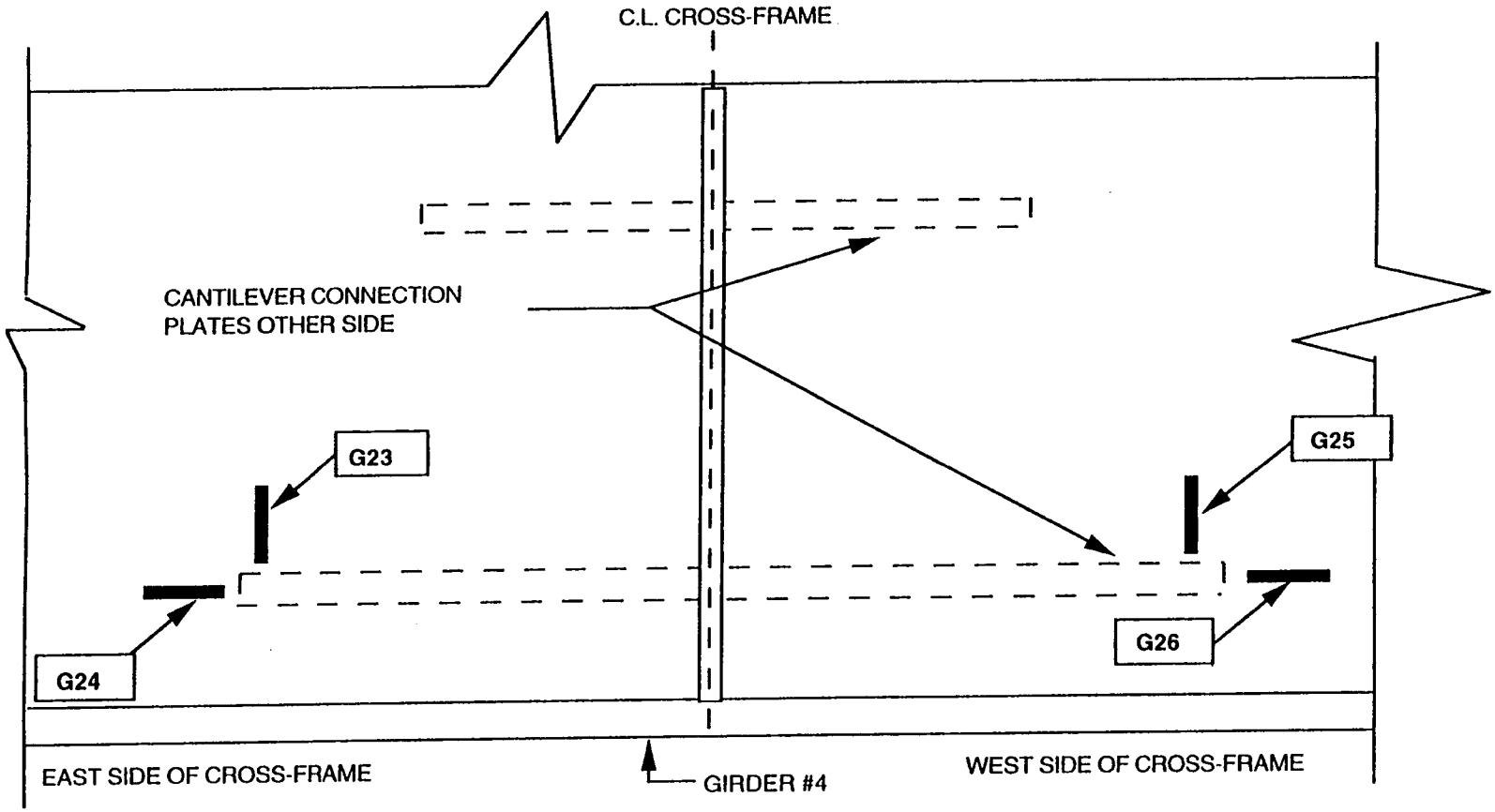
SECTION D-D



5

SAMPLE LOCATION #5 AT FAILURE LOCATION (1A)

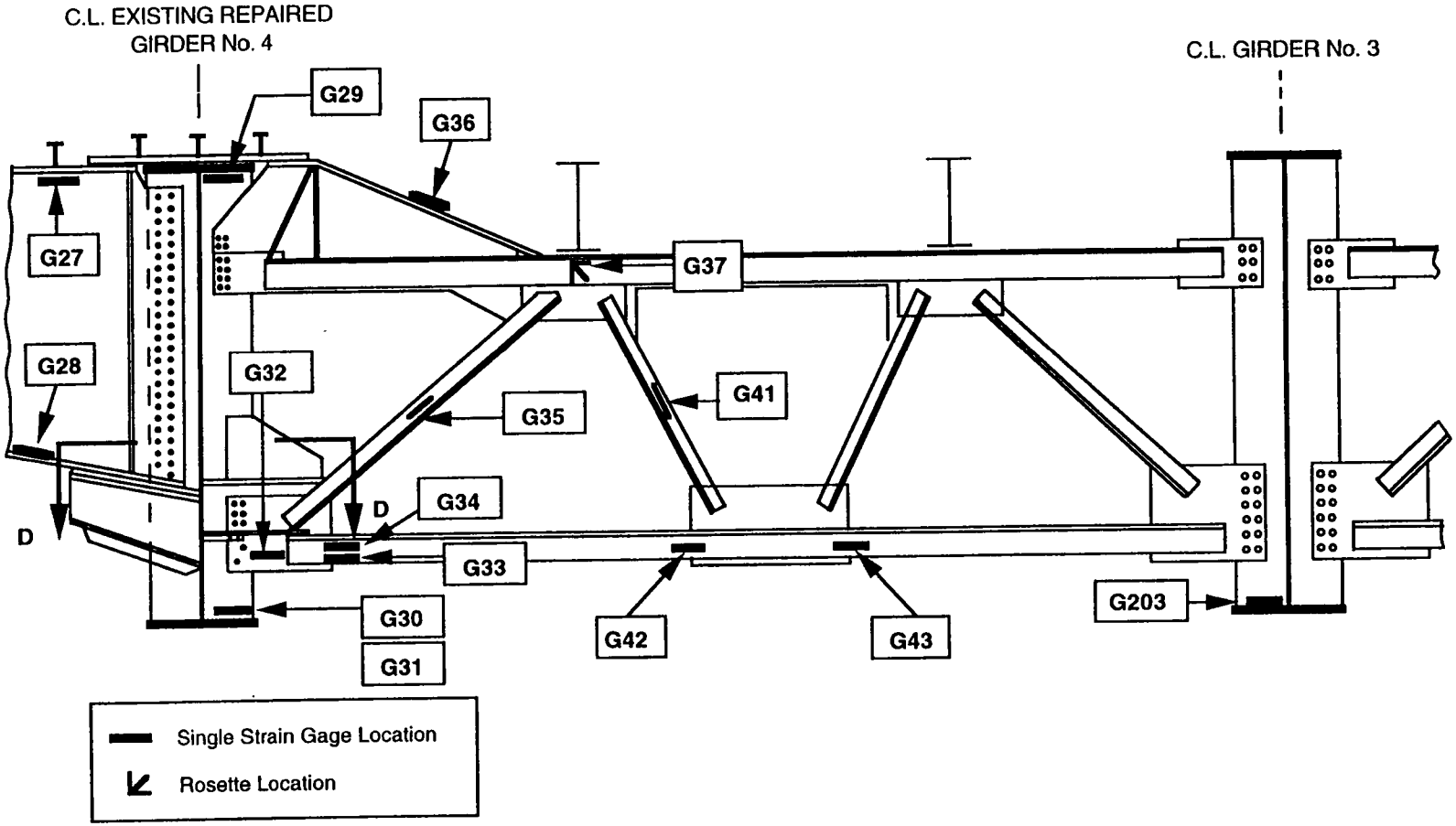
SECTION E-E



4

SAMPLE LOCATION #4

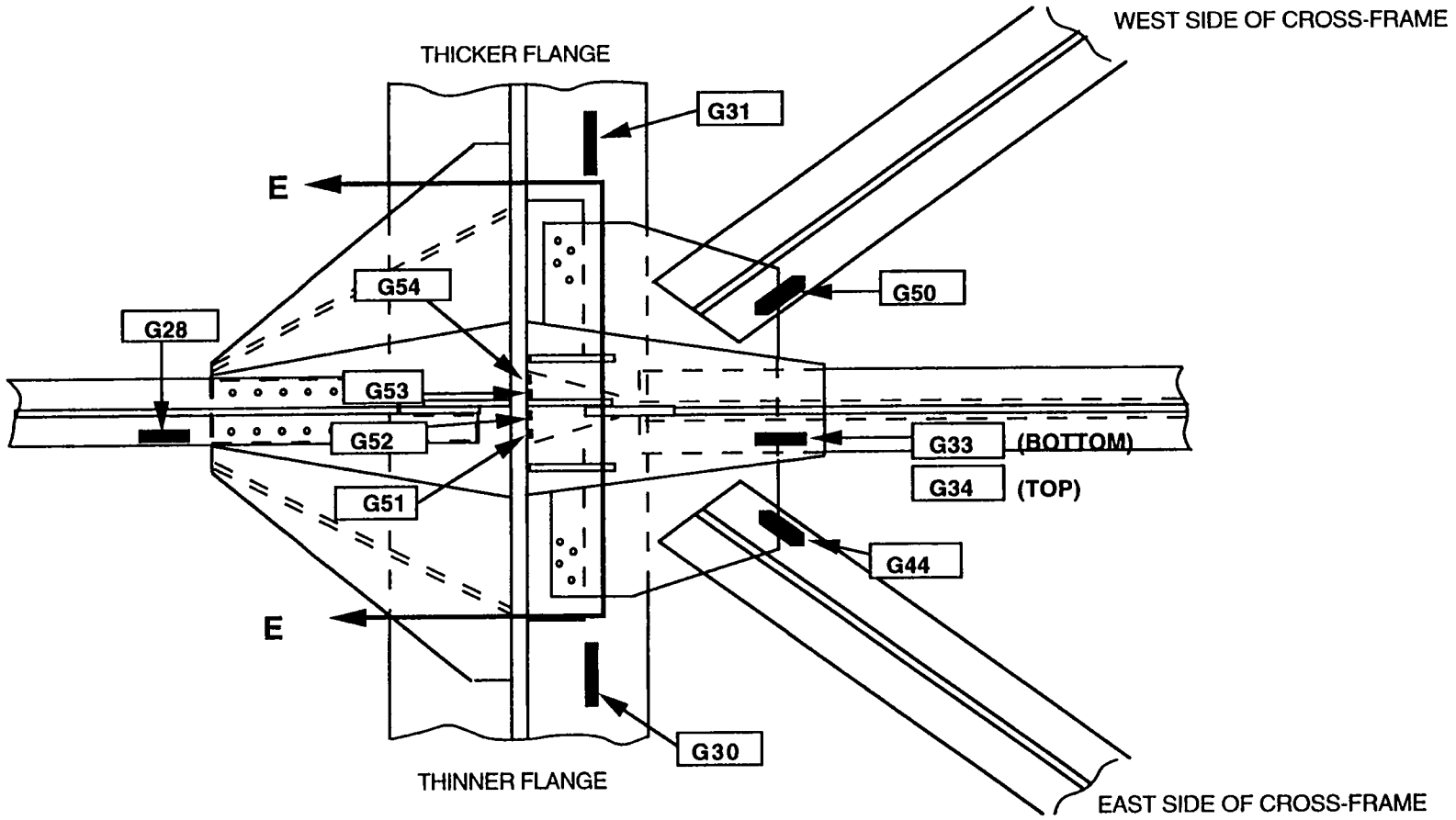
FIRST CROSS FRAME EAST OF FAILURE LOCATION (1A)
(CROSS-FRAME WITHOUT LATERAL BRACING)



1B

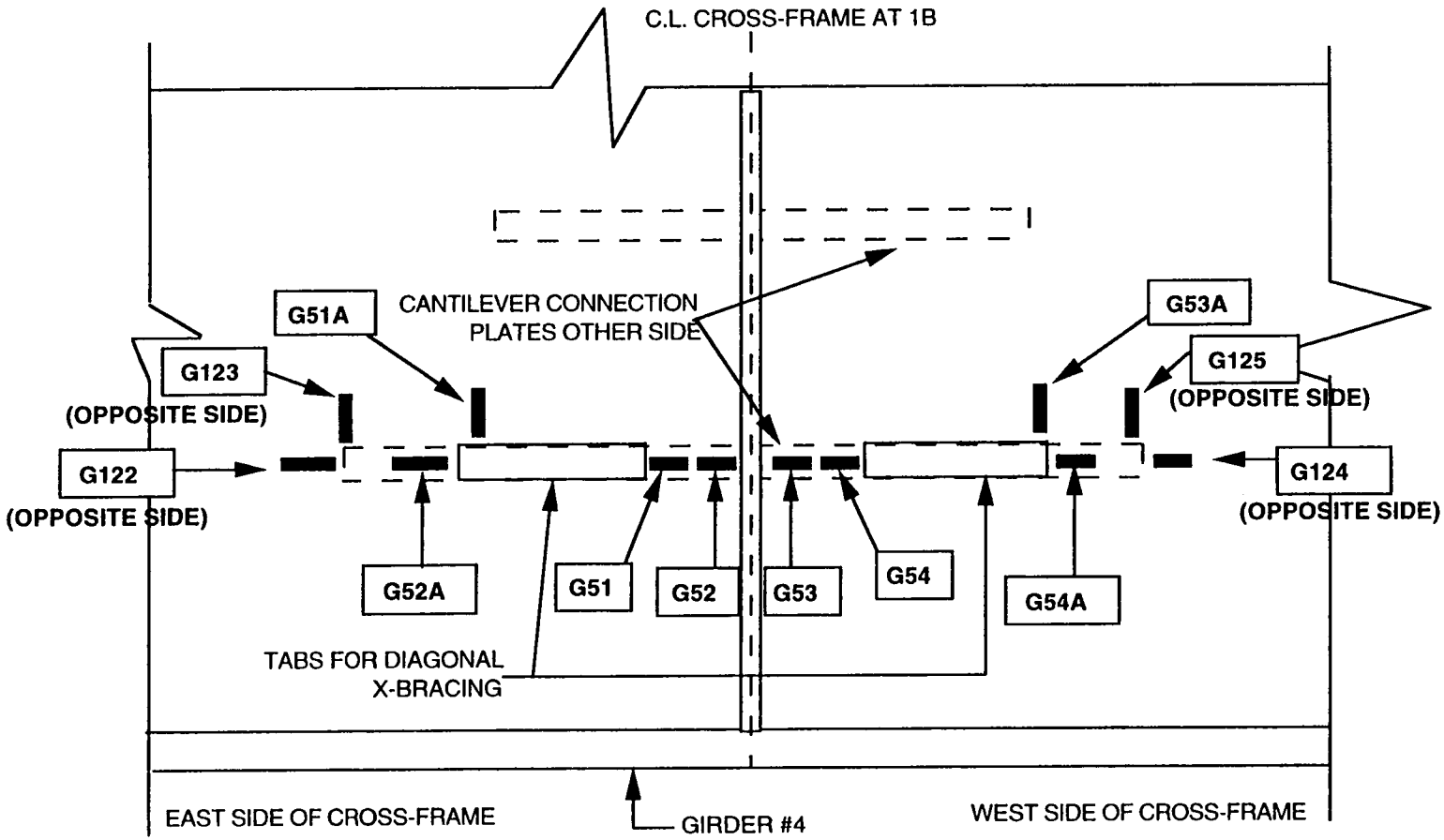
SAMPLE LOCATION #1B

THIRD CROSS-FRAME EAST OF FAILURE LOCATION (1A)



1B **SAMPLE LOCATION #1B**

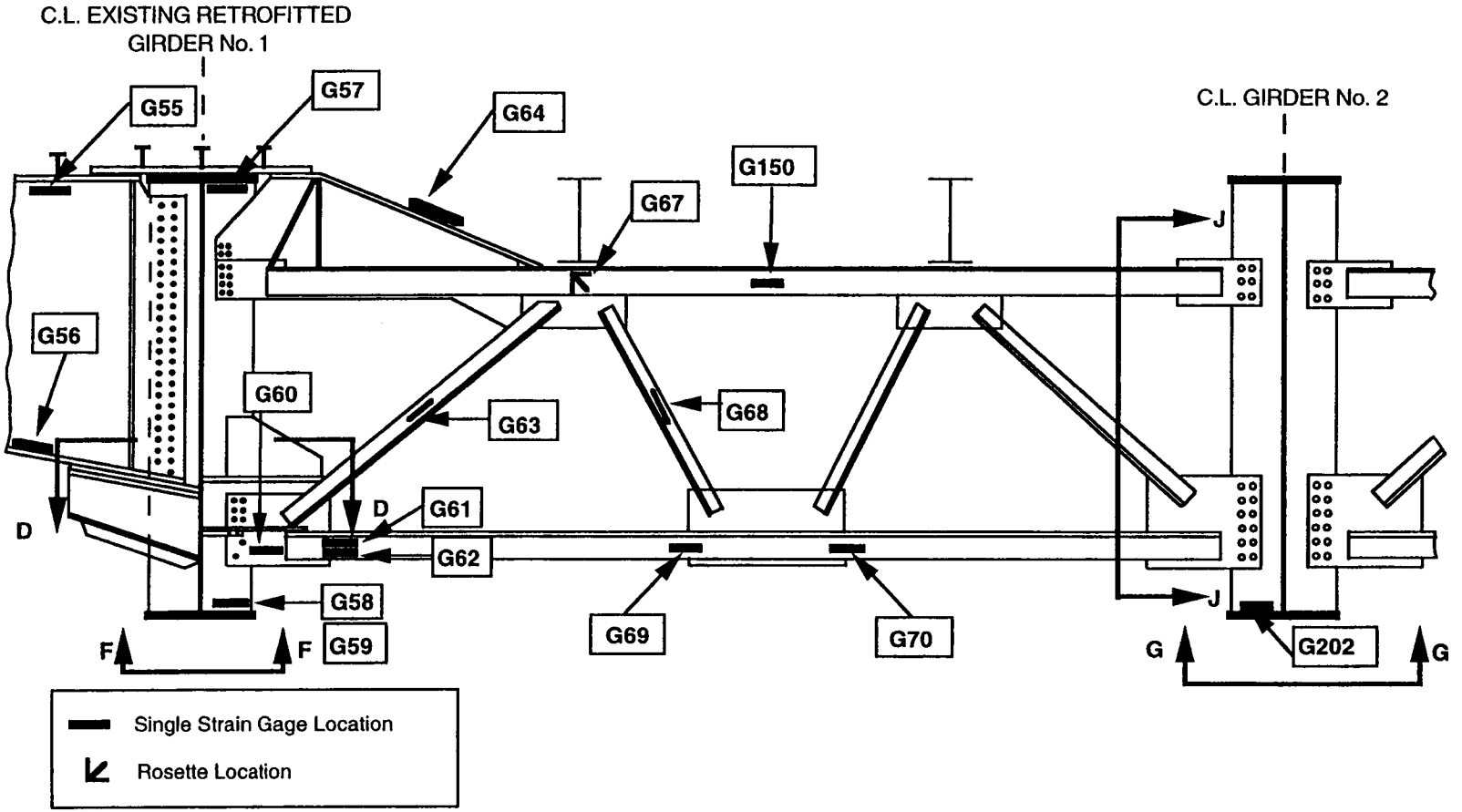
SECTION D-D



6

SAMPLE LOCATION #6 AT 1B

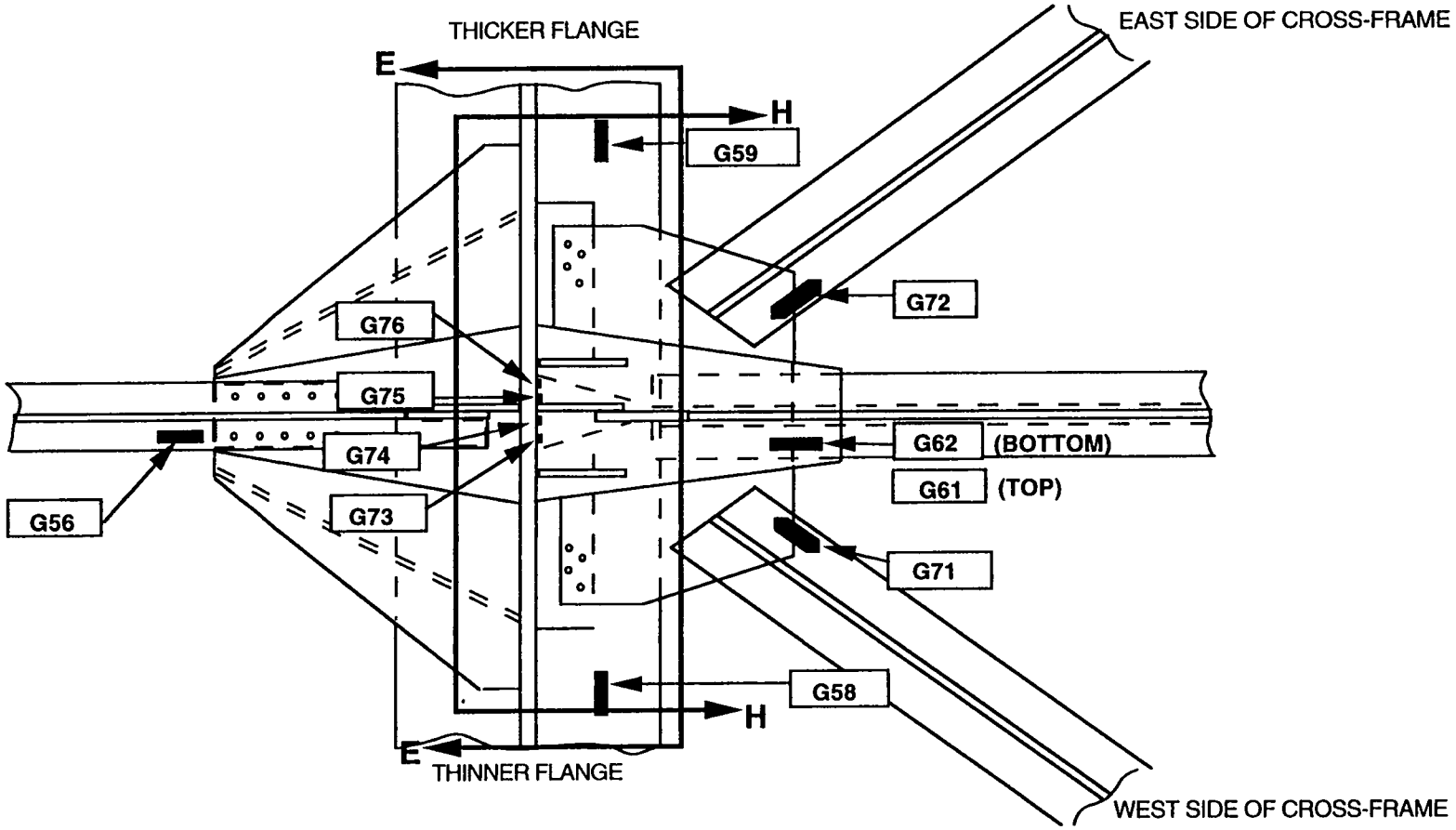
SECTION E-E



1C

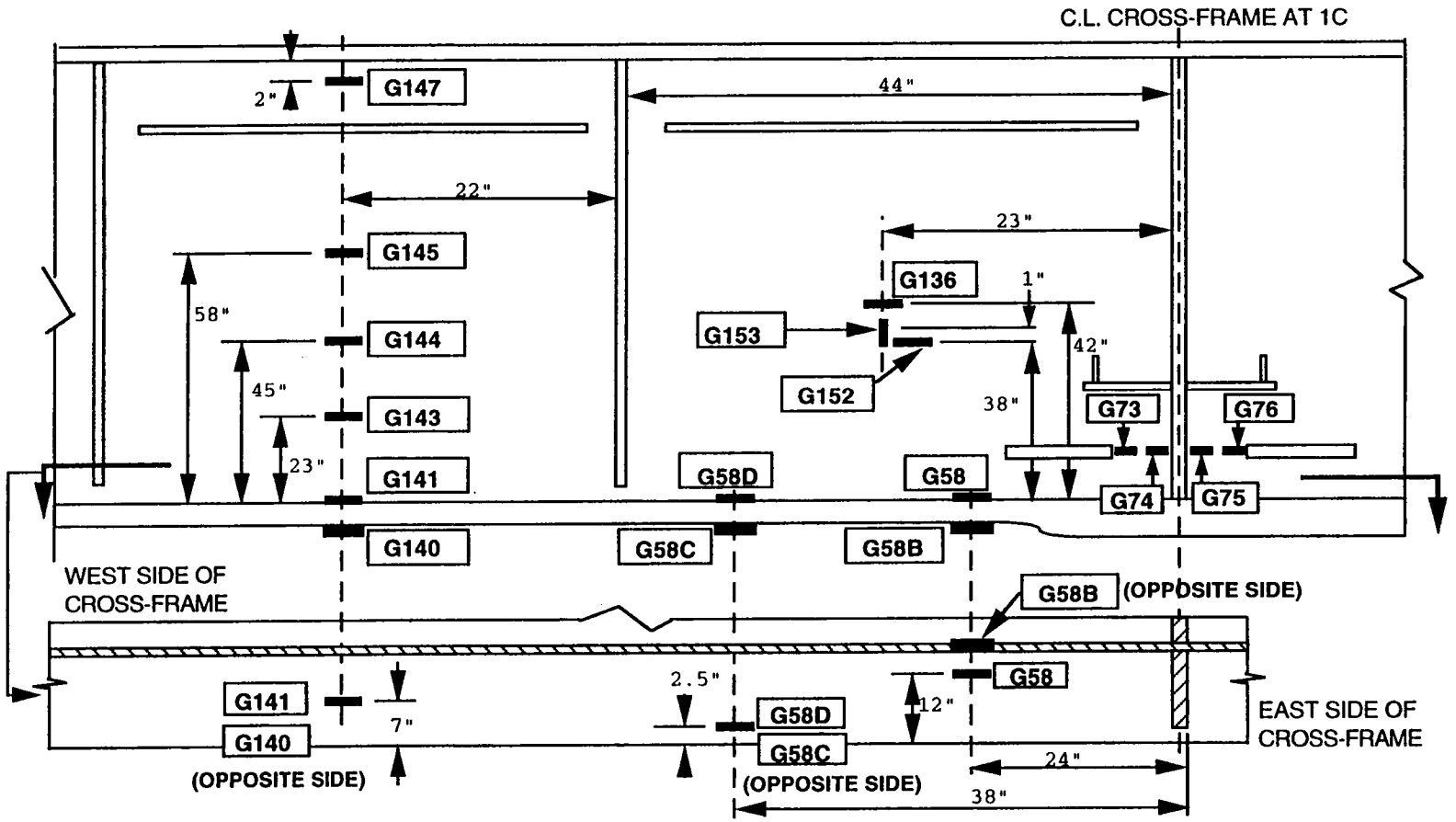
SAMPLE LOCATION #1C

CROSS-FRAME WEST BOUND ACROSS FROM FAILURE LOCATION (1A)



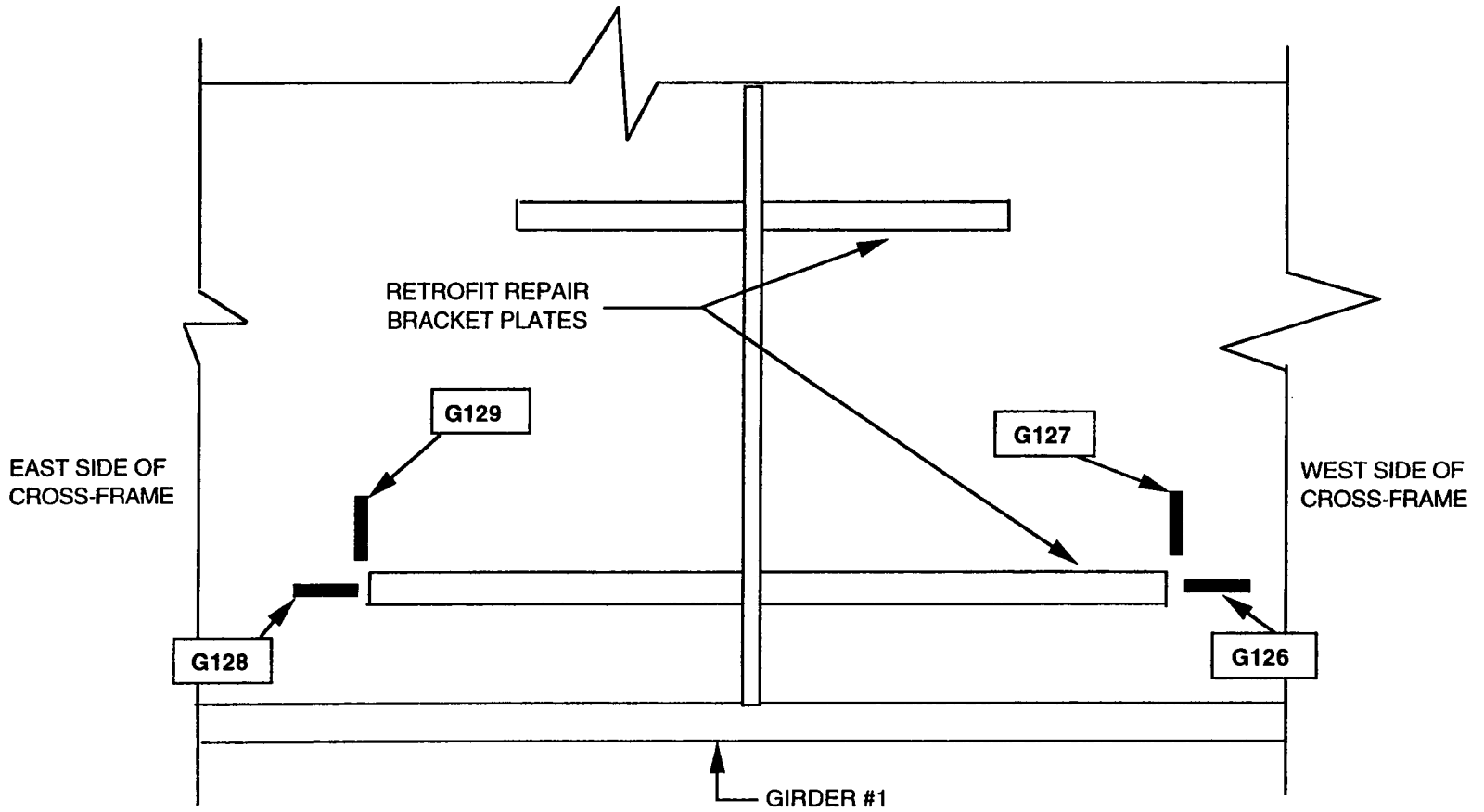
1C **SAMPLE LOCATION #1C**

SECTION D-D



1C **SAMPLE LOCATION #1C**

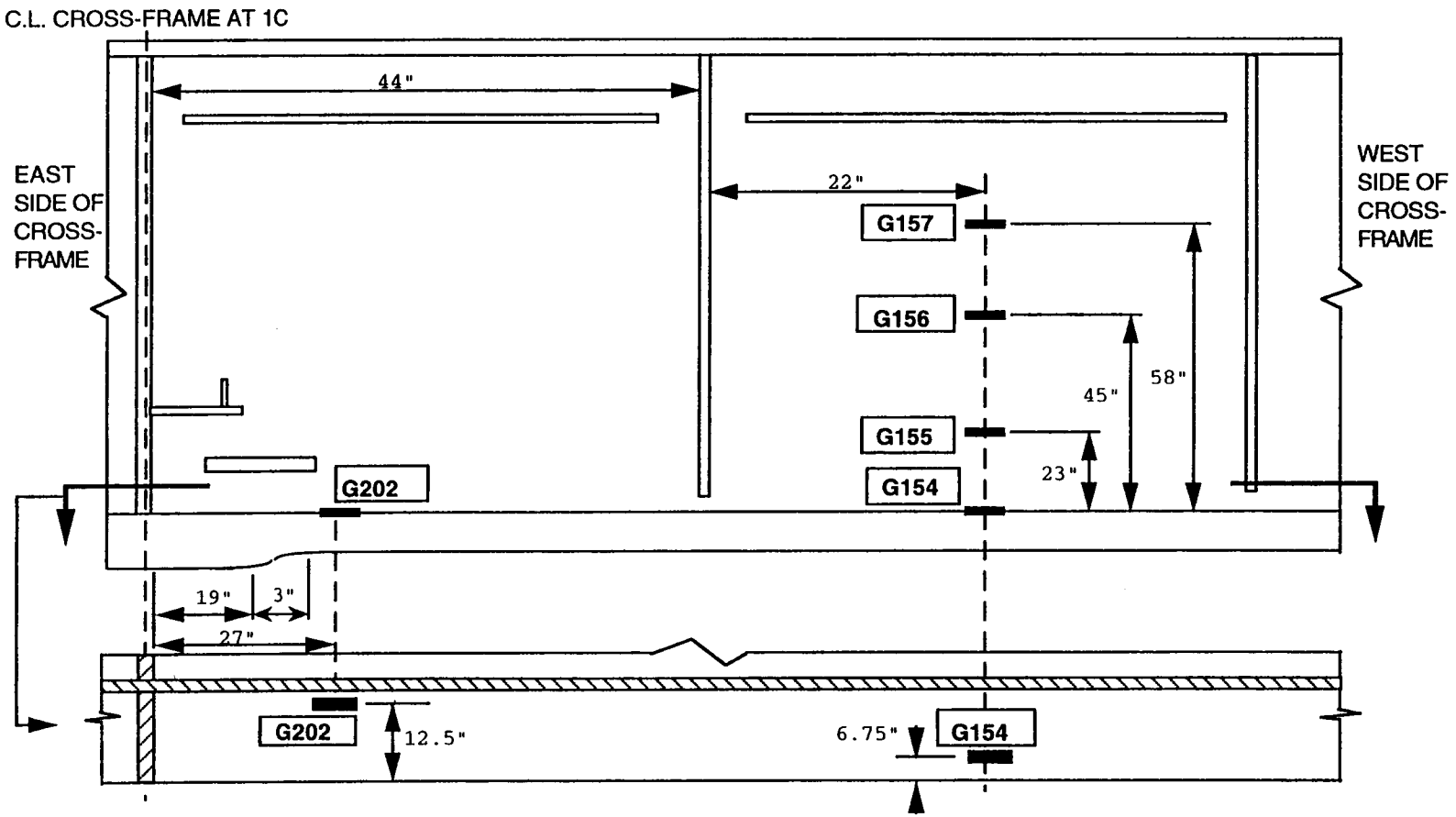
SECTION E-E



1C

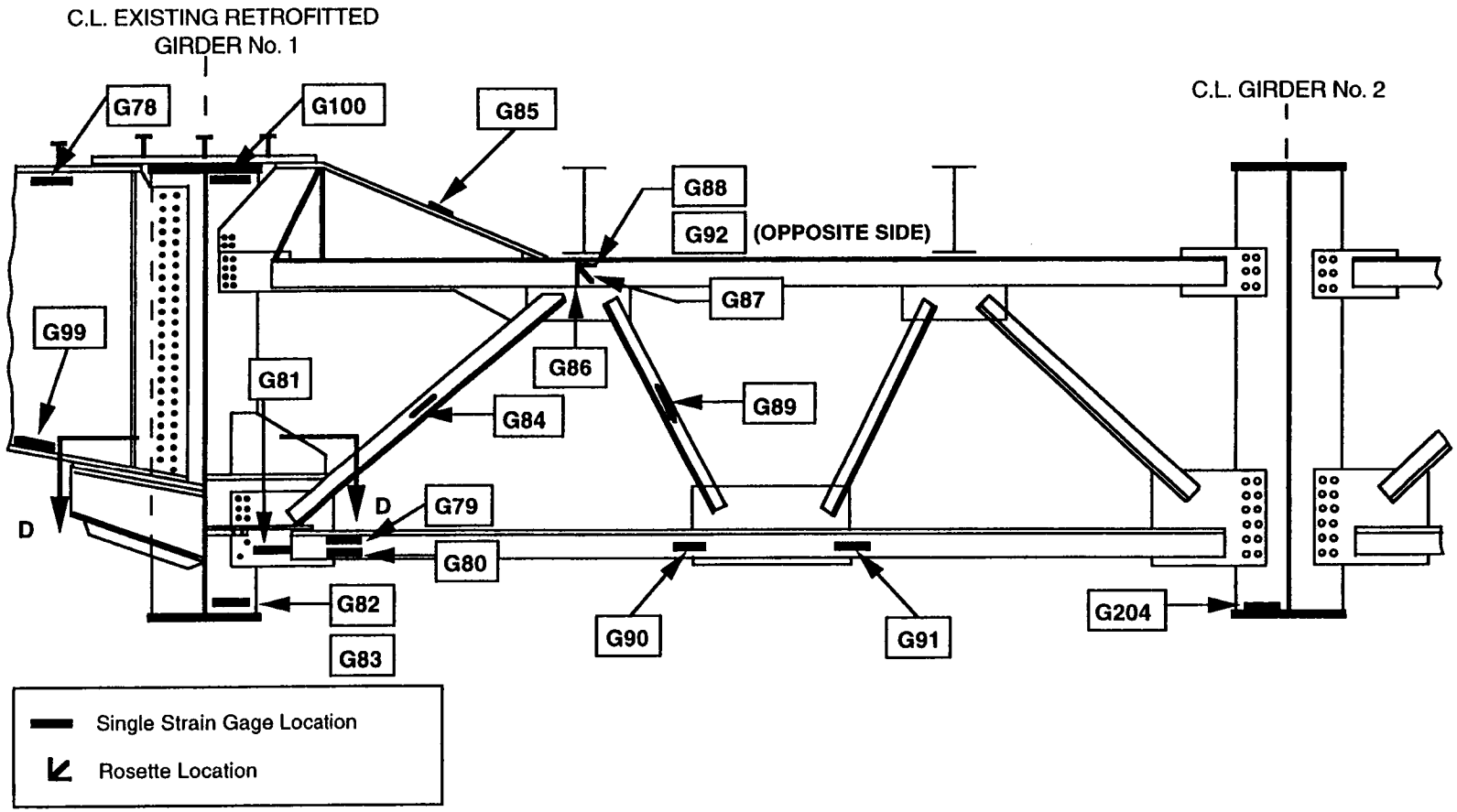
SAMPLE LOCATION #1C

SECTION H-H



1C **SAMPLE LOCATION #1C**

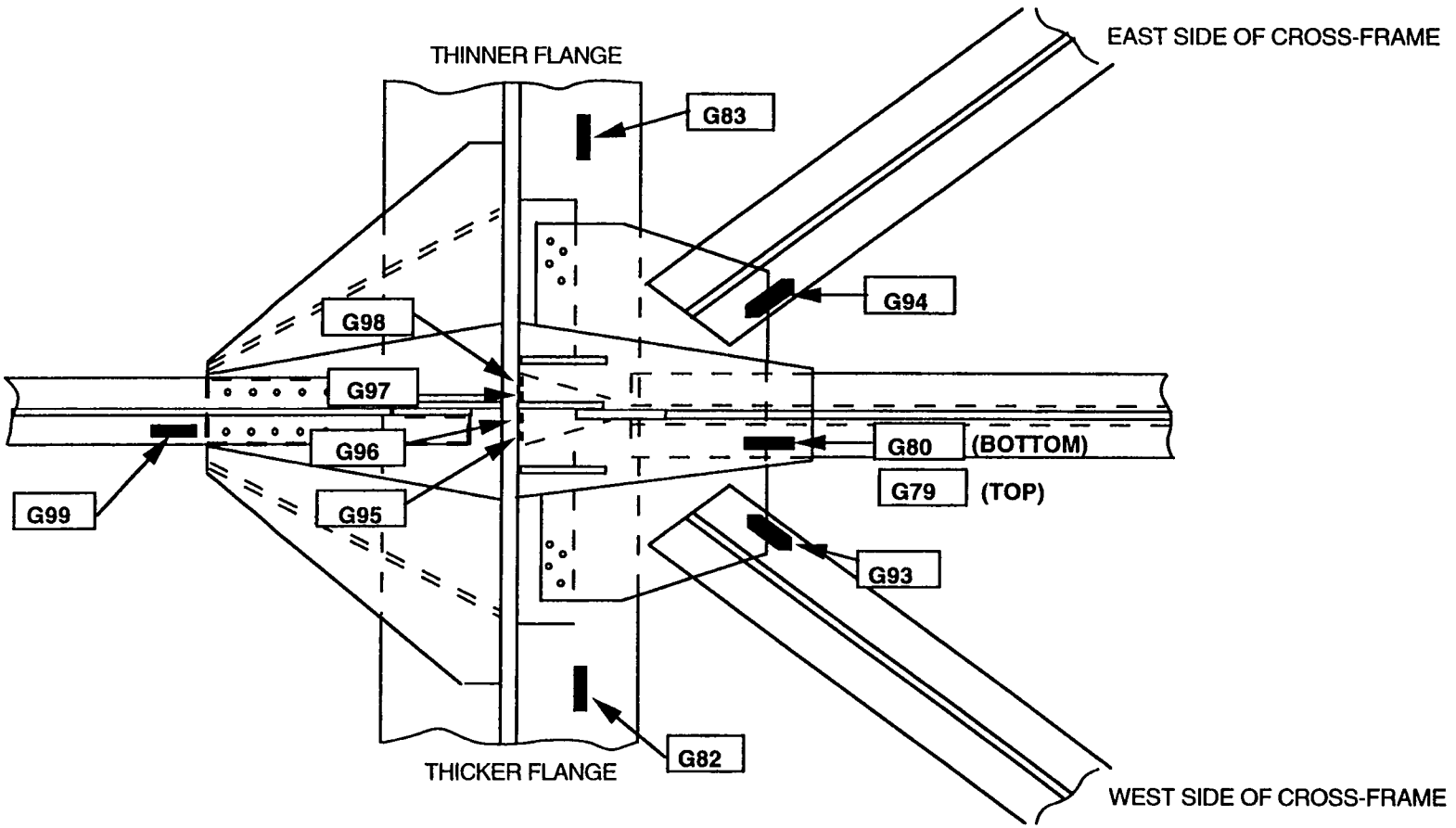
SECTION J-J



1D

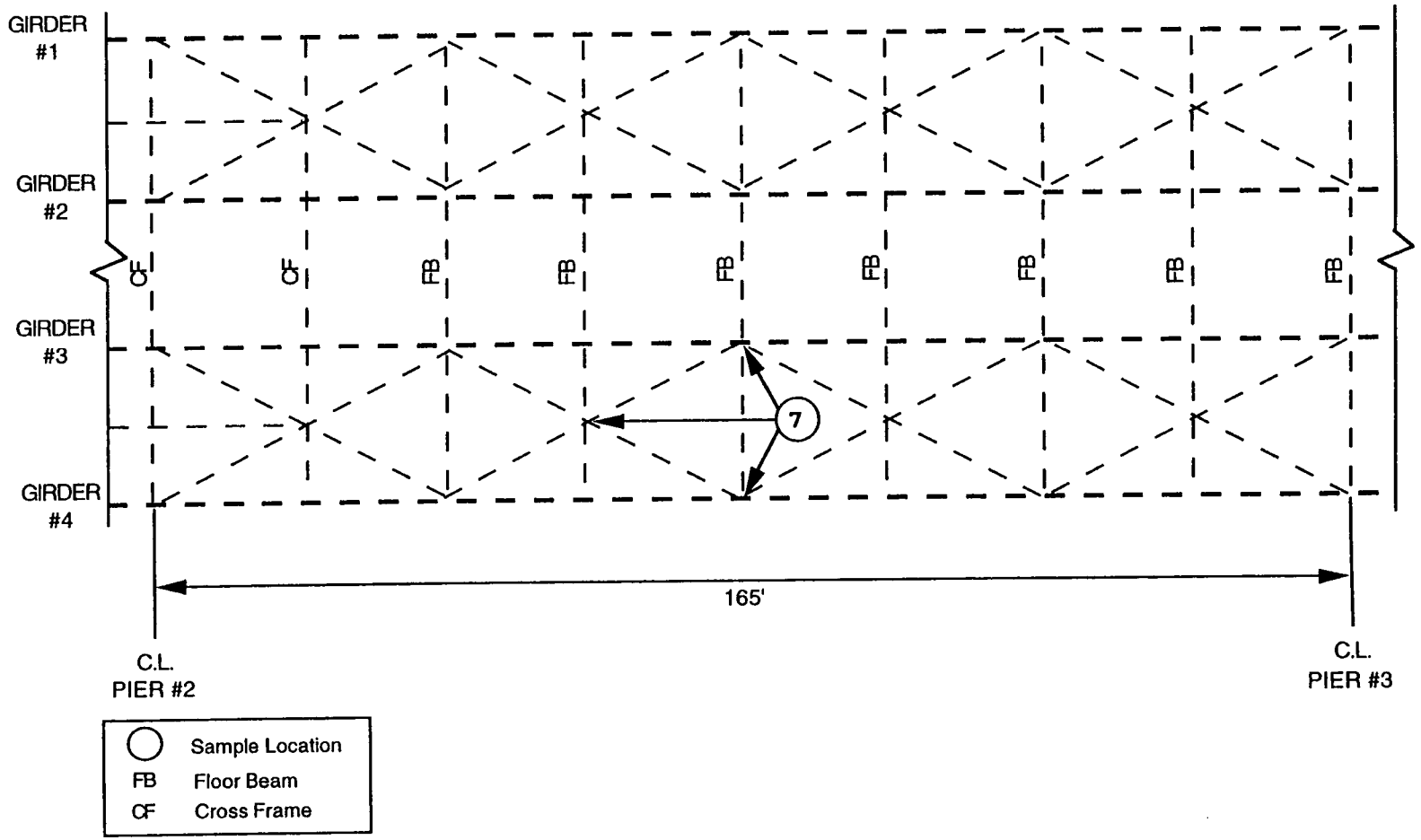
SAMPLE LOCATION #1D

CROSS-FRAME WEST BOUND ACROSS FROM 1B

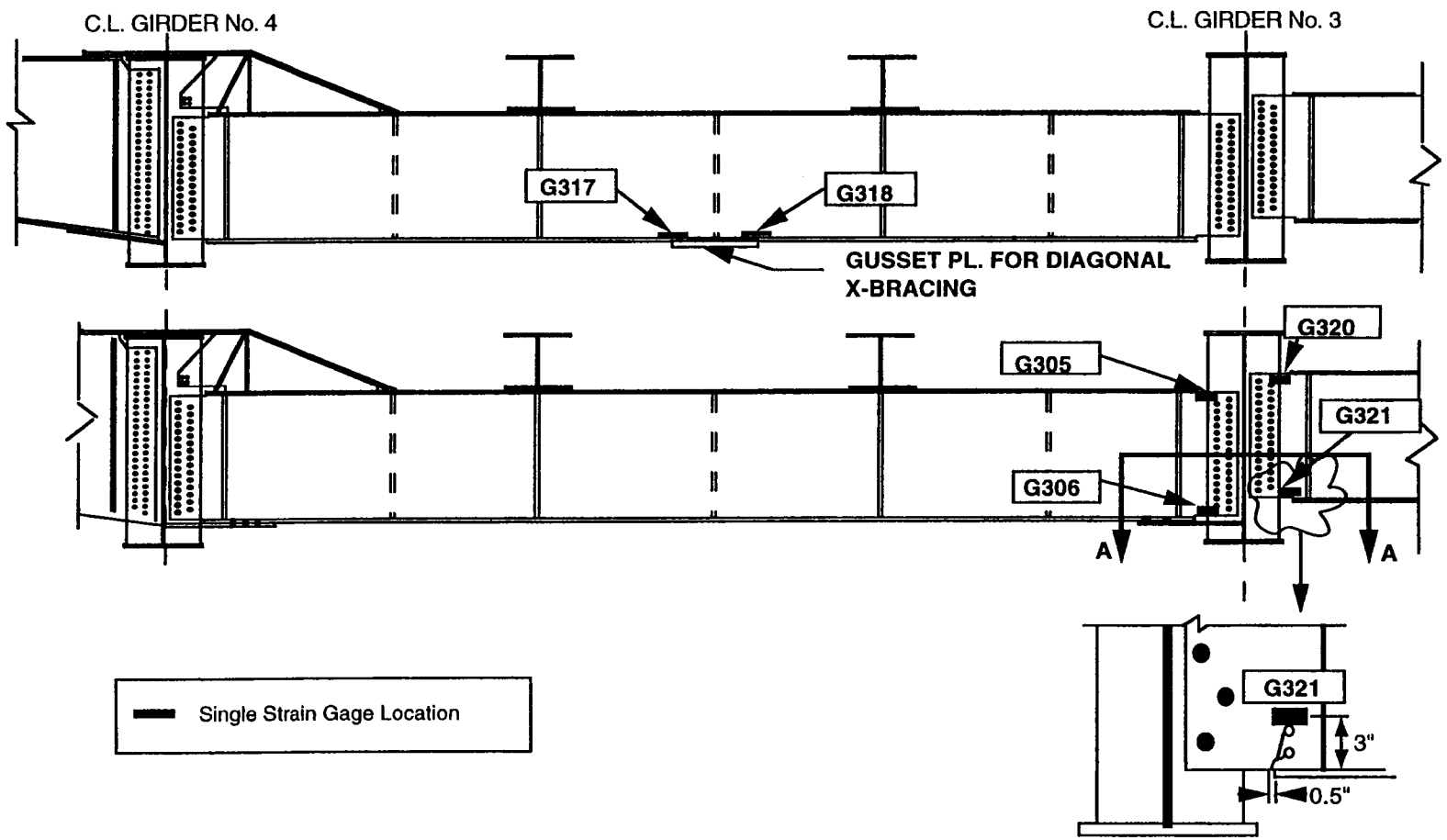


1D **SAMPLE LOCATION #1D**

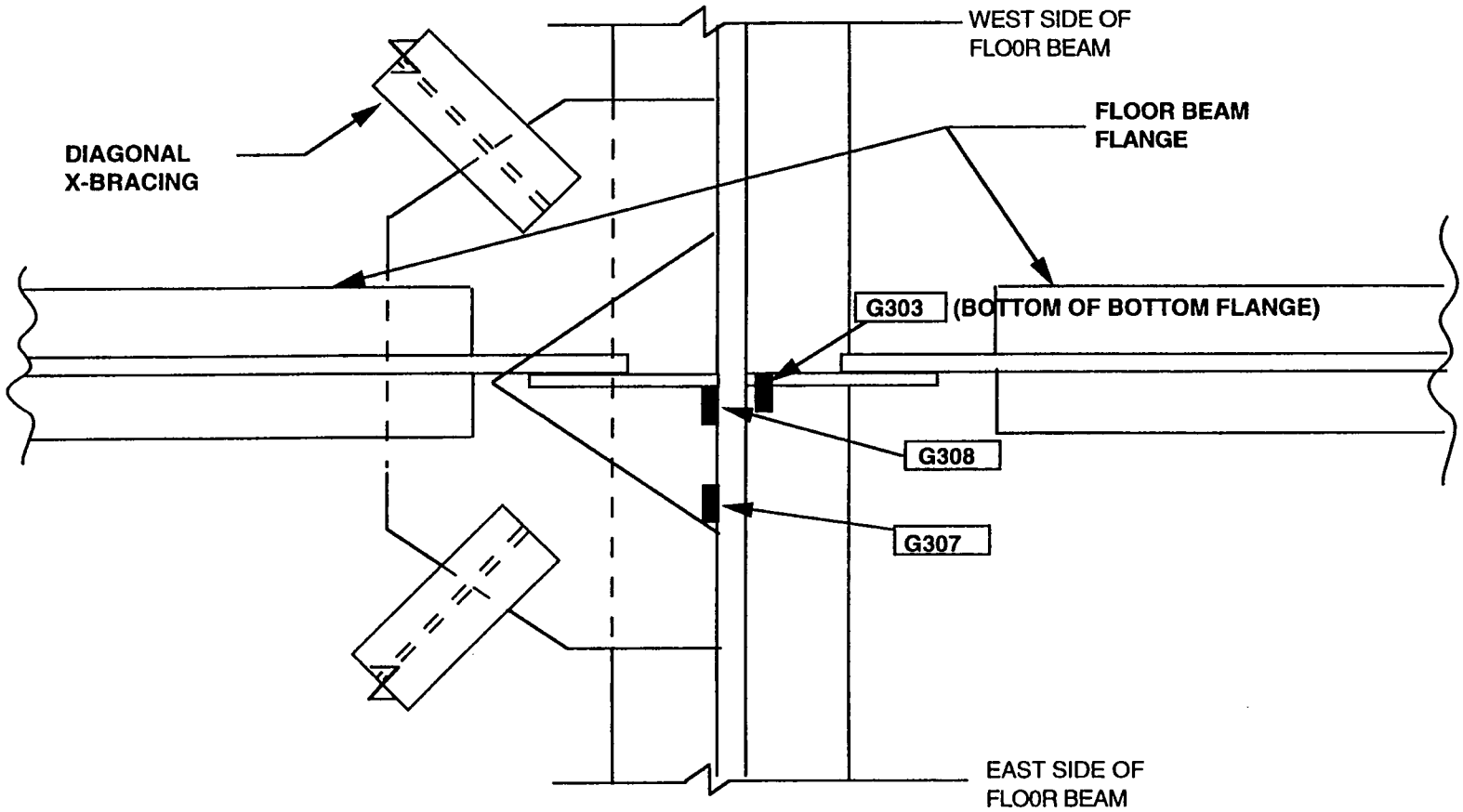
SECTION D-D



Plan View of Span 3



7 SAMPLE LOCATION #7



7 **SAMPLE LOCATION #7**

SECTION A-A

VITA

Shima Najem Clarke was born in Kabul, Afghanistan on August 22, 1958. She attended high school in Knoxville, Tennessee and graduated from West High School in May 1976. The following June she entered The University of Tennessee, Knoxville and in May 1980 received the degree of Bachelor of Science in Civil Engineering. She reentered The University of Tennessee, Knoxville in September 1983 and in March 1985 received a Master of Science in Civil Engineering with an emphasis in structures.

From 1980 to 1983, Shima was employed as a Civil/Structural Engineer by Bechtel Power Corporation in Gaithersburg, Maryland. From 1985 to 1988, Shima served as a principal engineer at Impell Corporation in Knoxville, Tennessee, working on various structural engineering projects and risk assessment projects. She later worked for TENERA Corporation as an engineering consultant in their nuclear power program. From 1990 to 1992, Shima was employed as a research assistant by The University of Tennessee Civil Engineering Department. From 1993 to 1996, Shima worked as a research associate with The University of Tennessee Transportation Center. Shima has taught structural analysis at The University of Tennessee, Knoxville.